

ปฏิบัติการถ่ายโอนโปรตอนที่หมู่ฟังก์ชันกรดทริฟลิกของแนฟิออน

นางสาวมยุรี พลเยี่ยม



วิทยานิพนธ์นี้เป็นส่วนหนึ่งของการศึกษาตามหลักสูตรปริญญาวิทยาศาสตรดุษฎีบัณฑิต

สาขาวิชาเคมี

มหาวิทยาลัยเทคโนโลยีสุรนารี

ปีการศึกษา 2554

PROTON TRANSFER REACTIONS AT TRIFLIC ACID
FUNCTIONAL GROUP OF NAFION[®]

Mayuree Phonyiem




A Thesis Submitted in Partial Fulfillment of the Requirements for the
Degree of Doctor of Philosophy in Chemistry
Suranaree University of Technology
Academic Year 2011

PROTON TRANSFER REACTIONS AT TRIFLIC ACID

FUNCTIONAL GROUP OF NAFION[®]

Suranaree University of Technology has approved this thesis submitted in partial fulfillment of the requirements for the Degree of Doctor of Philosophy.

Thesis Examining Committee


(Asst. Prof. Dr. Kunwadee Rangsiwatananon)

Chairperson


(Prof. Dr. Kritsana Sagarik)

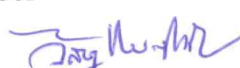
Member (Thesis Advisor)


(Assoc. Prof. Dr. Anan Tongraar)

Member


(Asst. Prof. Dr. Viwat Vchirawongkwin)


Member


(Asst. Prof. Dr. Visit Vao-Soongnern)

Member


(Prof. Dr. Sukit Limpijumnong)

Vice Rector for Academic Affairs


(Assoc. Prof. Dr. Prapun Manyum)

Dean of Institute of Science

มยุรี พลเยี่ยม : ปฏิริยาการถ่ายโอนโปรตอนที่หมู่ฟังก์ชันกรดทริฟลิกของแนฟิออน (PROTON TRANSFER REACTIONS AT TRIFLIC ACID FUNCTIONAL GROUP OF NAFION®) อาจารย์ที่ปรึกษา : ศาสตราจารย์ ดร.กฤษณะ ศาคริก, 177 หน้า.

วิทยานิพนธ์เรื่องนี้ศึกษาปฏิริยาการถ่ายโอนโปรตอนที่หมู่ฟังก์ชันกรดซัลโฟนิก ($-SO_3H$) ของแนฟิออน (Nafion®) โดยวิธีทางทฤษฎี โดยใช้สารเชิงซ้อนที่เกิดจากกรดทริฟลิก (triflic acid) ไฮออนไฮโดรเนียม (H_3O^+) และน้ำ (H_2O) เป็นแบบจำลอง การศึกษาเริ่มจากการคำนวณสารตั้งต้น (precursor) และสถานะการเปลี่ยน (transition state) ที่ระดับการไฮเดรตต่ำ โดยใช้วิธีเทสพาร์ทิเคิล (T-Model) จากนั้นนำสารตั้งต้นและสถานะการเปลี่ยนที่คำนวณได้ไปเป็นโครงสร้างเริ่มต้นในการจำลอง BOMD (Born-Oppenheimer molecular dynamics simulations) ที่อุณหภูมิ 298 K และ 350 K และนำข้อมูลเชิงพลวัตที่คำนวณได้ไปวิเคราะห์เพื่อจัดกลุ่ม ตลอดจนศึกษาปฏิริยามูลฐาน (elementary reactions) ของการถ่ายโอนโปรตอน ผลการคำนวณโดยวิธี density functional theory (DFT) แสดงวิถีการเกิดปฏิริยา (reaction pathway) ที่เป็นไปได้อย่างน้อยสองแบบ ได้แก่ การถ่ายโอนโปรตอนผ่านหมู่ฟังก์ชัน $-SO_3H$ ซึ่งมีการให้หรือรับโปรตอนที่อะตอมออกซิเจนของ $-SO_3H$ เรียกว่ากลไกการถ่ายโอนพาส-ทรู (pass-through mechanism) ในขณะที่แบบที่สอง โปรตอนถ่ายโอนผ่านพันธะไฮโดรเจนในสารประกอบซุนเดิล (Zundel complex, $H_5O_2^+$) ที่อยู่ในบริเวณใกล้เคียง เรียกว่ากลไกการถ่ายโอนพาส-บาย (pass-by mechanism)

การจำลอง BOMD ที่ 298 K แสดงว่า ปฏิริยาการถ่ายโอนโปรตอนที่หมู่ฟังก์ชัน $-SO_3H$ มีลักษณะไม่พร้อมเพรียงกัน (not concerted) เนื่องจากการกระเพื่อมของพลังงานความร้อน (thermal energy fluctuation) และมีสมมูลแบบพลวัตเสมือน (quasi-dynamics) เข้ามาเกี่ยวข้อง ในขณะที่เกิดปฏิริยา ผลการคำนวณแสดงด้วยว่าหมู่ฟังก์ชัน $-SO_3H$ ทำหน้าที่เป็นตัวกลาง สนับสนุนให้เกิดปฏิริยาการถ่ายโอนโปรตอนทั้งทางตรงและทางอ้อม โดยทำให้เกิดความบกพร่องโปรตอน (proton defect) และสถานะเปลี่ยน (transition state) ได้แก่ $-SO_3^-$ และ $-SO_3H_2^+$ ผลการวิเคราะห์ asymmetric O-H stretching frequencies (ν^{OH}) ของโปรตอนในพันธะไฮโดรเจนโดยวิธี DFT แสดงความถี่ขีดเริ่มเปลี่ยน (threshold asymmetric O-H stretching frequency, ν^{OH*}) ในช่วง $1700 - 2200\text{ cm}^{-1}$ ขณะที่การจำลอง BOMD ที่ 350 K ให้ความถี่ขีดเริ่มเปลี่ยนต่ำกว่าเล็กน้อย โดยแสดง asymmetric O-H stretching ที่สองความถี่ ($\nu_A^{OH,MD}$ และ $\nu_B^{OH,MD}$) ซึ่งเป็นลักษณะพิเศษของสารเชิงซ้อนพันธะไฮโดรเจนที่สามารถถ่ายโอนโปรตอนได้ โดยความถี่ที่ต่ำกว่า ($\nu_A^{OH,MD}$) สอดคล้องกับรูปแบบการสั่นกลับไปกลับมาของโปรตอนตรงกึ่งกลางพันธะไฮโดรเจน (oscillatory shuttling)

ในขณะที่ความถี่ที่สูงกว่า ($v_B^{OH,MD}$) เกิดจากการสั่นที่โปรตอนมีจุดศูนย์กลางการสั่นเคลื่อนไปยังอะตอมออกซิเจนข้างใดข้างหนึ่งเล็กน้อย (structural diffusion) การเปรียบเทียบผลที่ได้จากวิธีการจำลอง BOMD นี้ กับกรณีกลุ่มโมเลกุลไฮโดรเนียมในสารละลายน้ำ (protonated water clusters) แสดงว่า $-SO_3H$ ทำให้เกิดการลดพลังงานการสั่นสำหรับการเปลี่ยนไปมาระหว่างสถานะพลวัตทั้งสอง ($\Delta v_{BA}^{OH,MD}$) ส่งผลให้เกิดการเพิ่มจำนวนพันธะไฮโดรเจนที่มีแนวโน้มเกิดการถ่ายโอนโปรตอน ดังนั้นสรุปว่า หมู่ฟังก์ชัน $-SO_3H$ ของแนฟิออน ทำหน้าที่สร้างสถานะที่เหมาะสม ทั้งด้านโครงสร้าง พลังงานและพลวัต เพื่อให้กระบวนการถ่ายโอนโปรตอนมีประสิทธิภาพสูงสุด ผลการวิจัยยังแสดงวิธีการคำนวณแนวโน้มการถ่ายโอนโปรตอนในพันธะไฮโดรเจนเป็นครั้งแรก โดยใช้ $\Delta v_{BA}^{OH,MD}$ และได้เสนอพื้นฐานทางทฤษฎี ตลอดจนแนวทางในการทดลองเพื่อติดตามปฏิกิริยาการถ่ายโอนโปรตอนที่มีประสิทธิภาพในสารละลายน้ำ



สาขาวิชาเคมี

ปีการศึกษา 2554

ลายมือชื่อนักศึกษา

ลายมือชื่ออาจารย์ที่ปรึกษา

Dr. พชร วัฒน
Dr. ปรเมศ

MAYUREE PHONYIEM : PROTON TRANSFER REACTIONS AT
TRIFLIC ACID FUNCTIONAL GROUP OF NAFION®. THESIS
ADVISOR : PROF. KRITSANA SAGARIK, Ph.D. 177 PP.

PROTON TRANSFER REACTIONS/ NAFION®/ TRIFLIC ACID/ BOMD
SIMULATIONS/ VIBRATIONAL SPECTRA

Proton transfer reactions at the sulfonic acid groups in Nafion® were theoretically studied using complexes formed from triflic acid ($\text{CF}_3\text{SO}_3\text{H}$), H_3O^+ and H_2O , as model systems. The investigations began with searching for potential precursors and transition states at low hydration levels using the Test-particle model (T-Model), density functional theory (DFT) and *ab initio* calculations. They were employed as starting configurations in Born-Oppenheimer molecular dynamics (BOMD) simulations at 298 and 350 K, from which elementary reactions were analyzed and categorized. DFT calculations suggested at least two structural diffusion pathways at the $-\text{SO}_3\text{H}$ group namely, the “pass-through” and “pass-by” mechanisms. The former involves the protonation and deprotonation at the $-\text{SO}_3\text{H}$ group, whereas the latter the proton transfer in the adjacent Zundel complex. BOMD simulations at 298 K revealed that proton transfer reactions at $-\text{SO}_3\text{H}$ are not concerted, due to the thermal energy fluctuation and the existence of various quasi-dynamic equilibria, and $-\text{SO}_3\text{H}$ could directly and indirectly mediate proton transfer reactions through the formation of proton defects, as well as the $-\text{SO}_3^-$ and $-\text{SO}_3\text{H}_2^+$ transition states. Analyses of the asymmetric O-H stretching frequencies (ν^{OH}) of the hydrogen bond (H-bond) protons showed the threshold frequencies ($\nu^{\text{OH}*}$) of proton transfer in the

range of 1700 to 2200 cm^{-1} . BOMD simulations at 350 K anticipated slightly lower threshold frequencies ($\nu_{\text{A}}^{\text{OH}^*,\text{MD}}$), with two characteristic asymmetric O-H stretching frequencies ($\nu_{\text{A}}^{\text{OH,MD}}$ and $\nu_{\text{B}}^{\text{OH,MD}}$) being the spectral signatures of proton transfer in the H-bond complexes. The lower frequency ($\nu_{\text{A}}^{\text{OH,MD}}$) is associated with the oscillatory shuttling motion and the higher frequency ($\nu_{\text{B}}^{\text{OH,MD}}$) the structural diffusion motion. Comparison of the present results with BOMD simulations on protonated water clusters indicated that the $-\text{SO}_3\text{H}$ group facilitates proton transfer by reducing the vibrational energy for the interconversion between the two dynamic states ($\Delta\nu_{\text{BA}}^{\text{OH,MD}}$), resulting in a higher population of the H-bonds with the structural diffusion motion. One could therefore conclude that the $-\text{SO}_3\text{H}$ groups in Nafion[®] act as active binding sites which provide appropriate structural, energetic and dynamic conditions for effective structural diffusion processes in proton exchange membrane fuel cell (PEMFC). The present results suggested for the first time a possibility to discuss the tendency of proton transfer in H-bond using $\Delta\nu_{\text{BA}}^{\text{OH,MD}}$ and provided theoretical bases and guidelines for the investigations of proton transfer reactions in theory and experiment.

School of Chemistry

Academic Year 2011

Student's Signature

Advisor's Signature

ACKNOWLEDGEMENTS

I would like to express my sincere gratitude to Prof. Dr. Kritsana Sagarik for his exceptional generous support, academic guidance, advice and encouragement during my graduate career. I would like to thank to Asst. Prof. Dr. Kunwadee Rangsriwatananon, Assoc. Prof. Dr. Anan Tongraar, Asst. Prof. Dr. Viwat Vchirawongkwin, Asst. Prof. Dr. Visit Vao-Soongnern who are the thesis committees, for their time and useful suggestions. I would also like to express my great gratitude to all lecturers at the School of Chemistry, Suranaree University of Technology and Department of Chemistry, Faculty of Science, Ramkhamhaeng University for their good attitude and advices.

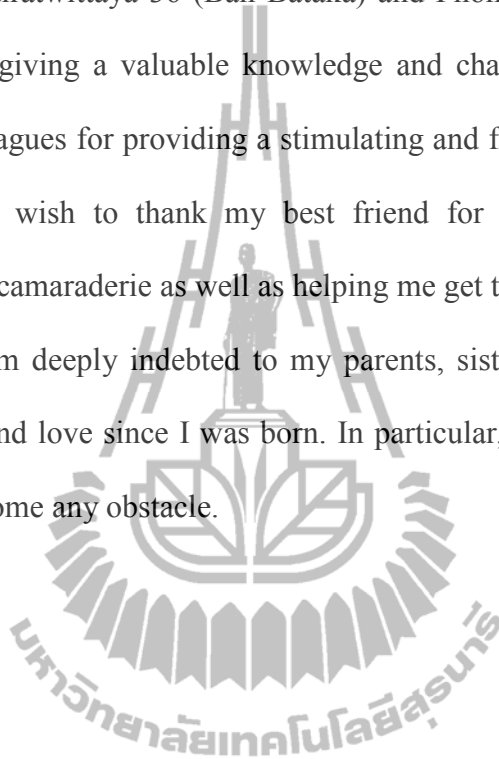
I would also like to acknowledge the financial support from the Thailand Research Fund (TRF) through the Royal Golden Jubilee (RGJ) Ph.D. program (Grant No. PHD/0110/2548). Special thanks should go to the School of Chemistry and the School of Mathematics, Institute of Science, Suranaree University of Technology (SUT), as well as the National Electronics and Computer Technology Center (NECTEC) and the National Nanotechnology Center (NANOTEC), for providing computer facilities.

I would like to express my sincere thanks to Prof. Dr. So Hirata and Dr. Kiyoshi Yagi at University of Illinois at Urbana-Champaign, United State of America, who provides me valuable advices, suggestions and new worthy research experiences.

Thanks to members of Hirata group for nice working atmosphere and all of my friends for their friendship and assistance.

I would like to take this opportunity to express my deepest gratitude to all of the teachers at Thairatwittaya 36 (Ban Bataka) and Phontongpattanawittaya Schools for their kindness giving a valuable knowledge and chances. I am indebted to my many student colleagues for providing a stimulating and fun environment in which to learn and grow. I wish to thank my best friend for all the emotional support, entertainment, and camaraderie as well as helping me get through the difficult times.

Finally, I am deeply indebted to my parents, sister and all cousins for their support, patience and love since I was born. In particular, their understandings make me strong to overcome any obstacle.



Mayuree Phonyiem

CONTENTS

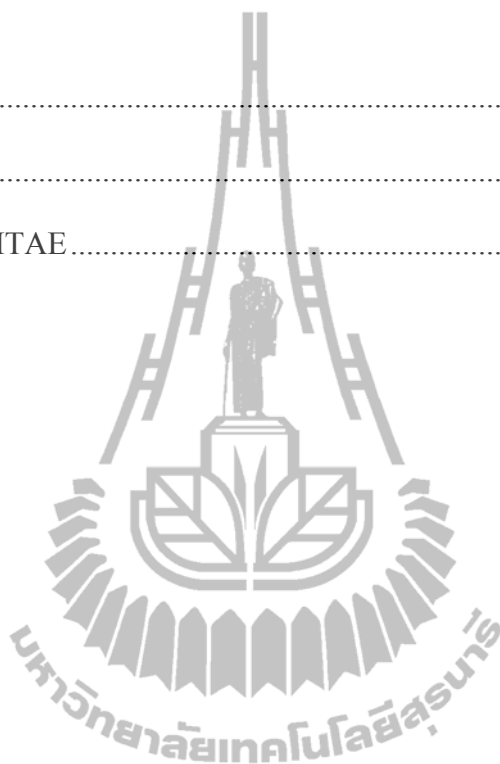
	Page
ABSTRACT IN THAI.....	I
ABSTRACT IN ENGLISH	III
ACKNOWLEDGEMENTS.....	V
CONTENTS.....	VII
LIST OF TABLES	X
LIST OF FIGURES	XII
LIST OF ABBREVIATIONS.....	XVII
CHAPTER	
I INTRODUCTION.....	1
II COMPUTATIONAL METHODOLOGY	10
2.1 The T-model potentials	12
2.2 Geometry refinement	15
Part I: B3LYP/6-31G (d,p) calculations	15
Part II: B3LYP/TZVP calculations.....	18
Characteristics of proton transfer in H-bond	20
2.3 Born-Oppenheimer MD simulations.....	21
Part I: NVE BOMD simulations	22
Proton transfer profiles	24
Part II: NVT BOMD simulations.....	24

CONTENTS (Continued)

		Page
	IR spectra	26
	Diffusion coefficients.....	27
III	RESULTS AND DISCUSSION	28
3.1	Part I.....	28
3.1.1	Static results	28
	Structures and energetic.....	28
	Potential energy profiles	45
3.1.2	Dynamic results	48
	Proton transfer profiles and elementary reactions	48
3.2	Part II	68
3.2.1	Static results.....	68
	Structures and energetic.....	68
	Harmonic IR frequencies	73
	Classifications of H-bonds.....	87
3.2.2	Dynamic results	91
	Average H-bond structures and IR spectra	91
	Diffusion coefficients.....	119
IV	CONCLUSIONS.....	123

CONTENTS (Continued)

	Page
REFERENCES	129
APPENDICES	142
CURRICULUM VITAE	177



LIST OF TABLES

Table	Page
3.1 Structures of the $\text{H}_3\text{O}^+\text{-H}_2\text{O}$ complexes, obtained from the T-model, DFT and <i>ab initio</i> geometry optimizations. (a) $\text{H}_3\text{O}^+\text{-H}_2\text{O}$ 1 : 1 complex. (b) $\text{H}_3\text{O}^+\text{-H}_2\text{O}$ 1 : 2 complex. (c) $\text{H}_3\text{O}^+\text{-H}_2\text{O}$ 1 : 3 complex.....	31
3.2 Structures of the $\text{CF}_3\text{SO}_3\text{H-H}_2\text{O}$ and $\text{CF}_3\text{SO}_3\text{H-H}_3\text{O}^+$ 1 : 1 complexes, obtained from T-model, DFT and <i>ab initio</i> geometry optimizations. a) - c) $\text{CF}_3\text{SO}_3\text{H-H}_2\text{O}$ 1 : 1 complexes. d) $\text{CF}_3\text{SO}_3\text{H-H}_3\text{O}^+$ 1 : 1 complex.....	33
3.3 Equilibrium structures of the $\text{CF}_3\text{SO}_3\text{H-H}_3\text{O}^+\text{-H}_2\text{O}$ 1 : 1 : 1 complexes a) - c), obtained from T-model, DFT and <i>ab initio</i> geometry optimizations. Interaction energy in kJ/mol, angle in degree and distance in Å.	35
3.4 Equilibrium structures of the $\text{CF}_3\text{SO}_3\text{H-H}_3\text{O}^+\text{-H}_2\text{O}$ 1 : 1 : 2 complexes a) – d), obtained from T-model, DFT and <i>ab initio</i> calculations. Interaction energy in kJ/mol and distance in Å.	40

LIST OF TABLES (Continued)

Table	Page
3.5 Energies of the $\text{CF}_3\text{SO}_3\text{H-H}_3\text{O}^+-n\text{H}_2\text{O}$ complexes, $1 \leq n \leq 3$, obtained from B3LYP/TZVP calculations, both in the gas phase and continuum aqueous solution. Energies are in kJ mol^{-1}	70
3.6 H-bond distances, asymmetric stretching coordinates (Δd_{DA}) and O-H stretching frequencies of the $\text{CF}_3\text{SO}_3\text{H-H}_3\text{O}^+-n\text{H}_2\text{O}$ complexes, $1 \leq n \leq 3$, obtained from B3LYP/TZVP calculations. They are in Å, Å and cm^{-1} , respectively.....	75
3.7 Dynamic results of the $\text{CF}_3\text{SO}_3\text{H-H}_3\text{O}^+-n\text{H}_2\text{O}$ complexes, $1 \leq n \leq 3$, obtained from BOMD simulations at 350 K. Distances, IR frequencies and proton diffusion coefficients are in Å, cm^{-1} and $\text{cm}^2 \text{s}^{-1}$, respectively.	97

LIST OF FIGURES

Figure	Page
1.1 Primary structure of Nafion [®] , a fluorocarbon backbones (A) and triflic acid group (-CF ₂ SO ₃ H) (B).	2
2.1 Basic steps employed the investigation of elementary reactions and dynamics of proton transfer in H-bond.....	12
2.2 Construction of T-model potentials.	14
2.3 Basic steps in MD simulations of N-particle system.	23
2.4 Definitions of the symmetric and asymmetric O-H stretching modes, as well as the O-O vibration.....	27
3.1 Potential energy profiles for single proton transfer, obtained from various theoretical methods. Interaction energy in kJ/mol and distance in Å. All minima on the potential energy curves were moved to zero for comparisons. a) H ₃ O ⁺ - H ₂ O 1 : 3 complex. b) H ₃ O ⁺ - H ₂ O 1 : 4 complex. c) - e) CF ₃ SO ₃ H - H ₃ O ⁺ - H ₂ O 1 : 1 : 1 complexes..	46
3.2 Examples of characteristic proton transfer profiles for the H ₃ O ⁺ - H ₂ O 1 : 1 complex, with snapshots of H-bond structures obtained in the course of BOMD. a) Large-amplitude vibrations. b) Small-amplitude vibrations. c) Snapshots of H-bond structures.	50

LIST OF FIGURES (Continued)

Figure	Page
3.3 Important elementary reactions in proton transfer in the $\text{H}_3\text{O}^+ - \text{H}_2\text{O}$ complexes obtained from BOMD simulations. The symbols are explained in the text.....	52
3.4 Examples of proton transfer profiles for the $\text{CF}_3\text{SO}_3\text{H} - \text{H}_3\text{O}^+ - \text{H}_2\text{O}$ 1 : 1 : 1 complexes, with snapshots H-bond structures observed in the course of BOMD. a) – b) BOMD starting from structure a in Figure 3.1. c) – d) Snapshots of H-bond structures.....	57
3.5 Important elementary reactions in proton transfer in the $\text{CF}_3\text{SO}_3\text{H} - \text{H}_3\text{O}^+ - \text{H}_2\text{O}$ 1 : 1 : 1 complexes, obtained from BOMD. The symbols are explained in the text.....	60
3.6 Important elementary reactions in proton transfer in the $\text{CF}_3\text{SO}_3\text{H} - \text{H}_3\text{O}^+ - \text{H}_2\text{O}$ 1 : 1 : 2 complexes, obtained from BOMD. The symbols are explained in the text.....	62
3.7 Important elementary reactions in proton transfer in the $\text{CF}_3\text{SO}_3\text{H} - \text{H}_3\text{O}^+ - \text{H}_2\text{O}$ 1 : 1 : 3 complexes, obtained from BOMD. The symbols are explained in the text.....	66

LIST OF FIGURES (Continued)

Figure	Page
<p>3.8 The trends of the interaction (ΔE) and solvation energies (ΔE^{sol}) with respect to the number of water molecules, obtained from B3LYP/TZVP calculations: $-\blacktriangle-$ = ΔE in the gas phase; $-\Delta-$ = ΔE in continuum aqueous solution; $-\blacksquare-$ = ΔE^{sol}</p>	72
<p>3.9 Static results of the $\text{CF}_3\text{SO}_3\text{H}\cdot\text{H}_3\text{O}^+\cdot n\text{H}_2\text{O}$ complexes obtained from B3LYP/TZVP calculations in the gas phase and continuum aqueous solution. a) Plot of Δd_{DA} and $R_{\text{O}\cdots\text{O}}$ for the pass-through mechanism. b) Plot of ν^{OH} and $R_{\text{O}\cdots\text{O}}$ for the pass-through mechanism. c) Plot of ν^{OH} and Δd_{DA} for the pass-through mechanism. d) Plot of Δd_{DA} and $R_{\text{O}\cdots\text{O}}$ for the pass-by mechanism. e) Plot of ν^{OH} and $R_{\text{O}\cdots\text{O}}$ for the pass-by mechanism. f) Plot of ν^{OH} and Δd_{DA} for the pass-by mechanism. (Δd_{DA} = asymmetric stretching coordinate; $R_{\text{O}\cdots\text{O}}$ = O-H...O H-bond distance; ν^{OH} = asymmetric O-H stretching frequency).....</p>	84
<p>3.10 The domains of ν^{OH} for the H-bond protons in Group 1 and 2, as well as Subgroup (I) to (IV). a) gas phase. b) continuum aqueous solution.....</p>	89

LIST OF FIGURES (Continued)

Figure	Page
<p>3.11 BOMD results on the Zundel complex at 350 K. a) – b) IR spectra of the transferring proton in the gas phase and continuum aqueous solution, respectively. c) Plot of $\sigma_{\text{R}_{\text{O-H}}}$ and $\langle \Delta d_{\text{DA}} \rangle$. d) Plot of $\Delta v_{\text{BA}}^{\text{OH,MD}}$ and $\langle \Delta d_{\text{DA}} \rangle$. e) Plot of $\text{P}_{\text{B}}/\text{P}_{\text{A}}$ and $\langle \Delta d_{\text{DA}} \rangle$. $\sigma_{\text{R}_{\text{O-H}}}$ = standard deviations of the O-H distances; $\langle \Delta d_{\text{DA}} \rangle$ = average asymmetric stretching coordinate; $\text{P}_{\text{B}}/\text{P}_{\text{A}}$ = probability of finding the structural diffusion motion relative to the oscillatory shuttling motion (Lao-ngam, Asawakun, Wannarat and Sagarik, 2011).</p>	93
<p>3.12 The BOMD results on the $\text{CF}_3\text{SO}_3\text{H}-\text{H}_3\text{O}^+-n\text{H}_2\text{O}$ complexes at 350 K. a) Plot of $\langle \Delta d_{\text{DA}} \rangle$ and $\langle \text{R}_{\text{O-O}} \rangle$ for the pass-through mechanism. b) Plot of ν^{OH} and $\langle \text{R}_{\text{O-O}} \rangle$ for the pass-through mechanism. c) Plot of ν^{OH} and $\langle \Delta d_{\text{DA}} \rangle$ for the pass-through mechanism. d) Plot of $\langle \Delta d_{\text{DA}} \rangle$ and $\langle \text{R}_{\text{O-O}} \rangle$ for the pass-by mechanism. e) Plot of ν^{OH} and $\langle \text{R}_{\text{O-O}} \rangle$ for the pass-by mechanism. f) Plot of ν^{OH} and $\langle \Delta d_{\text{DA}} \rangle$ for the pass-by mechanism. $\langle \Delta d_{\text{DA}} \rangle$ = average asymmetric stretching coordinate; $\langle \text{R}_{\text{O-O}} \rangle$ = average O-H..O H-bond distance; ν^{OH} = asymmetric O-H stretching frequency</p>	98

LIST OF FIGURES (Continued)

Figure	Page
<p>3.13 BOMD results on the Zundel complex at 350 K. a) – b) IR spectra of the transferring proton in the gas phase and continuum aqueous solution, respectively. c) Plot of $\sigma_{\text{R}_{\text{O-H}}}$ and $\langle \Delta d_{\text{DA}} \rangle$. d) Plot of $\Delta v_{\text{BA}}^{\text{OH,MD}}$ and $\langle \Delta d_{\text{DA}} \rangle$. e) Plot of $\mathbf{P}_{\text{B}}/\mathbf{P}_{\text{A}}$ and $\langle \Delta d_{\text{DA}} \rangle$. $\sigma_{\text{R}_{\text{O-H}}} =$ standard deviations of the O-H distances; $\langle \Delta d_{\text{DA}} \rangle =$ average asymmetric stretching coordinate; $\mathbf{P}_{\text{B}}/\mathbf{P}_{\text{A}} =$ probability of finding the structural diffusion motion relative to the oscillatory shuttling motion ..</p>	113
<p>3.14 Distributions of the diffusion coefficients (D) of the transferring proton in the $\text{CF}_3\text{SO}_3\text{H-H}_3\text{O}^+-n\text{H}_2\text{O}$ complexes, obtained from BOMD simulations at 350 K. a) gas phase. b) continuum aqueous solution.</p>	120

LIST OF ABBREVIATIONS

Å	=	Angström
au	=	Atomic unit
cm ⁻¹	=	Wavenumber
cm ² s ⁻¹	=	Diffusivity
fs	=	Femtosecond
ps	=	Picosecond
K	=	Kelvin
kJ/mol	=	Kilo joule per mole
A-H..B	=	Hydrogen-bond between the proton donor A and acceptor B
Oh..H..Ow	=	Hydrogen-bond between the hydronium ion and water molecule
CF ₃ SO ₃ H	=	Trifluoromethanesulfonic (triflic) acid
CF ₃ SO ₃ ⁻	=	Trifluoromethanesulfonate (triflate) anion
CO ₂	=	Carbon dioxide
H-bond	=	Hydrogen bond
H ₂ O	=	Water
H ₂ SO ₄	=	Sulfuric acid
HCl	=	Hydrochloric acid

LIST OF ABBREVIATIONS (Continued)

H_3O^+	=	Hydronium ion
H_5O_2^+	=	Zundel complex
H_7O_3^+	=	Two shared water complex
H_9O_4^+	=	Eigen complex
$-\text{SO}_3\text{H}$	=	Sulfonic acid group
$-\text{SO}_3^-$	=	Sulfonate anion group
$-\text{SO}_3\text{H}^+$	=	Sulfonic protonated group
1:1:1	=	$\text{CF}_3\text{SO}_3\text{H} - \text{H}_3\text{O}^+ - \text{H}_2\text{O}$ 1 : 1 : 1 complexes
1:1:2	=	$\text{CF}_3\text{SO}_3\text{H} - \text{H}_3\text{O}^+ - \text{H}_2\text{O}$ 1 : 1 : 2 complexes
1:1:3	=	$\text{CF}_3\text{SO}_3\text{H} - \text{H}_3\text{O}^+ - \text{H}_2\text{O}$ 1 : 1 : 3 complexes
I, II, III, IV, V	=	Important elementary reactions in proton transfer profiles
$\text{P}_1, \text{P}_2, \text{P}_3 \dots \text{P}_n$	=	Panels of the proton transfer profiles
$t_1, t_2, t_3 \dots t_n$	=	Time in femtosecond at structure reorganization
$\langle \tau_{\text{H}_5\text{O}_2^+}^{\text{I,A}} \rangle$	=	The average life times of structure A
$\langle \tau_{\text{H}_5\text{O}_2^+}^{\text{I,AB}} \rangle$	=	The average lifetimes of the quasi-dynamic equilibriums of structures A and B
$\langle \tau_{\text{H}_5\text{O}_2^+}^{\text{I,C}} \rangle$	=	The average life times of structure C

LIST OF ABBREVIATIONS (Continued)

$\langle \tau_{\text{H}_5\text{O}_2^+}^{\text{I,BC}} \rangle$	=	The average lifetimes of the quasi-dynamic equilibriums of structures B and C
$\langle \tau_{\text{H}_5\text{O}_2^+}^{\text{I,PT}_{\text{max}}} \rangle$	=	The average maximum proton transfer cycle time
$\langle \tau_{\text{H}_5\text{O}_2^+}^{\text{I,ABC}} \rangle$	=	The average lifetimes of the quasi-dynamic equilibriums of structures A, B and C
$g_{\text{H}_5\text{O}_2^+}^{\text{I}}$	=	The degree of coherence
$P_{\text{H}_5\text{O}_2^+}^{\text{I,forw}}$	=	The probability for proton transfer in the forward direction
I_{A}	=	IR intensity at $\nu_{\text{A}}^{\text{OH,MD}}$
I_{B}	=	IR intensity at $\nu_{\text{B}}^{\text{OH,MD}}$
k	=	Classical first-order rate constant
E_0	=	Ground-state electronic energy
ρ_0	=	Ground-state electron density
τ_{p}	=	Proton hopping time
τ	=	Lifetime of shared-proton complex
ε	=	Relative permittivity or dielectric constant
$\sigma_{\text{R}_{\text{O-H}}}$	=	Standard deviations of the O-H distances
$P_{\text{B}}/P_{\text{A}}$	=	Probability of finding the structural diffusion motion relative to the oscillatory shuttling motion

LIST OF ABBREVIATIONS (Continued)

R_{O-O}	=	O-O distance
R_{O-H}	=	O-H distance
Δd_{DA}	=	Asymmetric stretching coordinate
Δd_{DA}^*	=	Threshold asymmetric stretching coordinate
ν^{OH}	=	Asymmetric O-H stretching frequency
ν^{OH*}	=	Threshold asymmetric O-H stretching frequency
$\nu^{OH,MD}$	=	Characteristic asymmetric O-H stretching frequency from MD simulations
$\nu_A^{OH,MD}$	=	Characteristic asymmetric O-H stretching frequency associated with the oscillatory shuttling motion
$\nu_A^{OH*,MD}$	=	Threshold asymmetric O-H stretching frequency obtained from MD simulations
$\nu_B^{OH,MD}$	=	Characteristic asymmetric O-H stretching frequencies associated with the structural diffusion motion
ΔE	=	Interaction energy
ΔE^{sol}	=	Solvation energy
$\Delta E_{T-Model}$	=	T-Model energy
$\Delta \nu^{OH}$	=	Frequency shifts due to continuum aqueous solvent
$\Delta \nu_{BA}^{OH,MD}$	=	Vibrational energy for the interconversion between the oscillatory shuttling and structural diffusion motions

LIST OF ABBREVIATIONS (Continued)

$\langle \Delta d_{\text{DA}} \rangle$	=	Average asymmetric stretching coordinate
$\langle R_{\text{O-O}} \rangle$	=	Average O-O distance
$\langle R_{\text{O-H}} \rangle$	=	Average O-H distance
B3LYP	=	Becke three-parameters hybrid functional combined with Lee-Yang-Parr correlation function
BO	=	Born-Oppenheimer
BOMD	=	Born-Oppenheimer molecular dynamics
COSMO	=	Conductor-like screening model
CPU	=	Central processing unit
D	=	Diffusion coefficient
DFT	=	Density functional theory
FTIR	=	Fourier transform infrared spectroscopy
HF	=	Hartree-Fock
IR	=	Infrared
MC	=	Monte Carlo
MD	=	Molecular dynamics
MO	=	Molecular orbital
MP2	=	Second-order Møller-Plesset
MPI	=	Message Passing Interface
MSD	=	Mean-square displacement
NMR	=	Nuclear magnetic resonance

LIST OF ABBREVIATIONS (Continued)

NVE	=	Microcanonical ensemble
NVT	=	Canonical ensemble
OPT1	=	Partial geometry optimizations
OPT2	=	Full geometry optimizations
PEM	=	Polymer electrolyte membrane
PFSA	=	Perfluorosulfonic acid
PEMFC	=	Polymer electrolyte membrane fuel cells
PTFE	=	Polytetrafluoroethylene
PT	=	Proton transfer
QM	=	Quantum mechanics
QM/MM	=	Combined quantum mechanical and molecular mechanical calculations
SCF	=	Self-consistent field
SCRf	=	Self-consistent reaction field
T-model	=	Test-particle model
TZVP	=	Triple zeta valence plus polarization
VACF	=	Velocity autocorrelation function

CHAPTER I

INTRODUCTION

An energy crisis and environmental concerns about global warming, as well as the need to reduce CO₂ emissions, have provided strong motivation to seek ways of improving energy conversion technology. Proton exchange membrane fuel cell (PEMFC) has received much attention as one of the most promising energy suppliers for the future world (Koppel, 1999; Larminie and Dicks, 2001; Vincent and Scrosati, 1997). The polymer electrolyte membrane which has been widely used in PEMFC is Nafion[®], introduced by Dupont in 1967 (Kreuer, Paddison, Spohr and Schuster, 2004).

Nafion[®] is a perfluorinated polymer consisting of fluorocarbon backbones (Teflon[®]) and pendant polyether side chains. The side chains of Nafion[®] are terminated by trifluoromethanesulfonic (triflic) acid which is known to be one of the strongest acids in aqueous solutions (Gierke, Munn and Wilson, 1981). Experiments have shown that the triflic acid groups (-CF₂SO₃H) are preferentially hydrated, resulting in large interconnected hydrophilic domains which play important roles in proton transfer reactions (Hinatsu, Mizuhata and Takenaka, 1994). A possible structure of Nafion[®] is shown in Figure 1.1. Due to the extreme difference in the polarity of the fluorocarbon backbones and the sulfonic acid functional groups (-SO₃H), Nafion[®] membrane is quite well separated into hydrophilic and hydrophobic domains. Theoretical and experimental evidences have shown that strong and

extensive hydrogen bond (H-bond) networks in the hydrophilic domains facilitate and mediate proton conduction in Nafion[®]. This implies that PEMFC is not feasible to use at the temperature above 373 K, since the membrane would dry.

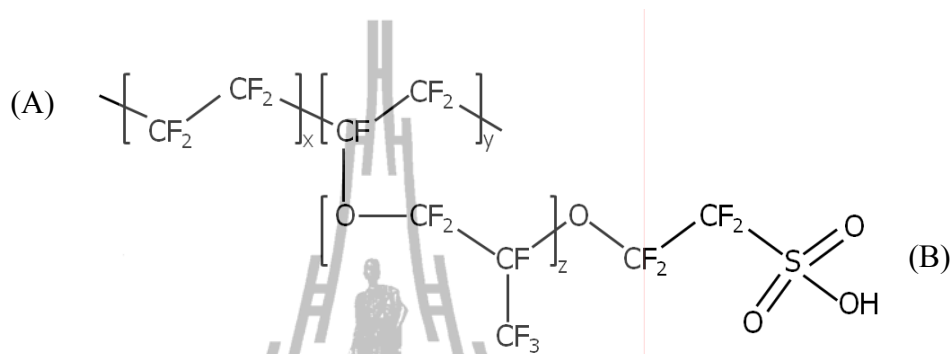


Figure 1.1 Primary structure of Nafion[®], a fluorocarbon backbones (A) and triflic acid group ($-\text{CF}_2\text{SO}_3\text{H}$) (B).

Therefore, a complete understanding of the elementary reactions in proton transfer processes in Nafion[®], especially at low-hydration level, is required for the development and improvement of PEMFC.

Although some basic information has been accumulated in the past decades, mechanisms of proton transfer reactions in Nafion[®], especially at the molecular level, are not well understood (Kreuer, 1996; Kreuer, Paddison, Spohr and Schuster, 2004; Paddison, 2003; Paddison and Zawodzinski, 1998). Some theoretical and experimental results pertinent to the present work will be summarized as follows.

Three basic molecular fragments, potentially involved in proton transfer reactions at the hydrophilic side chains in Nafion[®] are $-(\text{CF}_2\text{OCF}_2)-$, $-\text{CF}_2\text{SO}_3\text{H}$ and $-\text{CF}_2\text{SO}_3^-$. density functional theory (DFT) at B3LYP/6-31G(d,p) level (Paddison, Pratt and Zawodzinski, 1999; Paddison and Zawodzinski, 1998) suggested that, the H-bond between CF_3OCF_3 and H_2O is rather weak, due to the strong electron withdrawing effects from the two CF_3 groups. Therefore, $-(\text{CF}_2\text{OCF}_2)-$ might not be directly involved in proton transfer reactions in Nafion[®], which is in accordance with IR experiment (Laporta, Pegoraro and Zanderighi, 1999) and molecular dynamic (MD) simulations (Buzzoni, Bordiga, Ricchiardi, Spoto and Zecchina, 1995; Paddison, Bender, Kreuer, Nicoloso and Zawodzinski, 2000; Zecchina *et al.*, 1996). Experimental evidence has shown that, when sufficiently hydrated, the $-\text{CF}_2\text{SO}_3\text{H}$ groups in Nafion[®] are highly dissociated (Buzzoni, Bordiga, Ricchiardi, Spoto and Zecchina, 1995; Zecchina *et al.*, 1996). Spectroscopic measurements, in which the assignment and comparison of IR and Raman spectra of individual species in Nafion[®] were made, revealed that $-\text{CF}_2\text{SO}_3\text{H}$ could be completely dissociated depending upon experimental conditions. Dielectric spectroscopy (Paddison, Bender, Kreuer, Nicoloso and Zawodzinski, 2000) also showed a strong dependence of the dielectric constant and the specific conductivity of Nafion[®] with water content. Whereas ^{19}F NMR experiment (Boyle, McBrierty and Eisenberg, 1983) indicated that, there is a range of temperature over which the $-\text{CF}_2\text{SO}_3\text{H}$ groups in Nafion[®] go from being fully dissociated to being fully associated upon cooling.

Attempts have been made to probe the acidity of $\text{CF}_3\text{SO}_3\text{H}$, as well as to determine the transition state of ion-pair complex formed from CF_3SO_3^- and H_3O^+ in the gas phase (Paddison, Pratt, Zawodzinski and Reagor, 1998). It was reported that, with the inclusion of electrostatic free energy, the activation energy for the deprotonation of $\text{CF}_3\text{SO}_3\text{H}$ amounts to 19.6 kJ/mol, implying that the ion-pair complex are not stable in the gas phase and some water molecules are required to stabilize both CF_3SO_3^- and H_3O^+ . Mechanisms of proton dissociation from $\text{CF}_3\text{SO}_3\text{H}$ were examined by Paddison *et al.* (Paddison, 2001; Paddison, Pratt and Zawodzinski, 2001), by performing a series of B3LYP/6-31G(d,p) calculations on the $\text{CF}_3\text{SO}_3\text{H} - (\text{H}_2\text{O})_n$ complexes, $1 \leq n \leq 6$. Paddison *et al.* reported that, no proton dissociation was observed until three water molecules were included, and H_3O^+ could be stabilized through the formation of H-bonds with two water molecules and one oxygen atom of CF_3SO_3^- . This H-bond complex could represent one of the precursors for proton dissociation from $-\text{CF}_2\text{SO}_3\text{H}$. Interesting results were obtained when up to five water molecules were added, with H_3O^+ located progressively further away from CF_3SO_3^- , and when six water molecules were added, a complete separation of H_3O^+ from CF_3SO_3^- was observed. The results (Paddison, 2001; Paddison, Pratt and Zawodzinski, 2001) suggested a possible scenario for proton dissociation and showed how H_3O^+ moves away from CF_3SO_3^- .

Proton transfer reactions in minimally hydrated PEM were studied by molecular dynamic (MD) simulations on triflic acid monohydrate solid

$((\text{CF}_3\text{SO}_3\text{H}_3\text{O}^+)_4)$ (Eikerling, Paddison, Pratt and Zawodzinski, 2003). The MD results showed a relay-type mechanism, with a proton defect representing an intermediate state in the proton transfer pathway. The proton defect involves formation of the Zundel complex (H_5O_2^+) and the reorganization of the neighboring $-\text{SO}_3^-$ groups which share a proton between the oxygen atoms of the anionic sites. The proposed mechanism revealed a possibility of proton transfer along the hydrophilic groups, $-\text{SO}_3\text{H}$ and $-\text{SO}_3^-$.

A similar theoretical study was reported on short-side-chain perfluorosulfonic acids, in which large scale DFT calculations were conducted on fragments of Nafion[®], with and without water molecules and with distinct pendant chain separations (Paddison and Elliott, 2005; Paddison and Elliott, 2006; Paddison, Kreuer and Maier, 2006). B3LYP/6-311G(d,p) calculations revealed a possibility for proton transfer between two adjacent hydrophilic groups, along the H-bond networks of water connecting them. The proposed proton transfer pathway is mediated by formation of the $-\text{S}-\text{O} \cdots \text{H}^+ \cdots \text{O}-\text{H}$ H-bond and H_5O_2^+ (Paddison and Elliott, 2005). It was concluded that, the number of water molecules required to promote proton dissociation could be reduced when the $-\text{SO}_3\text{H}$ groups are brought closer to each other, through conformational changes in the backbone (Paddison and Elliott, 2006; Paddison, Kreuer and Maier, 2006).

The number of water molecules required to promote proton dissociation at the $-\text{SO}_3\text{H}$ group was investigated, using the H-bond complexes formed from

$\text{CF}_3\text{CF}_2\text{SO}_3\text{H}$ and $n\text{H}_2\text{O}$, $1 \leq n \leq 4$ (Glezakou, Dupuis and Mundy, 2007). Quantum chemical calculations and MD simulations revealed that, the neutral and ion-pair complexes for $n = 3$ are close in energy and are accessible in the fluctuation dynamics of proton transport. Whereas for $n \leq 2$, the only relevant complex is the neutral form. Most importantly, it was concluded based on the free energy surfaces of proton exchange that the $\text{CF}_3\text{CF}_2\text{SO}_3\text{H}_2^+ - \text{H}_2\text{O}$ and $\text{CF}_3\text{CF}_2\text{SO}_3\text{H} - \text{H}_3\text{O}^+$ complexes are nearly isoenergetic and $\text{CF}_3\text{CF}_2\text{SO}_3\text{H}_2^+$ could play important roles in proton transfer reactions at low hydration levels (Glezakou, Dupuis and Mundy, 2007).

Since one of the most important evidence of the H-bond formation in aqueous solution is the red shift of the high-frequency hydroxyl (O-H) stretching mode, accompanied by its intensity increase and band broadening (Asbury, Steinel and Fayer, 2004; Jiang, Chaudhuri, Lee and Chang, 2002; Wu, Chaudhuri, Jiang, Lee and H.C. Chang, 2004), attempt was made to correlate the O-H stretching frequency with the tendency of proton transfer in H-bonds (Buzzoni, Bordiga, Ricchiardi, Spoto and Zecchina, 1995; Iftimie, Thomas, Plessis, Marchand and Ayotte, 2008; Wu, Chaudhuri, Jiang, Lee and Chang, 2004). The broad and intense IR absorption bands ranging from 1000 to 3000 cm^{-1} were interpreted as spectral signatures of protonated water networks (Iftimie, Thomas, Plessis, Marchand and Ayotte, 2008), whereas the tendency of proton transfer was measured from strong red shift of the asymmetric O-H stretching frequency (ν^{OH}), compared with the corresponding “free” or “non-H-bonded” one (Wu, Chaudhuri, Jiang, Lee and Chang, 2004). The red shift cannot be determined easily in experiment due to the coupling and overlapping of various

vibrational modes, as well as the detection limit of IR equipment (Okumura, Yeh, Myers and Lee, 1990; Termath and Sauer, 1977; Wu, Jiang, Boo, Lin, Lee and Chang, 2000). Analyses of IR and Raman spectra of pure and concentrated solutions ($\text{H}_2\text{O}/\text{H}^+ = 3 - 4$) of H_2SO_4 , HCl and $\text{CF}_3\text{SO}_3\text{H}$ (Buzzoni, Bordiga, Ricchiardi, Spoto and Zecchina, 1995) and FTIR study of water in cast Nafion[®] films (Ludvigsson, Lindgren and Tegenfeld, 2000) revealed that the fingerprint of proton transfer from the undissociated $\text{CF}_3\text{SO}_3\text{H}$ to water at 1040 cm^{-1} could be masked by the strong C-F stretching bands at $1200 - 1300\text{ cm}^{-1}$, as well as the stretching bands in the $-\text{SO}_3\text{H}$ group at 910 and 1410 cm^{-1} . It was suggested that the classical interpretations of IR frequencies for concentrated acid solutions could be employed as criteria to roughly estimate the tendency of proton transfer (Pimentel and McClellan, 1960); the stretching frequencies for the H-bond proton are divided into three groups namely, the internal ($1300 - 2200\text{ cm}^{-1}$), external ($2500 - 3200\text{ cm}^{-1}$) and outerlayer groups ($3300 - 3400\text{ cm}^{-1}$). The H-bond proton in the internal group is considered to be susceptible to proton transfer.

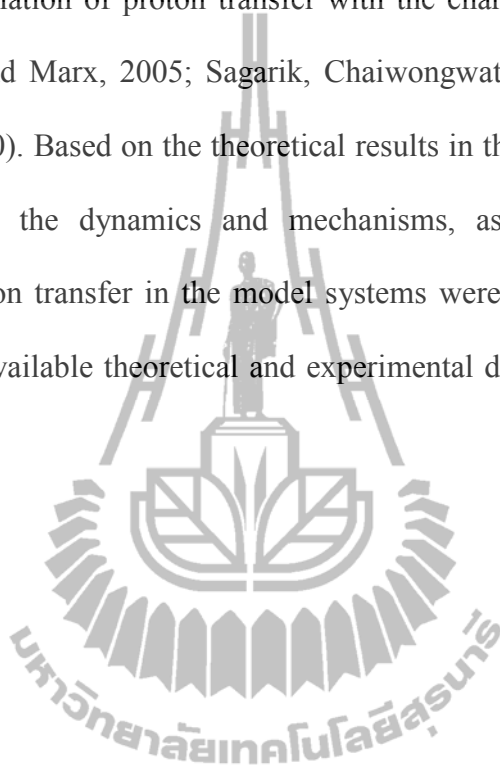
Characteristic IR frequencies of proton transfer in protonated water clusters were investigated using theoretical methods (Lao-ngam, Asawakun, Wannarat and Sagarik, 2011). DFT calculations revealed that the intermediate states in proton transfer pathways consist of the Zundel complex, with the threshold asymmetric O-H stretching frequencies (ν^{OH^*}) in the gas phase and aqueous solution at $\nu^{\text{OH}^*} = 1984$ and 1881 cm^{-1} , respectively. Born-Oppenheimer MD (BOMD) simulations predicted slightly lower threshold frequencies, $\nu^{\text{OH}^*,\text{MD}} = 1917$ and 1736 cm^{-1} , respectively, with two characteristic asymmetric O-H stretching frequencies ($\nu^{\text{OH},\text{MD}}$) being the IR

spectral signatures of proton transfer. The lower-frequency band (at $\nu_{\text{A}}^{\text{OH,MD}}$) could be associated with the “oscillatory shuttling motion”, whereas the higher-frequency band (at $\nu_{\text{B}}^{\text{OH,MD}}$) with the “structural diffusion motion” (Lao-ngam, Asawakun, Wannarat and Sagarik, 2011).

Although some important structural and dynamic results on the proton transfer reactions at the $-\text{SO}_3\text{H}$ group of Nafion[®] have been reported, several fundamental questions have to be answered, before the studies in condensed phases can be proceeded, as examples; (1) how to effectively monitor proton transfer reactions in condensed phases, both in theories and experiments; (2) according to IR spectral analyses (Lao-ngam, Asawakun, Wannarat and Sagarik, 2011; Sagarik, Chaiwongwattana, Vchirawongkwin and Prueksaaron, 2010), what are the characteristic and threshold frequencies of proton transfers in Nafion[®]; (3) what are the basic intermediate states in the proton transfer pathways and how to estimate the activation energies of proton transfers at and in the vicinities of the $-\text{SO}_3\text{H}$ group; (4) how the proton transfer reactions can be facilitated or mediated by the $-\text{SO}_3\text{H}$ group *etc.* The answers to these questions are important since they could be used as guidelines for the studies in condensed phases and IR experiments.

In order to answer these questions, proton transfer reactions at the $-\text{SO}_3\text{H}$ group of Nafion[®] were investigated in the present study, using the complexes formed from $\text{CF}_3\text{SO}_3\text{H}$, H_3O^+ and $n\text{H}_2\text{O}$, $1 \leq n \leq 3$, as model systems. The present work was divided into two parts. The first part (Part I) emphasized on how $-\text{CF}_2\text{SO}_3\text{H}$ facilitates or mediates transportation of an excess proton. Special attention was on

precursors and transition states, as well as dynamics in elementary reactions. In the second part (Part II), since the dynamics of proton transfer can be characterized by vibrational behavior of the transferring proton, attempt was made to correlate the tendency and population of proton transfer with the characteristic IR frequencies in H-bond (Benoit and Marx, 2005; Sagarik, Chaiwongwattana, Vchirawongkwin and Prueksaaron, 2010). Based on the theoretical results in the gas phase and continuum aqueous solutions, the dynamics and mechanisms, as well as the IR spectral signatures, of proton transfer in the model systems were analyzed and discussed in comparison with available theoretical and experimental data of the same and similar systems.



CHAPTER II

COMPUTATIONAL METHODOLOGY

Since mechanisms of proton conduction in Nafion[®] are complicated, care must be exercised in selecting model molecules and theoretical methods. Previous experience on strong H-bond clusters (Deeying and Sagarik, 2007; Sagarik, Chaiwongwattana and Sisot, 2004; Sagarik and Chaiyapongs, 2005; Sagarik and Dokmaisrijan, 2005; Sagarik and Rode, 2000) showed that, some structural and energetic information in the gas phase could provide bases for the discussion in aqueous solutions. Therefore, it was the strategy of the present work to explore proton transfer reactions at low hydration levels. Due to the fact that, superacid characters of Nafion[®] are localized at $-\text{CF}_2\text{SO}_3\text{H}$, the present study concentrated only on reactions among $-\text{CF}_3\text{SO}_3\text{H}$, H_3O^+ and $n\text{H}_2\text{O}$, using the complexes formed from $-\text{CF}_3\text{SO}_3\text{H}$, H_3O^+ and $n\text{H}_2\text{O}$ as model systems. For hydration of a single proton, according to experimental and theoretical investigations (Botti, Bruni, Imberti, Ricci and Soper, 2005; Hermida-Ramón and Karlström, 2004), there are at least three important H-bond structures involved in proton transfer reactions namely, H_3O^+ , H_5O_2^+ and the Eigen complex (H_9O_4^+). Based on neutron diffraction experiment, with hydrogen isotope substitutions and Monte Carlo (MC) simulations (Botti, Bruni, Imberti, Ricci and Soper, 2005), the first hydration shell of H_3O^+ consists of four water molecules and only three of them strongly H-bond to the hydrogen atoms of H_3O^+ . *Ab initio*

calculations (Newton, 1978) showed that the fourth water molecule, initially attached to the oxygen atom of H_3O^+ , eventually moves away to the second hydration shell. These findings and the fact that the size of the model systems must be reasonable and manageable by available computer resources, the $\text{CF}_3\text{SO}_3\text{H} - \text{H}_3\text{O}^+ - \text{H}_2\text{O}$ 1 : 1 : n complexes, $1 \leq n \leq 3$, were adopted in the theoretical investigations. It should be added that, previous theoretical investigations considered $-\text{CF}_2\text{SO}_3\text{H}$ as a primary source of proton, from which H_3O^+ and $-\text{CF}_2\text{SO}_3^-$ are generated. Therefore, proton transfer reactions among $-\text{CF}_3\text{SO}_3\text{H}$, H_3O^+ and $n\text{H}_2\text{O}$ have not been emphasized.

Literature survey showed that reactions and dynamics of proton transfer processes can be studied reasonably well using small model systems and the following three basic steps; (1) searching for all important equilibrium structures and intermediate states in the proton transfer pathways using the Test-particle model (T-model) potentials (Sagarik, 1999; Sagarik and Asawakun, 1997; Sagarik, Chaiwongwattana and Sisot, 2004; Sagarik and Chaiyapongs, 2005; Sagarik and Dokmaisrijan, 2005; Sagarik and Rode, 2000; Sagarik and Spohr, 1995; Sagarik and Ahlrichs, 1987; Sagarik, Pongpituk, Chaiyapongs and Sisot, 1991); (2) refining of the computed structures using the DFT method; (3) BOMD simulations starting from the refined structures. The three basic steps were adopted in the present investigations and summarized in Figure 2.1.

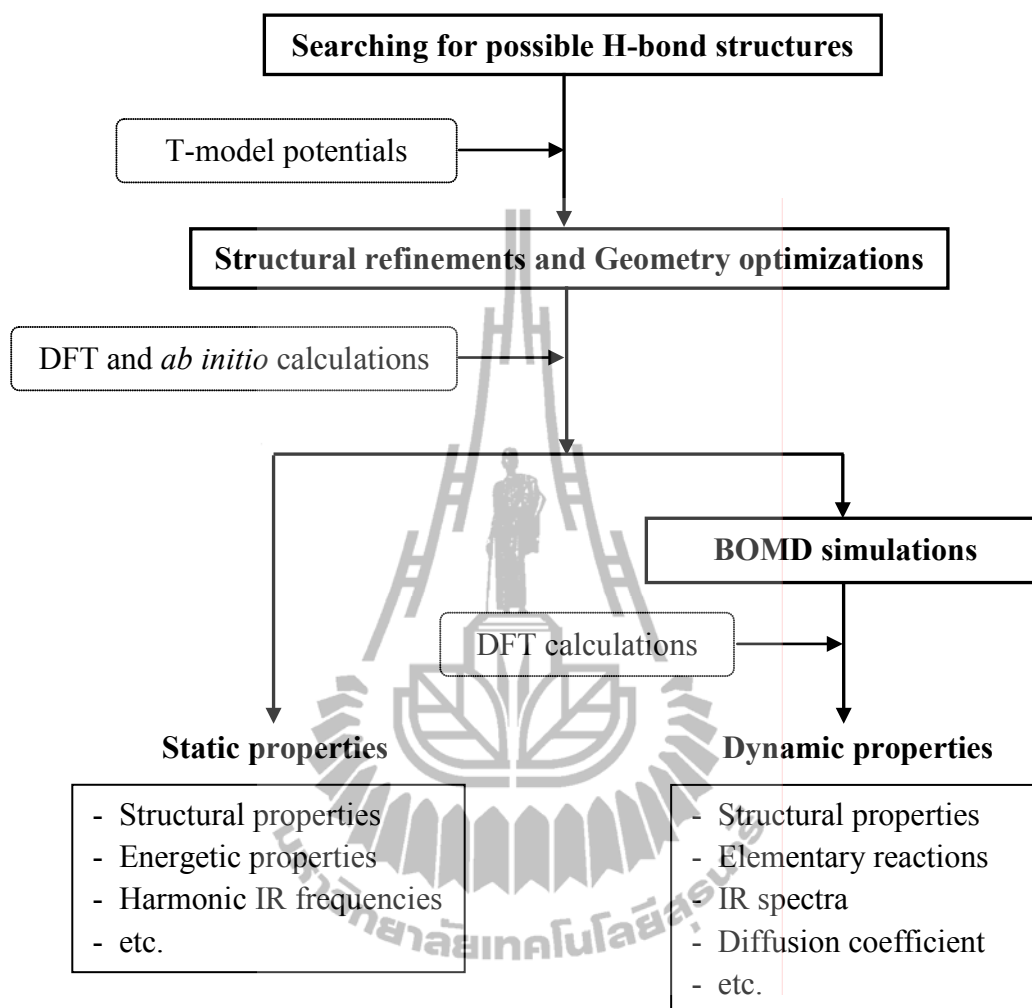


Figure 2.1 Basic steps employed the investigation of elementary reactions and dynamics of proton transfer in H-bond.

2.1 The T-model potentials

Since proton transfer reactions have been pointed out to be sensitive to the structures and dynamics in H-bond (Schmitt and Voth, 1999), all important H-bond structures in the model systems had to be identified, characterized and analyzed. Attention was focused on the H-bond structures, which could be precursors or

transition states in the proton transfer pathways. In order to effectively and systematically scan the potential energy surfaces, the T-model potentials were constructed and employed in the calculations of the equilibrium structures of the $\text{H}_3\text{O}^+ - \text{H}_2\text{O}$ and $\text{CF}_3\text{SO}_3\text{H} - \text{H}_3\text{O}^+ - n\text{H}_2\text{O}$ complexes, $1 \leq n \leq 3$. Since the T-model had been already discussed in details (Sagarik, 1999; Sagarik and Asawakun, 1997; Sagarik, Chaiwongwattana, and Sisot, 2004; Sagarik and Chaiyapongs, 2005; Sagarik and Rode, 2000; Sagarik and Spohr, 1995; Sagarik and Ahlrichs, 1987; Sagarik, Pongpituk, Chaiyapongs, and Sisot, 1991). Only some important aspects relevant to the geometry optimizations will be briefly summarized, using the Eigen complex as an example.

Experimental geometries (Giguere, 1979) of H_3O^+ and H_2O were kept constant in the T-model geometry optimizations. For the Eigen complex, a rigid H_3O^+ was placed at the origin of the Cartesian coordinate system. The coordinates of H_2O molecules were randomly generated in the vicinities of H_3O^+ . Based on the T-model potentials, equilibrium structures of the Eigen complex were searched using a minimization technique. For each H-bond complex, fifty configurations were generated randomly and employed as starting configurations in the T-model geometry optimizations. Similar methods were applied on the $\text{CF}_3\text{SO}_3\text{H} - \text{H}_3\text{O}^+ - n\text{H}_2\text{O}$ complexes, in which $\text{CF}_3\text{SO}_3\text{H}$ was placed at the origin of the Cartesian coordinate system, and the positions and orientations of H_3O^+ and $n\text{H}_2\text{O}$ were randomly assigned in its vicinities. For each H-bond complex, one hundred starting configurations were generated and employed as starting configurations in the T-model

geometry optimizations. The construction of the T-model potential is shown schematically in Figure 2.2.

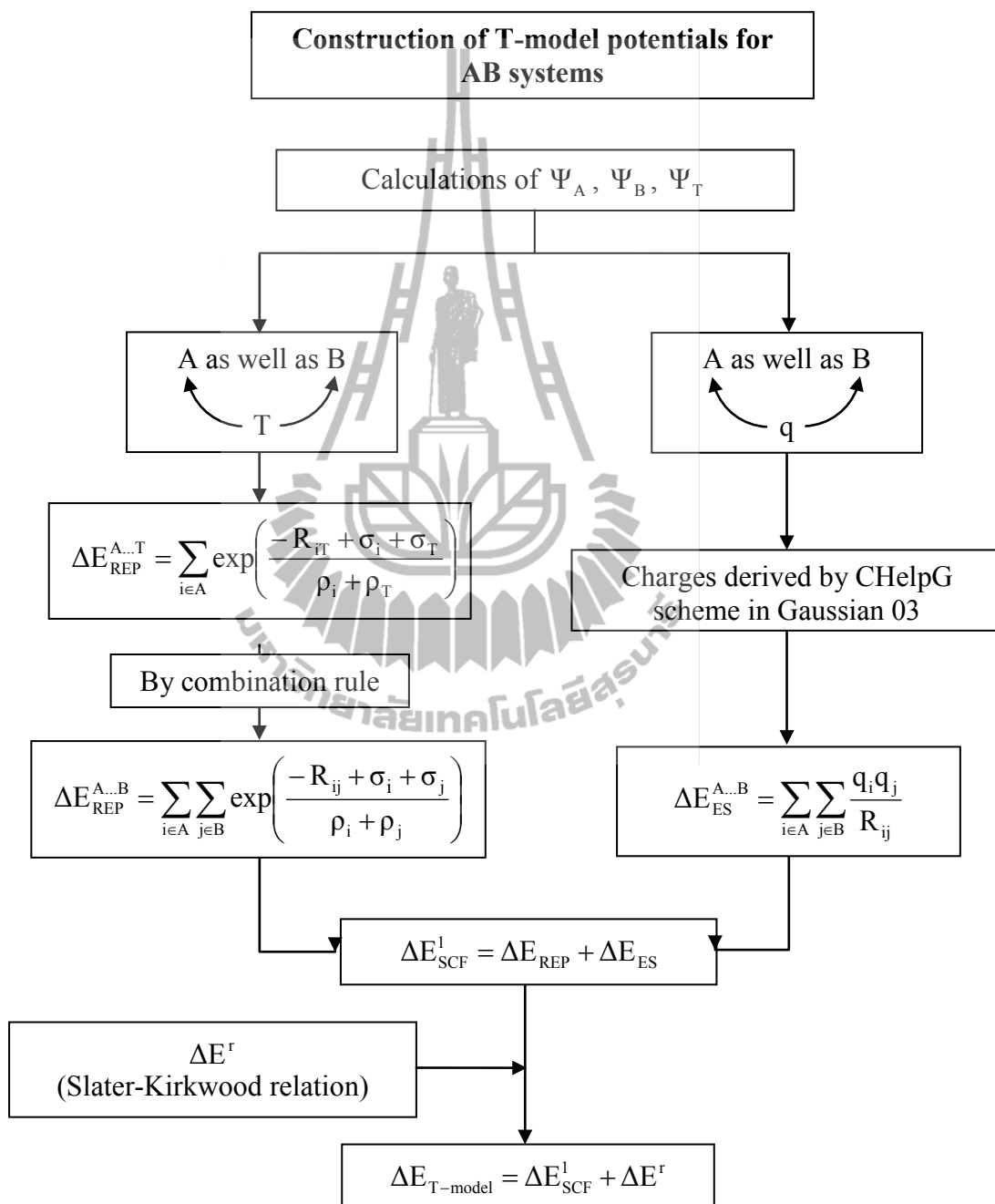


Figure 2.2 Construction of T-model potential (Deeying, 2005).

2.2 Geometry refinement

Part I: B3LYP/6-31G(d,p) calculations

Since the T-model potentials are based on rigid molecules, in which cooperative effects are neglected, further structural refinements had to be made using appropriate quantum chemical methods. As it is known in general that, sophisticated theoretical methods require more computer resources, and especially in the present case, MD simulations with thousands of time steps must be performed, it was necessary to compromise between the accuracy of theoretical methods and available computer resources. Literature survey showed that the DFT methods have been frequently chosen due to the ability to treat molecules of relatively large sizes with reasonable degree of accuracies, compared to other nonempirical methods. Especially for similar H-bond systems (Paddison, 2001; Paddison, 2003; Paddison and Elliott, 2005; Paddison, Pratt and Zawodzinski Jr., 1999; Paddison, Pratt and Zawodzinski, 2001; Paddison and Zawodzinski Jr, 1998), the DFT method at B3LYP/6-31G(d,p) level represents one of the most popular choice. Therefore, it was adopted as a primary candidate in the refinements of the T-model results. It should be noted that, although the DFT methods have been frequently chosen due to their ability to predict the effects of electron correlations with reasonable degree of accuracy and computational efforts, the performance of the DFT methods can be poor or fairly good, depending upon the chemical systems considered; the DFT methods tend to underestimate the interaction energies in van der Waals systems. Outstanding examples are the T-shaped and parallel-displaced (PD) structures of the phenol-benzene complex, from which the interplay between the electrostatic and dispersion interactions has been frequently studied (Kwac, Lee, Jung and Han, 2006); the

stability of the former is determined by the electrostatic interactions, whereas the latter by the dispersion interactions. B3LYP/6-311++G(d,p) calculations predicted that the PD structure is unstable, with a positive interaction energy (ΔE), whereas ΔE of the T-shaped structure (with the O-H... π H-bond) is -8.4 kJ/mol. This is considerably higher than the experimental value of -16.7 kJ/mol (ΔE of the cresol-benzene complex obtained from the picosecond photofragment spectroscopy) (Knee, Knundkar and Zewail, 1985). In Part I, a systematic comparison among B3LYP/6-31G(d,p), HF/6-311++G(d,p) and MP2/6-311++G(d,p) were conducted. The results on strong H-bond systems (Sagarik, 1999; Sagarik and Chaiyapongs, 2005; Sagarik and Rode, 2000) suggested that, *ab initio* calculations at MP2/6-311++G(d,p) or MP2/6-311++G(2d,2p) level could serve as benchmarks in this case.

The absolute and some local minimum energy geometries of the H-bond complexes, predicted from the T-model potentials, were employed as starting configurations in the DFT and *ab initio* geometry optimizations. Both partial and full geometry optimizations were performed, using the Berny algorithm included in Gaussian 03 (Frisch *et al.*, 2005). In partial geometry optimizations, monomer geometries were kept constant and only the intermolecular geometrical parameters were optimized. The purpose of the partial geometry optimizations was to verify the T-model optimized geometries, whereas the full geometry optimizations were aimed at structural refinements. In the present study, the partial and full geometry optimizations were denoted by OPT1 and OPT2, respectively.

Since the forces in MD simulations are computed from energy gradients, which are determined by structures of potential energy surface, and in order to compare the performance among candidate theoretical methods, potential energy profiles for single proton transfer event were constructed for selected H-bond complexes, using both DFT and *ab initio* calculations; by moving proton within a fixed H-bond distance. In this case, B3LYP/6-31G(d,p), HF/6-311++G(d,p) and MP2/6-311++G(d,p) calculations were employed in the calculations of the potential energy profiles. For the DFT method, additional calculations at B3LYP/6-31+G(d,p) level were made to examine the effects of diffuse functions.

It turned out that the size and shape of the potential energy surfaces for proton transfers in small protonated water clusters and the $\text{CF}_3\text{SO}_3\text{H}-\text{H}_3\text{O}^+-\text{H}_2\text{O}$ 1 : 1 : 1 complexes, obtained from B3LYP/6-31G(d,p) and MP2/6-311++G(d,p) calculations, were quite similar, whereas HF/6-311++G(d,p) calculations yielded different results; minima were observed at shorter distances and a double-well potential appeared for the cyclic H-bonds in the protonated water cluster. Since the forces in BOMD simulations are computed from energy gradients, which are determined by the structures of potential energy surfaces, the DFT method with the B3LYP functional was adopted in all successive studies. The choice is justified by BOMD simulations on similar systems, in which spectroscopic and dynamic results are compared well with experiments (Termath and Sauer, 1997).

Part II: B3LYP/TZVP calculations

As the electric field introduced by polar solvent can determine the potential energy surface, on which the transferring proton moves, a continuum model must be included in the model calculations. To account for the effects of the extended H-bond networks of water, a conductor-like screening model (COSMO), with the dielectric constant (ϵ) of 78, was employed in Part II. COSMO is a continuum solvent model (Ahlrichs, Bär, Häser, Horn and Kölmel, 1989; Treutler and Ahlrichs, 1995) in which solute molecule forms a cavity within a dielectric continuum solvent. The charge distribution of the solute molecule polarizes the dielectric solvent and the response of the solvent is described by the generation of screening charges on the cavity surface computed from atomic radii. Since the screening charges are updated in every cycle and the potential generated by these charges is included into the Hamiltonian, the variational principle is applied on both the molecular orbitals and the screening charges, allowing the gradients to be computed in the presence of the continuum fields of solvent. The continuum fields are therefore varied in the course of BOMD simulations. Since the surrounding solvent medium does not have explicit solvent molecules, our BOMD simulations do not require periodic boundary conditions.

The equilibrium structures of the H-bond complexes formed from $\text{CF}_3\text{SO}_3\text{H}$, H_3O^+ and $n\text{H}_2\text{O}$ obtained from the T-model potentials, were reoptimized using the DFT method, both in the gas phase and continuum aqueous solutions. In order to obtain reliable spectroscopic results, a tight SCF energy convergence criterion (less than 10^{-8} au), with the maximum norm of Cartesian gradients less than 10^{-4} au, was adopted in the DFT geometry optimizations. DFT calculations were performed using

the B3LYP hybrid functional (Becke, 1993; Lee, Yang and Parr, 1988), with the triple-zeta valence basis sets augmented by polarization functions (TZVP) (Schaefer, Huber and Ahlrichs, 1994). The performance of B3LYP calculations and the TZVP basis sets on similar systems was discussed in details (Santambrogio, Bruemmer, Woeste, Doeblner, Sierka, Sauer, Meijer and Asmis, 2008; Termath and Sauer, 1997). In the present work, B3LYP/TZVP calculations were performed using TURBOMOLE 6.0 software package (Ahlrichs, Bär, Häser, Horn and Kölmel, 1989; Treutler and Ahlrichs, 1995).

The interaction energies (ΔE) of the H-bond complexes (Lao-ngam, Asawakun, Wannarat and Sagarik, 2011), were computed as

$$\Delta E = E(\text{CF}_3\text{SO}_3\text{H} - \text{H}_3\text{O}^+ - n\text{H}_2\text{O}) - [E(\text{CF}_3\text{SO}_3\text{H}) + E(\text{H}_3\text{O}^+) + nE(\text{H}_2\text{O})] \quad (2.1)$$

where $E(\text{CF}_3\text{SO}_3\text{H} - \text{H}_3\text{O}^+ - n\text{H}_2\text{O})$ are the total energies of the H-bond complexes; $E(\text{CF}_3\text{SO}_3\text{H})$, $E(\text{H}_3\text{O}^+)$ and $E(\text{H}_2\text{O})$ the total energies of the isolated molecules at their optimized structures. The energetic effects of the continuum aqueous solvent (COSMO with $\varepsilon = 78$) were estimated from the solvation energy (ΔE^{sol})

$$\Delta E^{\text{sol}} = E(\text{CF}_3\text{SO}_3\text{H} - \text{H}_3\text{O}^+ - n\text{H}_2\text{O})^{\text{COSMO}} - E(\text{CF}_3\text{SO}_3\text{H} - \text{H}_3\text{O}^+ - n\text{H}_2\text{O}) \quad (2.2)$$

where $E(\text{CF}_3\text{SO}_3\text{H} - \text{H}_3\text{O}^+ - n\text{H}_2\text{O})^{\text{COSMO}}$ and $E(\text{CF}_3\text{SO}_3\text{H} - \text{H}_3\text{O}^+ - n\text{H}_2\text{O})$ are the total energies of the H-bond complexes, obtained from B3LYP/TZVP calculations with and without COSMO, respectively.

Characteristics of proton transfer in H-bond

In order to discuss the tendency of proton transfer through the structural diffusion mechanism, the asymmetric stretching coordinate (Δd_{DA}) (Benoit and Marx, 2005; Sagarik, Chaiwongwattana, Vchirawongkwin and Prueksaaron, 2010) and a concept of the “most active” H-bond were used (Marx, Tuckerman, Hutter and Parrinello, 1999). The H-bond susceptible to proton transfer can be alternatively characterized by low to nonexistence energy barrier along the proton transfer coordinate. This is manifested by a broad IR band with the asymmetric O-H stretching frequency (ν^{OH}) lower than a threshold frequency (ν^{OH*}) (Lao-ngam, Asawakun, Wannarat and Sagarik, 2011). In the present work, based on the well-optimized H-bond structures, harmonic IR frequencies were derived from numerical second derivatives, from which analyses of normal modes in terms of internal coordinates were made. NUMFORCE and AOFORCE programs, included in TURBOMOLE 6.0 software package (Ahlrichs, Bär, Häser, Horn and Kölmel, 1989; Treutler and Ahlrichs, 1995), were employed in the calculations of the second derivatives and the normal mode analyses, respectively. Since the vibrational frequencies obtained from quantum chemical calculations are generally overestimated compared to experiments, a scaling factor, which partially accounts for the anharmonicities and systematic errors, had to be applied; a scaling factor of 0.9614 (Scott and Radom, 1996) was shown to be appropriate for B3LYP/TZVP calculations (Lao-ngam, Asawakun, Wannarat and Sagarik, 2011; Sagarik, Chaiwongwattana, Vchirawongkwin and Prueksaaron, 2010). In order to quantitatively discuss the tendency of proton transfer in H-bond, ν^{OH} were plotted as a function of R_{O-O} and ν^{OH*} were determined from the plot of ν^{OH} and Δd_{DA} (Lao-ngam, Asawakun, Wannarat and Sagarik, 2011).

2.3 Born-Oppenheimer MD simulations

Dynamics of rapid covalent and H-bond formations and cleavages could be studied reasonably well using quantum MD simulations (Balbuena and Seminario, 1999), among which BOMD simulations have been widely used in recent years (Cramer, 2002; Young, 2001).

In the present work, the precursors and transition states in the proton transfer processes at $-\text{CF}_2\text{SO}_3\text{H}$ were studied using Born-Oppenheimer MD (BOMD) simulations (Barnett and Landman, 1993; Jing, Troullier, Dean, Binggeli, Chelikowsky, Wu and Saad, 1994). Within the framework of BOMD simulations, classical equations of motions of nuclei on the Born-Oppenheimer surfaces are integrated, whereas forces on nuclei are calculated in each MD step from quantum energy gradients, with the molecular orbitals (MO) updated by solving Schrodinger equations in the Born-Oppenheimer approximation. This makes BOMD simulations more accurate, as well as considerably CPU time consuming, compared to conventional classical MD simulations, in which forces on nuclei are determined from predefined empirical or quantum pair potentials. It should be noted that the high mobility of excess proton was initially attributed to QM tunneling (Leach, 1996). This has been challenged, for examples, by the results obtained from *ab initio* BOMD simulations (Schmitt and Voth, 1999) and conductivity measurements (Conway, Bockris and Linton, 1956), which showed that proton transfer reaction mechanisms could be explained reasonably well without assuming the proton tunneling to be the important pathways. The basics steps in MD simulations are illustrated in Figure 2.3.

Part I: NVE BOMD simulations

Since proton conduction, especially in aqueous solutions, involves dynamic processes with different timescales (Agmon, 1995; Giguere, 1979; Kreuer, 2000), the complexity of proton transfer reactions could be reduced using various approaches. The observation that the actual proton transfer occurs in femtosecond (fs) timescale (Giguere, 1979), which is in general faster than solvent reorganization (Agmon, 1995), made it reasonable to perform BOMD simulations by focusing only on short-lived phenomena, which take place before or after major H-bond structure reorganizations. To ensure that all important dynamics was taken into account, several BOMD trajectories were generated at 298 K, starting from the equilibrium structures of the $\text{H}_3\text{O}^+ - \text{H}_2\text{O}$ and $\text{CF}_3\text{SO}_3\text{H} - \text{H}_3\text{O}^+ - \text{H}_2\text{O}$ complexes computed in the previous sections. Since in aqueous solutions, rapid interconversion between the Zundel and Eigen complexes happens within about 100 fs (10^{-13} s) (Kreuer, 2000), the timestep used in solving dynamic equations was set to 0.5 fs. In each BOMD simulations, 500 fs was spent on equilibration, after which 2000 fs was devoted to property calculations.

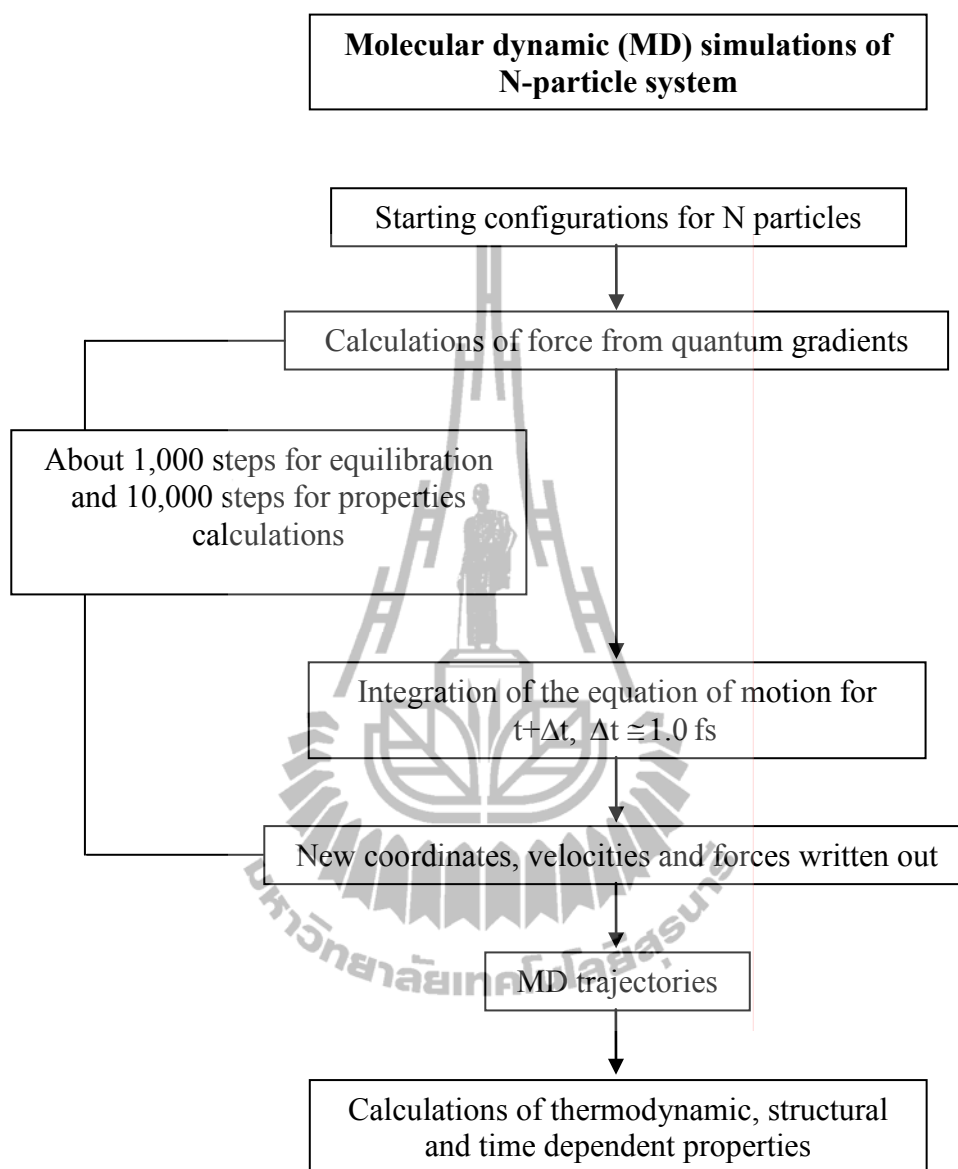


Figure 2.3 MD simulations of N-particle system (Deeying, 2005).

Proton transfer profiles

Since correlation exists between proton conductivity and H-bond structure (Kreuer, 2000), Jmol was employed to visualize molecular motions in the course of BOMD simulations. In addition, BOMD trajectories were analyzed in details by monitoring fluctuations and changes in the H-bond structures; some characteristic H-bond distances were plotted with MD simulation time. For example, the Oh..Ow, Ow-Hw and Oh-Hh distances were plotted with MD simulation time to study the dynamics in the Zundel and Eigen complexes; h = hydronium ion and w = water. The plots were regarded as proton transfer profiles in the present work. In combination with the molecular motions displayed by Jmol, precursors, transition states and the elementary reactions in proton transfer processes were analyzed and categorized. The average life times of the precursors, transition states and products were roughly estimated from the proton transfer profiles and further analyzed in details.

Part II: NVT BOMD simulations

BOMD simulations with the DFT method represent an appropriate combination due to the optimal accuracy versus CPU times (Lao-ngam, Asawakun, Wannarat and Sagarik, 2011; Sagarik, Chaiwongwattana, Vchirawongkwin and Prueksaaron, 2010). Therefore, BOMD simulations with the B3LYP/TZVP calculations were adopted in the present investigations.

All the equilibrium structures, including the intermediate states, obtained from the B3LYP/TZVP geometry optimizations, were employed as starting configurations in BOMD simulations at 350 K, an operating temperature in PEMFC. Canonical

(NVT) ensemble was employed in BOMD simulations, with a Nosé-Hoover chain thermostat, applied to each degree of freedom in the model system. Since, in aqueous solution, rapid interconversion between the Zundel and Eigen complexes takes place within 100 fs (Kreuer, 2000), the timestep used in solving dynamic equations was set to 1.0 fs. This choice is justified by the proton transfer profiles for the Zundel and the $\text{CF}_3\text{SO}_3\text{H-H}_3\text{O}^+-\text{H}_2\text{O}$ 1 : 1 : 1 complexes, in which the vibrations of normal O-H covalent bonds and those susceptible to proton transfers are clearly distinguished.

In each BOMD simulation, 1000 fs were spent on equilibration, after which about 10 ps were devoted to property calculations. The choices are justified by BOMD simulations on H_5O_2^+ and H_7O_3^+ (Termath and Sauer, 1997), from which insights into fast dynamic processes in H-bonds (*e.g.* H-bond structures and IR spectra) could be obtained from relatively short BOMD trajectories (~ 2 ps). All BOMD simulations were performed using FROG program included in TURBOMOLE 6.0 (Ahlich, Bär, Häser, Horn and Kölmel, 1989; Treutler and Ahlich, 1995); FROG program employs the Leapfrog Verlet algorithm to turn the electronic potential energy gradients into new atomic positions and velocities.

It should be noted that the applicability and performance of NVE and NVT BOMD simulations in the studies of proton transfer reactions in small H-bond systems were investigated and discussed in details (Sadeghi and Cheng, 1999). Since the energy released during the proton transfer process can be absorbed by the Nosé-Hoover thermostat bath, allowing the H-bond structure and the local temperature to maintain for a longer time (2-5 ps), NVT BOMD simulations were used in the present

investigations. The Nosé-Hoover thermostats were applied every twenty BOMD steps; for the most active H-bond structure, the average temperature was 349 K, with the standard deviation of 67 K, and the average total energy of -1191.7278058 au., with the standard deviation of 0.005439 au.

IR spectra

Since proton transfers in H-bond are coupled with various degrees of freedom (Cheng and Krause, 1997; Kreuer, 1996; Sagarik, Chaiwongwattana, Vchirawongkwin and Prueksaaron, 2010), attention was focused on the symmetric and asymmetric O-H stretching frequencies of the transferring protons, as well as the O-O vibrations. Definitions of the symmetric and asymmetric O-H stretching modes, as well as the O-O vibration are shown in Figure 2.4. In the present study, IR spectra of the transferring protons were computed from BOMD simulations, by Fourier transformations of the velocity autocorrelation function (VACF) (Bopp, 1986). This approach is appropriate as it allows the coupled vibrations to be distinguished, characterized and analyzed separately. Fourier transformations of VACF were made within a short time limit of about 1000 fs. This is supported by the observation that the average lifetime of the most important intermediate state, the Zundel complex, is about 100 fs (Kreuer, 2000).

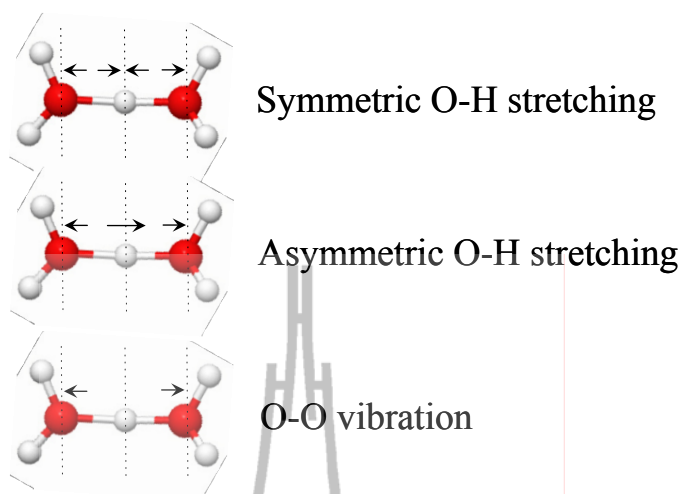


Figure 2.4 Definitions of the symmetric and asymmetric O-H stretching modes, as well as the O-O vibration (Kritsana Sagarik, Sermsiri Chaiwongwattana, Viwat Vchirawongkwin and Supakit Prueksaaron, 2010).

Diffusion coefficients

The diffusion coefficients (D) of the transferring protons were computed from BOMD simulations using the Einstein relation (Haile, 1997; Rapaport, 1995), for which D are determined from the slope of the mean-square displacements (MSD). Because the transferring proton is confined in a short H-bond distance, care must be exercised in selecting the time interval in which MSD are computed (Rapaport, 1995). Our experience showed that linear relationship between MSD and the simulation time could be obtained although the time intervals are not larger than 0.5 ps (Lao-ngam, Asawakun, Wannarat and Sagarik, 2011; Sagarik, Chaiwongwattana, Vchirawongkwin and Prueksaaron, 2010).

CHAPTER III

RESULTS AND DISCUSSION

In this chapter, all important results are discussed in comparison with available theoretical and experimental data. In Part I, the transition states and the elementary reactions in proton transfer processes were analyzed and categorized. The average life times of the precursors, transition states and products were estimated from the proton transfer profiles and analyzed in details. In Part II, the static results obtained from B3LYP/TZVP calculations were analyzed and used as guidelines for the interpretations of the BOMD results. The emphases were on the effects of the -SO₃H group on the H-bond structures, energetic and dynamics of proton transfer in the adjacent Zundel complex, as well as the tendency of protonation and deprotonation at the -SO₃H group.

3.1 Part I

3.1.1 Static results

Structures and energetic

The absolute and some lowest-lying minimum energy geometries of the H-bond complexes obtained from the T-model, DFT and *ab initio* calculations, together with the corresponding interaction energies and characteristic H-bond distances, are reported in the following subsections.

The $\text{H}_3\text{O}^+ - n\text{H}_2\text{O}$ complexes

For the $\text{H}_3\text{O}^+ - \text{H}_2\text{O}$ 1 : n complex, $1 \leq n \leq 3$, T-model, DFT and *ab initio* geometry optimizations suggested only one predominant H-bond structure; H_3O^+ acts as proton donor towards H_2O , structures **a**, **b** and **c** in Table 3.1.

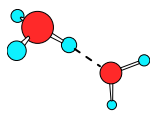
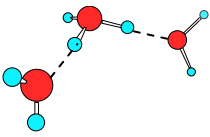
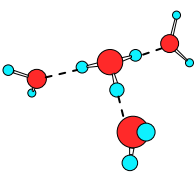
DFT and *ab initio* calculations with partial geometry optimizations predicted the same structures as T-model. The Zundel complex, in which a hydrogen atom is equally shared between two water molecules and considered as a defect in H-bond network (Eikerling, Paddison, Pratt and Zawodzinski, 2003), was obtained when DFT and *Ab initio* calculations with full geometry optimizations were applied. The Oh..H..Ow and Oh..H distances derived from B3LYP-OPT2 and MP2-OPT2 are almost the same, about 2.4 and 1.2 Å, respectively. The extraordinary short H-bond distance, as in the case of the Zundel complex, could be related to high possibility for proton transfer and, therefore, used as a criterion to monitor proton transfer reactions (Kreuer, 2000).

Similar trends were observed in the $\text{H}_3\text{O}^+ - \text{H}_2\text{O}$ 1 : 2 complexes. T-model, DFT and *Ab initio* calculations with partial geometry optimizations predicted the structure with two equivalent linear Oh-Hh..Ow H-bonds to be the most stable. Only slightly shorter Oh-Hh..Ow H-bond distances were observed when MP2-OPT2 and B3LYP-OPT2 were applied on the T-model results. All theoretical methods predicted longer Oh-Hh..Ow H-bond distances, when the number of water molecule was gradually increased from one to three. For the $\text{H}_3\text{O}^+ - \text{H}_2\text{O}$ 1 : 3 complex, T-model

suggested the Oh-Hh..Ow H-bond distance to be 2.58 Å, whereas the values obtained from MP2-OPT1 and B3LYP-OPT1 are 2.57 and 2.54 Å, respectively. MP2-OPT2 and B3LYP-OPT2 showed the same trend, with slightly shorter Oh-Hh covalent bonds in H_3O^+ .

As mentioned earlier that, H-bonds in the $\text{H}_3\text{O}^+ - \text{H}_2\text{O}$ complexes have been extensively studied using both experimental and theoretical treatments. It was generally concluded that, the introduction of an extra proton to cluster of water molecules in the gas phase or liquid water results in contraction of H-bonds, through the formation of proton defect which involves H_5O_2^+ (Kreuer, 2000). The isolated H_5O_2^+ was reported to possess very short H-bond distance, approximately 2.4 Å (Duan and Scheiner, 1992; Giguere, 1979; Schmitt and Voth, 1999). This is confirmed by all theoretical results obtained here. Both experiments and theories suggested the same trends when water molecules are added to H_5O_2^+ namely, the central H-bond in H_5O_2^+ is weaken to some extent, leading to relaxation of H-bonds. The H-bond distance in the Eigen complex was reported to be about 2.6 Å (Giguere, 1979; Kreuer, 2000; Schmitt and Voth, 1999), which is in excellent agreement with the present results.

Table 3.1 Structures of the $\text{H}_3\text{O}^+\text{-H}_2\text{O}$ complexes, obtained from the T-model, DFT and *ab initio* geometry optimizations. (a) $\text{H}_3\text{O}^+\text{-H}_2\text{O}$ 1:1 complex. (b) $\text{H}_3\text{O}^+\text{-H}_2\text{O}$ 1:2 complex. (c) $\text{H}_3\text{O}^+\text{-H}_2\text{O}$ 1:3 complex.

Structure	Method	$\Delta E/\text{kJ mol}^{-1}$	Oh-Hh..Ow/Å	Oh-Hh-Ow/°
a) 	T-model	-117.5	2.51	151.0
	MP2-OPT1	-135.5	2.46	175.9
	MP2-OPT2	-	2.39 ^a	174.0
	B3LYP-OPT1	-160.7	2.43	174.5
	B3LYP-OPT2	-	2.40 ^a	174.2
b) 	T-model	-229.9	2.52	152.6
	MP2-OPT1	-244.5	2.52	174.3
	MP2-OPT2	-	2.50	175.5
	B3LYP-OPT1	-287.6	2.49	174.0
	B3LYP-OPT2	-	2.47	174.6
c) 	T-model	-334.4	2.58	171.7
	MP2-OPT1	-334.0	2.57	175.6
	MP2-OPT2	-	2.57	175.9
	B3LYP-OPT1	-388.4	2.54	176.7
	B3LYP-OPT2	-	2.55	175.5

^a The Zundel complex; an excess proton equally shared between two water molecules.

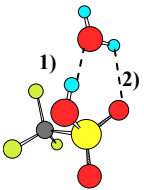
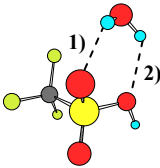
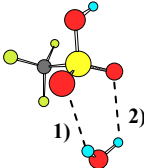
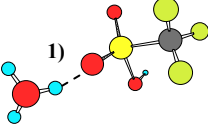
MP2-OPT1 = MP2/6-311++G(2d,2p) with partial geometry optimizations, MP2-OPT2 = MP2/6-311++G(2d,2p) with full geometry optimizations, B3LYP-OPT1 = B3LYP/6-31G(d,p) with partial geometry optimizations, B3LYP-OPT2 = B3LYP/6-31G(d,p) with full geometry optimizations.

The $\text{CF}_3\text{SO}_3\text{H}-\text{H}_2\text{O}$ and $\text{CF}_3\text{SO}_3\text{H}-\text{H}_3\text{O}^+$ complexes

For the $\text{CF}_3\text{SO}_3\text{H}-\text{H}_2\text{O}$ 1 : 1 complex, T-model, MP2-OPT1 and B3LYP-OPT2 predicted a cyclic H-bond structure, in which $\text{CF}_3\text{SO}_3\text{H}$ acts simultaneously as proton donor and acceptor, to be the global minimum energy geometry, structure **a** in Table 3.2; whereas other cyclic H-bond structures, in which $\text{CF}_3\text{SO}_3\text{H}$ acts only as proton acceptor, structures **b** and **c**, possess considerably lower stability. For the $\text{CF}_3\text{SO}_3\text{H}-\text{H}_3\text{O}^+$ 1 : 1 complex, both T-model and MP2-OPT1 predicted H_3O^+ to be stronger proton donor than $\text{CF}_3\text{SO}_3\text{H}$, structure **d** in Table 3.2.

The linear H-bond in structure **d** did not change substantially when B3LYP-OPT2 was applied. However, small but not negligible change was observed at the Oh-Hh..O H-bond. It becomes shorter and comparable with the Ow..H..Ow H-bond distance in the Zundel complex. The decrease in the H-bond distance is accompanied by an increase in the Oh-Hh covalent bond distance. This reflects a tendency for proton transfer from H_3O^+ to $\text{CF}_3\text{SO}_3\text{H}$, leading to a Zundel-like structure ($\text{CF}_3\text{SO}_3\text{H}_2^+ - \text{H}_2\text{O}$) (Glezakou, Dupuis and Mundy, 2007).

Table 3.2 Structures of the $\text{CF}_3\text{SO}_3\text{H} - \text{H}_2\text{O}$ and $\text{CF}_3\text{SO}_3\text{H} - \text{H}_3\text{O}^+$ 1 : 1 complexes, obtained from T-model, DFT and *ab initio* geometry optimizations. a) - c) $\text{CF}_3\text{SO}_3\text{H} - \text{H}_2\text{O}$ 1 : 1 complexes. d) $\text{CF}_3\text{SO}_3\text{H} - \text{H}_3\text{O}^+$ 1 : 1 complex.

Structure	Method	$\Delta E/\text{kJ mol}^{-1}$	H-bond	Distance/Å	Angle/°
a) 	T-model	-51.9	1)	2.71	158.4
			2)	2.79	111.6
	MP2-OPT1	-51.9	1)	2.68	166.2
			2)	2.93	133.3
	B3LYP-OPT2	-	1)	2.60	166.4
			2)	2.84	127.2
b) 	T-model	-15.7	1)	2.95	122.8
			2)	3.05	127.6
	MP2-OPT1	-13.2	1)	3.18	134.5
			2)	3.20	136.3
	B3LYP-OPT2	-	1)	3.01	138.9
			2)	3.22	102.3
c) 	T-model	-15.7	1)	2.95	122.8
			2)	3.05	127.6
	MP2-OPT1	-13.9	1)	3.21	127.5
			2)	3.24	123.6
	B3LYP-OPT2	-	1)	3.10	120.7
			2)	3.08	120.1
d) 	T-model	-68.1	1)	2.60	141.3
	MP2-OPT1	-114.6	1)	2.48	177.3
	B3LYP-OPT2	-	1)	2.40	177.4

MP2-OPT1 = MP2/6-311++G(d,p) with partial geometry optimizations. B3LYP-OPT2 = B3LYP/6-31G(d,p) with full geometry optimizations.

The $\text{CF}_3\text{SO}_3\text{H}-\text{H}_3\text{O}^+-n\text{H}_2\text{O}$ complexes

For the $\text{CF}_3\text{SO}_3\text{H}-\text{H}_3\text{O}^+-\text{H}_2\text{O}$ 1 : 1 : 1 complexes, T-model generated three important minimum energy geometries namely, structures **a**, **b** and **c** in Table 3.3. All of them adopt compact cyclic H-bond structures. The most stable one, structure **a**, consists of three H-bonds; H_3O^+ and H_2O act as proton donors towards two oxygen atoms of $\text{CF}_3\text{SO}_3\text{H}$. The stability of structure **b** is slightly lower than structure **a**, and structure **c** is quite different from structures **a** and **b**. In structure **c**, $\text{CF}_3\text{SO}_3\text{H}$ forms two separate cyclic H-bonds with H_3O^+ and H_2O . Both are located on the opposite side of $-\text{SO}_3\text{H}$. Some H-bonds in structures **b** and **c** were disrupted when MP2-OPT1 and B3LYP-OPT1 were applied on the T-model results, leading to linear H-bond structures. Comparison of the MP2-OPT1 and MP2-OPT2 results in details reveals the important trend; full geometry optimizations lead to shorter H-bond distances, especially where proton transfer could take place, e.g. the $\text{O}^{\text{H}}-\text{H}^{\text{H}}\cdots\text{O}^{\text{W}}$ H-bonds in structures **a** and **b**, as well as the $\text{O}^{\text{H}}-\text{H}^{\text{H}}\cdots\text{O}$ H-bonds in structures **b** and **c**. The latter reflect the possibility for proton transfer from H_3O^+ to $-\text{SO}_3\text{H}$, forming the previously proposed $\text{CF}_3\text{SO}_3\text{H}_2^+$ transition state. Starting from the T-model results, B3LYP-OPT2 did not bring about significant change in the H-bond structures. However, the possibilities for proton transfer in structures **a**, **b** and **c** become more evident. Compared with B3LYP-OPT1, all the H-bonds susceptible to proton transfer are systematically shorter, with hydrogen atoms located nearer to the centers.

Table 3.3 Equilibrium structures of the $\text{CF}_3\text{SO}_3\text{H} - \text{H}_3\text{O}^+ - \text{H}_2\text{O}$ 1 : 1 : 1 complexes

a) - c), obtained from T-model, DFT and *ab initio* geometry optimizations. Interaction energy in kJ/mol, angle in degree and distance in Å.

Structure	Method	$\Delta E/\text{kJ mol}^{-1}$	H-bond	Distance/Å
a) 	B3LYP-OPT2	-	1) Ow-Hw..Ow 2) Ow-Hw..O 3) Ow-H..Ow	2.71 2.78 2.41
	T-model	-229.3	1) Oh-Hh..O 2) Ow-Hw..O 3) Oh-Hh..Ow	2.54 2.96 2.51
	MP2-OPT1	-228.8	1) Oh-Hh..O 2) Ow-Hw..O 3) Oh-Hh..Ow	2.61 3.04 2.48
	B3LYP-OPT1	-257.8	1) Oh-Hh..O 2) Ow-Hw..O 3) Oh-Hh..Ow	2.60 2.99 2.46
	MP2-OPT2	-	1) Oh-Hh..O 2) Ow-Hw..O 3) Oh-Hh..Ow	2.64 2.87 2.42

MP2-OPT1 = MP2/6-311++G(d,p) with partial geometry optimizations, MP2-OPT2 = MP2/6-311++G(d,p) with full geometry optimizations, B3LYP-OPT1 = B3LYP/6-31G(d,p) with partial geometry optimizations, B3LYP-OPT2 = B3LYP/6-31G(d,p) with full geometry optimizations.

Table 3.3 (Continued).

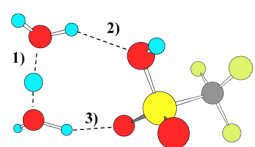
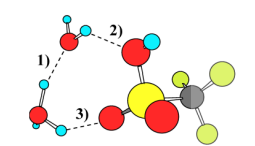
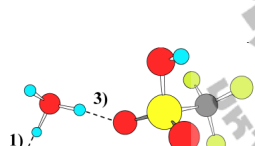
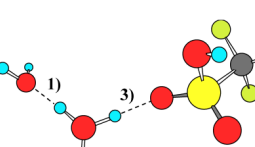
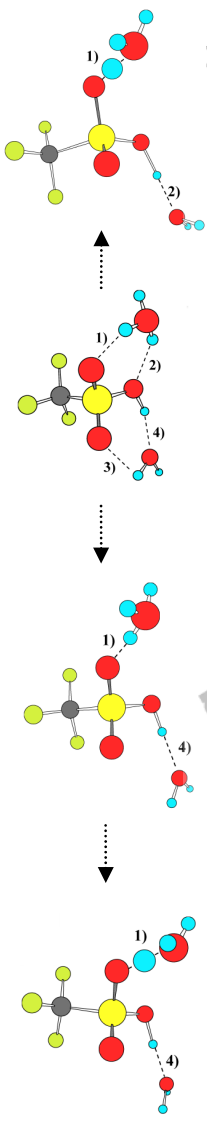
Structure	Method	$\Delta E/\text{kJ mol}^{-1}$	H-bond	Distance/Å
b)    	B3LYP-OPT2	-	1) Ow..H..Ow 2) Ow-Hw..O 3) Ow-Hw..O	2.44 3.07 2.60
	T-model	-226.4	1) Oh-Hh..Ow 2) Ow-Hw..O 3) Oh-Hh..O	2.50 3.05 2.53
	MP2-OPT1	-229.3	1) Oh-Hh..Ow 3) Oh-Hh..O	2.49 2.56
	B3LYP-OPT1	-254.7	1) Oh-Hh..Ow 3) Oh-Hh..O	2.48 2.56
	MP2-OPT2	-	1) Oh-Hh..Ow 3) Oh-Hh..O	2.47 2.53

Table 3.3 (Continued).

Structure	Method	$\Delta E/\text{kJ mol}^{-1}$	H-bond	Distance/Å
c) 	B3LYP-OPT2	-	1) Ow..H..O 2) O-H..Ow	2.43 2.46
	T-model	-165.9	1) Oh-Hh..O 2) Oh-Hh..O 3) Ow-Hw..O 4) Oh-H..Ow	2.57 2.75 2.80 2.61
	MP2-OPT1	-194.7	1) Oh-Hh..O 4) O-H..Ow	2.45 2.58
	B3LYP-OPT1	-212.4	1) Oh-Hh..O 4) O-H..Ow	2.45 2.56
	MP2-OPT2	-	1) Ow..H..O O..H Ow..H 4) O-H..Ow	2.39 1.14 1.25 2.48

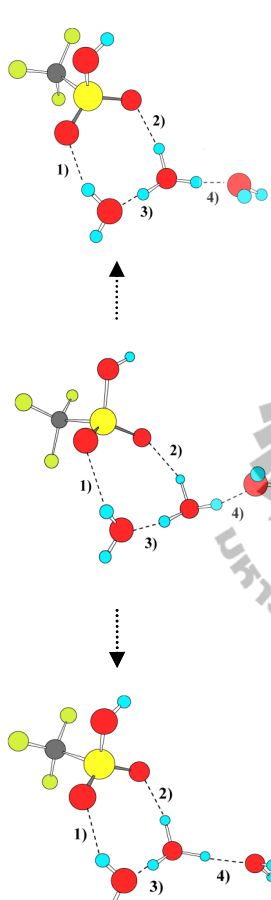
Since important information on theoretical methods had already been obtained, it was reasonable to investigate the $\text{CF}_3\text{SO}_3\text{H} - \text{H}_3\text{O}^+ - \text{H}_2\text{O}$ 1 : 1 : 2 complex using only T-model, MP2-OPT2 and B3LYP-OPT2. T-model predicted four important cyclic H-bond structures in Table 3.4. The most stable one consists of a basic unit similar to structure **a** in the $\text{CF}_3\text{SO}_3\text{H} - \text{H}_3\text{O}^+ - \text{H}_2\text{O}$ 1 : 1 : 1 complex, with the second water molecule hydrating at H_3O^+ . The stability of structure **b** is slightly lower than structure **a**. In structure **b**, both $\text{CF}_3\text{SO}_3\text{H}$ and H_3O^+ act as proton donors towards water molecules, and the second water molecule hydrating directly at H_3O^+ . The stability of structures **a** and **b** seems to result from a complete H-bond formation at H_3O^+ . Structures **c** and **d** are quite different from structures **a** and **b**; only two Oh-Hh covalent bonds in H_3O^+ are H-bonded. Comparison of interaction energies ($\Delta E_{\text{T-model}}$) suggested that the formation of a large cyclic H-bond tends to reduce the stability of the $\text{CF}_3\text{SO}_3\text{H} - \text{H}_3\text{O}^+ - \text{H}_2\text{O}$ 1 : 1 : 2 complexes. The T-model results did not change significantly, when B3LYP-OPT2 and MP2-OPT2 were applied; except for structures **c** and **d**, B3LYP-OPT2 showed higher possibility for the Zundel complex formation. In summary for the $\text{CF}_3\text{SO}_3\text{H} - \text{H}_3\text{O}^+ - \text{H}_2\text{O}$ 1 : 1 : 2 complexes, structures **a**, **b** and **d** reveal possibilities for proton transfer along the H-bond networks connecting the oxygen atoms of $-\text{SO}_3\text{H}$, whereas structure **c** shows a possibility for proton transfer through $-\text{SO}_3\text{H}$, e.g. a protonation at one oxygen atom followed by a deprotonation at the O-H group, or vice versa. This direct involvement of $-\text{SO}_3\text{H}$ in proton transfer is similar to the Grotthuss mechanism (Grotthuss, 1806). In the present case, a relay-type mechanism, in which proton hops across $-\text{SO}_3\text{H}$,

could take place through the formation of either $-\text{SO}_3\text{H}_2^+$ or $-\text{SO}_3^-$. It should be noted that, although limited number of H-bond structures was considered (Glezakou, Dupuis and Mundy, 2007), $-\text{SO}_3\text{H}_2^+$ was recognized in *ab initio* calculations and MD simulations, and pointed out to play important roles in proton transfer at low hydration levels. This was further investigated in MD simulations in the next sections.



Table 3.4 Equilibrium structures of the $\text{CF}_3\text{SO}_3\text{H} - \text{H}_3\text{O}^+ - \text{H}_2\text{O}$ 1 : 1 : 2 complexes

a) – d), obtained from T-model, DFT and *ab initio* calculations. Interaction energy in kJ/mol and distance in Å.

Structure	Method	$\Delta E/\text{kJ mol}^{-1}$	H-bond	Distance/Å
a) 	B3LYP-OPT2	-	1) Ow-Hw..O	2.86
			2) Oh-Hh..O	2.75
			3) Oh-Hh..Ow	2.49
			4) Oh-Hh..Ow	2.53
	T-model	-295.5	1) Ow-Hw..O	2.91
			2) Oh-Hh..O	2.62
			3) Oh-Hh..Ow	2.57
			4) Oh-Hh..Ow	2.56
	MP2-OPT2	-	1) Ow-Hw..O	2.91
			2) Oh-Hh..O	2.70
			3) Oh-Hh..Ow	2.51
			4) Oh-Hh..Ow	2.54

MP2-OPT2 = MP2/6-311++G(d,p) with full geometry optimizations, B3LYP-OPT2 = B3LYP/6-31G(d,p) with full geometry optimizations.

Table 3.4 (Continued).

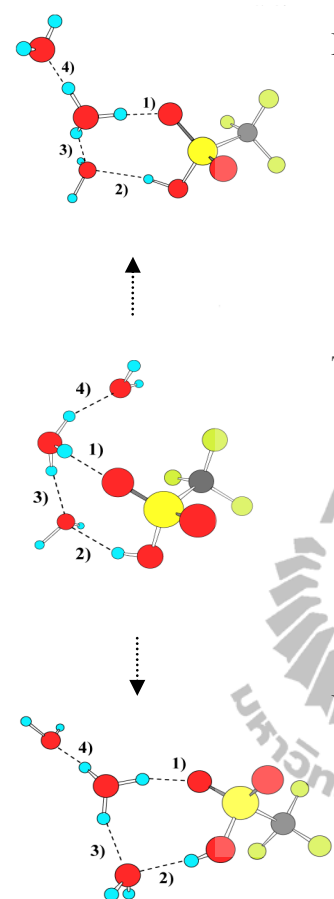
Structure	Method	$\Delta E/\text{kJ mol}^{-1}$	H-bond	Distance/Å
b) 	B3LYP-OPT2	-	1) Oh-Hh..O 2) O-H..Ow 3) Oh-Hh..Ow 4) Oh-Hh..Ow	2.53 2.81 2.70 2.50
	T-model	-285.5	1) Oh-Hh..O 2) O-H..Ow 3) Oh-Hh..Ow 4) Oh-Hh..Ow	2.49 2.88 2.61 2.53
	MP2-OPT2	-	1) Oh-Hh..O 2) O-H..Ow 3) Oh-Hh..Ow 4) Oh-Hh..Ow	2.53 2.86 2.72 2.50

Table 3.4 (Continued).

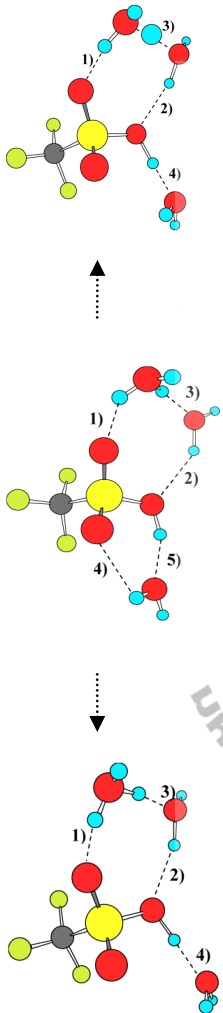
Structure	Method	$\Delta E/\text{kJ mol}^{-1}$	H-bond	Distance/Å
c) 	B3LYP-OPT2	-	1) Ow-Hw..Ow 2) Ow-Hw..O 3) Ow-H..Ow 4) O-H..Ow	2.59 2.85 2.42 2.50
	T-model	-252.4	1) Oh-Hh..O 2) Ow-Hw..O 3) Oh-Hh..Ow 4) Ow-Hw..O 5) O-H..Ow	2.57 2.96 2.54 2.86 2.68
	MP2-OPT2	-	1) Oh-Hh..O 2) Ow-Hw..O 3) Oh-Hh..Ow 4) O-H..Ow	2.58 2.84 2.43 2.52

Table 3.4 (Continued).

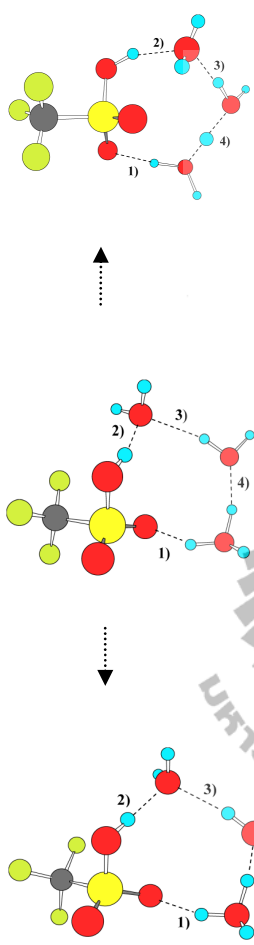
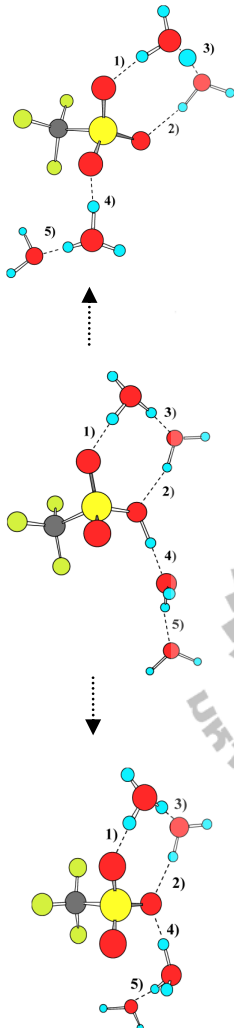
Structure	Method	$\Delta E/\text{kJ mol}^{-1}$	H-bond	Distance/Å
d) 	B3LYP-OPT2	-	1) Ow-Hw..O 2) O-H..Ow 3) Ow-Hw..Ow 4) Ow-H..Ow	2.60 2.71 2.77 2.43
	T-model	-246.5	1) Oh-Hh..O 2) O-H..Ow 3) Ow-Hw..Ow 4) Oh-Hh..Ow	2.61 2.74 3.11 2.52
	MP2-OPT2	-	1) Oh-Hh..O 2) O-H..Ow 3) Ow-Hw..Ow 4) Oh-Hh..Ow	2.45 2.74 2.89 2.45

Table 3.4 (Continued).

Structure	Method	$\Delta E/\text{kJ mol}^{-1}$	H-bond	Distance/Å
e) 	B3LYP-OPT2	-	1) Oh-Hh..O	2.54
			2) Ow-Hw..O	2.70
			3) Oh-Hh..Ow	2.43
			4) Oh-Hh..O	2.42
			5) Oh-Hh..Ow	2.52
	T-model	-282.1	1) Oh-Hh..O	2.53
			2) Ow-Hw..O	2.85
			3) Oh-Hh..Ow	2.45
			4) O-H..Ow	2.44
			5) Ow-Hw..Ow	2.70
	MP2-OPT2		1) Oh-Hh..O	2.55
			2) Ow-Hw..O	2.70
			3) Oh-Hh..Ow	2.42
			4) Oh-Hh..O	2.43
			5) Oh-Hh..Ow	2.52

For the $\text{CF}_3\text{SO}_3\text{H} - \text{H}_3\text{O}^+ - \text{H}_2\text{O}$ 1 : 1 : 3 complex, both linear and cyclic H-bonds were found in the optimized geometry, structure **e** in Figure 3.5. T-model, MP2-OPT2 and B3LYP-OPT2 predicted a similar trend namely, all H-bonds susceptible for proton transfer possess short H-bond distances. MP2-OPT2 and B3LYP-OPT2 also showed a possibility to form $-\text{SO}_3^-$, H_3O^+ and H_5O_2^+ within the $\text{CF}_3\text{SO}_3\text{H} - \text{H}_3\text{O}^+ - \text{H}_2\text{O}$ 1 : 1 : 3 complex. The appearance of $-\text{SO}_3^-$ and the ion-pair complex when $n = 3$ is in good agreement with the theoretical results in (Glezakou, Dupuis and Mundy, 2007).

Potential energy profiles

Comparison of the size and shape of the potential energy profiles for proton transfer in Figures 3.1a to 3.1d revealed that, B3LYP/6-31G(d,p), B3LYP/6-31+G(d,p) and MP2/6-311++G(d,p) yield similar trends; whereas HF/6-311++G(d,p) shows different results, *e.g.* minima are seen systematically at shorter distances. The discrepancies are quite obvious in Figures 3.1b to 3.1e; double-well potential is seen in the case of large cyclic H-bond of water; shoulders are seen in the case of $\text{CF}_3\text{SO}_3\text{H} - \text{H}_3\text{O}^+ - \text{H}_2\text{O}$ 1 : 1 : 1 complexes. Based on the above discussions and the fact that DFT requires lowest computational resources, one can conclude that B3LYP/6-31G(d,p) is the most appropriate choice for MD simulations.

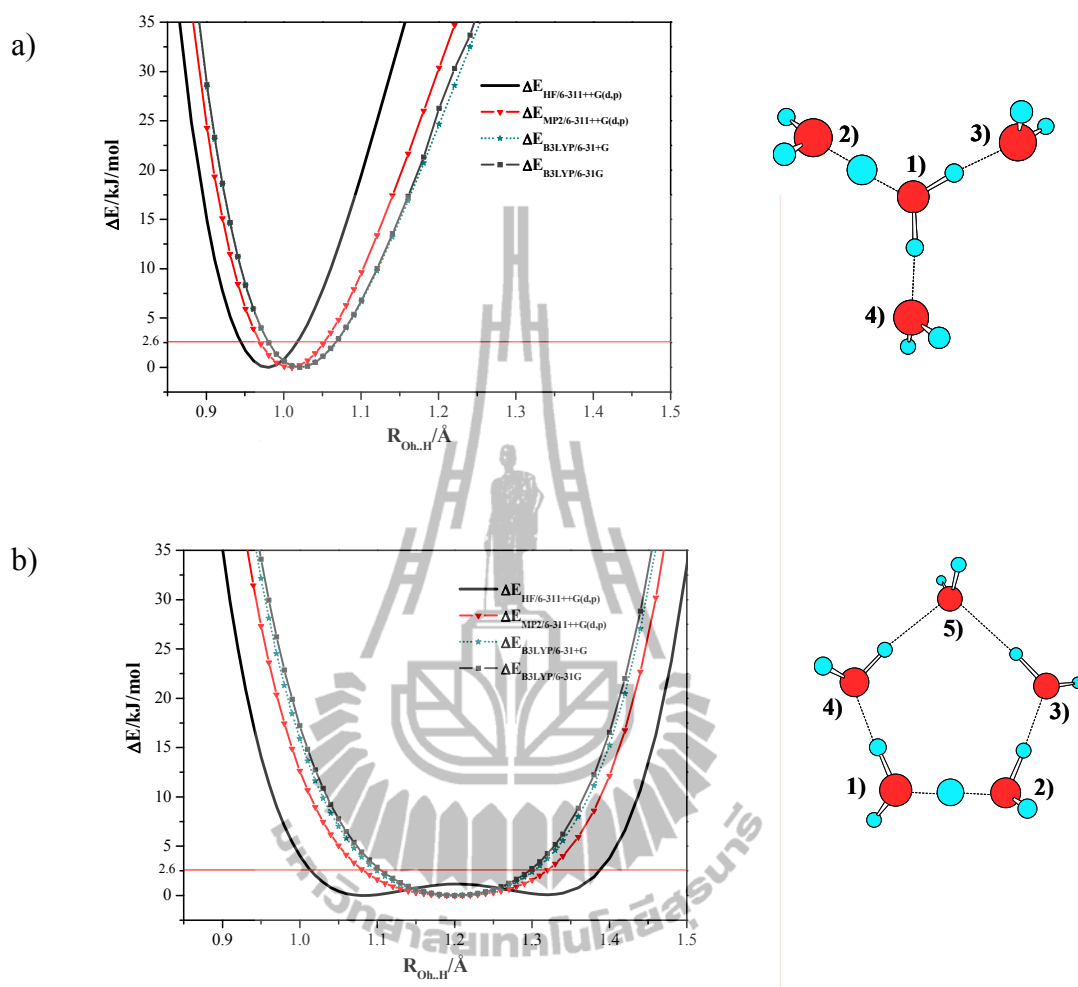


Figure 3.1 Potential energy profiles for single proton transfer, obtained from various theoretical methods. Interaction energy in kJ/mol and distance in Å. All minima on the potential energy curves were moved to zero for comparisons. a) $\text{H}_3\text{O}^+ - \text{H}_2\text{O}$ 1 : 3 complex. b) $\text{H}_3\text{O}^+ - \text{H}_2\text{O}$ 1 : 4 complex. c) - e) $\text{CF}_3\text{SO}_3\text{H} - \text{H}_3\text{O}^+ - \text{H}_2\text{O}$ 1 : 1 : 1 complexes.

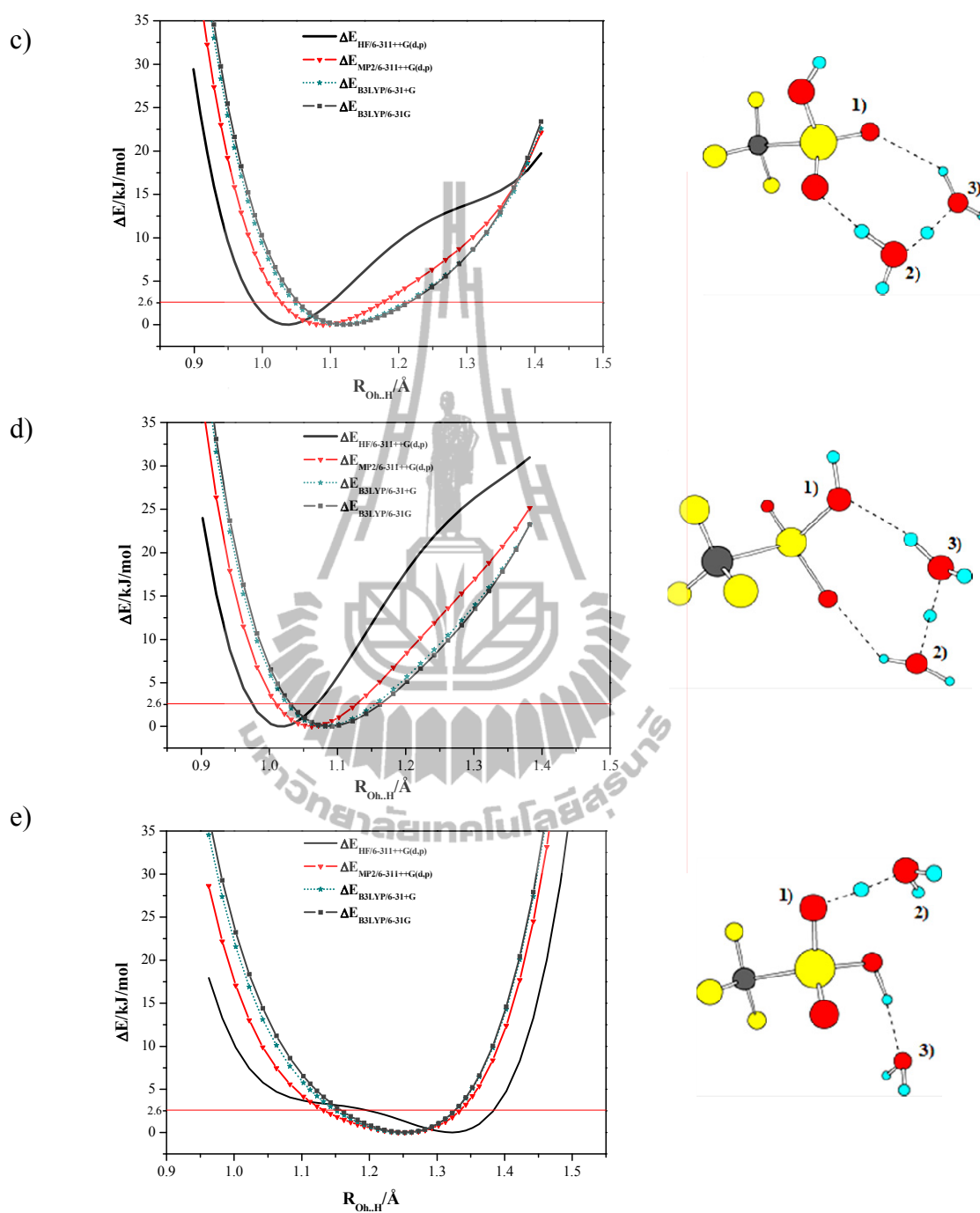


Figure 3.1 (Continued).

3.1.2 Dynamic results

Proton transfer profiles and elementary reactions

The $\text{H}_3\text{O}^+ - \text{H}_2\text{O}$ complexes

Since H-bond structures can vary in a quite wide range, care must be exercised in the discussion of proton transfer profiles. In order to study dynamics and elementary reactions in proton transfer processes, some characteristic structures in proton transfer profiles have to be interpreted, using BOMD results on the $\text{H}_3\text{O}^+ - \text{H}_2\text{O}$ 1 : 1 complex in Figures 3.2 and 3.3 as examples. It appeared in general that proton transfer in H_5O_2^+ depends strongly on the Oh-Hh..Ow H-bond distance, as well as its vibrational amplitude. Examples of two extreme cases namely, large- and small-amplitude vibrations, are shown in Figures 3.2a and 3.2b, respectively. In order to simplify the discussion, the proton transfer profiles are divided into panels, labeled with **P1**, **P2**, **P3**, ..., **P_n**, respectively.

For large-amplitude vibration, the Oh-Hh..Ow H-bond distance (O1-O2 in Figure 3.2a) varies in a quite wide range, from its equilibrium to about 3 Å. A periodic series, consisting of a quasi-dynamic equilibrium followed by an actual proton transfer, was observed in the course of BOMD simulations and could be considered as a part of proton transfer reaction mechanism. For H_5O_2^+ , the quasi-dynamic equilibrium is characterized by a proton shuttling back and forth in a narrow range within H-bond, before the actual proton transfer takes place, either in the forward or reverse direction. In Figure 3.2a, for example, a quasi-dynamic equilibrium is seen in panel **P2**, preceding the actual proton transfer in the forward direction at $t_3 = 2341$ fs.

The actual proton transfers are also seen at $t_1 = 2228$ fs, $t_2 = 2317$ fs and $t_4 = 2419$ fs. The life time of the quasi-dynamic equilibrium ($\tau_{\text{H}_5\text{O}_2^+}^{\text{I,ABC}}$) could be approximated from the width of panel **P2**, and the life times of H_3O^+ , $\tau_{\text{H}_5\text{O}_2^+}^{\text{I,C}}$ and $\tau_{\text{H}_5\text{O}_2^+}^{\text{I,A}}$, from panels **P1** and **P3**, respectively; the former is 24 fs and latter are 89 and 78 fs, respectively. The superscripts **A** and **C** in $\tau_{\text{H}_5\text{O}_2^+}^{\text{I,C}}$ and $\tau_{\text{H}_5\text{O}_2^+}^{\text{I,A}}$ represent the H-bond structures in Figure 3.2c, and **I**, the elementary reaction in Figure 3.3. The superscript **ABC** in $\tau_{\text{H}_5\text{O}_2^+}^{\text{I,ABC}}$ denotes the quasi-dynamic equilibrium established among structures **A**, **B** and **C**. Similar notations will be applied in the forthcoming discussions. Since $\tau_{\text{H}_5\text{O}_2^+}^{\text{I,A}}$ and $\tau_{\text{H}_5\text{O}_2^+}^{\text{I,C}}$ are longer than $\tau_{\text{H}_5\text{O}_2^+}^{\text{I,ABC}}$, the life times of the precursor H_3O^+ could be approximated as the rate-determining step for proton transfer reaction via large amplitude vibration in H_5O_2^+ .

For small-amplitude vibration, the Oh-Hh..Ow H-bond distance (O1-O2 in Figure 3.2b) varies in a narrow range near its equilibrium, between 2.3 and 2.7 Å. In this case, proton exchange between two water molecules takes place more often and quite randomly. For example, in Figure 3.2b, $\tau_{\text{H}_5\text{O}_2^+}^{\text{I,A}}$ and $\tau_{\text{H}_5\text{O}_2^+}^{\text{I,C}}$ vary from 19 to 39 fs, and up to three actual proton transfers occur between t_1 and t_4 . Interestingly, the O1-O2 vibration starts to damp at $t_1 = 1941$ fs, until a quasi-dynamic equilibrium, with $\tau_{\text{H}_5\text{O}_2^+}^{\text{I,ABC}} = 23$ fs, is reached at $t_5 = 2046$ fs; followed by a proton transfer at $t_6 = 2069$ fs. It should be noted that, although the life times of the precursor H_3O^+ ($\tau_{\text{H}_5\text{O}_2^+}^{\text{I,A}}$) for large- and small-amplitude vibrations are somewhat different, $\tau_{\text{H}_5\text{O}_2^+}^{\text{I,ABC}}$ are quite similar.

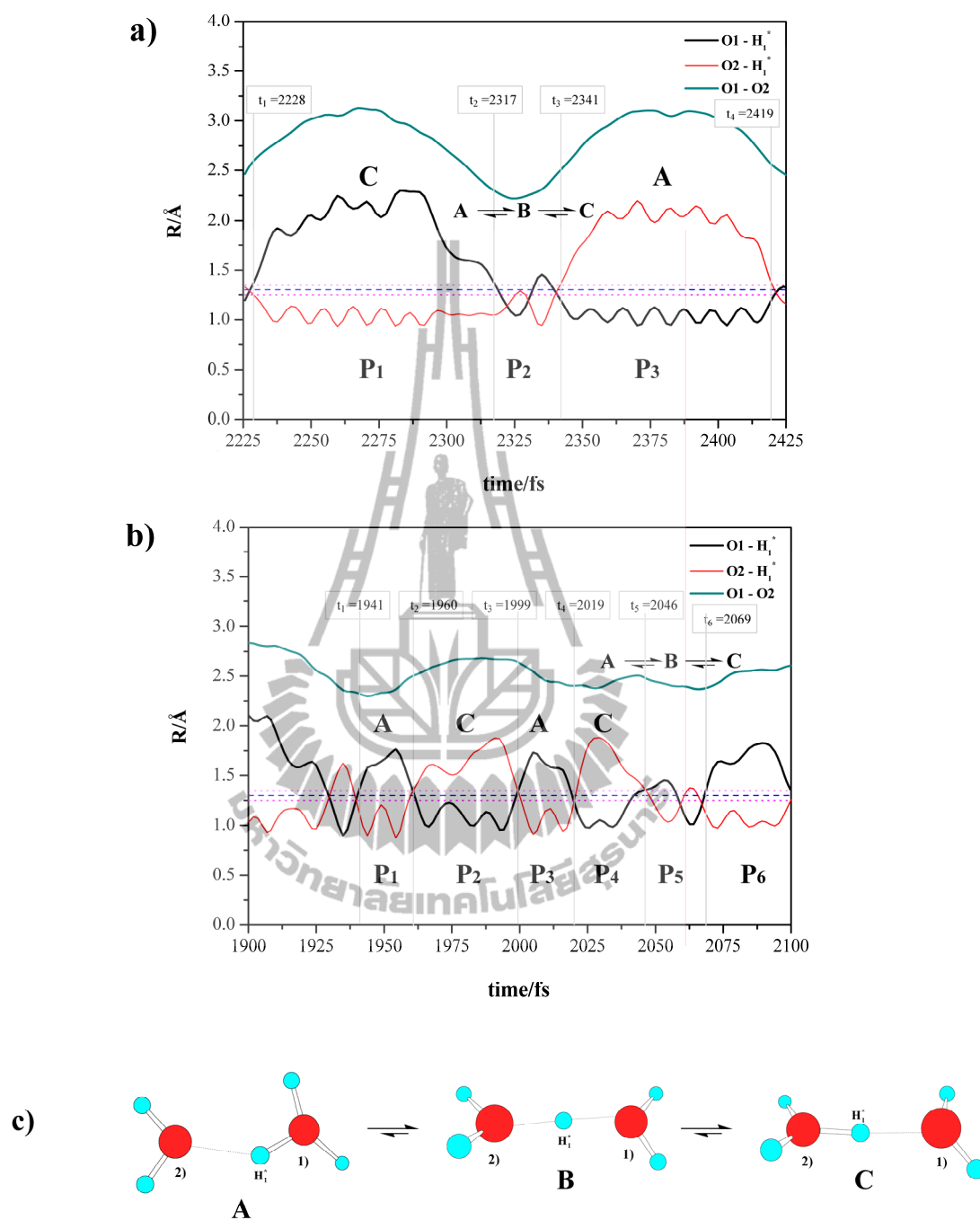


Figure 3.2 Examples of characteristic proton transfer profiles for the $\text{H}_3\text{O}^+ - \text{H}_2\text{O}$ 1 : 1 complex, with snapshots of H-bond structures obtained in the course of BOMD.

a) Large-amplitude vibrations. b) Small-amplitude vibrations. c) Snapshots of H-bond structures.

It could be recognized that, proton transfers in H_5O_2^+ are activated, when the Oh-Hh..Ow H-bond distance (O1-O2 in Figures 3.2a and 3.2b is close to its equilibrium, shorter than 2.4 Å, and only one actual proton transfer takes place for each large-amplitude vibration cycle. Therefore, maximum proton transfer cycle time ($\tau_{\text{H}_5\text{O}_2^+}^{\text{I,PT}_{\text{max}}}$) could be defined from large-amplitude vibration; from the time intervals between successive minima of the Oh-Hh..Ow H-bond distance. The proton transfer profiles in Figures 3.2a and 3.2b also revealed that. For the large-amplitude vibration, the O1-O2 and O1-H₁^{*} motions in panel **P**₁, as well as the O1-O2 and O2-H₁^{*} motions in panel **P**₃, are correlated, except during the quasi-dynamic equilibrium in **P**₂; whereas, for small-amplitude vibration, for which proton vibrates with higher frequency, such correlation is missing. Since the abnormal proton mobility in water has been pointed out to relate to incoherent effects (Agmon, 1995), it is reasonable to approximate the degree of coherence in H-bond. Similar to statistics and electromagnetic waves, the degree of coherence in the present study should measure the extent of correlation between vibrational motions in H-bonds, *e.g.* between the O-O and O-H vibrations. Since for large-amplitude vibration, $\tau_{\text{H}_5\text{O}_2^+}^{\text{I,A}}$ and $\tau_{\text{H}_5\text{O}_2^+}^{\text{I,PT}_{\text{max}}}$ are nearly the same, $\tau_{\text{H}_5\text{O}_2^+}^{\text{I,A}} / \tau_{\text{H}_5\text{O}_2^+}^{\text{I,PT}_{\text{max}}}$ could be adopted as a criteria to measure the degree of coherence ($g_{\text{H}_5\text{O}_2^+}^{\text{I}}$). Therefore, in Figure 3.2a, $g_{\text{H}_5\text{O}_2^+}^{\text{I}} \approx 1$ is attributed to the highest degree of coherence; whereas in Figure 3.2b, the short life times of the precursor H_3O^+ ($\tau_{\text{H}_5\text{O}_2^+}^{\text{I,A}}$ and $\tau_{\text{H}_5\text{O}_2^+}^{\text{I,C}}$) compared to $\tau_{\text{H}_5\text{O}_2^+}^{\text{I,PT}_{\text{max}}}$ reflect lower degree of coherence and higher frequency of proton transfer.

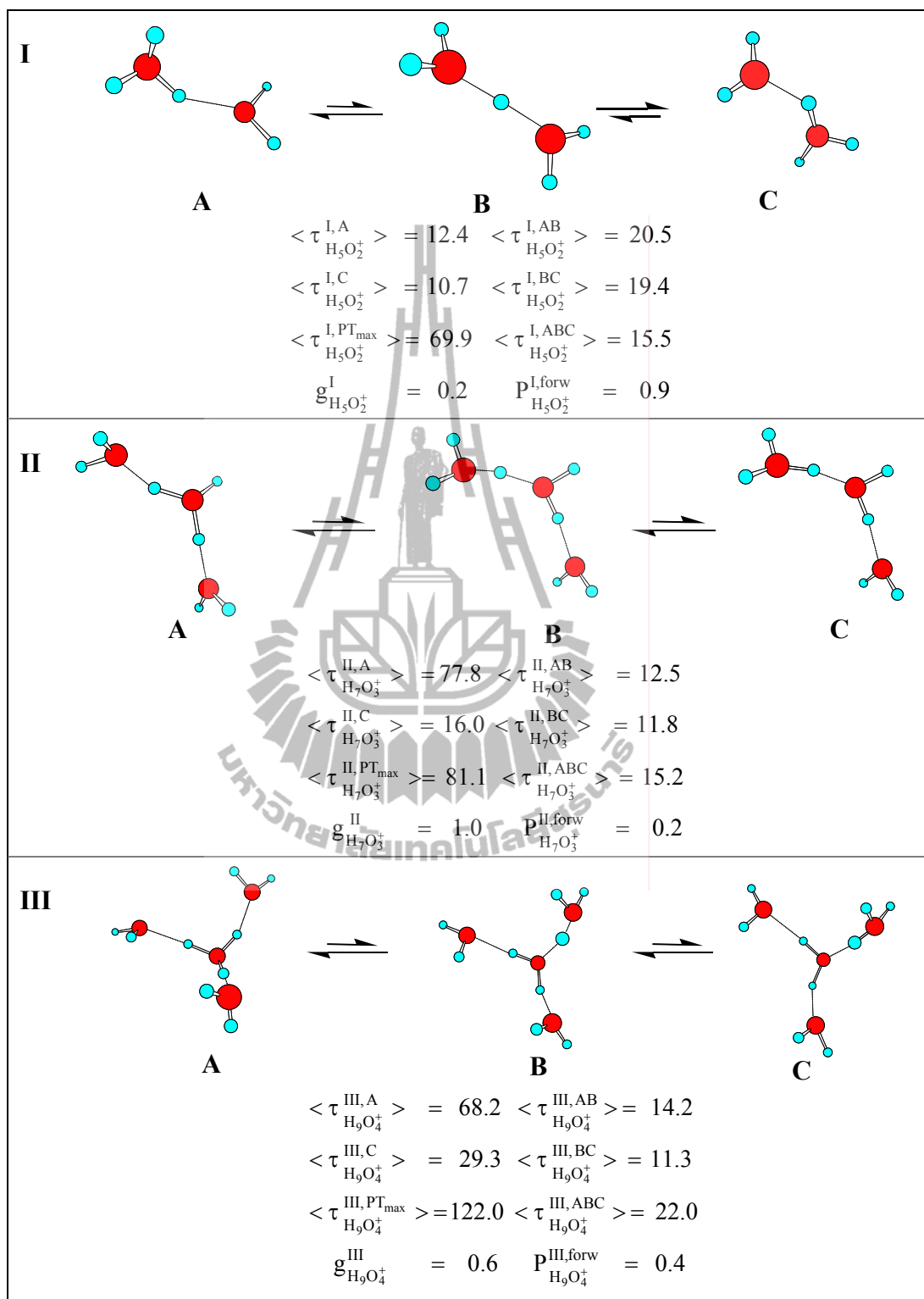


Figure 3.3 Important elementary reactions in proton transfer in the $\text{H}_3\text{O}^+ - \text{H}_2\text{O}$ complexes obtained from BOMD simulations. The symbols are explained in the text.

Proton transfer elementary reactions in the $\text{H}_3\text{O}^+ - \text{H}_2\text{O}$ 1 : n complexes, $1 \leq n \leq 3$, are listed in Figure 3.3. BOMD simulations predicted the average life times of the quasi-dynamic equilibria in H_5O_2^+ , $\langle \tau_{\text{H}_5\text{O}_2^+}^{\text{I,AB}} \rangle$, $\langle \tau_{\text{H}_5\text{O}_2^+}^{\text{I,BC}} \rangle$ and $\langle \tau_{\text{H}_5\text{O}_2^+}^{\text{I,ABC}} \rangle$, to be 20.5, 19.4 and 15.5 fs, respectively. Whereas the average life times of the precursor and product H_3O^+ , $\langle \tau_{\text{H}_5\text{O}_2^+}^{\text{I,A}} \rangle$ and $\langle \tau_{\text{H}_5\text{O}_2^+}^{\text{I,C}} \rangle$, are nearly the same, 12.4 and 10.7 fs, respectively. The average maximum proton transfer cycle time ($\langle \tau_{\text{H}_5\text{O}_2^+}^{\text{I,PT}_{\text{max}}} \rangle$) in this case amounts to 69.9 fs, with $g_{\text{H}_5\text{O}_2^+}^{\text{I}} = 0.2$. This confirms that, on average, small-amplitude vibration with low degree of coherence dominates in H_5O_2^+ . Due to the fact that, BOMD simulations were started from minimum energy geometries, it was not straight forward to predict the preferential proton transfer directions. However, for each proton transfer elementary reaction, the probability for proton transfer in the forward direction ($P_{\text{H}_5\text{O}_2^+}^{\text{I,forw}}$) could be conceivably associated with the average life time of product, which becomes a precursor in the next proton transfer step. Therefore, $P_{\text{H}_5\text{O}_2^+}^{\text{I,forw}}$ was approximated as $\langle \tau_{\text{H}_5\text{O}_2^+}^{\text{I,C}} \rangle / \langle \tau_{\text{H}_5\text{O}_2^+}^{\text{I,A}} \rangle$. Since the product and precursor are the same in H_5O_2^+ , $P_{\text{H}_5\text{O}_2^+}^{\text{I,forw}} = 1$ represents the upper limit of the relative probability for the proton transfer in the forward direction.

Characteristics of the proton transfer profiles for the $\text{H}_3\text{O}^+ - \text{H}_2\text{O}$ 1 : 2 complex (H_7O_3^+) are not substantially different from H_5O_2^+ . The presence of another strong Oh-Hh..Ow H-bond in H_7O_3^+ tends to increase the stability of the central H_3O^+ . Since BOMD results in Figure 3.3 suggested that, $\langle \tau_{\text{H}_7\text{O}_3^+}^{\text{II,A}} \rangle$ and $\langle \tau_{\text{H}_7\text{O}_3^+}^{\text{II,PT}_{\text{max}}} \rangle$

are comparable, one could conclude that, elementary reaction **II** favors large-amplitude vibration, with $g_{\text{H}_7\text{O}_3^+}^{\text{II}} \approx 1$, compared to 0.2 in H_5O_2^+ ; $\langle \tau_{\text{H}_7\text{O}_3^+}^{\text{II,PT}_{\text{max}}} \rangle$ and $\langle \tau_{\text{H}_7\text{O}_3^+}^{\text{II,A}} \rangle$ are 81.1 and 77.8 fs, respectively. In this case, the relative probability for proton transfer in the forward direction ($P_{\text{H}_7\text{O}_3^+}^{\text{II,A}} = \langle \tau_{\text{H}_7\text{O}_3^+}^{\text{II,C}} \rangle / \langle \tau_{\text{H}_7\text{O}_3^+}^{\text{II,A}} \rangle = 0.2$) is considerably lower than H_5O_2^+ . The increase in the stability of the central H_3O^+ is accompanied by shorter average life times of the quasi-dynamic equilibrium; $\langle \tau_{\text{H}_7\text{O}_3^+}^{\text{II,AB}} \rangle$ and $\langle \tau_{\text{H}_7\text{O}_3^+}^{\text{II,BC}} \rangle$ are 12.5 and 11.8 fs, respectively.

Due to couple motions among the three strong Oh-Hh..Ow H-bonds, as well as some H-bond structure reorganizations, proton transfer profiles for the $\text{H}_3\text{O}^+ - \text{H}_2\text{O}$ 1 : 3 complex are more complicated than H_5O_2^+ and H_7O_3^+ . Although the central H_3O^+ in the Eigen complex (H_9O_4^+) is more stabilized than in H_7O_3^+ , the fluctuations of surrounding water dipoles seem to help promote proton transfer reactions; similar to an extended local dynamic disorder which leads to a compression and breaking of H-bonds, as discussed (Kreuer, 1997). BOMD results suggested two important precursors for proton transfer elementary reactions in the $\text{H}_3\text{O}^+ - \text{H}_2\text{O}$ 1 : 3 complex namely, the Eigen complex and a linear H-bond structure. Since proton transfer profiles for the linear H-bond structure are similar to those in H_7O_3^+ , attention was focused on the Eigen complex. For elementary reaction **III** in Figure 3.3, both large- and small-amplitude vibrations were observed in the course of BOMD simulations. Analyses of proton transfer profiles revealed that, due to the couple vibrational

motions, the average life time of the central H_3O^+ ($\langle \tau_{\text{H}_3\text{O}^+}^{\text{III,A}} \rangle$) is shorter than in H_7O_3^+ ($\langle \tau_{\text{H}_7\text{O}_3^+}^{\text{II,A}} \rangle$), but still considerably longer than H_5O_2^+ ($\langle \tau_{\text{H}_5\text{O}_2^+}^{\text{I,A}} \rangle$), 68.2, 77.8 and 12.4 fs respectively. For the Eigen complex, the average maximum proton transfer cycle time ($\langle \tau_{\text{H}_9\text{O}_4^+}^{\text{III,PT,max}} \rangle = 122.0$ fs) is nearly twice longer than the average life time of the precursor ($\langle \tau_{\text{H}_9\text{O}_4^+}^{\text{III,A}} \rangle = 68.2$ fs). This implies that, on average, the probabilities for proton transfers through small- and large-amplitude vibrations are comparable; $g_{\text{H}_9\text{O}_4^+}^{\text{III}} = 0.6$ and $P_{\text{H}_9\text{O}_4^+}^{\text{III,forw}} = \langle \tau_{\text{H}_9\text{O}_4^+}^{\text{III,C}} \rangle / \langle \tau_{\text{H}_9\text{O}_4^+}^{\text{III,A}} \rangle = 0.4$. The former is lower than H_7O_3^+ , but still higher than H_5O_2^+ , whereas the latter could support the previous investigation that, the proton transfer rate is about one order of magnitude lower than the O-O vibration rate (Kreuer, 1997). Since small-amplitude vibration is a characteristic of the Zundel complex, one could conclude that, due to the thermal energy fluctuation and the couple motions among H-bonds, a quasi-dynamic equilibrium between the Eigen and Zundel complexes could be established in the course of BOMD simulations, and considered as the most fundamental elementary reaction in proton transfer process.

The most important property of H_3O^+ , which could be obtained from experiments, is the average life time. Based on approximate Eigen's relationship, the average life time of H_3O^+ was demonstrated to be sensitive to the concentration of acid (Eigen and Maeyer, 1958); as the concentration of the acid increases, so does the average lifetime. This could be one of the reasons, why the average life time of H_3O^+ reported in literatures varies in a quite wide range (Giguere, 1979). For examples,

through the measurements of proton conductance (Conway, Bockris and Linton, 1956), the average life time was estimated to be 240 fs, whereas a higher value, by about one order of magnitude, was derived from dielectric relaxation data (Eigen, 1963). While the measurement of the low frequency (1200 cm^{-1}) in the vibrational spectrum of H_3O^+ requires a minimum life time of only 30 fs (Giguere, 1979), the one obtained from the measurement of ^{17}O -induced proton relaxation in water and very dilute acids amounts to 2.2 ps (Glick and Tewari, 1966; Rabideau and Hetch, 1967). In the present study, the average life time of H_3O^+ in the Eigen complex is within this range. It should be added that, in our model systems, the lack of continuous H-bond network connecting the first and second hydration shells could restrict the mobility of proton, whereas the inclusion of strong interaction between proton and polar environment could lead to a retardation of proton transfer events (Kreuer, 1997). Our $\langle \tau_{\text{H}_3\text{O}^+}^{\text{III,A}} \rangle = 68.2\text{ fs}$ is, however, closer to the lowest limit, estimated from the low-frequency vibrational spectroscopy (Giguere, 1979).

The $\text{CF}_3\text{SO}_3\text{H} - \text{H}_3\text{O}^+ - n\text{H}_2\text{O}$ complexes

Figure 3.4 shows examples of proton transfer profiles for the $\text{CF}_3\text{SO}_3\text{H} - \text{H}_3\text{O}^+ - \text{H}_2\text{O}$ 1 : 1 : 1 complex, with snapshots of H-bond structures observed in the course of BOMD simulations. Three important elementary reactions were extracted from BOMD results and illustrated in Figure 3.5 with all other results. For the $\text{CF}_3\text{SO}_3\text{H} - \text{H}_3\text{O}^+ - \text{H}_2\text{O}$ 1 : 1 : 1 complexes, both large- and small-amplitude vibrations exist in the proton transfer profiles.

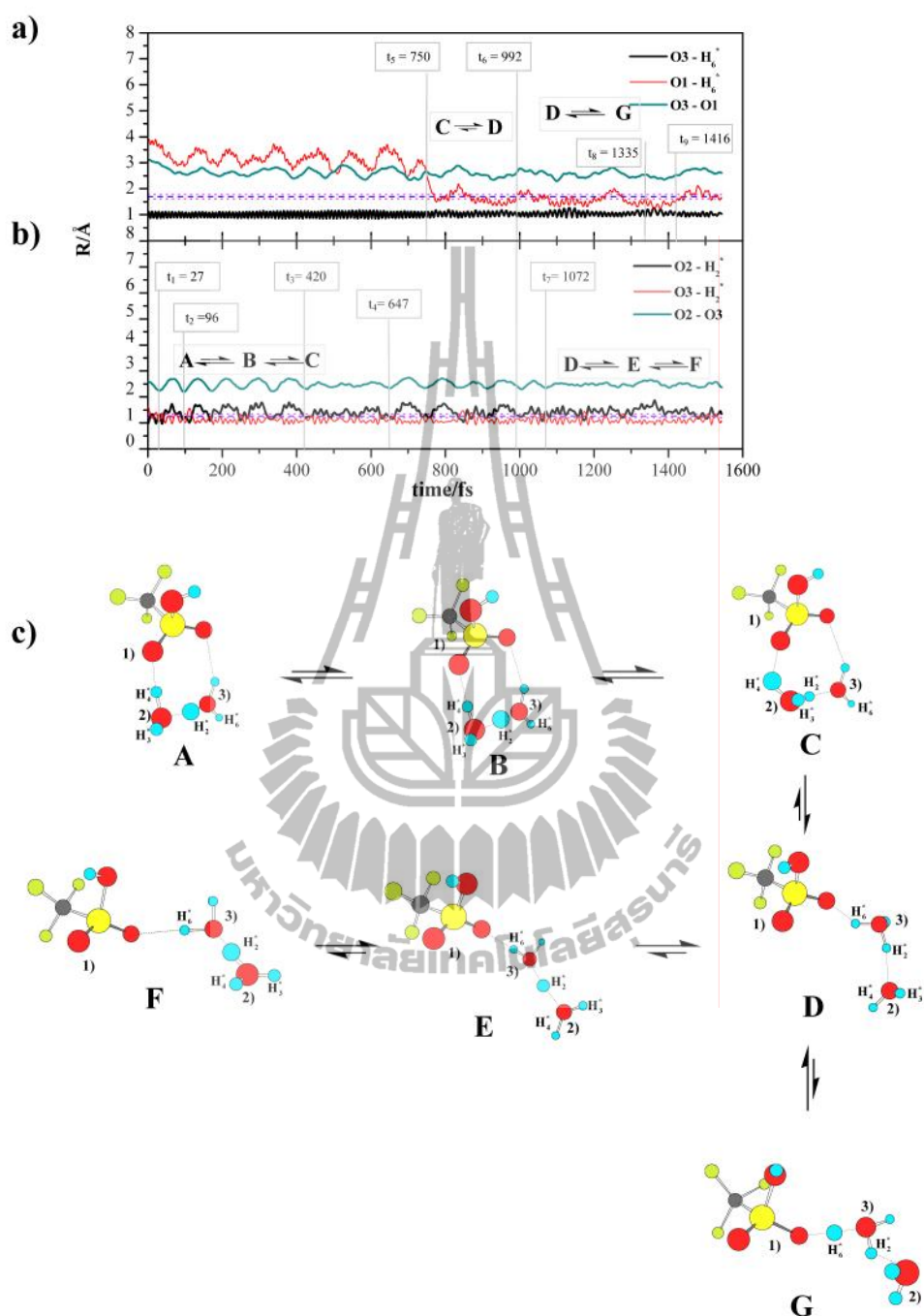


Figure 3.4 Examples of proton transfer profiles for the $\text{CF}_3\text{SO}_3\text{H} - \text{H}_3\text{O}^+ - \text{H}_2\text{O}$

1 : 1 : 1 complexes, with snapshots H-bond structures observed in the course of BOMD. a) – b) BOMD starting from structure **a** in Figure 3.1. c) – d) Snapshots of H-bond structures.

In Figure 3.4b, large-amplitude vibrations are seen, for example, between $t_1 = 27$ fs and $t_3 = 420$ fs, within which quasi-dynamic equilibria followed by actual proton transfers in the reverse direction are seen in general. Small-amplitude vibrations are, for example, from $t_3 = 420$ fs to $t_4 = 647$ fs. Starting from structure **a** in Table 3.3, the H-bond proton (H_2^* in Figure 3.4c) moved in the course of BOMD simulations from O2 to O3, resulting in structure **A** in Figure 3.4c. The proton transfer profile in Figure 3.4a and the snapshots in Figure 3.4c reveal an example of the H-bond structure reorganization from cyclic to linear. At $t_5 = 750$ fs, H_6^* forms H-bond with an oxygen atom of $-SO_3H$, then structure **C** changes to structure **D**. Structures **D**, **E** and **F** show a possibility for proton transfer away from $-SO_3H$, whereas structure **G** for proton transfer in the reverse direction; forming $-SO_3H_2^+$ between $t_8 = 1335$ fs and $t_9 = 1416$ fs. The probability for proton transfer through the formation of $-SO_3H_2^+$ is higher for structure **c** in Figure 3.1. Starting from structure **c**, $-SO_3H_2^+$ was generated right at the beginning of BOMD simulations. Snapshots in Figure 3.4d reveal that, structure **A** acts as a precursor and proton transfer could be mediated by $-SO_3H_2^+$ in both directions; from structures **A** to **B** to **C**, as well as from structures **A** to **D** to **E**. Since there is no water molecule to stabilize the product (H_3O^+), both structures **C** and **E** return to structure **A**, as also recognized in the case of $H_7O_3^+$.

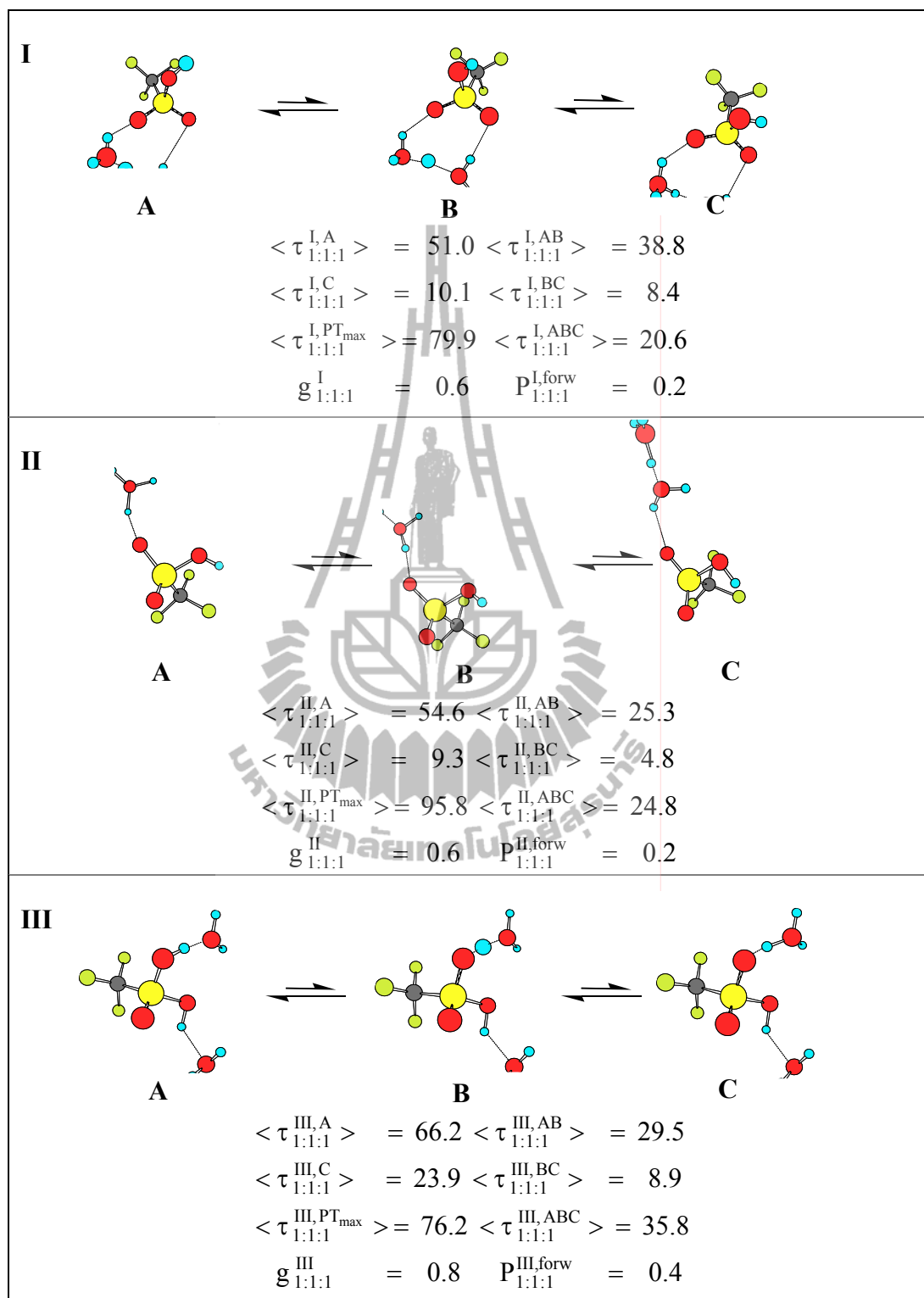


Figure 3.5 Important elementary reactions in proton transfer in the $\text{CF}_3\text{SO}_3\text{H} - \text{H}_3\text{O}^+ - \text{H}_2\text{O}$ 1 : 1 : 1 complexes, obtained from BOMD. The symbols are explained in details in the text.

The results in Figure 3.5 show that, due to limited number of water molecule, the products in elementary reactions **I** and **II** were observed in short times. $\langle \tau_{1:1:1}^{I,C} \rangle$ and $\langle \tau_{1:1:1}^{II,C} \rangle$ are 10.1 and 9.3 fs, respectively, compared to the life times of the precursors, $\langle \tau_{1:1:1}^{I,A} \rangle$ and $\langle \tau_{1:1:1}^{II,A} \rangle$, of 51.0 and 54.6 fs, respectively. For elementary reaction **I**, the quasi-dynamic equilibrium between the precursor and the transition state ($\langle \tau_{1:1:1}^{I,AB} \rangle$) is 38.8 fs, with the average maximum proton transfer cycle time ($\langle \tau_{1:1:1}^{I,PT_{max}} \rangle$) of 79.9 fs; whereas those of elementary reaction **II** are 25.3 and 95.8 fs, respectively. The values of $g_{1:1:1}^I$ and $P_{1:1:1}^{I,forw}$, as well as $g_{1:1:1}^{II}$ and $P_{1:1:1}^{II,forw}$ in Figure 3.5, indicate that, the degree of coherence in elementary reactions **I** and **II** are comparable with $H_9O_4^+$, with lower probability for proton transfer in the forward direction; $P_{1:1:1}^{I,forw}$ and $P_{1:1:1}^{II,forw}$ are only 0.2. Elementary reaction **III** in Figure 3.5 involves proton transfer through $-SO_3H_2^+$. Although elementary reaction **III** possesses the highest degree of coherence, $g_{1:1:1}^{III} = 0.8$, the probability for proton transfer from $-SO_3H_2^+$ and the life time of the product are the highest; $P_{1:1:1}^{III,forw} = 0.4$ and $\langle \tau_{1:1:1}^{III,C} \rangle = 23.9$ fs. These confirm the possibility that $-SO_3H_2^+$ could represent an effective transition state in proton transfer pathway at low hydration levels (Glezakou, Dupuis and Mundy, 2007).

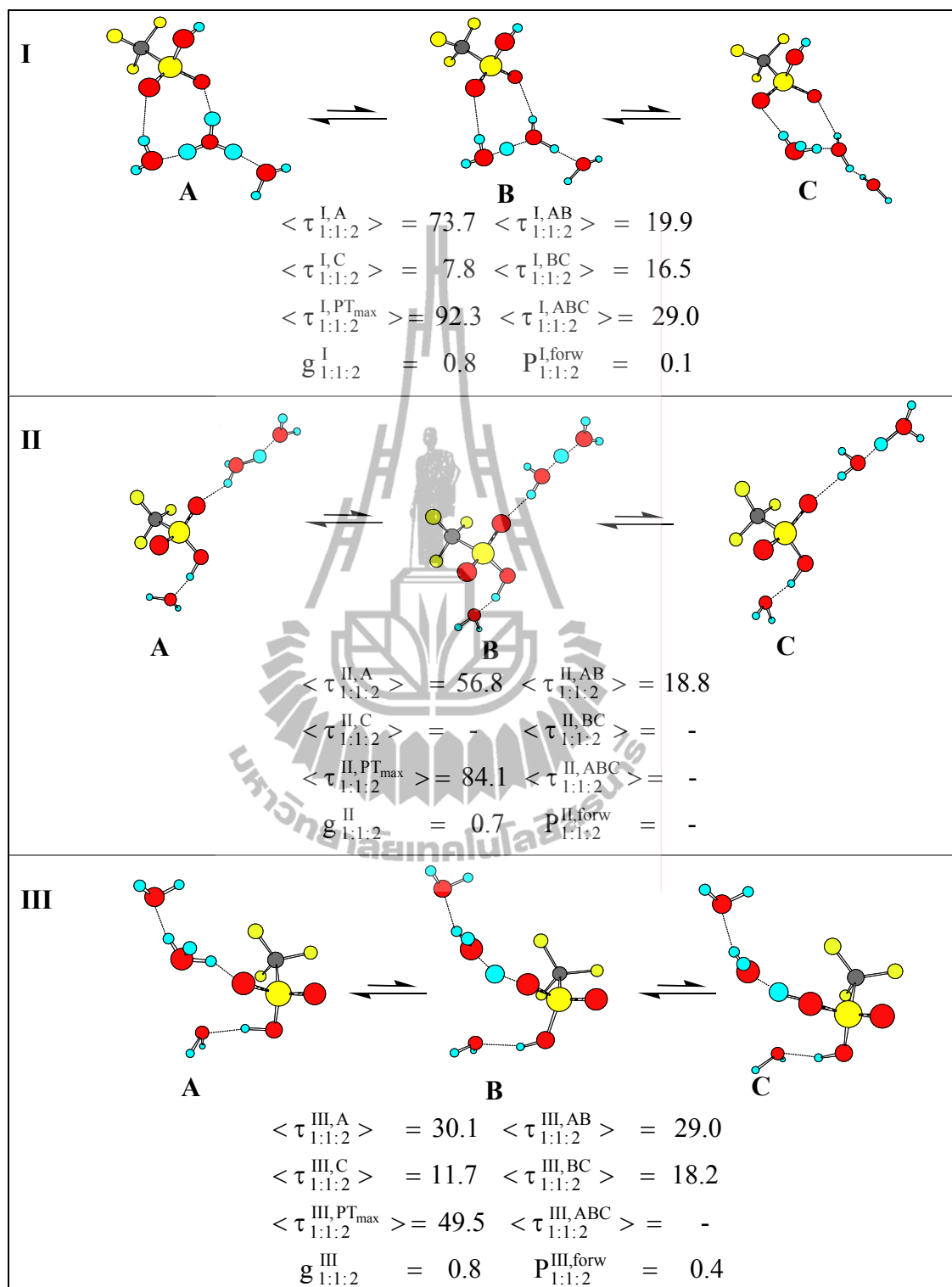


Figure 3.6 Important elementary reactions in proton transfer in the $\text{CF}_3\text{SO}_3\text{H} - \text{H}_3\text{O}^+ - \text{H}_2\text{O}$ 1 : 1 : 2 complexes, obtained from BOMD. The symbols are explained in details in the text.

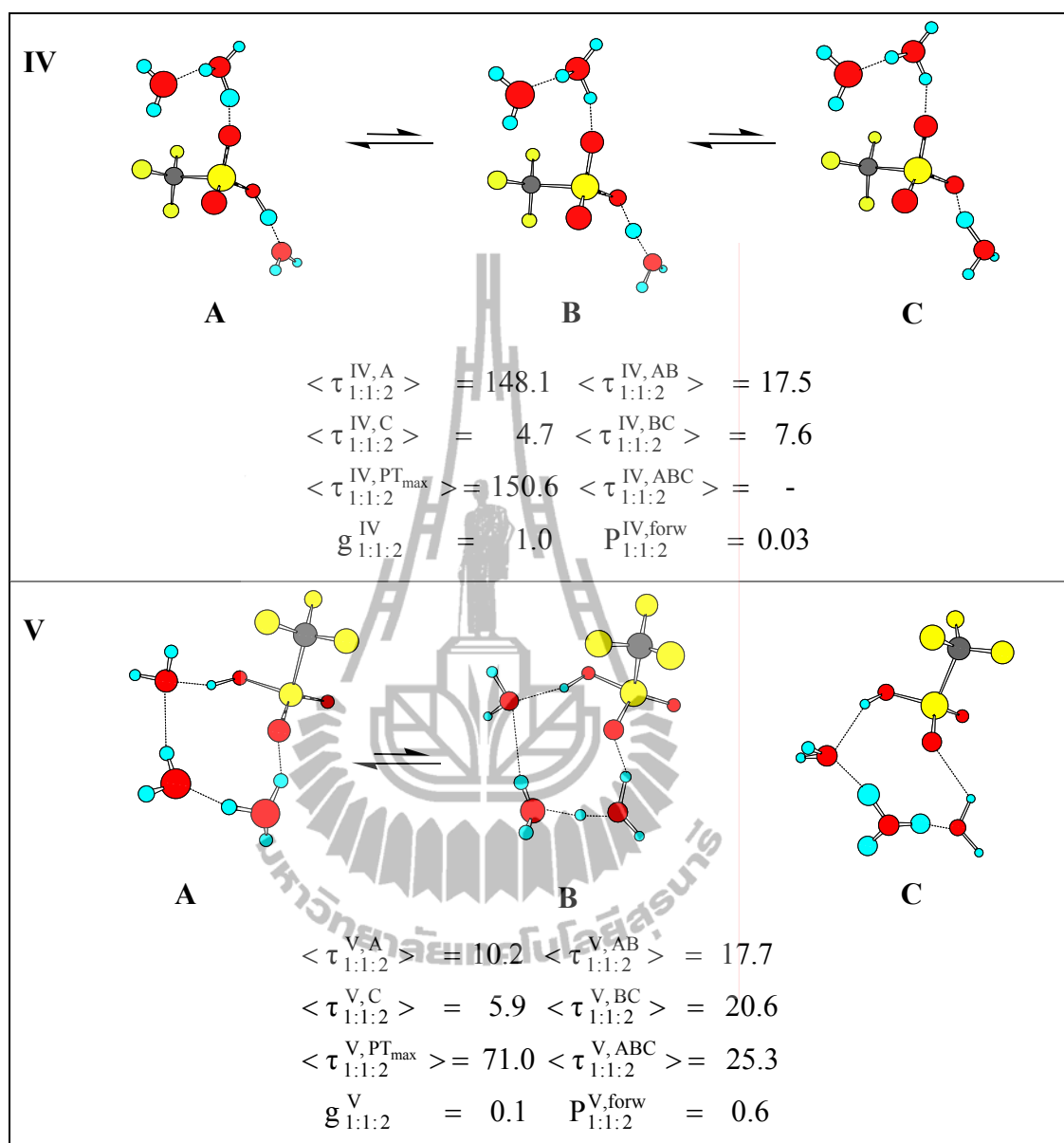


Figure 3.6 (Continued).

For the $\text{CF}_3\text{SO}_3\text{H} - \text{H}_3\text{O}^+ - \text{H}_2\text{O}$ 1 : 1 : 2 complexes, five important proton transfer elementary reactions could be extracted from BOMD results. The extension of the H-bond network in the vicinities of $-\text{SO}_3\text{H}$ could bring about both stabilization and destabilization effects to H_3O^+ , depending upon the H-bond structures. Comparison of the results in Figures 3.5 and 3.6 shows that, for elementary reaction **I**, the average life times of the precursor ($\langle \tau_{1:1:2}^{\text{I,A}} \rangle$), as well as the quasi-dynamic equilibrium ($\langle \tau_{1:1:2}^{\text{I,ABC}} \rangle$), are increased when H_3O^+ is triply H-bonded; the former is 73.7 fs, and the latter is 29.0 fs. These are accompanied by an increase in the degree of coherence and a decrease in the average life time of the product, $g_{1:1:2}^{\text{I}} = 0.8$ and $\langle \tau_{1:1:2}^{\text{I,C}} \rangle = 7.8$ fs, as well as a decrease in the probability for proton transfer in the forward direction, $P_{1:1:2}^{\text{I,forw}} = 0.1$.

Elementary reactions **II**, **III** and **IV** in Figure 3.6 represent three possibilities for proton transfers along the linear H-bonds at $-\text{SO}_3\text{H}$. For elementary **II**, the extension of the H-bond network, through the formation of the $\text{O}-\text{H} \cdots \text{Ow}$ H-bond, brings about higher stability to H_3O^+ . This makes it difficult for H_3O^+ to transfer proton to the adjacent water. Comparison of $P_{1:1:1}^{\text{II,forw}}$ and $P_{1:1:2}^{\text{II,forw}}$ in Figures 3.5 and 3.6 shows that, due to an increase in the stability of H_3O^+ in elementary reaction **II**, the probability for proton transfer away from $-\text{SO}_3\text{H}$ is considerably decreased; structure **C** which is the product was rarely found in the course of BOMD simulations. Comparison of elementary reaction **III** in Figures 3.5 and 3.6 reveals a similar trend

namely, the probability for H_3O^+ to protonate at $-\text{SO}_3\text{H}$ is reduced upon the Oh-Hh..Ow H-bond formation, with a shorter average life time of $-\text{SO}_3\text{H}_2^+$, $\langle \tau_{1:1:2}^{\text{III,C}} \rangle = 11.7$ fs, compared to $\langle \tau_{1:1:1}^{\text{III,A}} \rangle = 66.2$ fs. Elementary reaction **IV** shows a small probability to detect $-\text{SO}_3^-$ in the course of BOMD simulations, with $P_{1:1:2}^{\text{IV,forw}} = 0.03$. In this case, large-amplitude vibration with $g_{1:1:2}^{\text{IV}} \approx 1.0$, dominates and the charged product possesses very short average life time, $\langle \tau_{1:1:2}^{\text{IV,C}} \rangle = 4.7$ fs. The stability of H_3O^+ and the degree of coherence in H-bond are substantially reduced upon larger cyclic H-bond network formation; $\langle \tau_{1:1:2}^{\text{V,A}} \rangle$ and $g_{1:1:2}^{\text{V}}$ for elementary reaction **V** are 10.2 fs and 0.14, respectively. The values are close to those in H_5O_2^+ . Since the average life times of both precursor and the product are small, the probability for proton transfer in the forward direction is the highest among the $\text{CF}_3\text{SO}_3\text{H} - \text{H}_3\text{O}^+ - \text{H}_2\text{O}$ 1 : 1 : 2 complexes, with $P_{1:1:2}^{\text{V,forw}} = 0.6$.

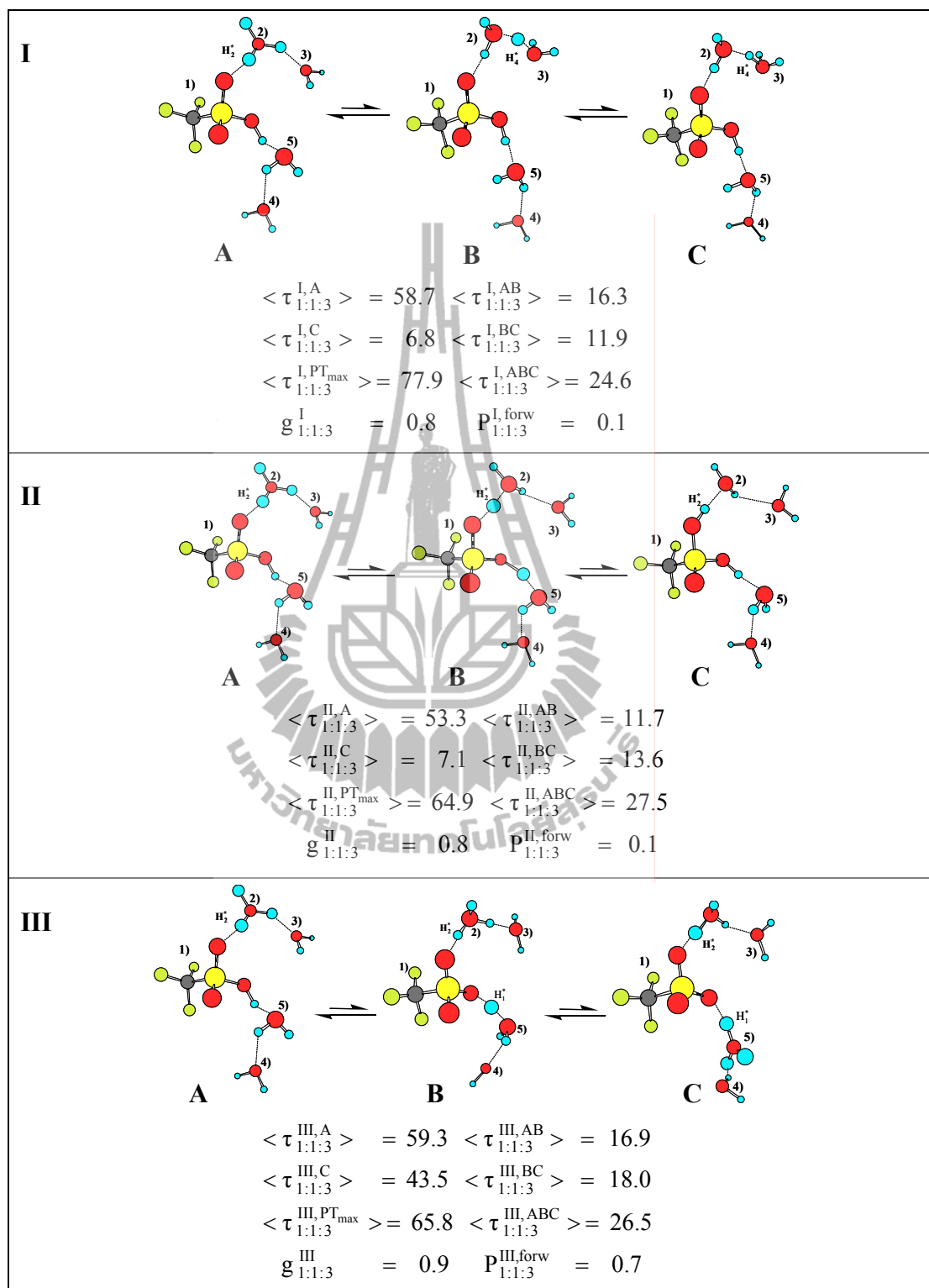


Figure 3.7 Important elementary reactions in proton transfer in the $\text{CF}_3\text{SO}_3\text{H} - \text{H}_3\text{O}^+ - \text{H}_2\text{O}$ 1 : 1 : 3 complexes, obtained from BOMD. The symbols are explained in details in the text.

Due to high degree of freedom in the $\text{CF}_3\text{SO}_3\text{H} - \text{H}_3\text{O}^+ - \text{H}_2\text{O}$ 1 : 1 : 3 complexes, only linear H-bonds were observed in the course of BOMD simulations. Elementary reactions **I**, **II** and **III** in Figure 3.7 represent three possibilities for proton transfer along the H-bond network passing through $-\text{SO}_3\text{H}$. Large-amplitude vibrations seem to dominate in elementary reactions **I** and **II**, with $g_{1:1:3}^{\text{I}}$ and $g_{1:1:3}^{\text{II}}$ of 0.8. Elementary reactions **I** and **II** show that, when the H-bond network is well connected on both sides of $-\text{SO}_3\text{H}$, the stability of H_3O^+ is increased. This tends to reduce the probability for the proton transfers from H_3O^+ to H_2O , as well as from H_3O^+ to $-\text{SO}_3\text{H}$; both $P_{1:1:3}^{\text{I,forw}}$ and $P_{1:1:3}^{\text{II,forw}}$ are only about 0.1. The former reflects the possibility for proton transfer away from $-\text{SO}_3\text{H}$, and the latter for the formation of $-\text{SO}_3\text{H}_2^+$. Elementary reaction **III** reveals a quite high possibility for proton transfer through the formation of $-\text{SO}_3^-$, through an ion-pair complex similar to structure **e** in Table 3.5. The results in Figure 3.7 indicate further that, for elementary reaction **III**, large-amplitude vibration dominates, with $g_{1:1:3}^{\text{III}} = 0.9$, and the probability for proton transfer in the forward direction is the highest among the $\text{CF}_3\text{SO}_3\text{H} - \text{H}_3\text{O}^+ - \text{H}_2\text{O}$ 1 : 1 : 3 complexes, with $P_{1:1:3}^{\text{III,forw}} = 0.7$. The latter is slightly higher than $P_{1:1:2}^{\text{V,forw}}$.

3.2 Part II

3.2.1 Static results

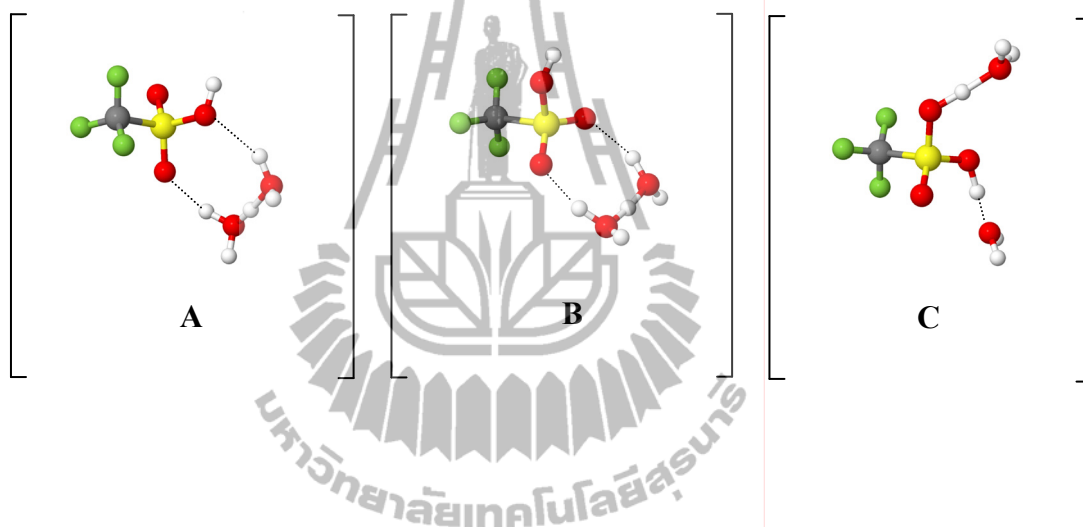
Structures and energetic

The equilibrium structures, ΔE and ΔE^{sol} of the $\text{CF}_3\text{SO}_3\text{H} - \text{H}_3\text{O}^+ - n\text{H}_2\text{O}$ complexes, $1 \leq n \leq 3$, in the gas phase and continuum aqueous solution are shown in Table 3.5, together with Δd_{DA} and v^{OH} . The trends of ΔE and ΔE^{sol} with respect to the number of water molecules are presented in Figure 3.8.

It appeared that the refined structures are the same as those obtained from B3LYP/6-31G(d,p) calculations (Table 3.4). The trends of ΔE with respect to the number of water molecules in the gas phase and continuum aqueous solution are similar, with smaller variations in continuum aqueous solution. The destabilization effects caused by the continuum aqueous solvent are quite large, ranging from 120 kJ/mol in the complex to 235 kJ/mol in the $\text{CF}_3\text{SO}_3\text{H} - \text{H}_3\text{O}^+ - 3\text{H}_2\text{O}$ complex; for the H-bond complexes with the same number of water molecules, the H-bonds inside the clusters experience comparable uniform electric field (COSMO). Figure 3.8 also revealed that ΔE^{sol} are not substantially different. The environmental effects on the stabilities of charged H-bonds were investigated using *ab initio* SCRF (self-consistent reaction field) calculations at the Hartree-Fock level, from which the dependence of ΔE on a wide range of dielectric constant (ϵ) was established (Chen, McAllister, Lee and Houk, 1998). It was demonstrated that small increases in ϵ from the gas-phase

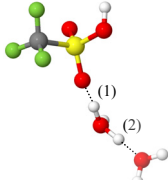
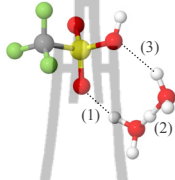
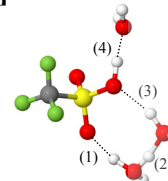
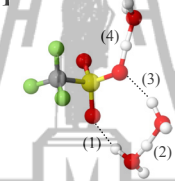
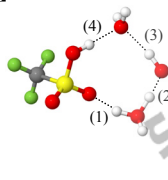
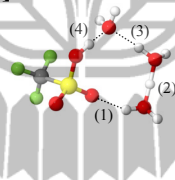
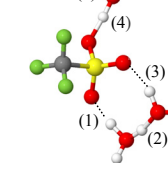
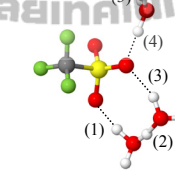
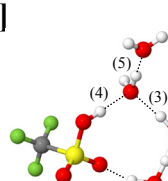
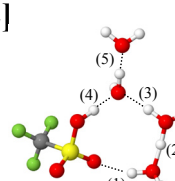
value ($\epsilon=1$) rapidly reduce the stabilities of the charged H-bonds, which is in accordance with the present results.

The results in Table 3.5 anticipated three $\text{CF}_3\text{SO}_3\text{H} - \text{H}_3\text{O}^+ - \text{H}_2\text{O}$ complexes as the most basic intermediate states in proton transfer pathways.



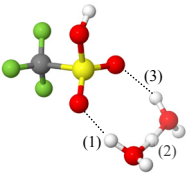
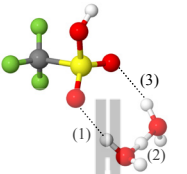
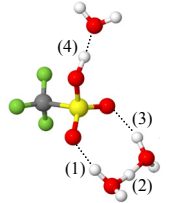
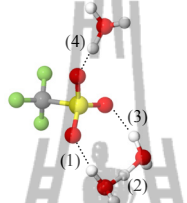
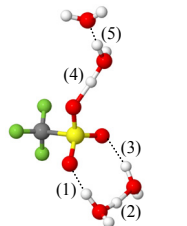
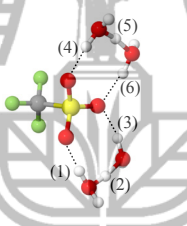
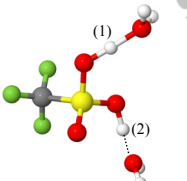
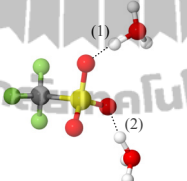
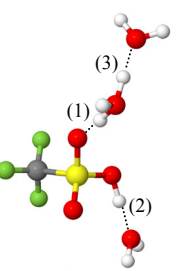
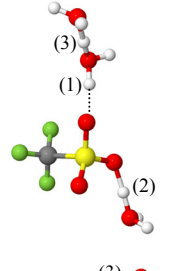
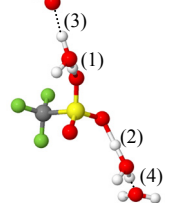
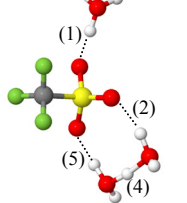
Structures **A** and **B** are represented by the Zundel complex H-bonding at two oxygen atoms of the $-\text{SO}_3\text{H}$ group. In structure **C**, $-\text{SO}_3\text{H}$ separates H_3O^+ and H_2O . The H-bonding features in structures **A**, **B** and **C** suggested two important structural diffusion mechanisms at the $-\text{SO}_3\text{H}$ group. Since the $-\text{SO}_3\text{H}$ group in structure **C** could be protonated or deprotonated and directly involved in proton transfer, one could regard the structural diffusion through structure **C** as the “pass-through” mechanism. Likewise, since the energetic and dynamics of the proton in the Zundel complex can be affected by the $-\text{SO}_3\text{H}$ group, one could consider the proton transfer through structures **A** and **B** as the “pass-by” mechanism.

Table 3.5 Energies of the $\text{CF}_3\text{SO}_3\text{H}\cdot\text{H}_3\text{O}^+\cdot n\text{H}_2\text{O}$ complexes, $1 \leq n \leq 3$, obtained from B3LYP/TZVP calculations, both in the gas phase and continuum aqueous solution. Energies are in kJ mol^{-1} .

	Gas	COSMO	ΔE	ΔE^{sol}
A1G		A1C 	-241.7(-63.5)	-272.3
A2G-[1]		A2C-[1] 	-316.9(-109.0)	-276.3
A2G-[2]		A2C-[2] 	-308.0(-115.6)	-291.9
A3G-[1]		A3C-[1] 	-398.3(-155.6)	-275.3
A3G-[2]		A3C-[2] 	-380.3(-146.1)	-283.8

ΔE = interaction energy; ΔE^{sol} = solution energy. (..) = continuum aqueous solution (COSMO).

Table 3.5 (Continued).

Gas	COSMO	ΔE	ΔE^{sol}
B1G 	B1C 	-239.8(-60.4)	-271.1
B2G 	B2C 	-327.6(-117.0)	-273.6
B3G 	B3C 	-398.7(-162.9)	-282.2
C1G 	C1C 	-225.5(-59.7)	-284.7
C2G 	C2C 	-323.8(-111.7)	-272.1
C3G 	C3C 	-387.1(-159.7)	-290.6

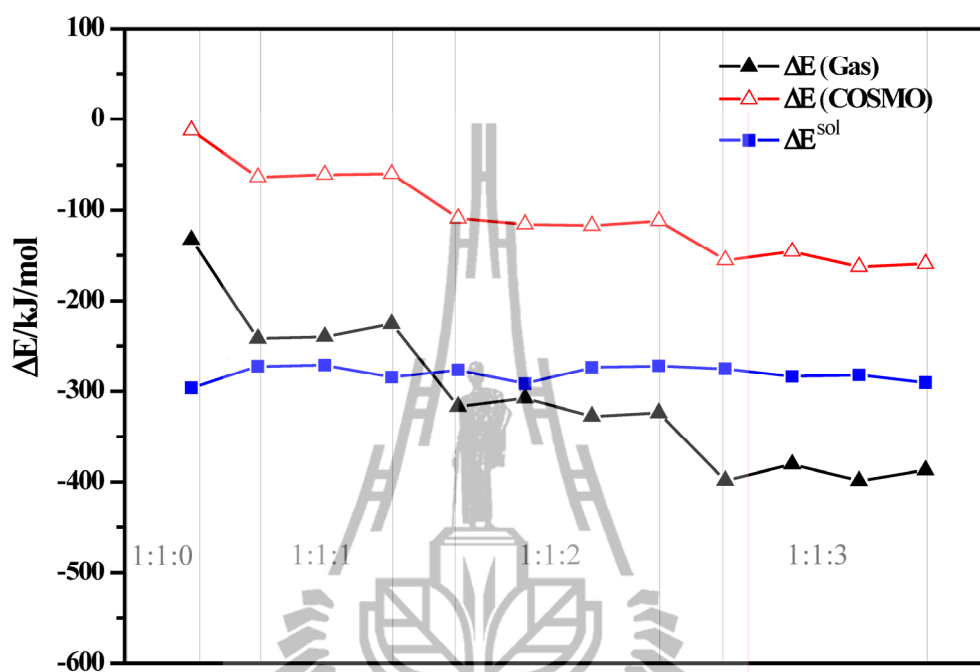


Figure 3.8 The trends of the interaction (ΔE) and solvation energies (ΔE^{sol}) with respect to the number of water molecules, obtained from B3LYP/TZVP calculations:

-▲- = ΔE in the gas phase; -△- = ΔE in continuum aqueous solution; -■- = ΔE^{sol} .

In order to simplify the discussion, the H-bond structures in Table 3.5 are labeled with three or four-character code; according to the basic intermediate states (**A**, **B** or **C**); the number of water molecules (**n**); in the gas phase (**G**) or continuum aqueous solution (**C**). Different H-bond structures with the same basic intermediate state and number of water molecule are distinguished by [**m**]. As examples, based on the four-character code, **A2G-[1]** and **A2G-[2]** represent different H-bond structures ([**1**] and [**2**]) with the same intermediate state and number of water molecules (**A2**) in the gas phase (**G**), whereas **A2G-[1]** and **A2C-[1]**, the same H-bond structure with two water molecules (**A2** and [**1**]) in the gas phase (**G**) and continuum aqueous solution (**C**), respectively.

Harmonic IR frequencies

H-bond distances (R_{O-O}), asymmetric stretching coordinates (Δd_{DA}) and O-H stretching frequency (ν^{OH}) are presented in Table 3.6. Attempt was made to distinguish between normal and strong H-bonds in the protonated water clusters (Lao-ngam, Asawakun, Wannarat and Sagarik, 2011). B3LYP/TZVP calculations showed that the “critical distance” (R_{O-O}^*), the H-bond distance at which symmetric double-well potential with a barrier at the center is transformed into single-well potential without barrier, and the threshold asymmetric O-H stretching frequencies for proton transfers (ν^{OH*}) could be approximated from the plots of Δd_{DA} and R_{O-O} , ν^{OH} and R_{O-O} , and ν^{OH} and Δd_{DA} . The relationship between Δd_{DA} and R_{O-O} could be represented by a linear function, ν^{OH} and R_{O-O} by an exponential function similar to the integrated rate expression for the first order reaction, and ν^{OH} and Δd_{DA} by an

exponential function resembling the normal distribution function. For the protonated water clusters (Lao-ngam, Asawakun, Wannarat and Sagarik, 2011) calculations of the second derivatives of the plots of ν^{OH} and Δd_{DA} gave two inflection points, in the gas phase at $\Delta d_{\text{DA}}^* = 0.33 \text{ \AA}$ and in continuum aqueous solution at $\Delta d_{\text{DA}}^* = 0.36 \text{ \AA}$. The values correspond to $\nu^{\text{OH}*} = 1984$ and 1881 cm^{-1} , respectively.

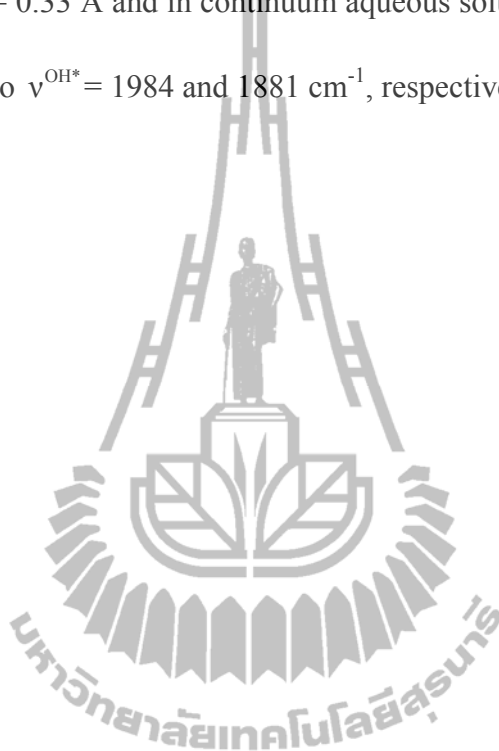


Table 3.6 H-bond distances, asymmetric stretching coordinates (Δd_{DA}) and O-H stretching frequencies of the $\text{CF}_3\text{SO}_3\text{H}-\text{H}_3\text{O}^+-n\text{H}_2\text{O}$ complexes, $1 \leq n \leq 3$, obtained from B3LYP/TZVP calculations. They are in Å, Å and cm^{-1} , respectively.

Gas				COSMO			
H-bond	$R_{\text{O-O}}$	Δd_{DA}	ν^{OH}	H-bond	$R_{\text{O-O}}$	Δd_{DA}	ν^{OH}
(1)	2.55	0.52	2788	(1)	2.75	0.83	3347
(2)	2.47	0.36	2218	(2)	2.43	0.20*	1223*
(3)	-	-	-	(3)	3.05	1.26	3577

$R_{\text{O-O}}$ = H-bond distance; Δd_{DA} = asymmetric stretching coordinate; ν^{OH} = asymmetric O-H stretching frequency; * = H-bond susceptible to proton transfer.

Table 3.6 (Continued).

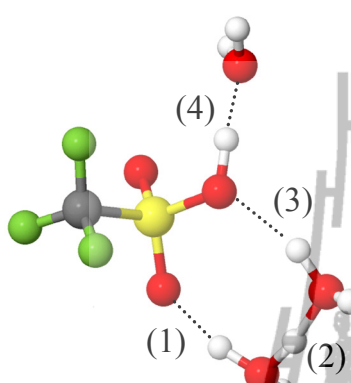
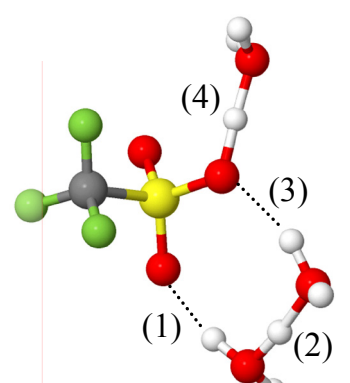
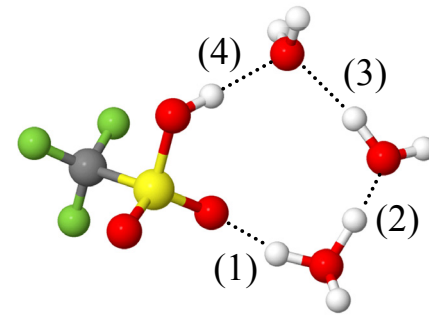
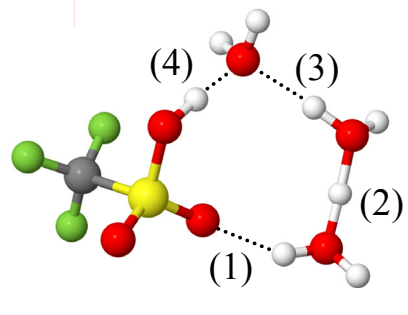
Gas				COSMO			
A2G-[1] 				A2C-[1] 			
H-bond	R _{O-O}	Δd_{DA}	ν^{OH}	H-bond	R _{O-O}	Δd_{DA}	ν^{OH}
(1)	2.59	0.62	3029	(1)	2.72	0.79	3320
(2)	2.44	0.27*	1893*	(2)	2.43	0.21*	1230*
(3)	2.89	1.01	3490	(3)	2.96	1.09	3525
(4)	2.54	0.47	2498	(4)	2.41	0.06*	905*
A2G-[2] 				A2C-[2] 			
H-bond	R _{O-O}	Δd_{DA}	ν^{OH}	H-bond	R _{O-O}	Δd_{DA}	ν^{OH}
(1)	2.54	0.56	2873	(1)	2.69	0.84	3422
(2)	2.45	0.30	1985	(2)	2.41	0.07*	823*
(3)	2.85	0.90	3396	(3)	2.79	0.84	3292
(4)	2.79	0.83	3233	(4)	2.57	0.51	2509

Table 3.6 (Continued).

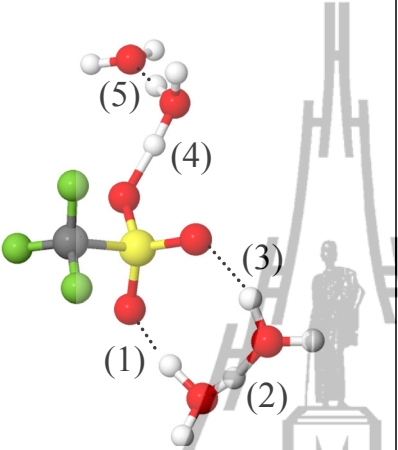
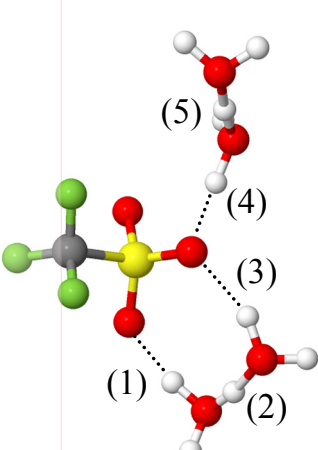
Gas				COSMO			
A3G-[1]				A3C-[1]			
							
H-bond	R _{O-O}	Δd_{DA}	ν^{OH}	H-bond	R _{O-O}	Δd_{DA}	ν^{OH}
(1)	2.54	0.50	2645	(1)	2.63	0.66	3071
(2)	2.44	0.27 [*]	1848 [*]	(2)	2.44	0.25 [*]	1345 [*]
(3)	2.74	0.84	3353	(3)	2.86	0.96	3449
(4)	2.43	0.27 [*]	1877 [*]	(4)	2.62	0.61	2876
(5)	2.54	0.48	2659	(5)	2.44	0.26 [*]	1735 [*]

Table 3.6 (Continued).

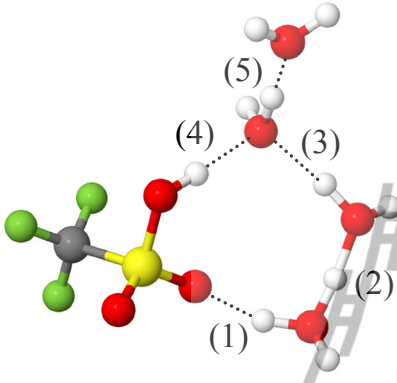
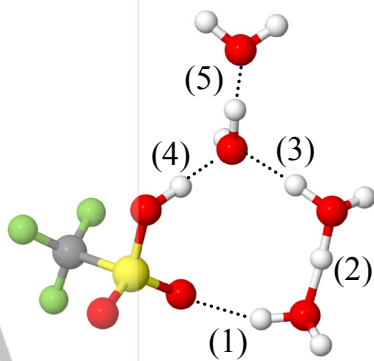
Gas				COSMO			
A3G-[2]				A3C-[2]			
							
H-bond	R _{O-O}	Δd_{DA}	ν^{OH}	H-bond	R _{O-O}	Δd_{DA}	ν^{OH}
(1)	2.56	0.58	2940	(1)	2.81	0.90	3460
(2)	2.43	0.21 [*]	1335 [*]	(2)	2.44	0.24 [*]	1374 [*]
(3)	2.73	0.75	3211	(3)	2.62	0.61	2910
(4)	2.70	0.71	2997	(4)	2.56	0.48	2373
(5)	2.65	0.65	3077	(5)	2.60	0.58	2731

Table 3.6 (Continued).

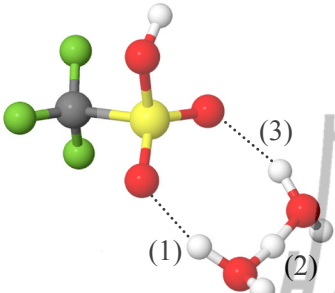
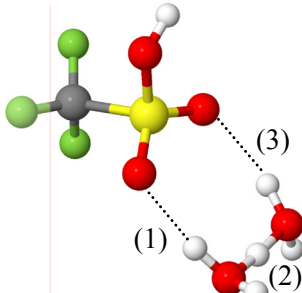
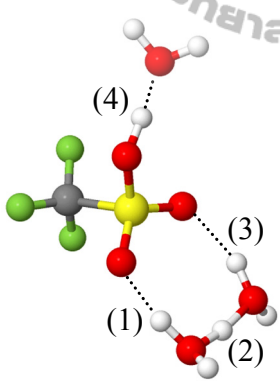
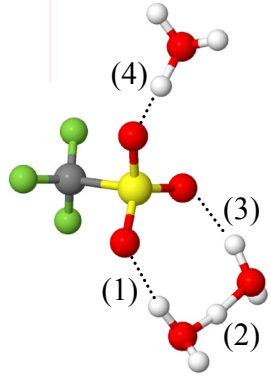
Gas				COSMO			
B1G 				B1C 			
H-bond	R _{O-O}	Δd_{DA}	ν^{OH}	H-bond	R _{O-O}	Δd_{DA}	ν^{OH}
(1)	2.70	0.76	3239	(1)	2.81	0.93	3439
(2)	2.42	0.14*	1100*	(2)	2.43	0.18*	1134*
(3)	2.80	0.96	3454	(3)	3.01	1.16	3537
B2G 				B2C 			
H-bond	R _{O-O}	Δd_{DA}	ν^{OH}	H-bond	R _{O-O}	Δd_{DA}	ν^{OH}
(1)	2.62	0.65	3026	(1)	2.69	0.73	3163
(2)	2.43	0.20*	1333*	(2)	2.43	0.17*	1068*
(3)	2.80	0.91	3422	(3)	2.81	0.91	3417
(4)	2.53	0.45	2434	(4)	2.45	0.30*	1843*

Table 3.6 (Continued).

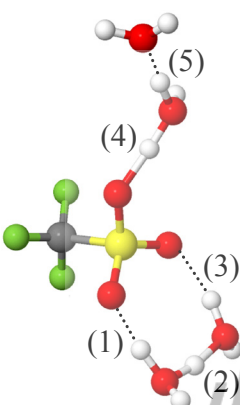
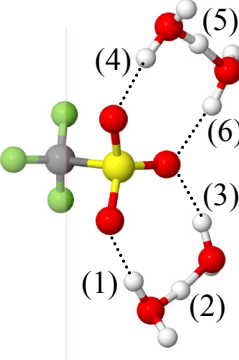
Gas				COSMO			
B3G 				B3C 			
H-bond	R _{O-O}	Δd_{DA}	ν^{OH}	H-bond	R _{O-O}	Δd_{DA}	ν^{OH}
(1)	2.55	0.51	2691	(1)	2.65	0.68	3085
(2)	2.44	0.25*	1407*	(2)	2.43	0.22*	1276*
(3)	2.74	0.83	3334	(3)	2.81	0.91	3416
(4)	2.43	0.26*	1526*	(4)	2.66	0.69	3109
(5)	2.54	0.50	2679	(5)	2.43	0.21*	1221*
(6)	-	-	-	(6)	2.81	0.90	3399

Table 3.6 (Continued).

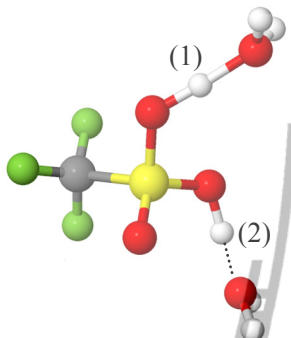
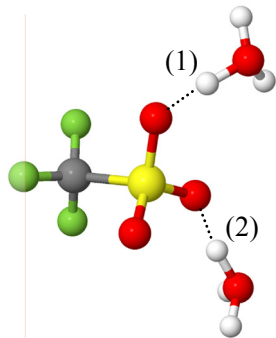
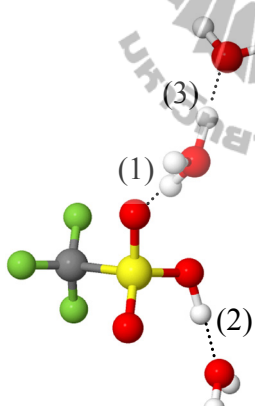
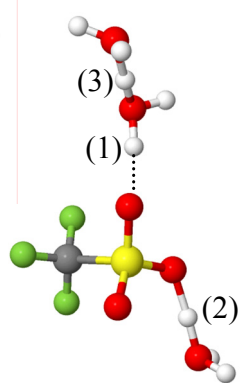
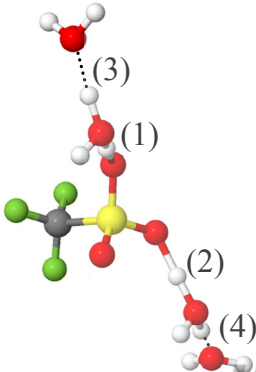
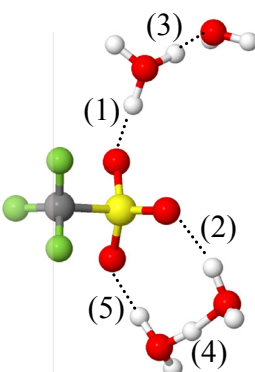
Gas				COSMO			
C1G 				C1C 			
H-bond	R _{O-O}	Δd_{DA}	ν^{OH}	H-bond	R _{O-O}	Δd_{DA}	ν^{OH}
(1)	2.44	0.23 [*]	1724 [*]	(1)	2.47	0.33	1970
(2)	2.49	0.37	2196	(2)	2.46	0.35	2076
C2G 				C2C 			
H-bond	R _{O-O}	Δd_{DA}	ν^{OH}	H-bond	R _{O-O}	Δd_{DA}	ν^{OH}
(1)	2.49	0.41	2324	(1)	2.61	0.61	2967
(2)	2.55	0.49	2599	(2)	2.43	0.21 [*]	1413 [*]
(3)	2.50	0.42	2516	(3)	2.45	0.27 [*]	1717 [*]

Table 3.6 (Continued).

Gas				COSMO			
C3G				C3C			
							
H-bond	R _{O-O}	Δd_{DA}	ν^{OH}	H-bond	R _{O-O}	Δd_{DA}	ν^{OH}
(1)	2.44	0.24 [*]	1809 [*]	(1)	2.59	0.57	2876
(2)	2.43	0.22 [*]	1708 [*]	(2)	2.65	0.66	3032
(3)	2.55	0.51	2715	(3)	2.45	0.29 [*]	1805 [*]
(4)	2.55	0.52	2760	(4)	2.43	0.20 [*]	1201 [*]
(5)	-	-	-	(5)	2.78	0.88	3390

In the present study, to estimate $\nu^{\text{OH}*}$, Δd_{DA} and $R_{\text{O-O}}$, ν^{OH} and $R_{\text{O-O}}$ and ν^{OH} and Δd_{DA} for the pass-through mechanism were plotted and shown in Figure 3.9a to 2c, respectively, whereas for the pass-by mechanism in Fig. 2d to 2f, respectively. The agreements between the fitted functions and the values obtained from B3LYP/TZVP calculations are shown in Figure 3.9. For the pass-through mechanism in the gas phase, the inflection point is seen in Figure 3.9c at $\nu^{\text{OH}*} = 2162 \text{ cm}^{-1}$ and $\Delta d_{\text{DA}}^* = 0.36 \text{ \AA}$, and in continuum aqueous solution at $\nu^{\text{OH}*} = 2001 \text{ cm}^{-1}$ and $\Delta d_{\text{DA}}^* = 0.36 \text{ \AA}$. For the pass-by mechanism, Figure 3.9f shows the inflection points in the gas phase at $\nu^{\text{OH}*} = 1829 \text{ cm}^{-1}$ and $\Delta d_{\text{DA}}^* = 0.29 \text{ \AA}$, and in continuum aqueous solution at $\nu^{\text{OH}*} = 1714 \text{ cm}^{-1}$ and $\Delta d_{\text{DA}}^* = 0.30 \text{ \AA}$. Comparison of $\nu^{\text{OH}*}$ for the pass-by mechanism and those of the protonated water clusters (Lao-ngam, Asawakun, Wannarat and Sagarik, 2011) suggested red-shifts of about 200 cm^{-1} due to the presence of the $-\text{SO}_3\text{H}$ group. It should be emphasized that the present work focused only on the asymmetric O-H stretching frequencies (ν^{OH}) which are directly related to the proton transfer processes. As ν^{OH} cannot be identified accurately in IR experiments, rigorous comparison cannot be made. One could however conclude that the asymmetric O-H stretching frequencies of the transferring protons in Table 3.6 are in good agreement with experiments (Buzzoni, Bordiga, Ricchiardi, Spoto and Zecchina, 1995; Ludvigsson, Lindgren and Tegenfeld, 2000).

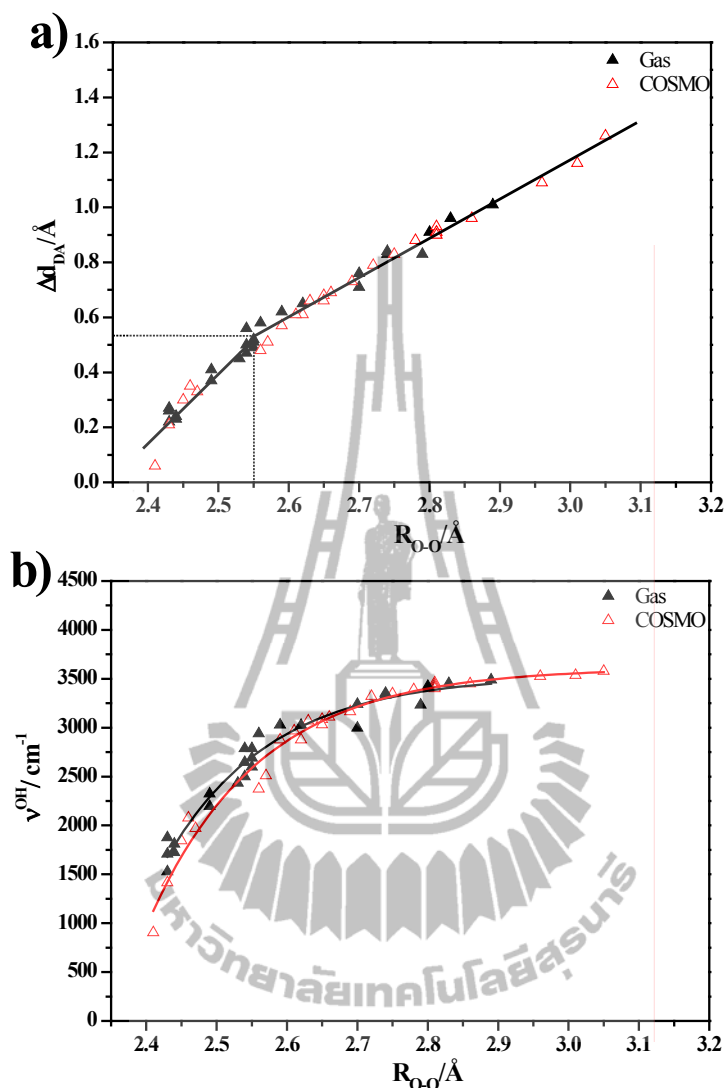


Figure 3.9 Static results of the $\text{CF}_3\text{SO}_3\text{H}-\text{H}_3\text{O}^+-n\text{H}_2\text{O}$ complexes obtained from B3LYP/TZVP calculations in the gas phase and continuum aqueous solution. a) Plot of Δd_{DA} and $R_{\text{O-O}}$ for the pass-through mechanism. b) Plot of ν^{OH} and $R_{\text{O-O}}$ for the pass-through mechanism. c) Plot of ν^{OH} and Δd_{DA} for the pass-through mechanism. d) Plot of Δd_{DA} and $R_{\text{O-O}}$ for the pass-by mechanism. e) Plot of ν^{OH} and $R_{\text{O-O}}$ for the pass-by mechanism. f) Plot of ν^{OH} and Δd_{DA} for the pass-by mechanism. (Δd_{DA} = asymmetric stretching coordinate; $R_{\text{O-O}}$ = O-H...O H-bond distance; ν^{OH} = asymmetric O-H stretching frequency)

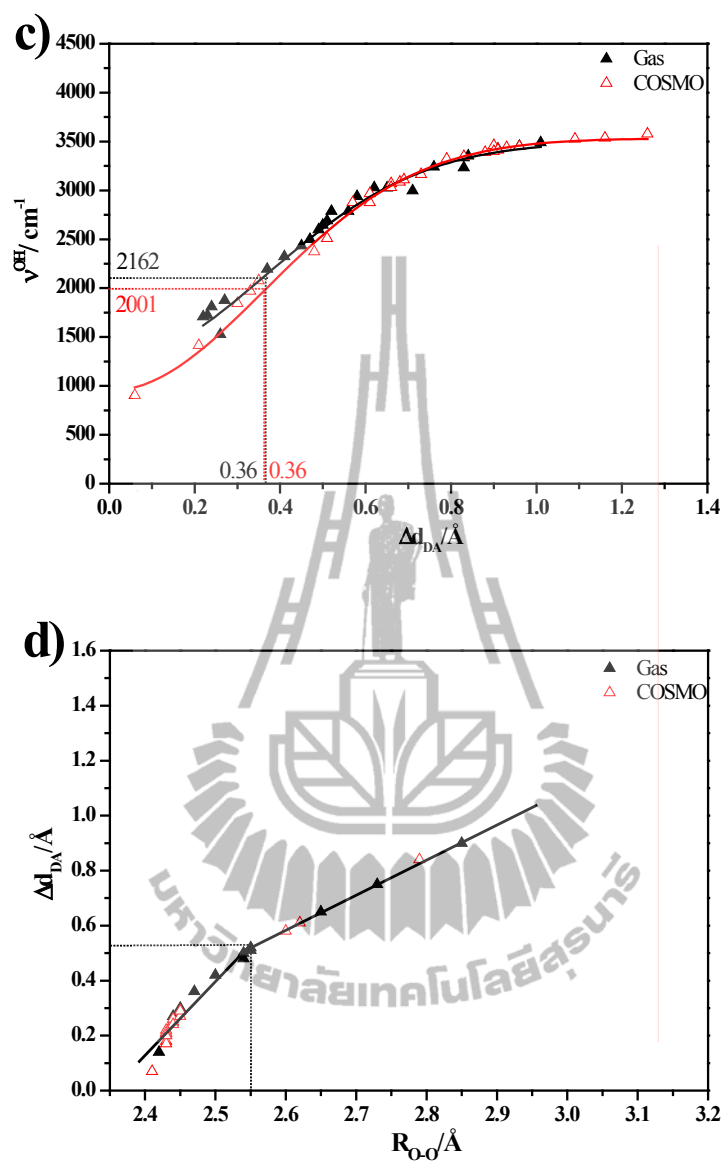


Figure 3.9 (Continued).

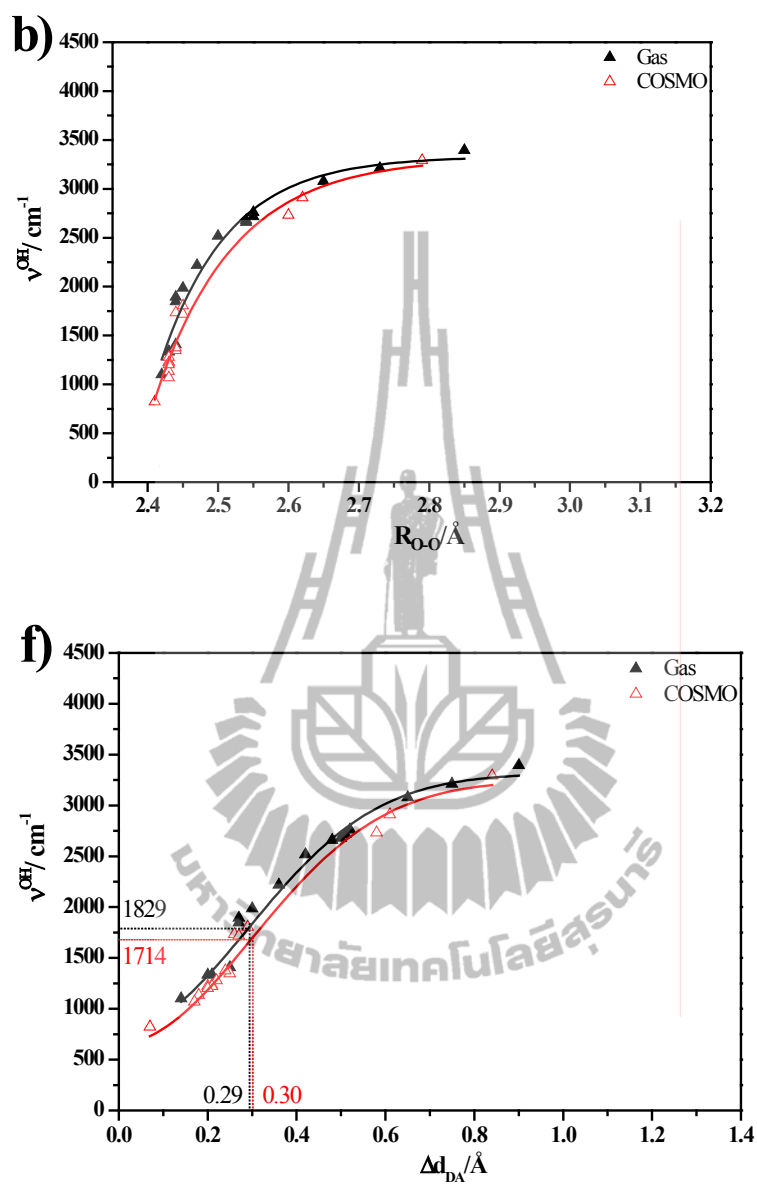


Figure 3.9 (Continued).

Although the H-bond structures in the gas phase and continuum aqueous solution are approximately the same, the trends of proton transfers are quite different. Δd_{DA} and ν^{OH} in Table 3.6 revealed that the $-SO_3H$ group is not preferentially dissociated in the gas phase, whereas in continuum aqueous solution, $-SO_3H$ tends to deprotonate, resulting in $-SO_3^-$ in close contact with H_3O^+ , with the highest tendency of proton dissociation in structure **A2C-[1]** ($\Delta d_{DA} = 0.06 \text{ \AA}$ and $\nu^{OH} = 905 \text{ cm}^{-1}$). Δd_{DA} and ν^{OH} also indicated that, in continuum aqueous solution, structure **A2C-[2]** possesses the highest tendency of proton transfer through the pass-by mechanism ($\Delta d_{DA} = 0.07 \text{ \AA}$ and $\nu^{OH} = 823 \text{ cm}^{-1}$).

Classifications of H-bonds

As in the case of IR experiments (Asbury, Steinel and Fayer, 2004; Jiang, Chaudhuri, Lee and Chang, 2002; Wu, Chaudhuri, Jiang, Lee and H.C. Chang, 2004) Table 3.6 showed that ν^{OH} can vary in a quite wide range; in the gas phase from 1100 to 3500 cm^{-1} , in continuum aqueous solution from 820 to 3600 cm^{-1} . To resolve these broad IR bands, the H-bonds in Table 1 were divided into two groups; the H-bonds connecting directly to the $-SO_3H$ or $-SO_3^-$ group belong to **Group 1** (potentially involved in the protonation or deprotonation at the $-SO_3H$ group, as well as the pass-through mechanism) and the H-bonds in the adjacent $H_3O^+-H_2O$ or Zundel complex to **Group 2** (potentially involved in the pass-by mechanism). Investigation of the H-bond structures in Table 3.6 in details, allowed **Group 1** and **2** to be further divided into four subgroups. The definitions of the groups and subgroups are summarized as follows:

- Group 1** H-bonds connecting directly to the $-\text{SO}_3\text{H}$ or $-\text{SO}_3^-$ group.
- Subgroup (I) Cyclic H-bonds between the Zundel complex or H_7O_3^+ and the two oxygen atoms of $-\text{SO}_3\text{H}$ or $-\text{SO}_3^-$, *e.g.* H-bonds **(1)** and **(3)** in structures **A1C** and **B1C**, and H-bonds **(1)** and **(4)** in structures **A2G[2]** and **A2C[2]**.
- Subgroup (II) Linear H-bond between an oxygen atom of the $-\text{SO}_3\text{H}$ or $-\text{SO}_3^-$ group and H_3O^+ , H_5O_2^+ or H_2O , *e.g.* H-bonds **(1)** and **(2)** in structures **C1C** and **C2C**, as well as H-bond **(1)** in structure **C3C**.
- Group 2** H-bonds in the adjacent Zundel complex.
- Subgroup (III) H-bond in the $\text{H}_3\text{O}^+ - \text{H}_2\text{O}$ contact structure or the Zundel complex in the structure with Subgroup (II), *e.g.* H-bond **(3)** in structure **C2G** and **C2C**, respectively.
- Subgroup (IV) H-bond of the Zundel complex in the structure with Subgroup (I), *e.g.* H-bond **(2)** in structures **A1C** and **B1C**.

The domains of ν^{OH} for the H-bond protons in **Group 1** (Subgroup (I) and (II)) and **Group 2** (Subgroup (III) to (IV)), in the gas phase and continuum aqueous solution, are shown in Figure 3.10.

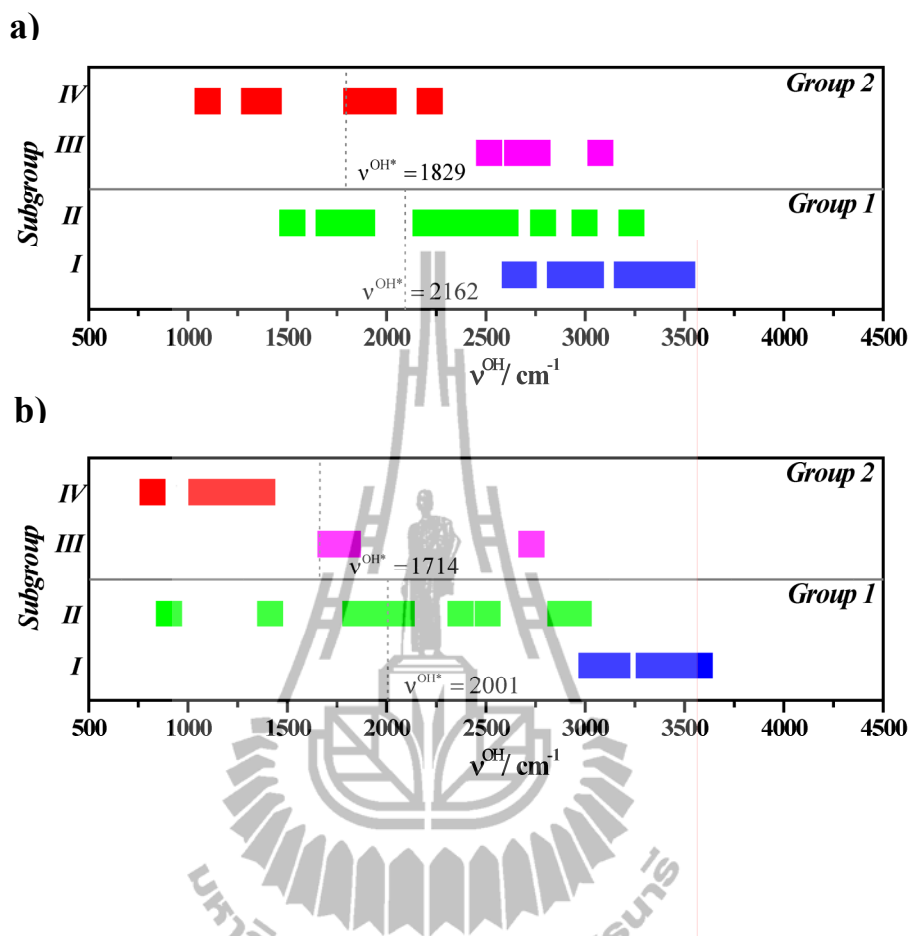


Figure 3.10 The domains of ν^{OH} for the H-bond protons in **Group 1** and **2**, as well as Subgroup (I) to (IV). a) gas phase. b) continuum aqueous solution.

Comparison of Figure 3.10a and 3.10b revealed that the electric field introduced by the continuum aqueous solvent brings about significant shifts of ν^{OH} , especially for the pass-by mechanism, in which all the H-bonds in Subgroup (IV) are red shifted to ν^{OH} lower than $\nu^{\text{OH}*}$. For the pass-through mechanism, only some linear H-bonds in Subgroup (II) are red shifted to ν^{OH} lower than $\nu^{\text{OH}*}$. The cyclic H-bonds between the two oxygen atoms of $-\text{SO}_3\text{H}$ and the Zundel complex (Subgroup (I)) tend to be destabilized in continuum aqueous solution, leading to blue shifts of ν^{OH} above 3000 cm^{-1} . The red shifts reflect higher tendency for the deprotonation of the $-\text{SO}_3\text{H}$ group, as well as the pass-through mechanism, in continuum aqueous solution.



3.2.2 Dynamic results

The neglect of extensive H-bond networks of water in the vicinities of the solute ($\text{CF}_3\text{SO}_3\text{H}$), as well as the thermal energy fluctuations in BOMD simulations, made it difficult to analyze the dynamics in the $\text{CF}_3\text{SO}_3\text{H}\cdot\text{H}_3\text{O}^+\cdot\text{H}_2\text{O}$ complexes. Therefore, attention was focused on the H-bond protons in the intermediate states.

Average H-bond structures and IR spectra

Before the dynamics in the $\text{CF}_3\text{SO}_3\text{H}\cdot\text{H}_3\text{O}^+\cdot n\text{H}_2\text{O}$ complexes are discussed, the characteristic vibrations in the protonated water clusters will be analyzed (Lao-ngam, Asawakun, Wannarat and Sagarik, 2011). The IR spectra of the H-bond proton in the Zundel complex obtained from BOMD simulations at 350 K are given in Figure 3.11a and 3.11b, in the gas phase and continuum aqueous solution, respectively. For the transferring proton ($\nu^{\text{OH}} < \nu^{\text{OH}^*}$), the static proton transfer potential (B3LYP/TZVP calculations) predicted only one asymmetric O-H stretching band, whereas BOMD simulations showed in addition a higher frequency band. The two IR bands are labeled with **A** and **B** in Figure 3.11a and 3.11b. Since the lower frequency band (at $\nu_{\text{A}}^{\text{OH,MD}}$) could be associated with the oscillatory shuttling motion and the higher frequency band (at $\nu_{\text{B}}^{\text{OH,MD}}$) with the structural diffusion motion (Lao-ngam, Asawakun, Wannarat and Sagarik, 2011), the vibrational energy for the interconversion between the two dynamic states ($\Delta\nu_{\text{BA}}^{\text{OH,MD}}$) can be approximated from the difference between $\nu_{\text{B}}^{\text{OH,MD}}$ and $\nu_{\text{A}}^{\text{OH,MD}}$, and the relative probability of finding these characteristic vibrations in the course of BOMD simulations could be estimated from the ratio of the IR intensities at **B** (I_{B}) and **A** (I_{A}) (Lao-ngam, Asawakun,

Wannarat and Sagarik, 2011); the lower I_B/I_A the higher the relative probability of finding the oscillatory shuttling motion. It should be noted that the discussion on $\Delta v_{BA}^{OH,MD}$ and I_B/I_A is meaningful only when the H-bond considered is susceptible to proton transfer, $v_A^{OH,MD} < v_A^{OH^*,MD}$.

The intensities of the IR bands at **A** and **B** in Figure 3.11a and 3.11b showed that the oscillatory shuttling motion dominates in the Zundel complex, especially in continuum aqueous solution; in the gas phase, $I_B/I_A = 0.5$, whereas in continuum aqueous solution, $I_B/I_A = 0.1$. The trend of I_B/I_A in the gas phase and continuum aqueous solution can be explained using $\Delta v_{BA}^{OH,MD}$; in the gas phase, $\Delta v_{BA}^{OH,MD} = 724 \text{ cm}^{-1}$, and in continuum aqueous solution, $\Delta v_{BA}^{OH,MD} = 808 \text{ cm}^{-1}$. The latter reflects a higher vibrational energy for the interconversion between the oscillatory shuttling and structural diffusion motions, resulting in a higher population of the oscillatory shuttling motion for the Zundel complex in continuum aqueous solution. It should be augmented that, due to a short BOMD simulation length, I_B/I_A may not be determined precisely. Therefore, attempt was made to alternatively estimate the relative population of the oscillatory shuttling and structural diffusion motions from $\Delta v_{BA}^{OH,MD}$. For the protonated water clusters, an interesting relationship was observed when $\Delta v_{BA}^{OH,MD}$ and $\langle \Delta d_{DA} \rangle$ were plotted. Together with the plot of the standard deviations of the O-H distances ($\sigma_{R_{O-H}}$) and $\langle \Delta d_{DA} \rangle$, energetic aspects of the two characteristic vibrations in the protonated water cluster could be studied.

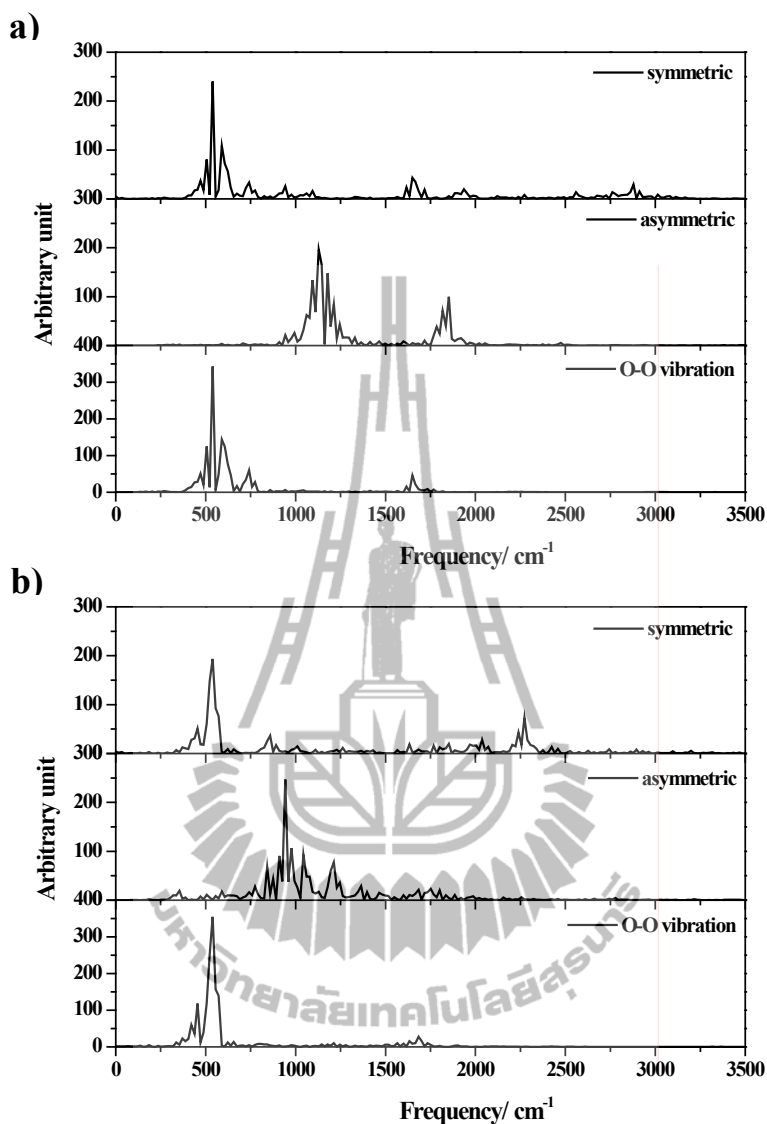


Figure 3.11 BOMD results on the Zundel complex at 350 K. a) – b) IR spectra of the transferring proton in the gas phase and continuum aqueous solution, respectively. c) Plot of $\sigma_{\text{RO-H}}$ and $\langle \Delta d_{\text{DA}} \rangle$. d) Plot of $\Delta v_{\text{BA}}^{\text{OH,MD}}$ and $\langle \Delta d_{\text{DA}} \rangle$. e) Plot of $\mathbf{P_B/P_A}$ and $\langle \Delta d_{\text{DA}} \rangle$. $\sigma_{\text{RO-H}}$ = standard deviations of the O-H distances; $\langle \Delta d_{\text{DA}} \rangle$ = average asymmetric stretching coordinate; $\mathbf{P_B/P_A}$ = probability of finding the structural diffusion motion relative to the oscillatory shuttling motion (Lao-ngam, Asawakun, Wannarat and Sagarik, 2011).

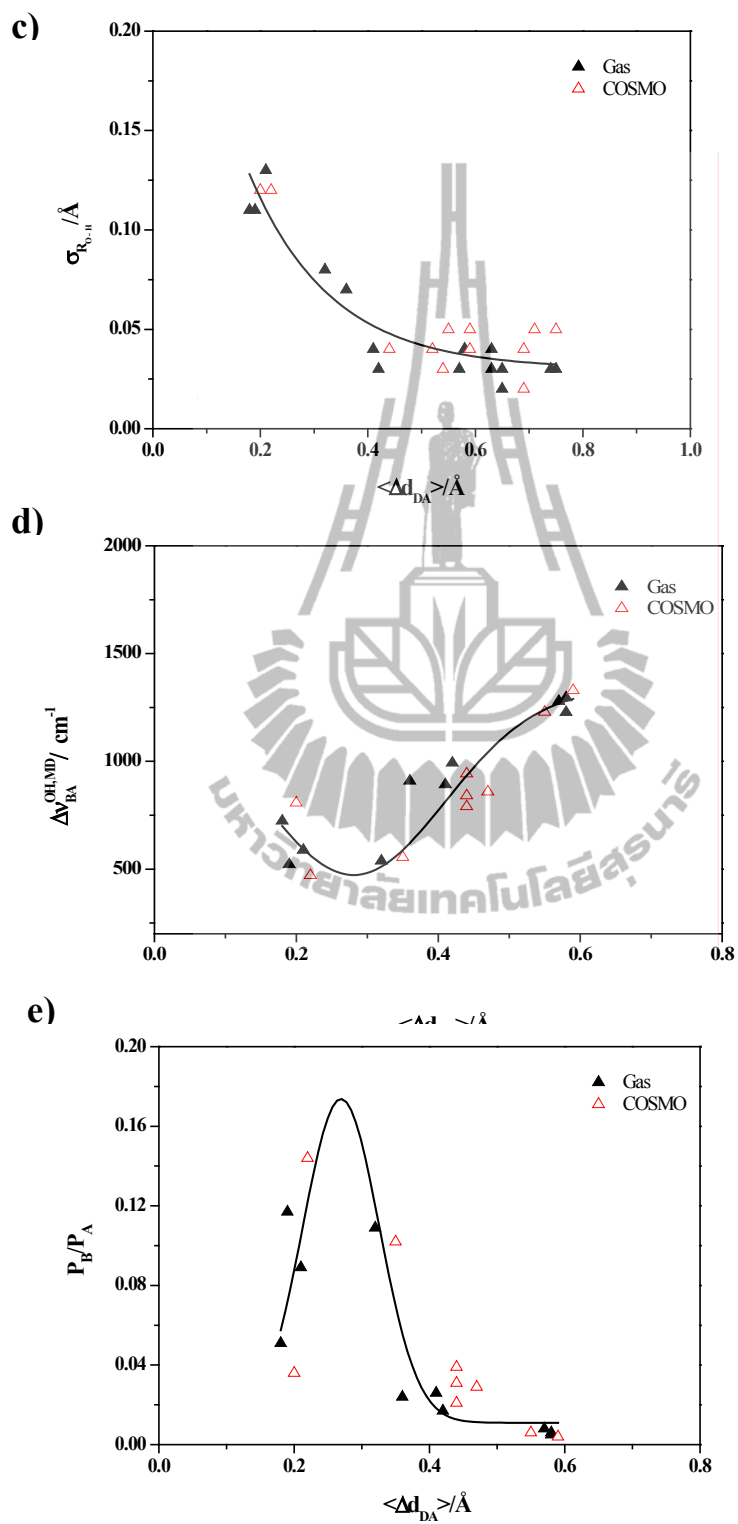


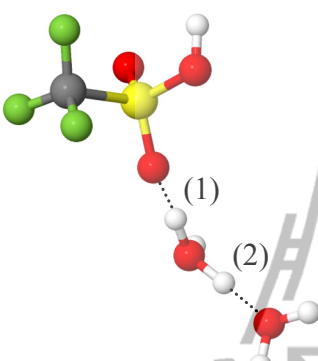
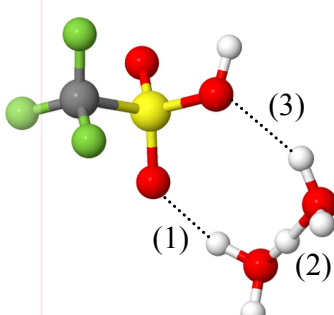
Figure 3.11 (Continued).

The plots of $\sigma_{\text{R}_{\text{O-H}}}$ and $\langle \Delta d_{\text{DA}} \rangle$ and $\Delta v_{\text{BA}}^{\text{OH,MD}}$ and $\langle \Delta d_{\text{DA}} \rangle$ are shown in Figures 3.11c and 3.11d, respectively. The former could be represented by an exponential decay function, whereas the latter by a reflected normal distribution function. Due to the thermal energy fluctuations and dynamics, $\sigma_{\text{R}_{\text{O-H}}}$, as well as $\Delta v_{\text{BA}}^{\text{OH,MD}}$, in the gas phase and continuum aqueous solution are not well separated. Therefore, the discussion on the relative population of the oscillatory shuttling and structural diffusion will be made based on a combined data set. It appeared that, for the protonated water clusters, $\sigma_{\text{R}_{\text{O-H}}}$ decreases exponentially with $\langle \Delta d_{\text{DA}} \rangle$, reflecting characteristics of the oscillatory shuttling and structural diffusion motions; the oscillatory shuttling motion dominates in the H-bond with small $\langle \Delta d_{\text{DA}} \rangle$. $\Delta v_{\text{BA}}^{\text{OH,MD}}$ decreases exponentially with $\langle \Delta d_{\text{DA}} \rangle$ and reaches a minimum at $\langle \Delta d_{\text{DA}} \rangle = 0.28 \text{ \AA}$ ($\langle \text{R}_{\text{O-O}} \rangle = 2.46 \text{ \AA}$), corresponding to the lowest vibrational energy for the interconversion between the oscillatory shuttling and the structural diffusion motions, $\Delta v_{\text{BA}}^{\text{OH,MD}} = 473 \text{ cm}^{-1}$ or 5.7 kJ/mol. Since the probability of finding a physical system in a certain energy state is proportional to the Boltzmann factor, the probability of finding the structural diffusion motion relative to the oscillatory shuttling motion ($\mathbf{P}_{\text{B}}/\mathbf{P}_{\text{A}}$) is proportional to $e^{-\Delta v_{\text{BA}}^{\text{OH,MD}}/RT}$. For the protonated water clusters, $\mathbf{P}_{\text{B}}/\mathbf{P}_{\text{A}}$ and $\langle \Delta d_{\text{DA}} \rangle$ is plotted and shown in Figure 3.11e. $\mathbf{P}_{\text{B}}/\mathbf{P}_{\text{A}}$ could be expressed in terms of $\langle \Delta d_{\text{DA}} \rangle$ using a normal distribution function. The agreement between the fitted function and the values obtained from BOMD simulations is included in Figure 3.11e. The fitted function suggested the maximum probability of finding the structural diffusion motion relative to the oscillatory shuttling motion, $\mathbf{P}_{\text{B}}/\mathbf{P}_{\text{A}} = 0.17$ at $\langle \Delta d_{\text{DA}} \rangle$

= 0.27 Å. At larger $\langle \Delta d_{DA} \rangle$, the H-bond becomes weaker and P_B/P_A decreases, especially when $v_A^{OH,MD} > v_A^{OH*,MD}$.

For the $CF_3SO_3H-H_3O^+-nH_2O$ complexes, the average H-bond structures, $\langle R_{O-O} \rangle$ and $\langle \Delta d_{DA} \rangle$, obtained from BOMD simulations at 350 K, are summarized in Table 3.7, together with, $v_A^{OH,MD}$, $v_B^{OH,MD}$ and the proton diffusion coefficients (D). The H-bonds susceptible to proton transfers are designated by asterisks. The plots between $\langle \Delta d_{DA} \rangle$ and $\langle R_{O-O} \rangle$, $v_A^{OH,MD}$ and $\langle R_{O-O} \rangle$, and $v_A^{OH,MD}$ and $\langle \Delta d_{DA} \rangle$ for the pass-through mechanism are shown in Figures 3.12a to 3.12c, respectively, and for the pass-by mechanism in Figures 3.12d to 3.12f, respectively. The same types of functions, as in the case of the B3LYP/TZVP calculations in Figure 3.12, were employed to represent the relationships in Figure 3.12. The agreements between the fitted functions and the values obtained from BOMD simulations are illustrated in Figure 3.12.

Table 3.7 Dynamic results of the $\text{CF}_3\text{SO}_3\text{H}-\text{H}_3\text{O}^+-n\text{H}_2\text{O}$ complexes, $1 \leq n \leq 3$, obtained from BOMD simulations at 350 K. Distances, IR frequencies and proton diffusion coefficients are in Å, cm^{-1} and $\text{cm}^2 \text{s}^{-1}$ respectively.

Gas						COSMO		
A1G						A1C		
H-bond	$\langle R_{\text{O-O}} \rangle$	$\sigma_{R_{\text{O-H}}}$	$\langle \Delta d_{\text{DA}} \rangle$	$\nu_{\text{A}}^{\text{OH,MD}}$	$\nu_{\text{B}}^{\text{OH,MD}}$	$P_{\text{B}}/P_{\text{A}}$	$D (10^{-5})$	
(1)	2.6	0.01	0.56	1750	2693	943	0.02	4.58
	-	-	-	-	-	-	-	-
(2)	2.5	0.03	0.36	1515	2154	673	0.06	2.48
	(2.4)	(0.05)	(0.17)*	(1043)*	(1700)	(657)	(0.07)	(1.69)
(3)	-	-	-	-	-	-	-	-
	-	-	-	-	-	-	-	-

$\langle R_{\text{O-O}} \rangle$ = average H-bond distance; $\sigma_{R_{\text{O-H}}}$ = standard deviation of the O-H distance;
 $\langle \Delta d_{\text{DA}} \rangle$ = average asymmetric stretching coordinate; $\nu_{\text{A}}^{\text{OH,MD}}$ and $\nu_{\text{B}}^{\text{OH,MD}}$ = asymmetric O-H stretching frequencies; $\Delta \nu_{\text{BA}}^{\text{OH,MD}}$ = vibrational energy for the interconversion between the oscillatory shuttling and structural diffusion motions;
 $P_{\text{B}}/P_{\text{A}}$ = relative probability of finding the oscillatory shuttling motion; D = proton diffusion coefficient; (..) = continuum aqueous solution (COSMO); * = H-bond susceptible to proton transfer.

Table 3.7 (Continued).

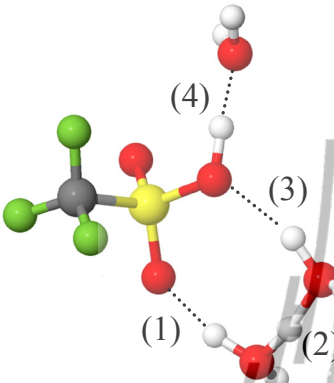
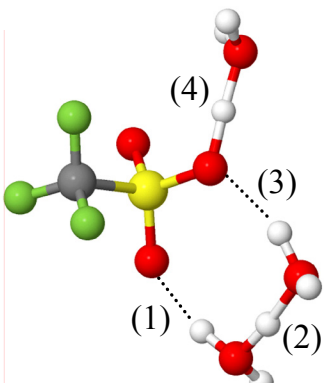
Gas					COSMO				
<div>A2G-[1] </div>					<div>A2C-[1] </div>				
H-bond	$\langle R_{O-O} \rangle$	$\sigma_{R_{O-H}}$	$\langle \Delta d_{DA} \rangle$	$v_A^{OH,MD}$	$v_B^{OH,MD}$	$\Delta v_{BA}^{OH,MD}$	P_B/P_A	$D (10^{-5})$	
(1)	2.6	0.02	0.65	1733	2962	1229	0.01	5.06	
	(2.7)	(0.01)	(0.91)	(1683)	(3501)	(1818)	(0.00)	(5.02)	
(2)	2.4	0.05	0.28*	1498*	2053	555	0.10	2.45	
	(2.4)	(0.08)	(0.21)*	(959)*	(1683)	(724)	(0.05)	(2.56)	
(3)	-	-	-	-	-	-	-	-	
	-	-	-	-	-	-	-	-	
(4)	2.5	0.02	0.55	1818	2693	875	0.03	2.46	
	(2.4)	(0.12)	(0.21)*	(948)*	(1717)	(769)	(0.04)	(2.67)	

Table 3.7 (Continued).

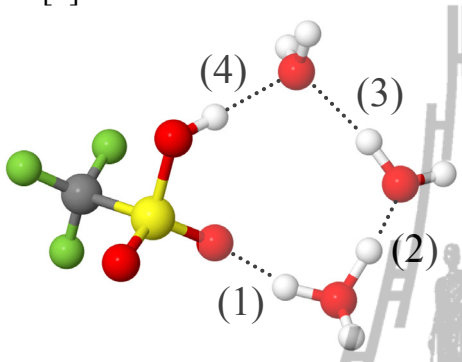
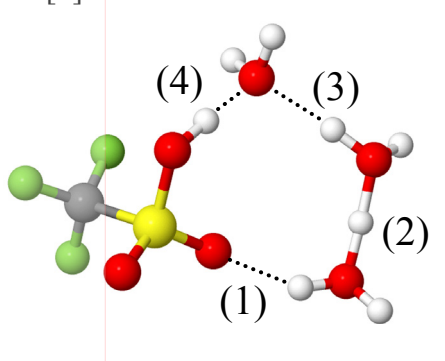
Gas					COSMO				
A2G-[2]					A2C-[2]				
									
H-bond	$\langle R_{O-O} \rangle$	$\sigma_{R_{O-H}}$	$\langle \Delta d_{DA} \rangle$	$\nu_A^{OH,MD}$	$\nu_B^{OH,MD}$	$\Delta \nu_{BA}^{OH,MD}$	P_B/P_A	$D (10^{-5})$	
(1)	2.5	0.02	0.58	1599	3046	1447	0.00	1.52	
	-	-	-	-	-	-	-	-	
(2)	2.5	0.08	0.26*	1531*	1969	438	0.17	1.77	
	(2.4)	(0.09)	(0.15)*	(875)*	(1834)	(959)	(0.02)	(2.91)	
(3)	-	-	-	-	-	-	-	-	
	(2.8)	(0.01)	(0.94)	(1666)	(3366)	(1700)	(0.00)	(7.42)	
(4)	-	-	-	-	-	-	-	-	
	(2.6)	(0.01)	(0.54)	(1296)	(2592)	(1296)	(0.00)	(2.91)	

Table 3.7 (Continued).

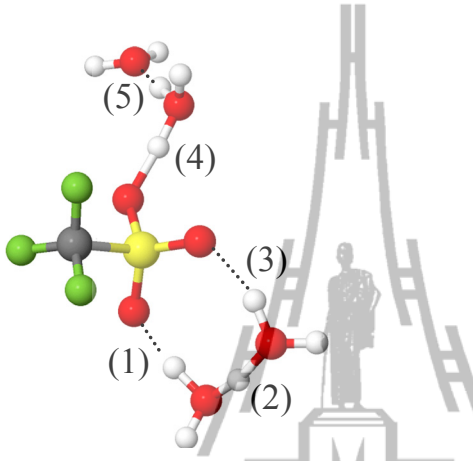
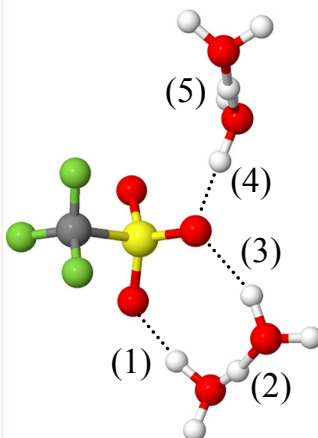
Gas					COSMO				
A3G-[1]					A3C-[1]				
									
H-bond	$\langle R_{O-O} \rangle$	$\sigma_{R_{O-H}}$	$\langle \Delta d_{DA} \rangle$	$V_A^{OH,MD}$	$V_B^{OH,MD}$	$\Delta V_{BA}^{OH,MD}$	P_B/P_A	$D (10^{-5})$	
(1)	2.5	0.02	0.53	1919	2558	639	0.07	2.98	
	(2.6)	(0.01)	(0.70)	(1717)	(3030)	(1313)	(0.00)	(3.01)	
(2)	2.4	0.06	0.27*	1363*	1935	572	0.10	1.65	
	(2.4)	(0.06)	(0.25)*	(1313)*	(1834)	(521)	(0.12)	(4.43)	
(3)	2.7	0.01	0.90	1548	3450	1902	0.00	2.51	
	-	-	-	-	-	-	-	-	
(4)	2.4	0.09	0.25*	1010*	1750	740	0.05	4.38	
	(2.6)	(0.01)	(0.66)	(1515)	(3080)	(1565)	(0.00)	(5.20)	
(5)	2.5	0.02	0.53	1801	2727	926	0.02	4.51	
	(2.4)	(0.07)	(0.26)*	(1313)*	(1733)	(420)	(0.18)	(3.29)	

Table 3.7 (Continued).

Gas					COSMO				
A3G-[2]					A3C-[2]				
H-bond	$\langle R_{O-O} \rangle$	$\sigma_{R_{O-H}}$	$\langle \Delta d_{DA} \rangle$	$V_A^{OH,MD}$	$V_B^{OH,MD}$	$\Delta V_{BA}^{OH,MD}$	P_B/P_A	$D (10^{-5})$	
(1)	2.6	0.02	0.64	1582	3013	1431	0.00	5.74	
	-	-	-	-	-	-	-	-	
(2)	2.4	0.08	0.20*	1094*	1717	623	0.08	2.00	
	(2.4)	(0.06)	(0.25)*	(1397)*	(1952)	(555)	(0.10)	(5.03)	
(3)	2.7	0.01	0.80	1801	3349	1548	0.00	3.79	
	(2.6)	(0.01)	(0.66)	(1599)	(3063)	(1464)	(0.00)	(6.17)	
(4)	2.7	0.01	0.75	1279	3232	1953	0.00	3.59	
	(2.7)	(0.02)	(0.53)	(1178)	(2659)	(1481)	(0.00)	(2.81)	
(5)	2.7	0.01	0.71	1885	3299	1414	0.00	3.55	
	(2.6)	(0.01)	(0.64)	(2323)	(3046)	(1060)	(0.01)	(4.10)	

Table 3.7 (Continued).

Gas					COSMO				
B1G					B1C				
H-bond	$\langle R_{O-O} \rangle$	$\sigma_{R_{O-H}}$	$\langle \Delta d_{DA} \rangle$	$v_A^{OH,MD}$	$v_B^{OH,MD}$	$\Delta v_{BA}^{OH,MD}$	P_B/P_A	$D (10^{-5})$	
(1)	2.7	0.01	0.80	1599	3400	1801	0.00	3.48	
	-	-	-	-	-	-	-	-	
(2)	2.4	0.07	0.14*	1077*	1750	673	0.06	2.18	
	(2.4)	(0.07)	(0.16)*	(993)*	(1700)	(707)	(0.05)	(2.52)	
(3)	-	-	-	-	-	-	-	-	
	-	-	-	-	-	-	-	-	

Table 3.7 (Continued).

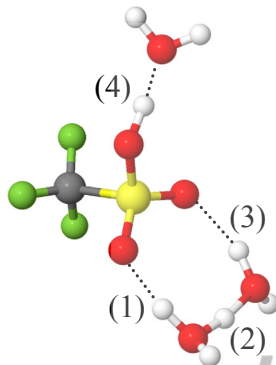
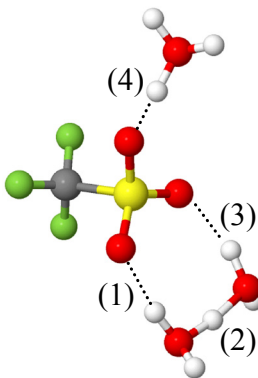
Gas					COSMO				
B2G					B2C				
									
H-bond	$\langle R_{O-O} \rangle$	$\sigma_{R_{O-H}}$	$\langle \Delta d_{DA} \rangle$	$\nu_A^{OH,MD}$	$\nu_B^{OH,MD}$	$\Delta \nu_{BA}^{OH,MD}$	P_B/P_A	$D (10^{-5})$	
(1)	-	-	-	-	-	-	-	-	
	(2.7)	(0.01)	(0.79)	(1666)	(3400)	(1734)	(0.00)	(3.32)	
(2)	2.4	0.08	0.20*	1066*	1868	802	0.04	2.57	
	(2.4)	(0.09)	(0.18)*	(976)*	(1700)	(724)	(0.03)	(2.12)	
(3)	-	-	-	-	-	-	-	-	
	-	-	-	-	-	-	-	-	
(4)	2.5	0.01	0.49	1447	2609	1162	0.01	1.17	
	(2.5)	(0.12)	(0.28)*	(1380)*	(1902)	(522)	(0.12)	(3.91)	

Table 3.7 (Continued).

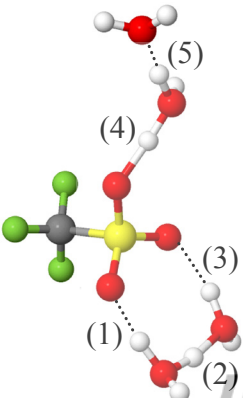
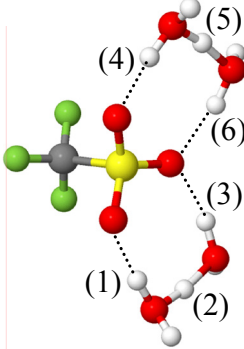
Gas					COSMO				
B3G					B3C				
									
H-bond	$\langle R_{O-O} \rangle$	$\sigma_{R_{O-H}}$	$\langle \Delta d_{DA} \rangle$	$v_A^{OH,MD}$	$v_B^{OH,MD}$	$\Delta v_{BA}^{OH,MD}$	P_B/P_A	$D(10^{-5})$	
(1)	2.6	0.02	0.54	1733	2592	859	0.03	3.36	
	(2.7)	(0.01)	(0.01)	(1666)	(3501)	(1835)	(0.00)	(4.32)	
(2)	2.4	0.07	0.26*	1313*	1952	639	0.07	3.27	
	(2.4)	(0.09)	(0.20)*	(1077)*	(1666)	(589)	(0.09)	(3.07)	
(3)	2.7	0.01	0.92	1565	3484	1919	0.00	5.56	
	(2.8)	(0.01)	(1.00)	(1548)	(3535)	(1987)	(0.00)	(2.64)	
(4)	2.4	0.09	0.22*	976*	1751	775	0.04	2.20	
	(2.7)	(0.01)	(0.77)	(1599)	(3282)	(1683)	(0.00)	(7.09)	
(5)	2.5	0.02	0.52	1851	2760	909	0.02	2.46	
	(2.4)	(0.08)	(0.20)*	(1066)*	(1717)	(651)	(0.07)	(4.58)	
(6)	-	-	-	-	-	-	-	-	
	-	-	-	-	-	-	-	-	

Table 3.7 (Continued).

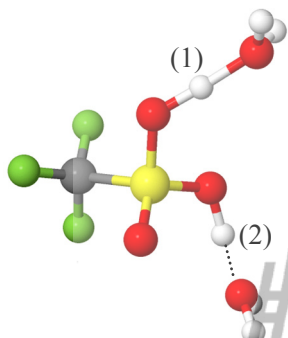
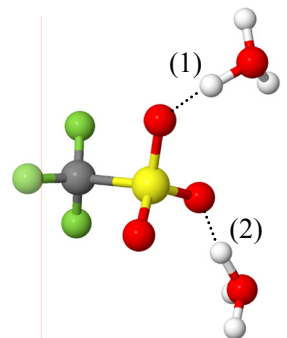
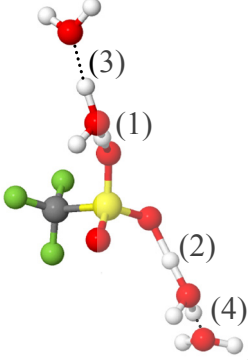
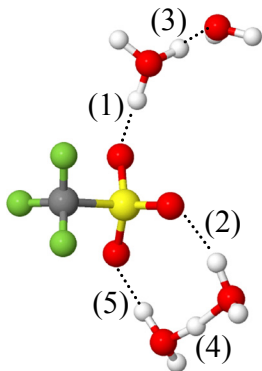
Gas					COSMO				
C1G					C1C				
									
H-bond	$\langle R_{O-O} \rangle$	$\sigma_{R_{O-H}}$	$\langle \Delta d_{DA} \rangle$	$v_A^{OH,MD}$	$v_B^{OH,MD}$	$\Delta v_{BA}^{OH,MD}$	P_B/P_A	$D(10^{-5})$	
(1)	2.4	0.06	0.26*	1499*	2003	504	0.13	1.33	
	(2.5)	(0.04)	(0.37)	(1767)	(2323)	(556)	(0.15)	(3.46)	
(2)	2.5	0.05	0.37	1902	2306	404	0.19	1.46	
	(2.5)	(0.08)	(0.33)	(1851)	(2356)	(505)	(0.13)	(3.15)	

Table 3.7 (Continued).

Gas					COSMO				
C2G					C2C				
H-bond	$\langle R_{O-O} \rangle$	$\sigma_{R_{O-H}}$	$\langle \Delta d_{DA} \rangle$	$v_A^{OH,MD}$	$v_B^{OH,MD}$	$\Delta v_{BA}^{OH,MD}$	P_B/P_A	$D(10^{-5})$	
(1)	2.5	0.02	0.44	2272	2592	320	0.18	1.91	
	-	-	-	-	-	-	-	-	
(2)	2.6	0.02	0.52	1582	2592	1010	0.06	2.27	
	(2.4)	(0.13)	(0.24)*	(1161)*	(2070)	(909)	(0.02)	(3.15)	
(3)	2.5	0.04	0.43	2171	2525	556	0.10	3.65	
	(2.5)	(0.07)	(0.27)*	(1414)*	(1750)	(336)	(0.25)	(3.01)	

Table 3.7 (Continued).

Gas					COSMO				
C3G					C3C				
									
H-bond	$\langle R_{O-O} \rangle$	$\sigma_{R_{O-H}}$	$\langle \Delta d_{DA} \rangle$	$v_A^{OH,MD}$	$v_B^{OH,MD}$	$\Delta v_{BA}^{OH,MD}$	P_B/P_A	$D(10^{-5})$	
(1)	2.4	0.11	0.26*	1228*	1868	640	0.07	2.74	
	(2.6)	(0.01)	(0.63)	(1868)	(3063)	(1195)	(0.01)	(4.39)	
(2)	2.4	0.11	0.22*	1117*	2003	886	0.03	3.05	
	(2.7)	(0.01)	(0.73)	(1834)	(3181)	(1347)	(0.00)	(6.82)	
(3)	-	-	-	-	-	-	-	-	
	(2.5)	(0.04)	(0.30)*	(1498)*	(1868)	(370)	(0.22)	(3.07)	
(4)	2.6	0.02	0.57	1548	2895	1347	0.00	4.25	
	(2.4)	(0.08)	(0.19)*	(1127)*	(1700)	(573)	(0.09)	(4.24)	
(5)	-	-	-	-	-	-	-	-	
	-	-	-	-	-	-	-	-	

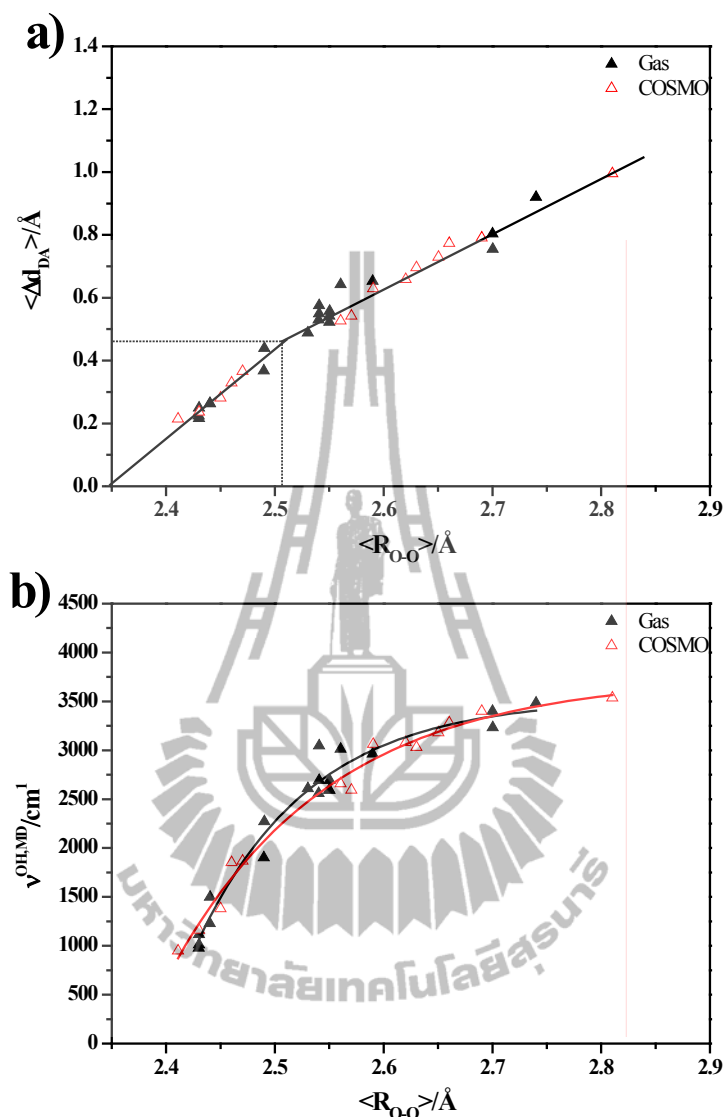


Figure 3.12 The BOMD results on the $\text{CF}_3\text{SO}_3\text{H}-\text{H}_3\text{O}^+-n\text{H}_2\text{O}$ complexes at 350 K. a) Plot of $\langle \Delta d_{DA} \rangle$ and $\langle R_{O-O} \rangle$ for the pass-through mechanism. b) Plot of ν^{OH} and $\langle R_{O-O} \rangle$ for the pass-through mechanism. c) Plot of ν^{OH} and $\langle \Delta d_{DA} \rangle$ for the pass-through mechanism. d) Plot of $\langle \Delta d_{DA} \rangle$ and $\langle R_{O-O} \rangle$ for the pass-by mechanism. e) Plot of ν^{OH} and $\langle R_{O-O} \rangle$ for the pass-by mechanism. f) Plot of ν^{OH} and $\langle \Delta d_{DA} \rangle$ for the pass-by mechanism. $\langle \Delta d_{DA} \rangle$ = average asymmetric stretching coordinate; $\langle R_{O-O} \rangle$ = average O-H...O H-bond distance; ν^{OH} = asymmetric O-H stretching frequency.

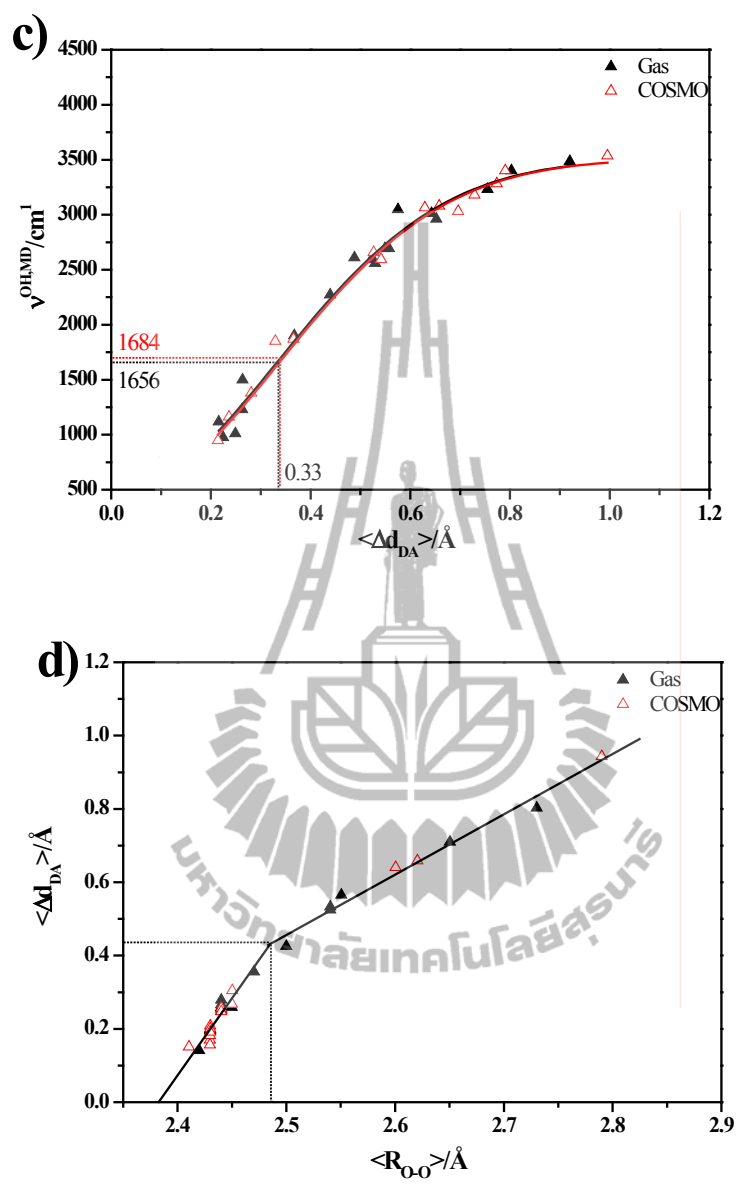


Figure 3.12 (Continued).

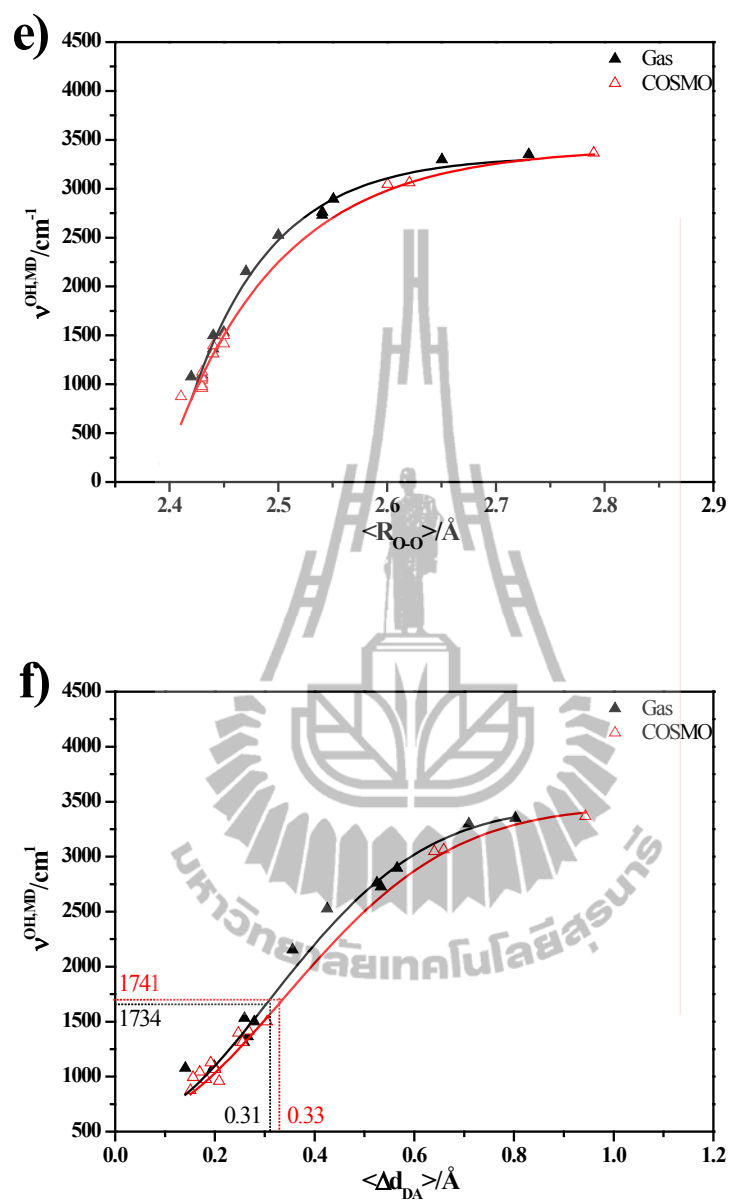
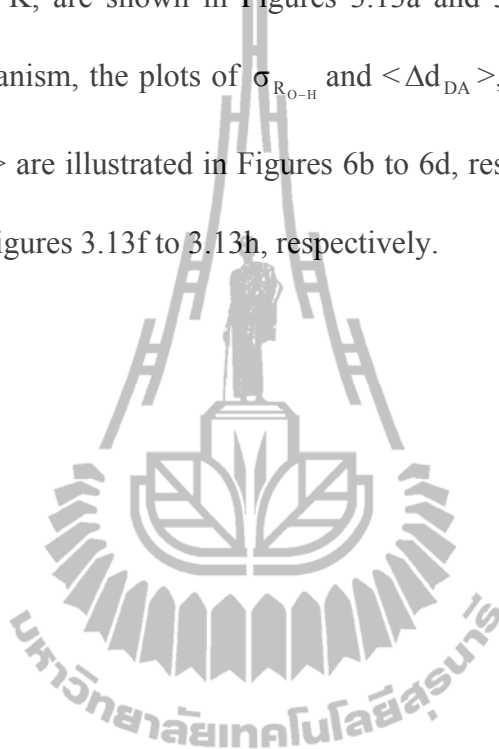


Figure 3.12 (Continued).

Since BOMD simulations were conducted in a short time, the average H-bond structures are not substantially different from the B3LYP/TZVP results. Comparison of $\nu_{\text{A}}^{\text{OH},\text{MD}}$ in Table 3.7 with ν^{OH} in Table 1 showed a general trend. The inclusion of the thermal energy fluctuations and dynamics in the model calculations brought about red shifts of the oscillatory shuttling bands both in the gas phase and continuum aqueous solution, except for structures **A2C-[1]** and **A2C-[2]** in continuum aqueous solution; B3LYP/TZVP calculations predicted the H-bonds **(4)** and **(2)** in structures **A2C-[1]** and **A2C-[2]** to possess the highest tendencies of proton transfer through the pass-through and pass-by mechanisms, respectively, and coupling among various modes of vibrations in BOMD simulations led to blue shifts of about 43 and 52 cm^{-1} , respectively.

As in the case of protonated water clusters, according to the thermal energy fluctuations and dynamics, the results in the gas phase and continuum aqueous solution are not well separated. Figure 3.12 showed the inflection points for the pass-through mechanism at $\nu_{\text{A}}^{\text{OH}^*,\text{MD}} = 1656$ and 1684 cm^{-1} , respectively, and for the pass-by mechanism at $\nu_{\text{A}}^{\text{OH}^*,\text{MD}} = 1733$ and 1741 cm^{-1} , respectively. The latter are 290 and 104 cm^{-1} lower than the corresponding values for the protonated water clusters (Lao-ngam, Asawakun, Wannarat and Sagarik, 2011). The red shifts represent energetic evidences for the promotion of proton transfer by the $-\text{SO}_3\text{H}$ group.

$\Delta v_{BA}^{OH,MD}$ and P_B/P_A for the H-bond protons in the $CF_3SO_3H-H_3O^+-H_2O$ complexes are included in Table 3.7. Examples of the characteristic asymmetric O-H stretching bands for the pass-through and pass-by mechanisms, obtained from BOMD simulations at 350 K, are shown in Figures 3.13a and 3.13e, respectively. For the pass-through mechanism, the plots of $\sigma_{R_{O-H}}$ and $\langle \Delta d_{DA} \rangle$, $\Delta v_{BA}^{OH,MD}$ and $\langle \Delta d_{DA} \rangle$, and P_B/P_A and $\langle \Delta d_{DA} \rangle$ are illustrated in Figures 6b to 6d, respectively, and for the pass-by mechanism in Figures 3.13f to 3.13h, respectively.



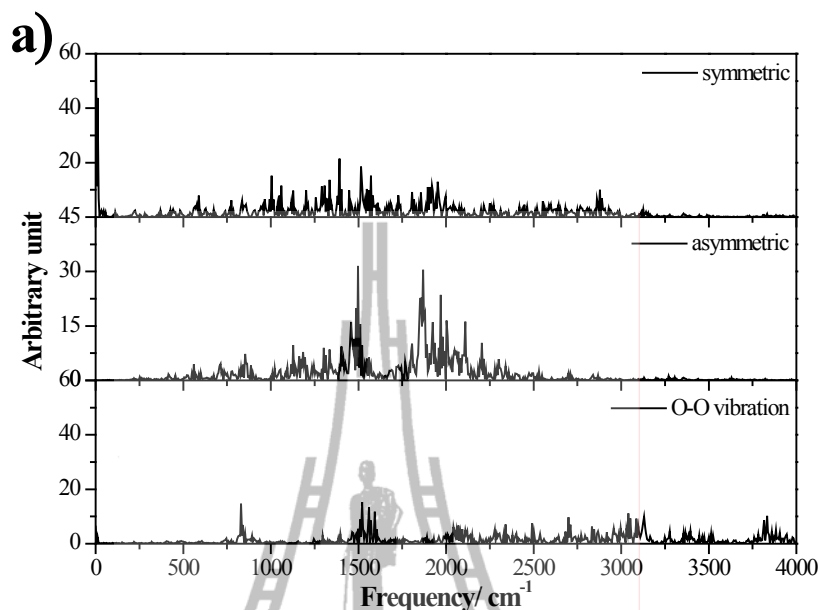


Figure 3.13 The BOMD results of the $\text{CF}_3\text{SO}_3\text{H}-\text{H}_3\text{O}^+-n\text{H}_2\text{O}$ complexes at 350 K. a) Example of the IR spectra of the transferring proton in the pass-through mechanism. b) Plot of $\sigma_{\text{RO-H}}$ and $\langle\Delta d_{\text{DA}}\rangle$ for the pass-through mechanism. c) Plot of $\Delta v_{\text{BA}}^{\text{OH,MD}}$ and $\langle\Delta d_{\text{DA}}\rangle$ for the pass-through mechanism.. d) Plot of $\mathbf{P_B/P_A}$ and $\langle\Delta d_{\text{DA}}\rangle$ for the pass-through mechanism. e) Example of the IR spectra of the transferring proton in the pass-by mechanism. f) Plot of $\sigma_{\text{RO-H}}$ and $\langle\Delta d_{\text{DA}}\rangle$ for the pass-by mechanism. g) Plot of $\Delta v_{\text{BA}}^{\text{OH,MD}}$ and $\langle\Delta d_{\text{DA}}\rangle$ for the pass-by mechanism. h) Plot of $\mathbf{P_B/P_A}$ and $\langle\Delta d_{\text{DA}}\rangle$ for the pass-by mechanism. $\sigma_{\text{RO-H}}$ = standard deviations of the O-H distances; $\langle\Delta d_{\text{DA}}\rangle$ = average asymmetric stretching coordinate; $\mathbf{P_B/P_A}$ = probability of finding the structural diffusion motion relative to the oscillatory shuttling motion.

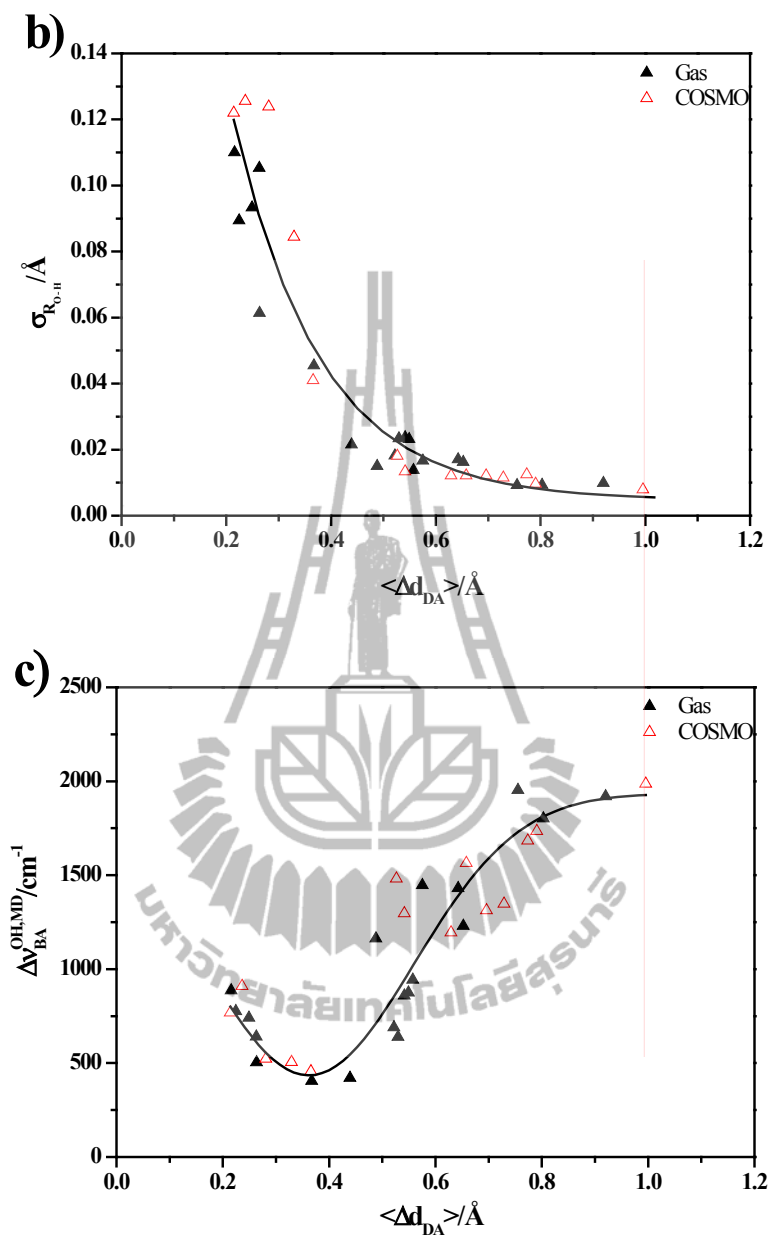


Figure 3.13 (Continued).

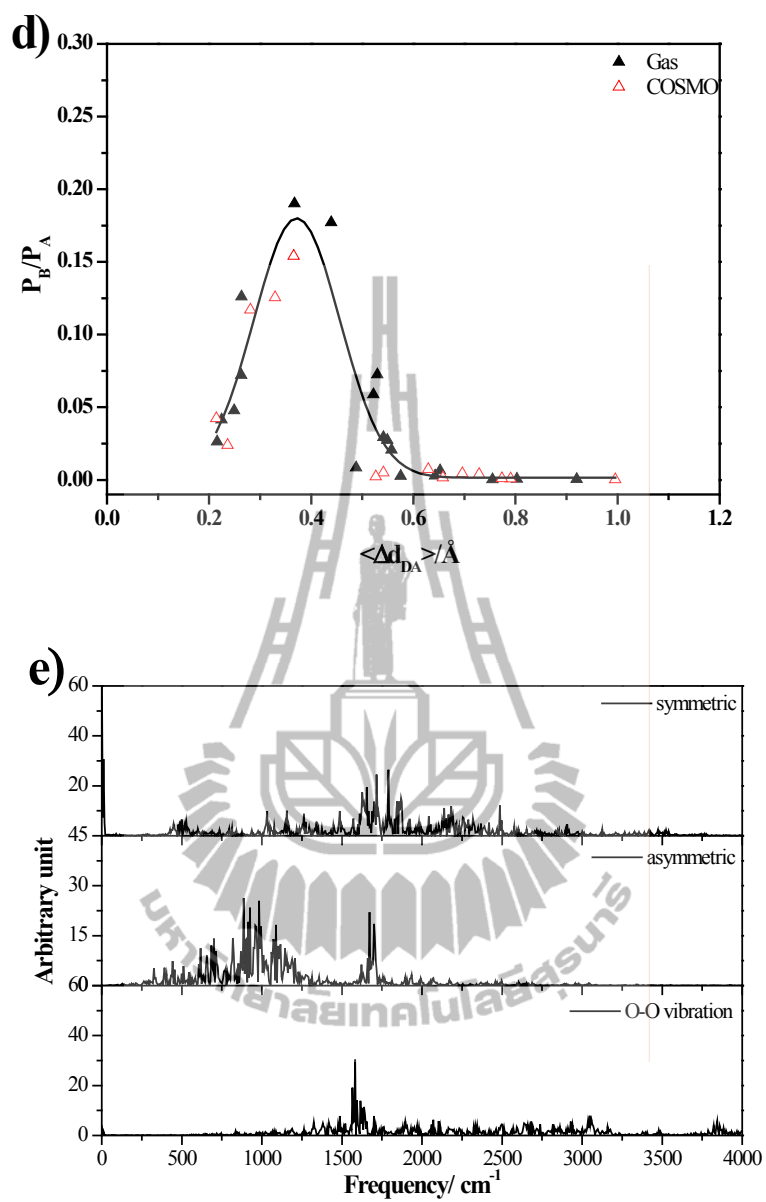


Figure 3.13 (Continued).

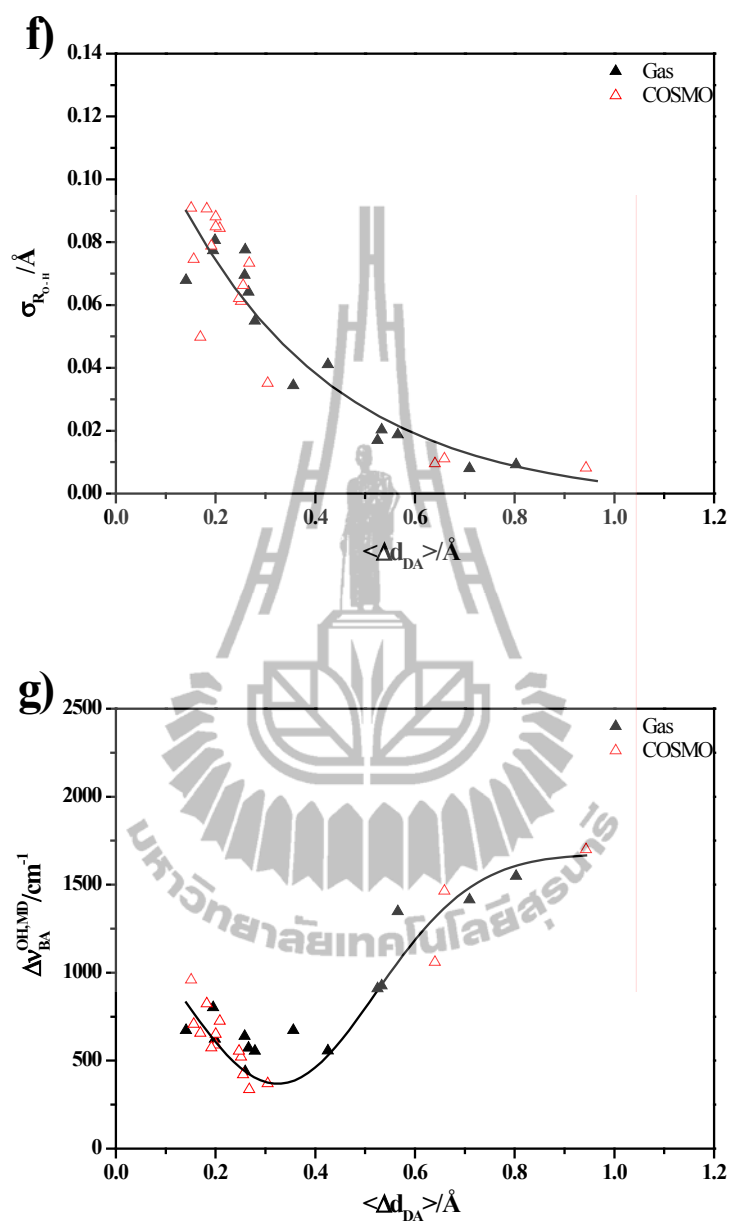


Figure 3.13 (Continued).

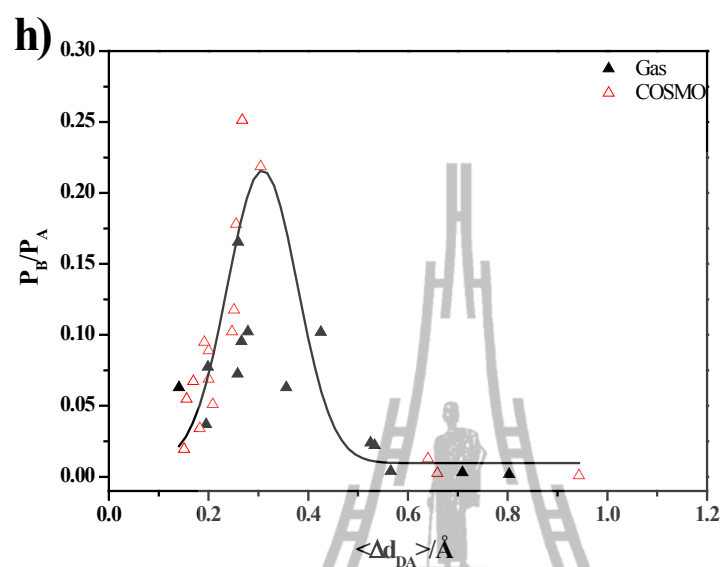


Figure 3.13 (Continued).

All the outstanding features discussed in the protonated water clusters were observed in the $\text{CF}_3\text{SO}_3\text{H}-\text{H}_3\text{O}^+-n\text{H}_2\text{O}$ complexes. The same types of functions, as in the case of the protonated water clusters in Figure 3.11, represent the relationships in Figure 3.13 quite well. For the pass-through mechanism, $\Delta v_{\text{BA}}^{\text{OH,MD}}$ in Figure 3.13c decreases exponentially with $\langle \Delta d_{\text{DA}} \rangle$ and reaches a minimum at $\Delta v_{\text{BA}}^{\text{OH,MD}} = 469 \text{ cm}^{-1}$, corresponding to the maximum probability of finding the structural diffusion motion ($\mathbf{P_B/P_A}$) of 0.17; the H-bonds in the vicinities of the maximum are, for examples, H-bond (1) in structures **C1G** and **C1C**, and H-bond (2) in structure **C2G**. For the pass-by mechanism, due to the presence of the $-\text{SO}_3\text{H}$ group, the vibrational energy for the interconversion between the oscillatory shuttling and the structural diffusion motions are decreased, from $\Delta v_{\text{BA}}^{\text{OH,MD}} = 473 \text{ cm}^{-1}$ in the protonated water clusters to $\Delta v_{\text{BA}}^{\text{OH,MD}} = 398 \text{ cm}^{-1}$ in the $\text{CF}_3\text{SO}_3\text{H}-\text{H}_3\text{O}^+-n\text{H}_2\text{O}$ complexes. The values correspond to an increase in the relative probability of finding the structural diffusion motion, from $\mathbf{P_B/P_A} = 0.17$ in the protonated water clusters to 0.21 in the $\text{CF}_3\text{SO}_3\text{H}-\text{H}_3\text{O}^+-n\text{H}_2\text{O}$ complexes. The H-bonds in the vicinities of maximum $\mathbf{P_B/P_A}$ are, for examples, H-bond (3) in structures **C2C** and **C3C**, and H-bond (5) in structure **A3G-[1]**.

Diffusion coefficients

To discuss the dynamics of proton transfer in the $\text{CF}_3\text{SO}_3\text{H-H}_3\text{O}^+-n\text{H}_2\text{O}$ complexes, the distributions of the proton diffusion coefficients (D) for the H-bonds susceptible to proton transfer ($v_{\text{A}}^{\text{OH,MD}} < v_{\text{A}}^{\text{OH}^*,\text{MD}}$) were computed and shown in Figure 3.14. It appeared that D can vary in a quite wide range, with maxima at 2.5×10^{-5} and $3.2 \times 10^{-5} \text{ cm}^2 \text{ s}^{-1}$, in the gas phase and continuum aqueous solution, respectively; the latter is represented by the H-bonds in **Group 2** (pass-by mechanism) and could be used in the discussion of the effects of the $-\text{SO}_3\text{H}$ group, by comparison with the results in the protonated water clusters (Lao-ngam, Asawakun, Wannarat and Sagarik, 2011). It should be noted that the proton diffusion coefficients computed in the present work are comparable with the self-diffusion coefficient of liquid water ($2.3 \times 10^{-5} \text{ cm}^2 \text{ s}^{-1}$), but considerably lower than those in the protonated water clusters (Lao-ngam, Asawakun, Wannarat and Sagarik, 2011; Wu, Chen, Wang, Paesani and G.A. Voth, 2008).

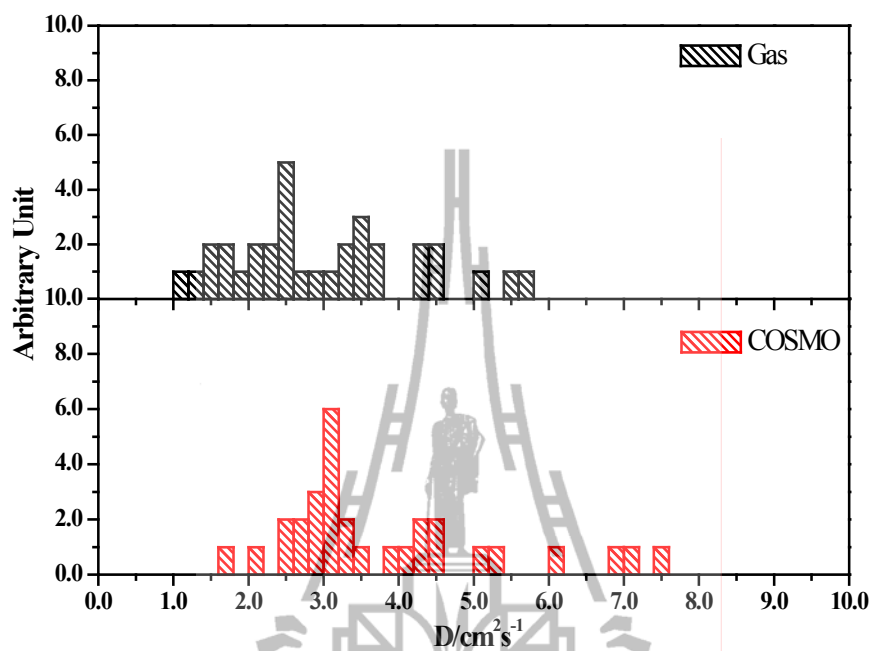


Figure 3.14 Distributions of the diffusion coefficients (D) of the transferring proton in the $\text{CF}_3\text{SO}_3\text{H}-\text{H}_3\text{O}^+-n\text{H}_2\text{O}$ complexes, obtained from BOMD simulations at 350 K. a) gas phase. b) continuum aqueous solution.

In order to obtain additional kinetics information from BOMD simulations, the lifetimes (τ) of the H-bonds with high relative probability of finding the structural diffusion motion (P_B/P_A) were computed from VACF of the O-O vibrations (Bopp, 1986); based on the observation that the relaxation behavior of the envelope of VACF can be approximated by an exponential function and the shared-proton structures possess shorter life times than the contact structures ($O-H^+..O$) (Kreuer, 2000). The classical first-order rate constants (k) for the interconversion between these two limiting structures were approximated from the lifetimes. In the present study, the lifetimes of H-bond (1) in structure **C1C** and H-bond (3) in structure **C2C** are given as examples; $\tau = 90$ and 114 fs, respectively, and corresponding to $k = 15.4$ and 12.1 ps^{-1} , respectively. The lifetimes are shorter and the first-order rate constants are larger than those obtained for the protonated water cluster (Lao-ngam, Asawakun, Wannarat and Sagarik, 2011); in continuum aqueous solution, the shared-proton structure with the highest P_B/P_A possesses $\tau = 233 \text{ fs}$ and $k = 6.0 \text{ ps}^{-1}$. The values reflected a higher rate for the interconversion between the shared-proton and contact structures in the presence of the $-SO_3H$ group.

Remarks should be made on the dynamics and kinetics in the presence of the $-SO_3H$ group. Comparison of the most probable proton diffusion coefficient in the $CF_3SO_3H-H_3O^+-nH_2O$ complexes ($D = 3.2 \times 10^{-5} \text{ cm}^2 \text{ s}^{-1}$, in continuum aqueous solution) and the corresponding value in the protonated water clusters (Lao-ngam, Asawakun, Wannarat and Sagarik, 2011) leads to an important conclusion; the transferring proton in the protonated water cluster with an extended H-bond network possesses $D = 8.9 \times 10^{-5}$ and $8.2 \times 10^{-5} \text{ cm}^2 \text{ s}^{-1}$, in the gas phase and continuum

aqueous solution, respectively. The values suggested that the $-\text{SO}_3\text{H}$ group suppresses the mobility of the transferring proton in the intermediate state, which could be explained by an increase of the electrostatic effect in the shared-proton structure. This result in lower proton diffusion coefficients in the $\text{CF}_3\text{SO}_3\text{H}-\text{H}_3\text{O}^+-n\text{H}_2\text{O}$ complexes compared to the protonated water clusters. The increase of the electrostatic effect is accompanied by a decrease of $\Delta v_{\text{BA}}^{\text{OH,MD}}$ and an increase in the relative probability of finding the structural diffusion motion ($\text{P}_\text{B}/\text{P}_\text{A}$) in the shared-proton structure, leading eventually to higher first-order rate constants (k) in the $\text{CF}_3\text{SO}_3\text{H}-\text{H}_3\text{O}^+-n\text{H}_2\text{O}$ complexes. One could therefore conclude that the $-\text{SO}_3\text{H}$ groups in Nafion[®] act as active binding sites which provide appropriate structural, energetic and dynamic conditions for effective structural diffusion processes in the intermediate states of proton transfer reactions.

CHAPTER IV

CONCLUSION

Proton transfer reactions at the sulfonic acid groups in Nafion[®] were theoretically studied using complexes formed from triflic acid (CF₃SO₃H), H₃O⁺ and H₂O, as model systems. The investigations began with searching for potential precursors and transition states at low hydration levels using the Test-particle model (T-Model), density functional theory (DFT) and *ab initio* calculations. They were employed as starting configurations in Born-Oppenheimer molecular dynamics (BOMD) simulations at 298 and 350 K, from which elementary reactions were analyzed and categorized.

Attempt has been made in Part I to study proton transfer reactions at a hydrophilic functional group in model Nafion[®], using a theoretical method which takes into account dynamics of formation and cleavage of covalent and H-bonds. Complexes formed from CF₃SO₃H, H₃O⁺ and n H₂O were employed as model systems, from which dynamics of an excess proton and proton defects at and in the vicinities of -SO₃H were systematically studied, with the emphasis on how -SO₃H facilitates or mediates proton transfer reactions at low hydration levels. It was found in general that all characteristic H-bond structures and trends of proton transfer in the H₃O⁺ - H₂O 1 : n and CF₃SO₃H - H₃O⁺ - H₂O 1 : 1 : n complexes, $1 \leq n \leq 3$,

could be predicted reasonably well by T-model, B3LYP/6-31G(d,p) and MP2/6-311++G(d,p) calculations. The theoretical results revealed possibilities for proton transfer along the H-bond network of water connecting the oxygen atoms of $-\text{SO}_3\text{H}$, as well as by relay-type mechanisms, in which proton hops across $-\text{SO}_3\text{H}$ through the formations of the $-\text{SO}_3\text{H}_2^+$ and $-\text{SO}_3^-$ transition states.

A series of BOMD simulations at 298 K was performed based on B3LYP/6-31G(d,p) calculations. Attention was focused on the precursors and transition states with H-bonds susceptible to proton transfers. Since the Zundel and Eigen complexes play the most important role in proton transfer reactions in aqueous solutions, their basic dynamic behavior was initially studied. It appeared that, proton transfer in H_5O_2^+ depends strongly on the $\text{O}_\text{h}\text{--}\text{H}_\text{h}\text{--}\text{O}_\text{w}$ H-bond separation, as well as its vibrational amplitude. Two extreme cases namely, large- and small-amplitude vibrations, were analyzed and discussed in details based on proton transfer profiles. The BOMD results showed that, due to the thermal energy fluctuation and couple motions among H-bonds, a quasi-dynamic equilibrium between the Eigen and Zundel complexes could be established and considered to be one of the most important elementary reactions in the proton transfer process. Although the model systems lack of continuous H-bond network connecting the first and second hydration shells, the average life time of H_3O^+ in the Eigen complex is in reasonable agreement with the lowest limit estimated from low-frequency vibrational spectroscopy.

For the $\text{CF}_3\text{SO}_3\text{H} - \text{H}_3\text{O}^+ - \text{H}_2\text{O}$ complexes, various temporary proton defects in H-bond structures were observed in the course of BOMD simulations. Due to the thermal energy fluctuation and dynamics at 298 K, proton transfer reactions at $-\text{SO}_3\text{H}$ seem to comprise of various elementary reactions in quasi-dynamic equilibriums. These prohibit proton transfer reactions from being concerted, and confirm the observations that, the proton motion is too fast to be rate-determining step. Due to large- and small-amplitude vibrations in H-bond separations, the internal conversions between covalent and H-bonds, similar to the Grotthuss mechanism, were concluded to form general basis for proton transfer processes at $-\text{SO}_3\text{H}$. Attempt was also made to describe these proton-relay type mechanisms in terms of coherence and incoherence effects. BOMD simulations showed that, the proton-relay type mechanisms could take place among $-\text{SO}_3\text{H}$, H_3O^+ and H_2O , providing some effective proton transfer pathways, through the formations of the $-\text{SO}_3^-$, $-\text{SO}_3\text{H}_2^+$ and H_5O_2^+ transition states. The analyses of the average life times of the precursors and elementary reactions suggested that, when the H-bond structures are right, in order that $-\text{SO}_3\text{H}$ could effectively function as a mediator in proton transfer reactions, the probabilities for the elementary reactions to proceed in the forward and reverse directions should be somewhat equivalent, otherwise proton would be trapped at $-\text{SO}_3\text{H}$.

It should be emphasized that, the present BOMD simulations focused on proton transfer processes at and in the vicinities of a single $-\text{SO}_3\text{H}$ group, and within

a narrow timescale. Therefore, H-bond structure reorganizations and molecular diffusions, which could contribute to proton conduction in different timescales, were not taken into account. It should also be added that, the present theoretical investigations were performed at low hydration levels, in which the H-bond networks are not as extensive as in aqueous solutions, and strong interaction between proton and the polar environment could lead to a retardation of proton transfer. Therefore, direct comparisons between our model calculations and experiments seem not appropriate. However, some important insights, especially the interplays between local H-bond structures and dynamics, as well as the potential precursors and the proton transfer elementary reactions in an excess proton condition, could be obtained. The present BOMD results also iterated that, equilibrium structures and energetic obtained from MM or *ab initio* geometry optimizations could not provide complete information on chemical reactions, especially the reaction pathways. It appeared that the theoretical methods and the analyses adopted in the present work could provide practical bases for the study of proton transfer reactions in larger H-bond systems.

In Part II, proton transfer reactions and dynamics at a hydrophilic group of Nafion[®] were investigated at low hydration levels using the complexes formed from $\text{CF}_3\text{SO}_3\text{H}$, H_3O^+ and $n\text{H}_2\text{O}$, $1 \leq n \leq 3$, as model systems. Following the strategies in Part I, the H-bond structures, asymmetric stretching coordinates (Δd_{DA}) and asymmetric O-H stretching frequencies (ν^{OH}) obtained from B3LYP/TZVP calculations were analyzed and categorized. The B3LYP/TZVP results suggested two types of structural diffusion mechanisms namely, the pass-through mechanism, involving the protonation and deprotonation at the $-\text{SO}_3\text{H}$ group, and the pass-by

mechanism, the proton transfer in the adjacent Zundel complex. The plots of ν^{OH} and Δd_{DA} predicted the threshold frequencies ($\nu^{\text{OH}*}$) for the proton transfer through the pass-through mechanism at 2162 and 2001 cm^{-1} , in the gas phase and continuum aqueous solution, respectively, whereas for the pass-by mechanism at 1829 and 1714 cm^{-1} , respectively. The latter are about 200 cm^{-1} lower than those in the protonated water clusters and, therefore, represent a spectroscopic evidence for the promotion of proton transfer in the intermediate states (the shared-proton complexes) by the $-\text{SO}_3\text{H}$ group.

Inclusion of the thermal energy fluctuations and dynamics in the model calculations made it difficult to differentiate the results in the gas phase and continuum aqueous solution. For the pass-by mechanism, BOMD simulations at 350 K predicted similar characteristic asymmetric O-H stretching frequencies ($\nu_{\text{A}}^{\text{OH,MD}}$), with slightly lower threshold frequencies for proton transfer, $\nu_{\text{A}}^{\text{OH*,MD}} = 1733$ and 1740 cm^{-1} , respectively. Additionally, BOMD simulations showed second asymmetric O-H stretching band at a higher frequency ($\nu_{\text{B}}^{\text{OH,MD}}$). As in the case of protonated water clusters, $\nu_{\text{A}}^{\text{OH,MD}}$ and $\nu_{\text{B}}^{\text{OH,MD}}$ could be associated with the oscillatory shuttling and structural diffusion motions, respectively; the characteristic motions of the transferring proton in H-bond. The analyses of $\nu_{\text{A}}^{\text{OH,MD}}$ and $\nu_{\text{B}}^{\text{OH,MD}}$ suggested the lowest vibrational energies for the interconversion between the oscillatory shuttling and structural diffusion motions ($\Delta \nu_{\text{BA}}^{\text{OH,MD}}$), for the pass-through and pass-by mechanisms of 469 and 398 cm^{-1} , respectively. The latter is about 75 cm^{-1} lower than the protonated water clusters; an indication of a decrease of the vibrational energy for

the interconversion between the oscillatory shuttling and structural diffusion motions in the presence of the $-\text{SO}_3\text{H}$ group.

Comparison of the proton diffusion coefficients obtained in the present work and those in the protonated water clusters indicated that the $-\text{SO}_3\text{H}$ group suppresses the mobility of the transferring proton in the intermediate states, by introducing strong electrostatic effect at the shared-proton structures. These are however accompanied by a decrease of the vibrational energy for the interconversion between the oscillatory shuttling and structural diffusion motions and a higher relative probability of finding the structural diffusion motion in the $\text{CF}_3\text{SO}_3\text{H}\cdot\text{H}_3\text{O}^+\cdot n\text{H}_2\text{O}$ complexes, compared to those in the protonated water clusters. One could, therefore, conclude that the $-\text{SO}_3\text{H}$ groups in Nafion[®] act as active binding sites which provide appropriate structural, energetic and dynamic conditions for effective structural diffusion processes in the intermediate states of proton transfer reactions. The present results confirmed that, due to the coupling among various vibrational modes in H-bonds, the discussions on proton transfer reactions cannot be made based solely on static proton transfer potentials. Inclusion of thermal energy fluctuations and dynamics in the model calculations, as in the case of BOMD simulations, together with systematic IR spectral analyses, has been proved to be the most appropriate theoretical approaches.



REFERENCES

REFERENCES

- Agmon, N. (1995). The Grotthuss mechanism. **Chemical Physics Letters**. 244: 456-462.
- Ahlrichs, R., Bär, M., Häser, M., Horn, H. and Kölmel, C. (1989). Electronic structure calculations on workstation computers: The program system turbomole. **Chemical Physics Letters**. 162: 165-169.
- Asbury, J. B., Steinel, T. and Fayer, M. D. (2004). Vibrational echo correlation spectroscopy probes of hydrogen bond dynamics in water and methanol. **Journal of Luminescence**. 107: 271-286.
- Balbuena, P. B. and Seminario, J. M. (1999). **Theoretical and Computational Chemistry 7**. Amsterdam: Elsevier.
- Barnett, R. N. and Landman, U. (1993). Born-Oppenheimer molecular-dynamics simulations of finite systems: Structure and dynamics of (H₂O)₂. **Physical Review B**. 48: 2081-2097.
- Becke, A. D. (1993). Density-functional thermochemistry. III. The role of exact exchange. **The Journal of Chemical Physics**. 98: 5648-5652.
- Benoit, M. and Marx, D. (2005). The shapes of protons in hydrogen bonds depend on the bond length. **ChemPhysChem**. 6: 1738-1741.
- Bopp, P. (1986). A study of the vibrational motions of water in an aqueous CaCl₂ solution. **Chemical Physics**. 106: 205-212.

- Botti, A., Bruni, F., Imberti, S., Ricci, M. A. and Soper, A. K. (2005). Solvation shell of H^+ ions in water. **Journal of Molecular Liquids**. 117: 77-79.
- Boyle, N. G., McBrierty, V. J. and Eisenberg, A. (1983). NMR investigation of molecular motion in Nafion membranes. **Macromolecules**. 16: 80-84.
- Buzzoni, R., Bordiga, S., Ricchiardi, G., Spoto, G. and Zecchina, A. (1995). Interaction of H_2O , CH_3OH , $(CH_3)_2O$, CH_3CN , and pyridine with the superacid perfluorosulfonic membrane Nafion: An IR and Raman study. **The Journal of Physical Chemistry**. 99: 11937-11951.
- Chen, J., McAllister, M. A., Lee, J. K. and Houk, K. N. (1998). Short, strong hydrogen bonds in the gas phase and in solution: Theoretical exploration of pKa matching and environmental effects on the strengths of hydrogen bonds and their potential roles in enzymatic catalysis. **The Journal of Organic Chemistry**. 63: 4611-4619.
- Cheng, H. P. and Krause, J. L. (1997). The dynamics of proton transfer in $H_5O_2^+$. **The Journal of Chemical Physics**. 107: 8461-8468.
- Conway, B. E., Bockris, J. O. M. and Linton, H. (1956). Proton conductance and the existence of the H_3O^+ ion. **The Journal of Chemical Physics**. 24: 834-850.
- Cramer, C. J. (2002). **Essentials of Computational Chemistry: Theory and models**. New York: John Wiley & Sons, Ltd.
- Deeying, N. (2005). **Influence of metal ion and solute conformation change on hydration of small amino acid**. Ph.D. Dissertation, Suranaree University of Technology, Thailand.

- Deeying, N. and Sagarik, K. (2007). Effects of metal ion and solute conformation change on hydration of small amino acid. **Biophysical Chemistry**. 125: 72-91.
- Devanathan, R., Venkatnathan, A. and Dupuis, M. (2007). Atomistic simulation of Nafion membrane. 2. Dynamics of water molecules and hydronium Ions. **The Journal of Physical Chemistry B**. 111: 13006-13013.
- Duan, X. and Scheiner, S. (1992). Analytic functions fit to proton transfer potentials. **Journal of Molecular Structure**. 270: 173-185.
- Eigen, M. (1964). Proton transfer, acid-base catalysis, and enzymatic hydrolysis. Part 1: elementary processes. **Angewandte Chemie**. 3: 1-19.
- Eigen, M. and Maeyer, L. D. (1958). Self-Dissociation and Protonic Charge Transport in Water and Ice. **Proceedings of the Royal Society**. 247: 505-533.
- Eikerling, M., Paddison, S. J., Pratt, L. R. and Zawodzinski, T. A. (2003). Defect structure for proton transport in a triflic acid monohydrate solid. **Chemical Physics Letters**. 368: 108-114.
- Fridgen, T. D., McMahon, T. B., MacAleese, L., Lemaire, J. and Maitre, P. (2004). Infrared spectrum of the protonated water dimer in the gas phase. **The Journal of Physical Chemistry A**. 108: 9008-9010.

- Frisch, M. J., Trucks, G. W., Schlegel, H. B., Scuseria, G. E., Robb, M. A., Cheeseman, J. R., Zakrzewski, V. G., Montgomery, J. A., Stratmann, R. E., Burant, J. C., Dapprich, S., Millam, J. M., Daniel, A. D., Kudin, K. N., Strain, M. C., Farkas, O., Tomasi, J., Barone, V., Cossi, M., Cammi, R., Mennucci, B., Pomelli, C., Adamo, C., Clifford, S., Ochterski, J., Petersson, G. A., P.Y. Ayala, Q. C., Morokuma, K., Salvador, P., Dannenberg, J. J., Malick, D. K., Rabuck, A. D., Raghavachari, K., J. B. Foresman, Cioslowski, J., Ortiz, J. V., Baboul, A. G., Stefanov, B. B., Liu, G., Liashenko, A., Piskorz, P., Komaromi, I., Gomperts, R., Martin, R. L., Fox, D. J., T. Keith, M. A. A. L., Peng, C. Y., Nanayakkara, A., Challacombe, M., Gill, B. J., Chen, W., Wong, M. W., Gonzalez, C. and Pople, J. A. (2005). Gaussian 03 (Revision D.1): Gaussian, Inc.
- Gierke, T. D., Munn, G. E. and Wilson, F. C. (1981). The morphology in nafion perfluorinated membrane products, as determined by wide- and small-angle x-ray studies. **Journal of Polymer Science: Polymer Physics Edition**. 19: 1687- 1704.
- Giguere, P. A. (1979). The great fallacy of the H^+ ion: And the true nature of H_3O^+ . **Journal of Chemical Education**. 56: 571-576.
- Glezakou, V. A., Dupuis, M. and Mundy, C. J. (2007). Acid/base equilibria in clusters and their role in proton exchange membranes: Computational insight. **Physical Chemistry Chemical Physics**. 9: 5752-5760.
- Glick, R. E. and Tewari, K. C. (1966). Proton Nuclear Magnetic Relaxation Studies on Water: The Rates of Acid- and Base-Catalyzed Proton Exchange. **Journal of Chemical Physics**. 44: 546-547.

- Grotthuss, C. J. T. de. (1806). Sur la décomposition de l'eau et des corps qu'elle tient en dissolution à l'aide de l'électricité galvanique. **Annali di chimica (Paris)** 58: 54-73.
- Haile, J. M. (1997). **Molecular Dynamics Simulations**. New York: John Wiley & Sons Ltd.
- Hermida-Ramón, J. M. and Karlström, G. (2004). Study of the hydronium ion in water. A combined quantum chemical and statistical mechanical treatment. **Journal of Molecular Structure: THEOCHEM**. 712: 167-173.
- Hinatsu, J. T., Mizuhata, M. and Takenaka, H. (1994). Water Uptake of Perfluorosulfonic Acid Membranes from Liquid Water and Water Vapor. **Journal of The Electrochemical Society**. 141: 1493-1498.
- Iftimie, R., Thomas, V., Plessis, S., Marchand, P. and Ayotte, P. (2008). Spectral signatures and molecular origin of acid dissociation intermediates. **Journal of the American Chemical Society**. 130: 5901-5907.
- Jiang, J. C., Chaudhuri, C., Lee, Y. T. and Chang, H. C. (2002). Hydrogen bond rearrangements and interconversions of $\text{H}^+(\text{CH}_3\text{OH})_4\text{H}_2\text{O}$ cluster isomers. **The Journal of Physical Chemistry A**. 106: 10937-10944.
- Jing, X., Troullier, N., Dean, D., Binggeli, N., Chelikowsky, J. R., Wu, K. and Saad, Y. (1994). Ab initio molecular-dynamics simulations of Si clusters using the higher-order finite-difference-pseudopotential method. **Physical Review B**. 50: 12234-12237.
- Knee, J. L., Knundkar, L. R. and Zewail, A. H. (1985). Picosecond mass spectrometry of a collisionless photodissociation reaction. **Journal of Chemical Physics** 82: 4715-4716.

- Koppel, T. (1999). **Powering the Future: The ballard fuel cell and the race to change the world**. New York: John Wiley & Sons Ltd.
- Kreuer, K. D. (1996). Proton conductivity: Materials and applications. **Chemistry of Materials**. 8: 610-641.
- Kreuer, K. D. (1997). Fast proton conductivity: A phenomenon between the solid and the liquid state? **Solid State Ionics**. 94: 55-62.
- Kreuer, K. D. (2000). On the complexity of proton conduction phenomena. **Solid State Ionics** 136: 149-160.
- Kreuer, K. D., Paddison, S. J., Spohr, E. and Schuster, M. (2004). Transport in proton conductors for fuel-cell applications: Simulations, elementary reactions, and phenomenology. **Chemical Reviews**. 104: 4637-4678.
- Kwac, K., Lee, C., Jung, Y. and Han, J. (2006). Phenol-benzene complexation dynamics: Quantum chemistry calculation, molecular dynamics simulations, and two dimensional IR spectroscopy. **Journal of Chemical Physics** 125: 244508-244516.
- Lao-ngam, C., Asawakun, P., Wannarat, S. and Sakarik, K. (2011). Proton transfer reactions and dynamics in protonated water clusters. **Physical Chemistry Chemical Physics**. 13: 4562-4575.
- Laporta, M., Pegoraro, M. and Zanderighi, L. (1999). Perfluorosulfonated membrane (Nafion): FT-IR study of the state of water with increasing humidity. **Physical Chemistry Chemical Physics**. 1: 4619-4628.
- Larminie, J. and Dicks, A. (2001). **Fuel Cell Systems Explained**. Chichester: John Wiley & Son, Ltd.

- Leach, A. R. (1996). **Molecular Modelling: Principles and Applications**. Essex: Addison Wesley Longman, Ltd.
- Lee, C., Yang, W. and Parr, R. G. (1988). Development of the Colle-Salvetti correlation-energy formula into a functional of the electron density. **Physical Review B**. 37: 785-789.
- Ludvigsson, M., Lindgren, J. and Tegenfeld, J. (2000). FTIR study of water in the case Nafion films. **Electrochimica Acta**. 45: 2267-2271.
- Marx, D., Tuckerman, M. E., Hutter, J. and Parrinello, M. (1999). The nature of the hydrated excess proton in water. **Nature**. 397: 601-604.
- Mauritz, K. A. and Moore, R. B. (2004). State of understanding of Nafion. **Chemical Reviews**. 104: 4535-4586.
- Okumura, M., Yeh, L. I., Myers, J. D. and Lee, Y. T. (1990). Infrared spectra of the solvated hydronium ion: Vibrational predissociation spectroscopy of mass-selected $\text{H}_3\text{O}^+(\text{H}_2\text{O})_n(\text{H}_2)_m$. **The Journal of Physical Chemistry**. 94: 3416-3427.
- Paddison, S. J. (2001). The modeling of molecular structure and ion transport in sulfonic acid based ionomer membranes. **Journal of New Materials for Electrochemical Systems**. 4: 197-207.
- Paddison, S. J. (2003). Proton conduction mechanisms at low degrees of hydration in sulfonic acid-based polymer electrolyte membranes. **Annual Review of Materials Research**. 33: 289-319.

- Paddison, S. J., Bender, G., Kreuer, K. D., Nicoloso, N. and Zawodzinski Jr., T. A. (2000). The microwave region of the dielectric spectrum of hydrated Nafion and other sulfonated membranes. **Journal of New Materials for Electrochemical Systems**. 3: 291-300.
- Paddison, S. J. and Elliott, J. A. (2005). Molecular modeling of the short-side-chain perfluorosulfonic acid membrane. **The Journal of Physical Chemistry A**. 109: 7583-7593.
- Paddison, S. J. and Elliott, J. A. (2006). The effects of backbone conformation on hydration and proton transfer in the 'short-side-chain' perfluorosulfonic acid membrane. **Solid State Ionics**. 177: 2385-2390.
- Paddison, S. J. and Elliott, J. A. (2006). On the consequences of side chain flexibility and backbone conformation on hydration and proton dissociation in perfluorosulfonic acid membranes. **Physical Chemistry Chemical Physics**. 8: 2193-2203.
- Paddison, S. J., Pratt, L. R. and Zawodzinski Jr., T. A. (1999). Conformations of perfluoroether sulfonic acid side chains for the modeling of Nafion. **Journal of New Materials for Electrochemical Systems**. 2: 183-188.
- Paddison, S. J., Pratt, L. R. and Zawodzinski Jr., T. A. (2001). Variation of the Dissociation Constant of Triflic Acid with Hydration. **The Journal of Physical Chemistry A**. 105: 6266-6268.
- Paddison, S. J., R. Pratt, L., Zawodzinski Jr., T. A. and Reagor, D. W. (1998). Molecular modeling of trifluoromethanesulfonic acid for solvation theory. **Fluid Phase Equilibria**. 150-151: 235-243.

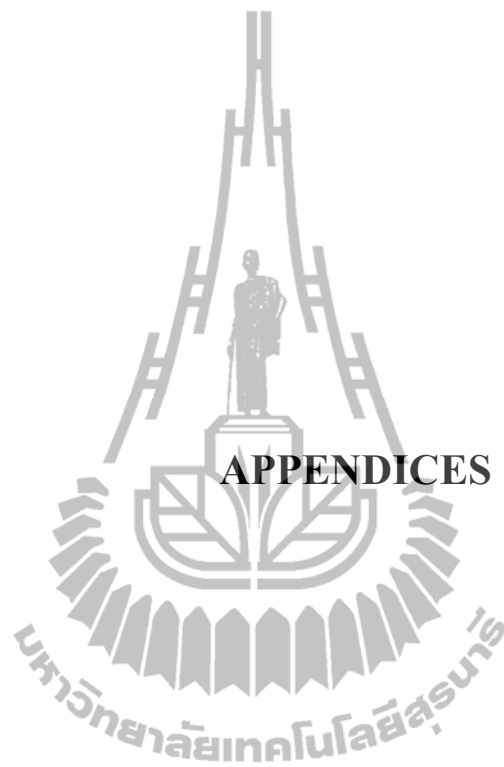
- Paddison, S. J. and Zawodzinski Jr, T. A. (1998). Molecular modeling of the pendant chain in Nafion. **Solid State Ionics**. 115: 333-340.
- Park, M., Shin, I., Singh, N. J. and Kim, K. S. (2007). Eigen and Zundel forms of small protonated water clusters: Structures and infrared spectra. **The Journal of Physical Chemistry A**. 111: 10692-10702.
- Pimentel, G. C. and McClellan, A. L. (1960). **The Hydrogen Bond**. San Francisco: W. H. Freeman.
- Phonyiem, M., Chaiwongwattana, S., Lao-ngam, C. and Sagarik, K. (2011). Proton transfer reactions and dynamics of sulfonic acid group of Nafion[®]. **Physical Chemistry Chemical Physics**. 13: 10923-10939.
- Rabideau, S. W. and Hetch, H. G. (1967). Oxygen-17 NMR Linewidths as Influenced by Proton Exchange in Water. **Journal of Chemical Physics**. 47: 544-546.
- Rapaport, D. C. (1995). **The Art of Molecular Dynamics Simulation**. London: Cambridge University Press.
- Sadeghi, R. R. and Cheng, H. P. (1999). The dynamics of proton transfer in a water chain. **The Journal of Chemical Physics**. 111: 2086-2094.
- Sagarik, K. (1999). Theoretical studies on hydrogen bonding in hydroxylamine clusters and liquid. **Journal of Molecular Structure: THEOCHEM**. 465: 141-155.
- Sagarik, K. and Ahlrichs, R. (1987). A test particle model potential for formamide and molecular dynamics simulations of the liquid. **The Journal of Chemical Physics**. 86: 5117-5126.
- Sagarik, K. and Asawakun, P. (1997). Intermolecular potential for phenol based on the test particle model. **Chemical Physics**. 219: 173-191.

- Sagarik, K., Chaiwongwattana, S. and Sisot, P. (2004). A theoretical study on clusters of benzoic acid-water in benzene solutions. **Chemical Physics**. 306: 1-12.
- Sagarik, K., Chaiwongwattana, S., Vchirawongkwin, V. and Prueksaaron, S. (2010). Proton transfer reactions and dynamics in $\text{CH}_3\text{OH}-\text{H}_3\text{O}^+-\text{H}_2\text{O}$ complexes. **Physical Chemistry Chemical Physics**. 12: 918-929.
- Sagarik, K. and Chaiyapongs, S. (2005). Structures and stability of salt-bridge in aqueous solution. **Biophysical Chemistry**. 117: 119-140.
- Sagarik, K., Phonyiem, M., Lao-ngam, C. and Chaiwongwattana, S. (2008). Mechanisms of proton transfer in Nafion: Elementary reactions at the sulfonic acid groups. **Physical Chemistry Chemical Physics**. 10: 2098-2112.
- Sagarik, K., Pongpituk, V., Chaiyapongs, S. and Sisot, P. (1991). Test-particle model potentials for hydrogen-bonded complexes: Complexes formed from HCN, HF, H_2O , NH_3 , HCONH_2 , HCONHCH_3 , guanine and cytosine. **Chemical Physics**. 156: 439-456.
- Sagarik, K. and Rode, B. M. (2000). Intermolecular potential for benzoic acid-water based on the test-particle model and statistical mechanical simulations of benzoic acid in aqueous solutions. **Chemical Physics**. 260: 159-182.
- Sagarik, K. and Spohr, E. (1995). Statistical mechanical simulations on properties of liquid pyridine. **Chemical Physics**. 199: 73-82.
- Santambrogio, G., Brummer, M., Woste, L., Dobler, J., Sierka, M., Sauer, J., Meijer, G. and Asmis, K. R. (2008). Gas phase vibrational spectroscopy of mass-selected vanadium oxide anions. **Physical Chemistry Chemical Physics**. 10: 3992-4005.

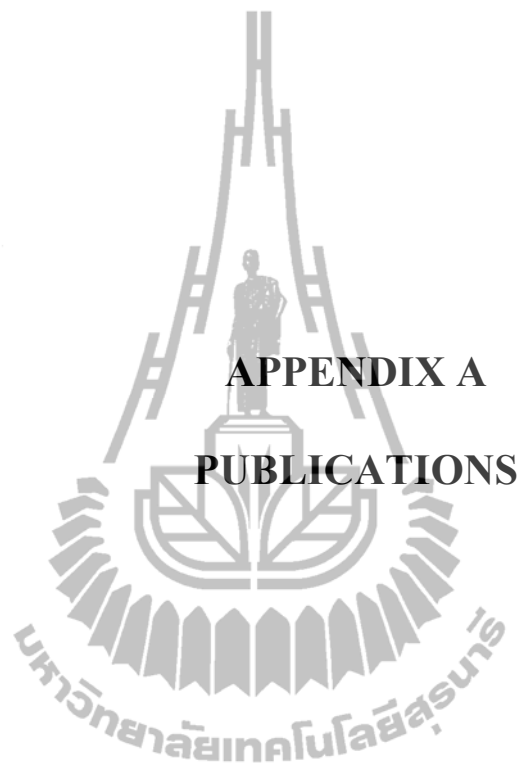
- Schafer, A., Huber, C. and Ahlrichs, R. (1994). Fully optimized contracted Gaussian basis sets of triple zeta valence quality for atoms Li to Kr. **The Journal of Chemical Physics**. 100: 5829-5835.
- Schmitt, U. W. and Voth, G. A. (1999). The computer simulation of proton transport in water. **The Journal of Chemical Physics**. 111: 9361-9381.
- Scott, A. P. and Radom, L. (1996). Harmonic vibrational frequencies: An evaluation of Hartree-Fock, Moller-Plesset, quadratic configuration interaction, density functional theory, and semiempirical scale factors. **The Journal of Physical Chemistry**. 100: 16502-16513.
- Termath, V. and Sauer, J. (1997). *Ab initio* molecular dynamics simulation of H_5O_2^+ and H_7O_3^+ gas phase clusters based on density functional theory **Molecular Physics**. 91: 963-975.
- Treutler, O. and Ahlrichs, R. (1995). Efficient molecular numerical integration schemes. **The Journal of Chemical Physics**. 102: 346-354.
- Vincent, C. A. and Scrosati, B. (1997). **Modern batteries: an introduction to electrochemical power sources**. New York: John Wiley & Sons Ltd.
- Wu, C. C., Chaudhuri, C., Jiang, J. C., Lee, Y. T. and Chang, H. C. (2003). Structural isomerism and competitive proton solvation between methanol and water in $\text{H}^+(\text{CH}_3\text{OH})_m(\text{H}_2\text{O})_n$, $m + n = 4$. **The Journal of Physical Chemistry A**. 108: 2859-2866.
- Wu, C. C., Jiang, J. C., Boo, D. W., Lin, S. H., Lee, Y. T. and Chang, H. C. (2000). Behaviors of an excess proton in solute-containing water clusters: A case study of $\text{H}^+(\text{CH}_3\text{OH})(\text{H}_2\text{O})_{1-6}$. **The Journal of Chemical Physics**. 112: 176-188.

- Wu, Y., Chen, H., Wang, F., Paesani, F. and Voth, G. A. (2007). An improved multistate empirical valence bond model for aqueous proton solvation and transport. **The Journal of Physical Chemistry B**. 112: 467-482.
- Young, D. C. (2001). **Computational Chemistry: A practical guide for applying techniques to real world problems**. New York: Wiley Interscience.
- Zecchina, A., Geobaldo, F., Spoto, G., Bordiga, S., Ricchiardi, G., Buzzoni, R. and Petrini, G. (1996). FTIR Investigation of the Formation of Neutral and Ionic Hydrogen-Bonded Complexes by Interaction of H-ZSM-5 and H-Mordenite with CH₃CN and H₂O: Comparison with the H-NAFION Superacidic System. **The Journal of Physical Chemistry**. 100: 16584-16599.





APPENDICES

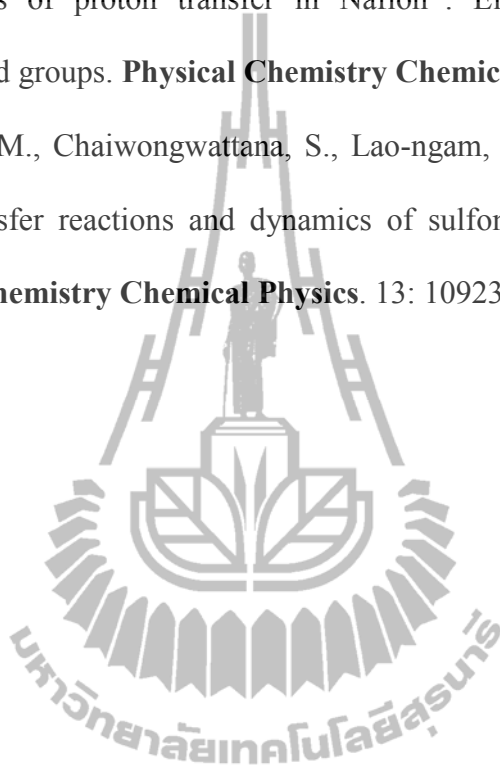


APPENDIX A

PUBLICATIONS

Publications:

1. Sagarik, K., Phonyiem, M., Lao-ngam, C. and Chaiwongwattana, S. (2008). Mechanisms of proton transfer in Nafion[®]: Elementary reactions at the sulfonic acid groups. **Physical Chemistry Chemical Physics**. 10: 2098-2112.
2. Phonyiem, M., Chaiwongwattana, S., Lao-ngam, C. and Sagarik, K. (2011). Proton transfer reactions and dynamics of sulfonic acid group of Nafion[®]. **Physical Chemistry Chemical Physics**. 13: 10923-10939.



Mechanisms of proton transfer in Nafion[®]: elementary reactions at the sulfonic acid groups

Kritsana Sagarik,^{*ab} Mayuree Phonyiem,^a Charoensak Lao-ngam^a and Sernsiri Chaiwongwattana^a

Received 29th November 2007, Accepted 17th January 2008

First published as an Advance Article on the web 21st February 2008

DOI: 10.1039/b718480h

Proton transfer reactions at the sulfonic acid groups in Nafion[®] were theoretically studied, using complexes formed from triflic acid (CF₃SO₃H), H₃O⁺ and H₂O, as model systems. The investigations began with searching for potential precursors and transition states at low hydration levels, using the test-particle model (T-model), density functional theory (DFT) and *ab initio* calculations. They were employed as starting configurations in Born–Oppenheimer molecular dynamics (BOMD) simulations at 298 K, from which elementary reactions were analyzed and categorized. For the H₃O⁺–H₂O complexes, BOMD simulations suggested that a quasi-dynamic equilibrium could be established between the Eigen and Zundel complexes, and that was considered to be one of the most important elementary reactions in the proton transfer process. The average lifetime of H₃O⁺ obtained from BOMD simulations is close to the lowest limit, estimated from low-frequency vibrational spectroscopy. It was demonstrated that proton transfer reactions at –SO₃H are not concerted, due to the thermal energy fluctuation and the existence of various quasi-dynamic equilibria, and –SO₃H could directly and indirectly mediate proton transfer reactions through the formation of proton defects, as well as the –SO₃[–] and –SO₃H₂⁺ transition states.

1. Introduction

An energy crisis and environmental concerns about global warming, as well as the need to reduce CO₂ emissions, have provided strong motivation to seek ways of improving energy conversion technology. The proton exchange membrane fuel cell (PEMFC) has received much attention as one of the most promising energy suppliers for the future world.^{1–3} The polymer electrolyte membrane which has been widely used in PEMFCs is Nafion[®], introduced by Dupont in 1967.² Nafion[®] is a perfluorinated polymer with hydrophobic Teflon backbone and randomly attached hydrophilic side chains. The backbones and the side chains of Nafion[®] are terminated by trifluoromethanesulfonic (triflic) acid, which is known to be one of the strongest acids. The triflic acid functional groups (–CF₂SO₃H) are preferentially hydrated and play important roles in proton transfer reactions in PEMFCs. Experiments have shown that hydrated –CF₂SO₃H form aggregates, resulting in large interconnected hydrophilic domains.⁴ Since the hydrophilic and hydrophobic domains are quite well separated,^{5,6} theoretical and experimental investigations could emphasize only the hydrophilic domains, in which proton conduction takes place. It was observed in general that the degree of hydration at –CF₂SO₃H, the morphology of

PEM and the size of the hydrophilic domains are directly related to the efficiency of proton conduction in Nafion[®].^{5,7–9} Although some theoretical and experimental information has been accumulated, the complete mechanisms of proton conduction in Nafion[®] seem not available, especially at the molecular level.^{5,7–9} Since basic chemistry of Nafion[®] has been discussed in details in many review articles, only some information relevant to the present study will be briefly summarized.

Three basic molecular fragments, potentially involved in proton transfer reactions at the hydrophilic side chains in Nafion[®], are –(CF₂OCF₂)–, –CF₂SO₃H and –CF₂SO₃[–]. Density functional theory (DFT) at B3LYP/6-31G(d,p) level^{10,11} suggested that, the hydrogen-bond (H-bond) between CF₃OCF₃ and H₂O is rather weak, due to the strong electron withdrawing effects from the two CF₃ groups. Therefore, –(CF₂OCF₂)– might not be directly involved in proton transfer reactions in Nafion[®], which is in accordance with IR experiment¹² and molecular dynamic (MD) simulations.¹³ Experimental evidence has shown that when sufficiently hydrated, the –CF₂SO₃H groups in Nafion[®] are highly dissociated.^{14–16} Spectroscopic measurements in which the assignment and comparison of IR and Raman spectra of individual species in Nafion[®] were made^{14,15} revealed that –CF₂SO₃H could be completely dissociated, depending upon the experimental conditions. Dielectric spectroscopy¹⁶ also showed a strong dependence of the dielectric constant and the specific conductivity of Nafion[®] with water content. Whereas ¹⁹F NMR experiment¹⁷ indicated that there is a range of temperatures over which the –CF₂SO₃H groups in

^a School of Chemistry, Institute of Science, Suranaree University of Technology, Nakhon Ratchasima 30000, Thailand. E-mail: kritsana@sut.ac.th; Fax: (6644) 224635; Tel: (6644) 224635

^b National Nanotechnology Center (NANOTEC), National Science and Technology Development Agency (NSTDA), Pathumthani 12120, Thailand

Nafion[®] go from being fully dissociated to being fully associated upon cooling.

Attempts have been made to probe the acidity of CF₃SO₃H, as well as to determine the transition state ion-pair complex formed from CF₃SO₃[−] and H₃O⁺ in the gas phase.¹⁸ It was reported that, with the inclusion of electrostatic free energy, the activation energy for the deprotonation of CF₃SO₃H amounts to 19.6 kJ mol^{−1}, implying that, the ion-pair complex are not stable in the gas phase and some water molecules are required to stabilize both CF₃SO₃[−] and H₃O⁺. Mechanisms of proton dissociation from CF₃SO₃H were examined by Paddison *et al.*,^{19,20} by performing a series of B3LYP/6-31G(d,p) calculations on clusters of the CF₃SO₃H-(H₂O)_n complexes, 1 ≤ n < 6. Paddison *et al.* reported that, no proton dissociation was observed until three water molecules were included, and H₃O⁺ could be stabilized through the formation of H-bonds with two water molecules and one oxygen atom of CF₃SO₃[−]. This H-bond complex could represent one of the precursors for proton dissociation from CF₃SO₃H. Interesting results were obtained when up to five water molecules were added, with H₃O⁺ located progressively further away from CF₃SO₃[−], and when six water molecules were added, a complete separation of H₃O⁺ from CF₃SO₃[−] was observed. The results in ref. 19 and 20 suggested a possible scenario for proton dissociation and showed how H₃O⁺ moves away from CF₃SO₃[−].

Mechanisms of proton dissociation at -CF₂SO₃H in minimally hydrated PEM were proposed based on DFT-MD simulations on triflic acid monohydrate solid ((CF₃SO₃[−]H₃O⁺)₄).²¹ DFT-MD simulations suggested a relay-type mechanism, in which a proton defect represents an intermediate state; the defect involves formation of the Zundel complex (H₅O₂⁺) and the reorganization of the neighboring -CF₂SO₃[−] groups, which share a proton between the oxygen atoms of the anionic sites. The proposed mechanism also revealed a possibility for proton conduction along the hydrophilic head groups, -CF₂SO₃H and -CF₂SO₃[−]. The results in ref. 21 are in good agreement with the activation energy for proton transfer in minimally hydrated Nafion[®] reported in ref. 22.

Similar theoretical studies were carried out on short-side-chain perfluorosulfonic acids, in which large scale DFT geometry optimizations were conducted on fragments of Nafion[®], with and without water molecules and with distinct pendant chain separations.^{23–25} B3LYP/6-311G(d,p) revealed a possibility for proton transfer between two adjacent hydrophilic groups, along the H-bond networks of water connecting them. The proposed proton transfer pathway is mediated by the formations of the -S-O⋯H⋯O-H H-bond, as well as H₅O₂⁺.²³ It was suggested in ref. 24 and 25 that the number of water molecules required to promote proton dissociation could be reduced when the -CF₂SO₃H groups are brought closer to each other through conformational change in the backbone. These show the importance of side chain flexibility and backbone conformation in proton transfer in short-side-chain perfluorosulfonic acid membranes at low water content.

Ab initio calculations and MD simulations on the complexes formed from CF₃CF₂SO₃H and nH₂O, 1 ≤ n ≤ 4, available to us after the manuscript has been completed, indicated that for n = 3, the neutral and ion-pair complexes are close in energy

and are accessible in the fluctuation dynamics of proton transport,²⁶ whereas for n ≤ 2, the only relevant complex is the neutral form. Most importantly, it was suggested in ref. 26 that, based on the free energy surface for proton exchange, the CF₃CF₂SO₃H₂⁺-H₂O and CF₃CF₂SO₃H-H₃O⁺ complexes are nearly isoenergetic, and CF₃CF₂SO₃H₂⁺ could play important roles in proton conduction at low hydration levels.

In the present study, a theoretical method which takes into account the dynamics of formation and cleavage of covalent and H-bonds was employed in the study of proton transfer reactions at a hydrophilic functional group in model Nafion[®]. While the other theoretical investigations^{18–20} focused on conditions and mechanisms of proton dissociation from -CF₂SO₃H, as well as proton conduction from the dissociated species (-CF₂SO₃[−]), the present study emphasized on how -CF₂SO₃H facilitates or mediates transportation of an excess proton. Special attention was given to precursors and transition states, as well as dynamics in elementary reactions. The complexes formed from CF₃SO₃H, H₃O⁺ and H₂O were employed as model systems, from which dynamics of an excess proton and proton defects at and in the vicinity of -CF₂SO₃H was systematically studied. In order to obtain information specifically at -CF₂SO₃H, as well as to reduce complexity of H-bonds in the model systems, the present investigations were restricted to reactions at low hydration levels and at short time. Since H₃O⁺ plays the most important role in proton transfer reactions in aqueous solutions, its basic dynamic information was obtained based on the same approaches, using the complexes formed from H₃O⁺ and H₂O as model systems. Characteristic proton transfer reactions in the H₃O⁺-H₂O complexes were described and used in the discussions of the CF₃SO₃H-H₃O⁺-H₂O complexes.

2. Computational methods

For hydration of a single proton, according to experimental and theoretical investigations,^{27,28} there are at least three important H-bond structures involved in proton transfer reactions, namely, H₃O⁺, H₅O₂⁺ and the Eigen complex (H₉O₄⁺). Based on a neutron diffraction experiment, with hydrogen isotope substitutions and Monte Carlo simulations (MC),²⁸ the first hydration shell of H₃O⁺ consists of four water molecules and only three of them strongly H-bond to the hydrogen atoms of H₃O⁺. *Ab initio* calculations in ref. 29 showed that the fourth water molecule, initially attached to the oxygen atom of H₃O⁺, eventually moves away to the second hydration shell. Therefore, in the present study, up to three water molecules were considered in the investigation of basic elementary reactions in the proton transfer process at H₃O⁺.

Since mechanisms of proton conduction in Nafion[®] are complicated, care must be exercised in selecting model molecules and theoretical methods. Our previous experience on strong H-bond clusters^{30–34} showed that some structural and energetic information in the gas phase could provide the basis for discussion in aqueous solutions. Therefore, it was our strategy to explore proton transfer reactions at low hydration levels. Due to the fact that, superacid characters of Nafion[®] are localized at -CF₂SO₃H, the present study concentrated only on reactions among -CF₂SO₃H, H₃O⁺ and H₂O, using

the complexes formed from $\text{CF}_3\text{SO}_3\text{H}$, H_3O^+ and H_2O as model systems; including H_3O^+ in the model systems could promote proton transfer reactions by creating proton defect which involves the formation of H_5O_2^+ , as in the case of water³⁵ and triflic acid monohydrate solid.²¹ Because the size of the model systems must be reasonable and manageable by our computer resources, the $\text{CF}_3\text{SO}_3\text{H}-\text{H}_3\text{O}^+-\text{H}_2\text{O}$ 1 : 1 : n complexes, $1 \leq n \leq 3$, were adopted. It should be added that previous theoretical investigations considered $-\text{CF}_2\text{SO}_3\text{H}$ as a primary source of proton, from which H_3O^+ and $-\text{CF}_2\text{SO}_3^-$ are generated. Therefore, proton transfer reactions among $-\text{CF}_2\text{SO}_3\text{H}$, H_3O^+ and H_2O have not been emphasized.

2.1 T-model

Since proton transfer reactions have been pointed out to be sensitive to structures and dynamics of the H-bond,³⁶ all important H-bond structures in the model systems had to be identified, characterized and analyzed. Attention was focused on H-bond structures, which could be precursors or transition states in proton transfer pathways. In order to effectively and systematically scan the potential energy surfaces, T-model potentials were constructed and employed in the calculations of the equilibrium structures of the $\text{H}_3\text{O}^+-\text{H}_2\text{O}$ and $\text{CF}_3\text{SO}_3\text{H}-\text{H}_3\text{O}^+-\text{H}_2\text{O}$ complexes. Since the T-model had been discussed in details in our previous studies,^{30–34,37–41} only some important aspects of geometry optimizations will be briefly summarized.

For the $\text{H}_3\text{O}^+-\text{H}_2\text{O}$ complexes, a rigid H_3O^+ was placed at the origin of the Cartesian coordinate system. The coordinates of water molecules were randomly generated in the vicinity of H_3O^+ . Based on the T-model potentials, equilibrium structures of the $\text{H}_3\text{O}^+-\text{H}_2\text{O}$ complexes were searched, using a minimization technique. Similar methods were applied on the $\text{CF}_3\text{SO}_3\text{H}-\text{H}_3\text{O}^+-\text{H}_2\text{O}$ complexes, in which $\text{CF}_3\text{SO}_3\text{H}$ was placed at the origin of the Cartesian coordinate system, and the positions and orientations of H_3O^+ and H_2O were randomly assigned in its vicinity. For each H-bond complex, one-hundred starting configurations were generated and employed as starting configurations in the T-model geometry optimizations.

2.2 DFT and *ab initio* calculations

Since the T-model potentials are based on rigid molecules, in which cooperative effects are neglected, further structural refinements had to be made using appropriate quantum chemical methods. As it is known in general that sophisticated theoretical methods require more computer resources, and especially in the present case, MD simulations with thousands of timesteps must be performed, it was necessary to compromise between the accuracy of theoretical methods and the available computer resources. A literature survey showed that DFT methods have been frequently chosen due to the ability to treat molecules of relatively large sizes with a reasonable degree of accuracy, compared to other nonempirical methods. Especially for similar H-bond systems,^{7,10,11,19,20,23} the DFT method at B3LYP/6-31G(d,p) level represents one of the most popular choices. Therefore, it was adopted as a primary candidate in the refinement of the T-model results. It should

be noted, however, that the performance of DFT methods can be poor or fairly good, depending upon the chemical systems considered. As in the present case, the existence of three fluorine atoms in $\text{CF}_3\text{SO}_3\text{H}$ could bring about strong electron correlation effects, and thus made it necessary to examine the applicability of B3LYP/6-31G(d,p) in details. Our experience on strong H-bond systems^{30,33,39} suggested that *ab initio* calculations at MP2/6-311++G(d,p) or MP2/6-311++G(2d,2p) level could serve as a benchmark in this case.

The absolute and some local minimum energy geometries of the H-bond complexes, predicted from the T-model potentials, were employed as starting configurations in DFT and *ab initio* geometry optimizations. Both partial and full geometry optimizations were performed, using the Berny algorithm in Gaussian 03.⁴² In partial geometry optimizations, monomer geometries were kept constant and only the intermolecular geometrical parameters were optimized. The purpose of the partial geometry optimizations was to verify the T-model optimized geometries, whereas the full geometry optimizations were aimed at structural refinements. In the present study, the partial and full geometry optimizations were denoted by OPT1 and OPT2, respectively. Since forces in MD simulations are computed from energy gradients, which are determined by structures of potential energy surface, and in order to compare the performance among candidate theoretical methods, the potential energy profiles for a single proton transfer event were constructed for selected H-bond complexes, using both DFT and *ab initio* calculations; by moving a proton within a fixed H-bond distance. In the present case, B3LYP/6-31G(d,p), HF/6-311++G(d,p) and MP2/6-311++G(d,p) calculations were employed in the calculations of the potential energy profiles. For the DFT method, additional calculations at B3LYP/6-31+G(d,p) level were made to examine the effects of diffuse functions.

2.3 MD simulations

The dynamics of rapid covalent and H-bond formation and cleavage could be studied reasonably well using theoretical approaches that incorporate quantum chemical methods into MD simulations,⁴³ among which DFT-MD simulations have been widely used in recent years.^{44,45}

In the present work, the precursors and transition states, as well as elementary reactions, in proton transfer processes at $-\text{CF}_2\text{SO}_3\text{H}$ were studied using Born–Oppenheimer MD (BOMD) simulations.^{46,47} Within the framework of BOMD simulations, classical equations of motions of nuclei on the Born–Oppenheimer surfaces are integrated, whereas forces on nuclei are calculated in each MD step from quantum energy gradients, with the molecular orbitals (MOs) updated by solving Schrodinger equations in the Born–Oppenheimer approximation. This makes BOMD simulations more accurate, as well as considerably CPU time consuming, compared to conventional classical MD simulations, in which forces on nuclei are determined from predefined empirical or quantum pair potentials. It should be noted that the high mobility of the excess proton was initially attributed to QM tunneling.⁴⁸ This has been challenged, for example, by the results obtained from *ab initio* BOMD simulations³⁶ and conductivity

measurements,⁴⁹ which showed that proton transfer reaction mechanisms could be explained reasonably well without assuming the proton tunneling to be the important pathway.

Since proton conduction, especially in aqueous solutions, involves dynamic processes with different timescales,^{35,50,51} the complexity of proton transfer reactions could be reduced using various approaches. The observation that the actual proton transfer occurs on a femtosecond (fs) timescale,⁵¹ which is in general faster than solvent reorganization,⁵⁰ made it reasonable to perform BOMD simulations by focusing only on short-lived phenomena which take place before or after major H-bond structure reorganizations. To ensure that all important dynamics was taken into account, several BOMD-trajectories were generated at 298 K, starting from the equilibrium structures of the $\text{H}_3\text{O}^+-\text{H}_2\text{O}$ and $\text{CF}_3\text{SO}_3\text{H}-\text{H}_3\text{O}^+-\text{H}_2\text{O}$ complexes computed in the previous sections. Since in aqueous solutions, rapid interconversion between the Zundel and Eigen complexes happens within about 100 fs (10^{-13} s),³⁵ the time-step used in solving dynamic equations was set to 0.5 fs. In each BOMD simulation, 500 fs was spent on equilibration, after which 2000 fs was devoted to property calculations.

Since correlation exists between proton conductivity and H-bond structure,³⁵ JMOL⁵² was employed to visualize molecular motions in the course of BOMD simulations. In addition, BOMD trajectories were analyzed in details by monitoring fluctuations and changes in H-bond structures; some characteristic H-bond distances were plotted with MD simulation time. For example, the $\text{O}_\text{h}\cdots\text{O}_\text{w}$, $\text{O}_\text{w}-\text{H}_\text{w}$ and $\text{O}_\text{h}-\text{H}_\text{h}$ distances were plotted with MD simulation time to study the dynamics in the Zundel and Eigen complexes; h = hydronium ion and w = water. The plots were regarded as proton transfer profiles in the present work. In combination with the molecular motions displayed by JMOL, precursors, transition states and the elementary reactions in proton transfer pro-

cesses were analyzed and categorized. The average lifetimes of the precursors, transition states and products were roughly estimated from the proton transfer profiles and further analyzed in details. The analyses of the proton transfer profiles will be discussed in the forthcoming sections.

3. Results and discussion

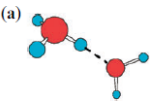
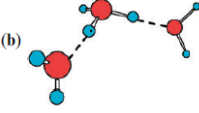
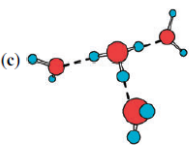
3.1 Structures and energetic

The absolute and some lowest-lying minimum energy geometries of the H-bond complexes, together with corresponding interaction energies and characteristic H-bond distances, are displayed in Tables 1 and 2, as well as Fig. 1 and 2.

3.1.1 The $\text{H}_3\text{O}^+-\text{H}_2\text{O}$ complexes. For the $\text{H}_3\text{O}^+-\text{H}_2\text{O}$ 1 : n complex, $1 \leq n \leq 3$, T-model, DFT and *ab initio* geometry optimizations suggested only one predominant H-bond structure; H_3O^+ acts as proton donor towards H_2O , structures a, b and c in Table 1. DFT and *ab initio* calculations with partial geometry optimizations predicted the same structures as the T-model. The Zundel complex, in which a hydrogen atom is equally shared between two water molecules and considered as a defect in the H-bond network,²¹ was obtained when DFT and *ab initio* calculations with full geometry optimizations being applied. The $\text{O}_\text{h}\cdots\text{H}\cdots\text{O}_\text{w}$ and $\text{O}_\text{h}\cdots\text{H}$ distances derived from B3LYP-OPT2 and MP2-OPT2 are almost the same, about 2.4 and 1.2 Å, respectively. The extraordinary short H-bond distance, as in the case of the Zundel complex, could be related to a high possibility for proton transfer and, therefore, used as a criterion to monitor proton transfer reactions.³⁵

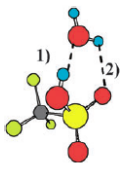
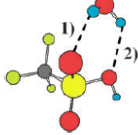
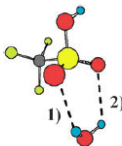
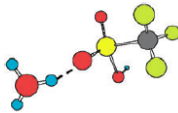
Similar trends were observed in the $\text{H}_3\text{O}^+-\text{H}_2\text{O}$ 1 : 2 complexes. T-model, DFT and *ab initio* calculations with partial geometry optimizations predicted the structure with two

Table 1 Structures of the $\text{H}_3\text{O}^+-\text{H}_2\text{O}$ complexes, obtained from the T-model, DFT and *ab initio* geometry optimizations. (a) $\text{H}_3\text{O}^+-\text{H}_2\text{O}$ 1 : 1 complex. (b) $\text{H}_3\text{O}^+-\text{H}_2\text{O}$ 1 : 2 complex. (c) $\text{H}_3\text{O}^+-\text{H}_2\text{O}$ 1 : 3 complex

	Method	$\Delta E/\text{kJ mol}^{-1}$	$\text{O}_\text{h}-\text{H}_\text{h}\cdots\text{O}_\text{w}/\text{\AA}$	$\text{O}_\text{h}-\text{H}_\text{h}-\text{O}_\text{w}/^\circ$
	T-model	-117.5	2.51	151.0
	MP2-OPT1	-135.5	2.46	175.9
	MP2-OPT2	—	2.39 ^a	174.0
	B3LYP-OPT1	-160.7	2.43	174.5
	B3LYP-OPT2	—	2.40 ^a	174.2
	T-model	-229.9	2.52	152.6
	MP2-OPT1	-244.5	2.52	174.3
	MP2-OPT2	—	2.50	175.5
	B3LYP-OPT1	-287.6	2.49	174.0
	B3LYP-OPT2	—	2.47	174.6
	T-model	-334.4	2.58	171.7
	MP2-OPT1	-334.0	2.57	175.6
	MP2-OPT2	—	2.57	175.9
	B3LYP-OPT1	-388.4	2.54	176.7
	B3LYP-OPT2	—	2.55	175.5

^a The Zundel complex; an excess proton equally shared between two water molecules. MP2-OPT1 = MP2/6-311++G(2d,2p) with partial geometry optimizations. MP2-OPT2 = MP2/6-311++G(2d,2p) with full geometry optimizations. B3LYP-OPT1 = B3LYP/6-31G(d,p) with partial geometry optimizations. B3LYP-OPT2 = B3LYP/6-31G(d,p) with full geometry optimizations.

Table 2 Structures of the $\text{CF}_3\text{SO}_3\text{H}-\text{H}_2\text{O}$ and $\text{CF}_3\text{SO}_3\text{H}-\text{H}_3\text{O}^+$ 1 : 1 complexes, obtained from the T-model, DFT and *ab initio* geometry optimizations. (a)–(c) $\text{CF}_3\text{SO}_3\text{H}-\text{H}_2\text{O}$ 1 : 1 complexes. (d) $\text{CF}_3\text{SO}_3\text{H}-\text{H}_3\text{O}^+$ 1 : 1 complex

	Method	$\Delta E/\text{kJ mol}^{-1}$	H-bond	Distance/Å	Angle/°
(a) 	T-model	−51.9	(1) O–H...Ow	2.71	158.4
	MP2-OPT1	−51.9	(2) Ow–Hw...O	2.79	111.6
	B3LYP-OPT2	—		2.68	166.2
				2.93	133.3
				2.60	166.4
				2.84	127.2
(b) 	T-model	−15.7	(1) Ow–Hw...O	2.95	122.8
	MP2-OPT1	−13.2	(2) Ow–Hw...O	3.05	127.6
	B3LYP-OPT2	—		3.18	134.5
				3.20	136.3
				3.01	138.9
				3.22	102.3
(c) 	T-model	−15.7	(1) Ow–Hw...O	2.95	122.8
	MP2-OPT1	−13.2	(2) Ow–Hw...O	3.05	127.6
	B3LYP-OPT2	—		3.21	127.5
				3.24	123.6
				3.10	120.7
				3.08	120.1
(d) 	T-model	−68.1	Oh–Hh...O	2.60	141.3
	MP2-OPT1	−114.6		2.48	177.3
	B3LYP-OPT2	—			
				2.40	177.4

MP2-OPT1 = MP2/6-311++G(d,p) with partial geometry optimizations. B3LYP-OPT2 = B3LYP/6-31G(d,p) with full geometry optimizations.

equivalent linear $\text{Oh}-\text{Hh}\cdots\text{Ow}$ H-bonds to be the most stable. Only slightly shorter $\text{Oh}-\text{Hh}\cdots\text{Ow}$ H-bond distances were observed when MP2-OPT2 and B3LYP-OPT2 were applied on the T-model results. All theoretical methods predicted longer $\text{Oh}-\text{Hh}\cdots\text{Ow}$ H-bond distances when the number of water molecule was gradually increased from one to three. For the $\text{H}_3\text{O}^+-\text{H}_2\text{O}$ 1 : 3 complex, the T-model suggested the $\text{Oh}-\text{Hh}\cdots\text{Ow}$ H-bond distance to be 2.58 Å, whereas the values obtained from MP2-OPT1 and B3LYP-OPT1 are 2.57 and 2.54 Å, respectively. MP2-OPT2 and B3LYP-OPT2 showed the same trend, with slightly shorter $\text{Oh}-\text{Hh}$ covalent bonds in H_3O^+ .

As mentioned earlier, H-bonds in the $\text{H}_3\text{O}^+-\text{H}_2\text{O}$ complexes have been extensively studied using both experimental and theoretical treatments. It was generally concluded that the introduction of an extra proton to the cluster of water molecules in the gas phase or liquid water results in contraction of H-bonds, through the formation of proton defect which involves H_5O_2^+ .³⁵ The isolated H_5O_2^+ was reported to possess a very short H-bond distance, approximately 2.4 Å.^{36,51,53,54} This is confirmed by all theoretical results obtained here. Both experiments and theories suggested the same trends when water molecules are added to H_5O_2^+ , namely, the central H-bond in H_5O_2^+ is weakened to some extent, leading to relaxation of H-bonds. The H-bond distance in the Eigen complex was reported to be about 2.6 Å,^{35,36,51} which is in excellent agreement with the present results.

3.1.2 The $\text{CF}_3\text{SO}_3\text{H}-\text{H}_2\text{O}$ and $\text{CF}_3\text{SO}_3\text{H}-\text{H}_3\text{O}^+$ complexes. For the $\text{CF}_3\text{SO}_3\text{H}-\text{H}_2\text{O}$ 1 : 1 complex, T-model, MP2-OPT1 and B3LYP-OPT2 predicted a cyclic H-bond structure in which $\text{CF}_3\text{SO}_3\text{H}$ acts simultaneously as proton donor and acceptor, to be the global minimum energy geometry, structure a in Table 2; whereas other cyclic H-bond structures, in which $\text{CF}_3\text{SO}_3\text{H}$ acts only as proton acceptor, structures b and c, possess considerably lower stability. For the $\text{CF}_3\text{SO}_3\text{H}-\text{H}_3\text{O}^+$ 1 : 1 complex, both the T-model and MP2-OPT1 predicted H_3O^+ to be a stronger proton donor than $\text{CF}_3\text{SO}_3\text{H}$, structure d in Table 2. The linear H-bond in structure d did not change substantially when B3LYP-OPT2 was applied. However, small but not negligible change was observed at the $\text{Oh}-\text{Hh}\cdots\text{O}$ H-bond. It becomes shorter and comparable with the $\text{Ow}\cdots\text{H}\cdots\text{Ow}$ H-bond distance in the Zundel complex. The decrease in the H-bond distance is accompanied by an increase in the $\text{Oh}-\text{Hh}$ covalent bond distance. This reflects a tendency for proton transfer from H_3O^+ to $\text{CF}_3\text{SO}_3\text{H}$, leading to a Zundel-like structure ($\text{CF}_3\text{SO}_3\text{H}_2^+-\text{H}_2\text{O}$) as proposed in ref. 26.

3.1.3 $\text{CF}_3\text{SO}_3\text{H}-\text{H}_3\text{O}^+-\text{H}_2\text{O}$ complexes. For the $\text{CF}_3\text{SO}_3\text{H}-\text{H}_3\text{O}^+-\text{H}_2\text{O}$ 1 : 1 : 1 complexes, the T-model generated three important minimum energy geometries, namely, structures a, b and c in Fig. 1. All of them adopt compact cyclic H-bond structures. The most stable one, structure a,

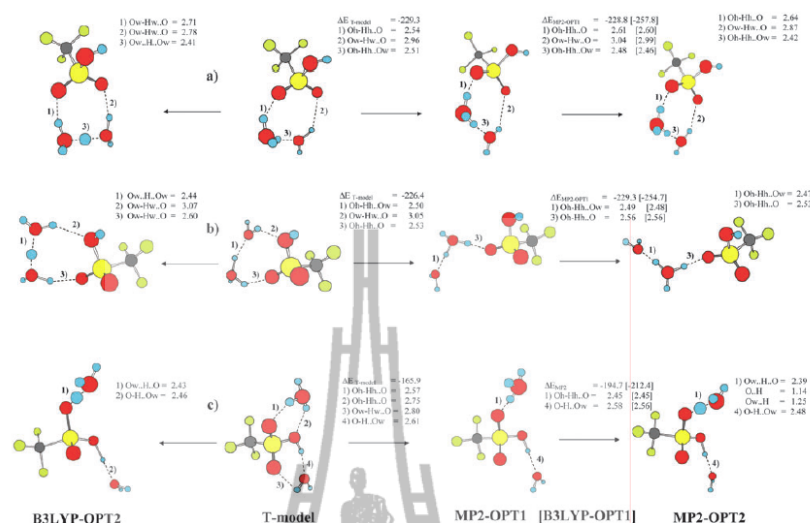


Fig. 1 Equilibrium structures of the $\text{CF}_3\text{SO}_3\text{H}-\text{H}_3\text{O}^+-\text{H}_2\text{O}$ 1 : 1 : 1 complexes, obtained from the T-model, DFT and *ab initio* geometry optimizations. Interaction energy is given in kJ mol^{-1} , angle in degrees and distance in Å. MP2-OPT1 = MP2/6-311++G(d,p) with partial geometry optimizations. MP2-OPT2 = MP2/6-311++G(d,p) with full geometry optimizations. B3LYP-OPT1 = B3LYP/6-31G(d,p) with partial geometry optimizations. B3LYP-OPT2 = B3LYP/6-31G(d,p) with full geometry optimizations. [..] = Values obtained from B3LYP-OPT1.

consists of three H-bonds; H_3O^+ and H_2O act as proton donors towards two oxygen atoms of $\text{CF}_3\text{SO}_3\text{H}$. The stability of structure **b** is slightly lower than structure **a** and structure **c** is quite different from structures **a** and **b**. In structure **c**, $\text{CF}_3\text{SO}_3\text{H}$ forms two separate cyclic H-bonds with H_3O^+ and H_2O . Both are located on the opposite sides of $-\text{SO}_3\text{H}$. Some H-bonds in structures **b** and **c** were disrupted when MP2-OPT1 and B3LYP-OPT1 were applied on the T-model results, leading to linear H-bond structures. The comparison of the MP2-OPT1 and MP2-OPT2 results in details reveals the important trend; full geometry optimizations lead to shorter H-bond distances, especially where proton transfer could take place, e.g. the $\text{Ow-Hh}\cdots\text{Ow}$ H-bonds in structures **a** and **b**, as well as the $\text{Ow-Hh}\cdots\text{O}$ H-bonds in structures **b** and **c**. The latter reflect the possibility for proton transfer from H_3O^+ to $-\text{SO}_3\text{H}$, forming the previously proposed $\text{CF}_3\text{SO}_3\text{H}_2^+$ transition state. Starting from the T-model results, B3LYP-OPT2 did not bring about a significant change in the H-bond structures. However, the possibilities for proton transfer in structures **a**, **b** and **c** become more evident. Compared with B3LYP-OPT1, all the H-bonds susceptible to proton transfer are systematically shorter, with hydrogen atoms located nearer to the centers.

Since important information on theoretical methods had already been obtained, it was reasonable to investigate the $\text{CF}_3\text{SO}_3\text{H}-\text{H}_3\text{O}^+-\text{H}_2\text{O}$ 1 : 1 : 2 complex using only the T-model, MP2-OPT2 and B3LYP-OPT2. The T-model predicted four important cyclic H-bond structures in Fig. 2. The most stable one consists of a basic unit similar to structure **a** in the $\text{CF}_3\text{SO}_3\text{H}-\text{H}_3\text{O}^+-\text{H}_2\text{O}$ 1 : 1 : 1 complex, with the second water molecule hydrates at H_3O^+ . The stability of structure **b** is slightly lower than that in structure **a**. In structure **b**, both $\text{CF}_3\text{SO}_3\text{H}$ and H_3O^+ act as proton donors towards water

molecules, and the second water molecule hydrates directly at H_3O^+ . The stability of structures **a** and **b** seems to result from a complete H-bond formation at H_3O^+ . Structures **c** and **d** are quite different from structures **a** and **b**; only two Ow-Hh covalent bonds in H_3O^+ are H-bonded. Comparison of interaction energies ($\Delta E_{\text{T-model}}$) suggested that the formation of a large cyclic H-bond tends to reduce the stability of the $\text{CF}_3\text{SO}_3\text{H}-\text{H}_3\text{O}^+-\text{H}_2\text{O}$ 1 : 1 : 2 complexes. The T-model results did not change significantly when B3LYP-OPT2 and MP2-OPT2 were applied, except for structures **c** and **d**, B3LYP-OPT2 showed a higher possibility for the Zundel complex formation. In summary, for the $\text{CF}_3\text{SO}_3\text{H}-\text{H}_3\text{O}^+-\text{H}_2\text{O}$ 1 : 1 : 2 complexes, structures **a**, **b** and **d** reveal possibilities for proton transfer along the H-bond networks connecting the oxygen atoms of $-\text{SO}_3\text{H}$, whereas structure **c** shows a possibility for proton transfer through $-\text{SO}_3\text{H}$, e.g., a protonation at one oxygen atom followed by a deprotonation at the O-H group, or *vice versa*. This direct involvement of $-\text{SO}_3\text{H}$ in proton transfer is similar to the Grotthuss mechanism.⁵⁵ In the present case, a relay-type mechanism, in which a proton hops across $-\text{SO}_3\text{H}$, could take place through the formation of either $-\text{SO}_3\text{H}_2^+$ or $-\text{SO}_3^-$. It should be noted that, although a limited number of H-bond structures was considered in ref. 26, $-\text{SO}_3\text{H}_2^+$ was recognized in *ab initio* calculations and MD simulations, and pointed out to play important roles in proton transfer at low hydration levels. This was further investigated in our MD simulations in the next sections.

For the $\text{CF}_3\text{SO}_3\text{H}-\text{H}_3\text{O}^+-\text{H}_2\text{O}$ 1 : 1 : 3 complex, both linear and cyclic H-bonds were found in the optimized geometry, structure **e** in Fig. 2. The T-model, MP2-OPT2 and B3LYP-OPT2 predicted a similar trend, namely, all H-bonds susceptible for proton transfer possess short H-bond distances. MP2-OPT2 and B3LYP-OPT2 also showed a possibility to form

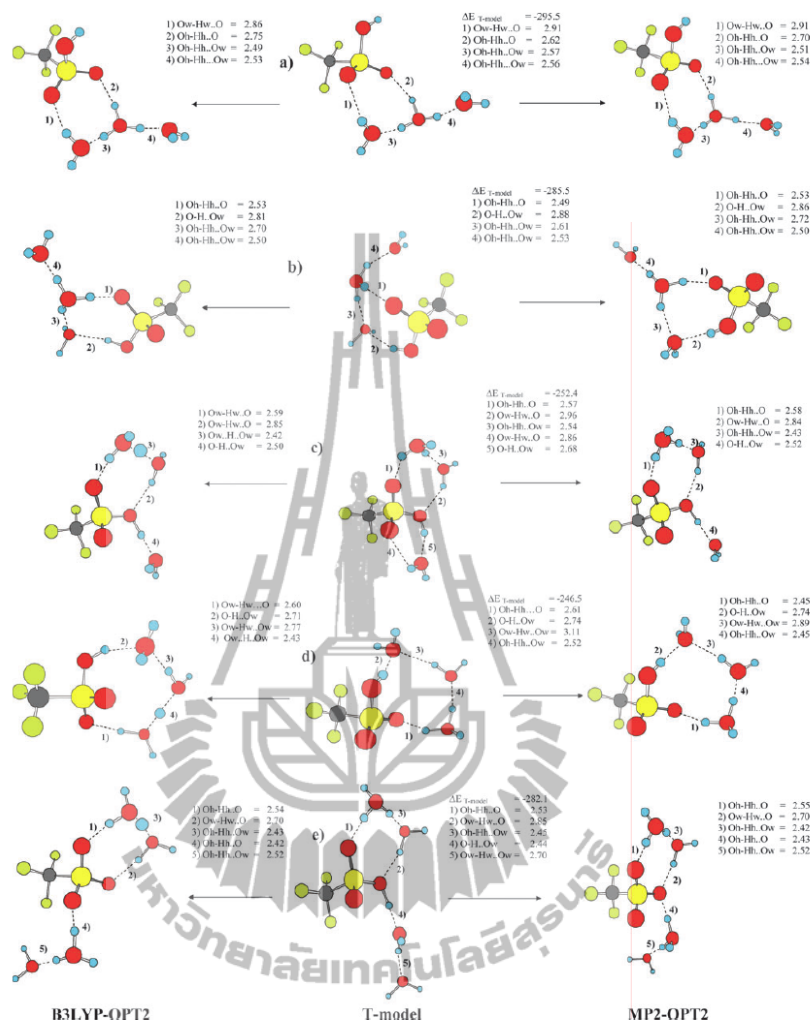


Fig. 2 Equilibrium structures of the $\text{CF}_3\text{SO}_3\text{H}-\text{H}_3\text{O}^+-\text{H}_2\text{O}$ 1 : 1 : 2 and 1 : 1 : 3 complexes, obtained from the T-model, DFT and *ab initio* calculations. Interaction energy in kJ mol^{-1} and distance in Å. (a)–(d) $\text{CF}_3\text{SO}_3\text{H}-\text{H}_3\text{O}^+-\text{H}_2\text{O}$ 1 : 1 : 2 complexes. (e) $\text{CF}_3\text{SO}_3\text{H}-\text{H}_3\text{O}^+-\text{H}_2\text{O}$ 1 : 1 : 3 complex. MP2-OPT2 = MP2/6-311++G(d,p) with full geometry optimizations. B3LYP-OPT2 = B3LYP/6-31G(d,p) with full geometry optimizations.

$-\text{SO}_3^-$, H_3O^+ and H_5O_2^+ within the $\text{CF}_3\text{SO}_3\text{H}-\text{H}_3\text{O}^+-\text{H}_2\text{O}$ 1 : 1 : 3 complex. The appearance of $-\text{SO}_3^-$ and the ion-pair complex when $n = 3$ is in good agreement with the theoretical results in ref. 26.

Comparison of the size and shape of the potential energy profiles for proton transfer in Fig. 3a to 3d revealed that B3LYP/6-31G(d,p), B3LYP/6-31+G(d,p) and MP2/6-311++G(d,p) yield similar trends; whereas HF/6-311++G(d,p) shows different results, *e.g.* the minima are seen systematically at shorter distances. The discrepancies are quite obvious in Fig. 3b to 3e; double-well potential is seen in the case of large cyclic H-bond of water; shoulders are seen in the case of $\text{CF}_3\text{SO}_3\text{H}-\text{H}_3\text{O}^+-\text{H}_2\text{O}$ 1 : 1 : 1 complexes. Based on the above discussions and the fact that DFT requires

lowest computational resources, we concluded that B3LYP/6-31G(d,p) is the most appropriate choice for our MD simulations.

3.2 Dynamics and elementary reactions

3.2.1 The $\text{H}_3\text{O}^+-\text{H}_2\text{O}$ complexes. Since H-bond structures can vary in a rather wide range, care must be exercised in the discussion of proton transfer profiles. In order to study dynamics and elementary reactions in proton transfer processes, some characteristic structures in proton transfer profiles have to be interpreted, using BOMD results on the $\text{H}_3\text{O}^+-\text{H}_2\text{O}$ 1 : 1 complex in Fig. 4 and 5 as examples. It appeared, in general, that the proton transfer in H_5O_2^+

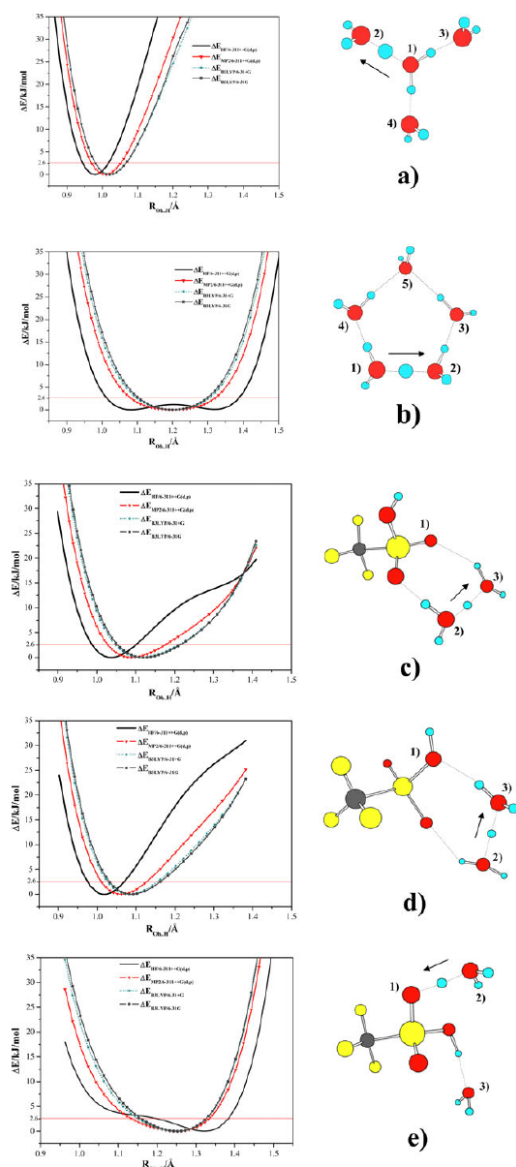


Fig. 3 Potential energy profiles for single proton transfer, obtained from various theoretical methods. Interaction energy in kJ mol^{-1} and distance in \AA . All minima on the potential energy curves were moved to zero for comparison. (a) $\text{H}_3\text{O}^+-\text{H}_2\text{O}$ 1 : 3 complex. (b) $\text{H}_3\text{O}^+-\text{H}_2\text{O}$ 1 : 4 complex. (c)–(e) $\text{CF}_3\text{SO}_3\text{H}-\text{H}_3\text{O}^+-\text{H}_2\text{O}$ 1 : 1 : 1 complexes.

depends strongly on the Oh–Hh...Ow H-bond distance, as well as its vibrational amplitude. Examples of two extreme cases, namely, large- and small-amplitude vibrations, are shown in Fig. 4a and 4b, respectively. In order to simplify the discussion, the proton transfer profiles are divided into panels, labeled as P_1 , P_2 , P_3 , ..., P_n , respectively.

For large-amplitude vibration, the Oh–Hh...Ow H-bond distance (O1–O2 in Fig. 4a) varies in quite a wide range, from its equilibrium to about 3 \AA . A periodic series, consisting of a quasi-dynamic equilibrium followed by an actual proton transfer, was observed in the course of BOMD simulations and could be considered as a part of proton transfer reaction mechanism. For H_5O_2^+ , the quasi-dynamic equilibrium is characterized by a proton shuttling back and forth in a narrow range within the H-bond, before the actual proton transfer takes place, either in the forward or reverse direction. In Fig. 4a, for example, a quasi-dynamic equilibrium is seen in panel P_2 , preceding the actual proton transfer in the forward direction at $t_3 = 2341$ fs. The actual proton transfers are also seen at $t_1 = 2228$ fs, $t_2 = 2317$ fs and $t_4 = 2419$ fs. The lifetime of the quasi-dynamic equilibrium ($\tau_{\text{H}_5\text{O}_2^+}^{\text{I,ABC}}$) could be approximated from the width of panel P_2 , and the lifetimes of H_3O^+ , $\tau_{\text{H}_5\text{O}_2^+}^{\text{I,C}}$ and $\tau_{\text{H}_5\text{O}_2^+}^{\text{I,A}}$, from panels P_1 and P_3 , respectively; the former is 24 fs and the latter are 89 and 78 fs, respectively. The superscripts A and C in $\tau_{\text{H}_5\text{O}_2^+}^{\text{I,C}}$ and $\tau_{\text{H}_5\text{O}_2^+}^{\text{I,A}}$ represent the H-bond structures in Fig. 4c, and I, the elementary reaction in Fig. 5. The superscript ABC in $\tau_{\text{H}_5\text{O}_2^+}^{\text{I,ABC}}$ denotes the quasi-dynamic equilibrium established among structures A, B and C. Similar notations will be applied in the forthcoming discussions. Since $\tau_{\text{H}_5\text{O}_2^+}^{\text{I,A}}$ and $\tau_{\text{H}_5\text{O}_2^+}^{\text{I,C}}$ are longer than $\tau_{\text{H}_5\text{O}_2^+}^{\text{I,ABC}}$, the lifetimes of the precursor H_3O^+ could be approximated as the rate-determining step for a proton transfer reaction *via* large amplitude vibration in H_5O_2^+ .

For small-amplitude vibration, the Oh–Hh...Ow H-bond distance (O1–O2 in Fig. 4b) varies in a narrow range near its equilibrium, between 2.3 and 2.7 \AA . In this case, proton exchange between two water molecules takes place more often and quite randomly. For example, in Fig. 4b, $\tau_{\text{H}_5\text{O}_2^+}^{\text{I,A}}$ and $\tau_{\text{H}_5\text{O}_2^+}^{\text{I,C}}$ vary from 19 to 39 fs, and up to three actual proton transfers occur between t_1 and t_4 . Interestingly, the O1–O2 vibration starts to damp at $t_1 = 1941$ fs, until a quasi-dynamic equilibrium, with $\tau_{\text{H}_5\text{O}_2^+}^{\text{I,ABC}} = 23$ fs, is reached at $t_5 = 2046$ fs; followed by a proton transfer at $t_6 = 2069$ fs. It should be noted that, although the lifetimes of the precursor H_3O^+ ($\tau_{\text{H}_5\text{O}_2^+}^{\text{I,A}}$) for large- and small-amplitude vibrations are somewhat different, $\tau_{\text{H}_5\text{O}_2^+}^{\text{I,ABC}}$ are quite similar.

It could be recognized that proton transfers in H_5O_2^+ are activated, when the Oh–Hh...Ow H-bond distance (O1–O2 in Fig. 4a and 4b) is close to its equilibrium, shorter than 2.4 \AA , and only one actual proton transfer takes place for each large-amplitude vibration cycle. Therefore, maximum proton transfer cycle time ($\tau_{\text{H}_5\text{O}_2^+}^{\text{I,PTmax}}$) could be defined from large-amplitude vibration; from the time intervals between successive minima of the Oh–Hh...Ow H-bond distance. The proton transfer profiles in Fig. 4a and 4b also revealed that, for large-amplitude vibration, the O1–O2 and O1–H₁* motions in panel P_1 , as well as the O1–O2 and O2–H₁* motions in panel P_3 , are correlated, except during the quasi-dynamic equilibrium in P_2 ; whereas, for small-amplitude vibration, for which proton vibrates with higher frequency, such correlation seems missing. Since the abnormal proton mobility in water has been pointed out to relate to incoherent effects,⁵⁰ it is reasonable to approximate the degree of coherence in the H-bond. Similar to statistics and electromagnetic waves, the degree of coherence in the present study should measure the extent of correlation between vibrational motions in the H-bonds, *e.g.* between the

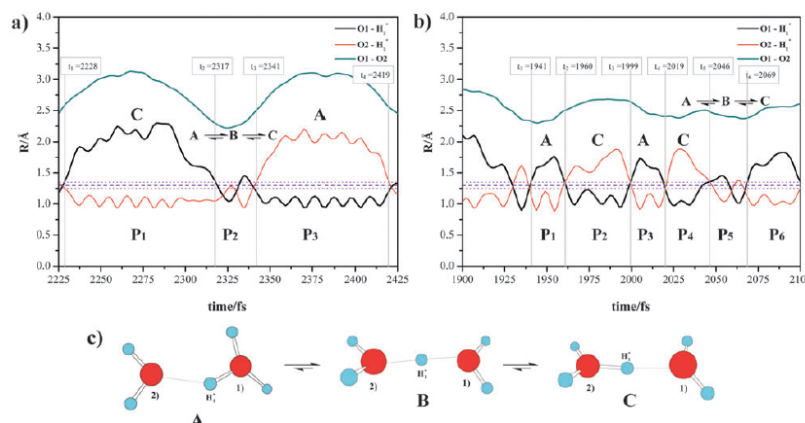


Fig. 4 Examples of characteristic proton transfer profiles for the $\text{H}_3\text{O}^+-\text{H}_2\text{O}$ 1 : 1 complex, with snapshots of H-bond structures obtained in the course of BOMD simulations. (a) Large-amplitude vibrations. (b) Small-amplitude vibrations (c) Snapshots of H-bond structures.

O–O and O–H vibrations. Since, for large-amplitude vibration, $\tau_{\text{H}_3\text{O}_2^+}^{\text{I,A}}$ and $\tau_{\text{H}_3\text{O}_2^+}^{\text{I,PTmax}}$ are nearly the same, $\tau_{\text{H}_3\text{O}_2^+}^{\text{I,A}}/\tau_{\text{H}_3\text{O}_2^+}^{\text{I,PTmax}}$ could be adopted as a criterium to measure the degree of coherence ($g_{\text{H}_3\text{O}_2^+}^{\text{I}}$). Therefore, in Fig. 4a, $g_{\text{H}_3\text{O}_2^+}^{\text{I}} \approx 1$ is attributed to the highest degree of coherence; whereas in Fig. 4b, the short lifetimes of the precursor H_3O^+ ($\tau_{\text{H}_3\text{O}_2^+}^{\text{I,A}}$ and $\tau_{\text{H}_3\text{O}_2^+}^{\text{I,C}}$) compared to $\tau_{\text{H}_3\text{O}_2^+}^{\text{I,PTmax}}$ reflect a lower degree of coherence and higher frequency of proton transfer.

Proton transfer elementary reactions in the $\text{H}_3\text{O}^+-\text{H}_2\text{O}$ 1 : n complexes, $1 \leq n \leq 3$, are listed in Fig. 5. BOMD simulations predicted the average lifetimes of the quasi-

dynamic equilibria in H_3O_2^+ , $\langle \tau_{\text{H}_3\text{O}_2^+}^{\text{I,AB}} \rangle$, $\langle \tau_{\text{H}_3\text{O}_2^+}^{\text{I,BC}} \rangle$ and $\langle \tau_{\text{H}_3\text{O}_2^+}^{\text{I,ABC}} \rangle$, to be 20.5, 19.4 and 15.5 fs, respectively, whereas the average lifetimes of the precursor and product H_3O^+ , $\langle \tau_{\text{H}_3\text{O}_2^+}^{\text{I,A}} \rangle$ and $\langle \tau_{\text{H}_3\text{O}_2^+}^{\text{I,C}} \rangle$, are nearly the same, 12.4 and 10.7 fs, respectively. The average maximum proton transfer cycle time ($\langle \tau_{\text{H}_3\text{O}_2^+}^{\text{I,PTmax}} \rangle$) in this case amounts to 69.9 fs, with $g_{\text{H}_3\text{O}_2^+}^{\text{I}} = 0.2$. This confirms that, on average, small-amplitude vibration with a low degree of coherence dominates in H_3O_2^+ . Due to the fact that BOMD simulations were started from minimum energy geometries, it was not straightforward to predict the preferential proton transfer directions. However, for each proton transfer elementary reaction, the probability

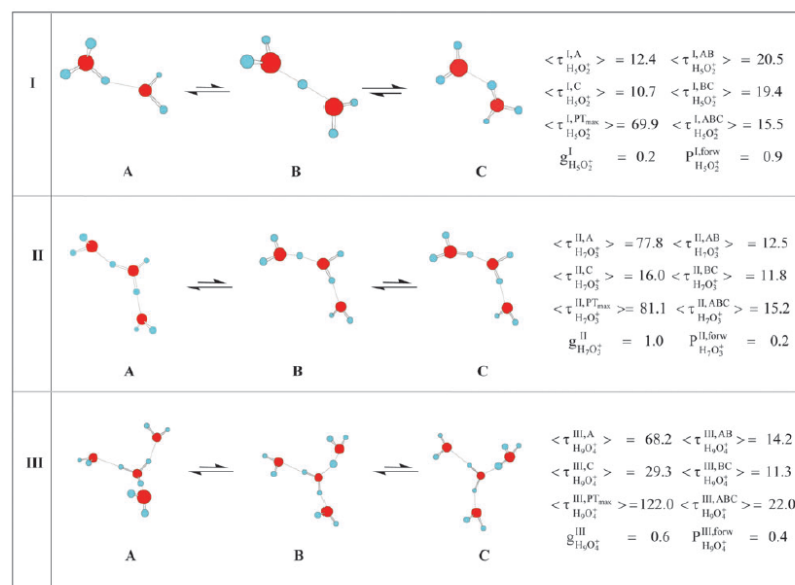


Fig. 5 Important elementary reactions in proton transfer in the $\text{H}_3\text{O}^+-\text{H}_2\text{O}$ complexes obtained from BOMD simulations. The symbols are explained in details in the text.

for proton transfer in the forward direction ($P_{\text{H}_3\text{O}_2^+}^{\text{I,forw}}$) could be conceivably associated with the average lifetime of the product, which becomes a precursor in the next proton transfer step. Therefore, $P_{\text{H}_3\text{O}_2^+}^{\text{I,forw}}$ was approximated as $\langle\tau_{\text{H}_3\text{O}_2^+}^{\text{I,C}}\rangle/\langle\tau_{\text{H}_3\text{O}_2^+}^{\text{I,A}}\rangle$. Since the product and precursor are the same in H_3O_2^+ , $P_{\text{H}_3\text{O}_2^+}^{\text{I,forw}} = 1$ represents the upper limit of the relative probability for proton transfer in the forward direction.

The characteristics of proton transfer profiles for the $\text{H}_3\text{O}^+ - \text{H}_2\text{O}$ 1 : 2 complex (H_7O_3^+) are not substantially different from H_5O_2^+ . The presence of another strong Oh-Hh...Ow H-bond in H_7O_3^+ tends to increase the stability of the central H_3O^+ . Since BOMD results in Fig. 5 suggested that $\langle\tau_{\text{H}_7\text{O}_3^+}^{\text{II,A}}\rangle$ and $\langle\tau_{\text{H}_7\text{O}_3^+}^{\text{II,PTmax}}\rangle$ are comparable, one could conclude that the elementary reaction II favors large-amplitude vibration, with $g_{\text{H}_7\text{O}_3^+}^{\text{II}} \approx 1$, compared to 0.2 in H_5O_2^+ ; $\langle\tau_{\text{H}_7\text{O}_3^+}^{\text{II,PTmax}}\rangle$ and $\langle\tau_{\text{H}_7\text{O}_3^+}^{\text{II,A}}\rangle$ are 81.1 and 77.8 fs, respectively. In this case, the relative probability for proton transfer in the forward direction ($P_{\text{H}_7\text{O}_3^+}^{\text{II,A}} = \langle\tau_{\text{H}_7\text{O}_3^+}^{\text{II,C}}\rangle/\langle\tau_{\text{H}_7\text{O}_3^+}^{\text{II,A}}\rangle = 0.2$) is considerably lower than H_5O_2^+ . The increase in the stability of the central H_3O^+ is accompanied by shorter average lifetimes of the quasi-dynamic equilibrium; $\langle\tau_{\text{H}_7\text{O}_3^+}^{\text{II,AB}}\rangle$ and $\langle\tau_{\text{H}_7\text{O}_3^+}^{\text{II,BC}}\rangle$ are 12.5 and 11.8 fs, respectively.

Due to coupled motions among the three strong Oh-Hh...Ow H-bonds, as well as some H-bond structure reorganizations, proton transfer profiles for the $\text{H}_3\text{O}^+ - \text{H}_2\text{O}$ 1 : 3 complex are more complicated than H_5O_2^+ and H_7O_3^+ . Although the central H_3O^+ in the Eigen complex (H_9O_4^+) is more stabilized than in H_7O_3^+ , the fluctuations of the surrounding water dipoles seem to help promote proton transfer reactions; similar to an extended local dynamic disorder which leads to a compression and breaking of H-bonds, as discussed in ref. 56. BOMD results suggested two important precursors for proton transfer elementary reactions in the $\text{H}_3\text{O}^+ - \text{H}_2\text{O}$ 1 : 3 complex, namely, the Eigen complex and a linear H-bond structure. Since the proton transfer profiles for the linear H-bond structure are similar to those in H_7O_3^+ , attention was focused on the Eigen complex. For elementary reaction III in Fig. 5, both large- and small-amplitude vibrations were observed in the course of BOMD simulations. Analyses of proton transfer profiles revealed that, due to the coupled vibrational motions, the average lifetime of the central H_3O^+ ($\langle\tau_{\text{H}_9\text{O}_4^+}^{\text{III,A}}\rangle$) is shorter than in H_7O_3^+ ($\langle\tau_{\text{H}_7\text{O}_3^+}^{\text{II,A}}\rangle$), but still considerably longer than H_5O_2^+ ($\langle\tau_{\text{H}_5\text{O}_2^+}^{\text{I,A}}\rangle$), 68.2, 77.8 and 12.4 fs, respectively. For the Eigen complex, the average maximum proton transfer cycle time ($\langle\tau_{\text{H}_9\text{O}_4^+}^{\text{III,PTmax}}\rangle = 122.0$ fs) is nearly twice longer than the average lifetime of the precursor ($\langle\tau_{\text{H}_9\text{O}_4^+}^{\text{III,A}}\rangle = 68.2$ fs). This implies that, on average, the probabilities for proton transfers through small- and large-amplitude vibrations are comparable; $g_{\text{H}_9\text{O}_4^+}^{\text{III}} = 0.6$ and $P_{\text{H}_9\text{O}_4^+}^{\text{III,forw}} = \langle\tau_{\text{H}_9\text{O}_4^+}^{\text{III,C}}\rangle/\langle\tau_{\text{H}_9\text{O}_4^+}^{\text{III,A}}\rangle = 0.4$. The former is lower than H_7O_3^+ , but still higher than H_5O_2^+ , whereas the latter could support the previous investigation that the proton transfer rate is about one order of magnitude lower than the O-O vibration rate.⁵⁶ Since small-amplitude vibration is a characteristic of the Zundel complex, one could conclude that, due to the thermal energy fluctuation and the coupled motions among H-bonds, a quasi-dynamic equilibrium between the Eigen and Zundel complexes could be established in the course

of BOMD simulations, and considered as the most fundamental elementary reaction in proton transfer process.

The most important property of H_3O^+ , which could be obtained from experiments, is the average lifetime. Based on an approximate Eigen's relationship, the average lifetime of H_3O^+ was demonstrated to be sensitive to the concentration of acid;⁵⁷ as the concentration of the acid increases, so does the average lifetime. This could be one of the reasons why the average lifetime of H_3O^+ reported in literatures varies in a rather wide range.⁵¹ For example, through the measurements of proton conductance,⁴⁹ the average lifetime was estimated to be 240 fs, whereas a higher value, by about one order of magnitude, was derived from dielectric relaxation data.⁵⁸ While the measurement of the low frequency (1200 cm^{-1}) in the vibrational spectrum of H_3O^+ requires a minimum lifetime of only 30 fs,⁵¹ the one obtained from the measurement of ^{17}O -induced proton relaxation in water and very dilute acids amounts to 2.2 ps.^{59,60} In the present study, the average lifetime of H_3O^+ in the Eigen complex is within this range. It should be added that, in our model systems, the lack of continuous H-bond network connecting the first and second hydration shells could restrict the mobility of proton, whereas the inclusion of strong interaction between proton and polar environment could lead to a retardation of proton transfer events.⁵⁶ Our $\langle\tau_{\text{H}_9\text{O}_4^+}^{\text{III,A}}\rangle = 68.2$ fs is, however, closer to the lowest limit, estimated from the low-frequency vibrational spectroscopy.⁵¹

3.2.2 The $\text{CF}_3\text{SO}_3\text{H} - \text{H}_3\text{O}^+ - \text{H}_2\text{O}$ complexes. Fig. 6 shows examples of proton transfer profiles for the $\text{CF}_3\text{SO}_3\text{H} - \text{H}_3\text{O}^+ - \text{H}_2\text{O}$ 1 : 1 : 1 complex, with snapshots of H-bond structures observed in the course of BOMD simulations. Three important elementary reactions were extracted from BOMD results and illustrated in Fig. 7 with all other results. For the $\text{CF}_3\text{SO}_3\text{H} - \text{H}_3\text{O}^+ - \text{H}_2\text{O}$ 1 : 1 : 1 complexes, both large- and small-amplitude vibrations exist in the proton transfer profiles. In Fig. 6b, large-amplitude vibrations are seen, for example, between $t_1 = 27$ fs and $t_3 = 420$ fs, within which quasi-dynamic equilibria, followed by actual proton transfers in the reverse direction are seen in general. Small-amplitude vibrations are, for example, from $t_3 = 420$ fs to $t_4 = 647$ fs. Starting from structure a in Fig. 1, the H-bond proton (H_2^* in Fig. 6c) moved in the course of BOMD simulations from O2 to O3, resulting in structure A in Fig. 6c. The proton transfer profile in Fig. 6a and the snapshots in Fig. 6c reveal an example of the H-bond structure reorganization from cyclic to linear. At $t_5 = 750$ fs, H_6^* forms H-bond with an oxygen atom of $-\text{SO}_3\text{H}$, then structure C changes to structure D. Structures D, E and F show a possibility for proton transfer away from $-\text{SO}_3\text{H}$; whereas structure G for proton transfer in the reverse direction; forming $-\text{SO}_3\text{H}_2^+$ between $t_8 = 1335$ fs and $t_9 = 1416$ fs. The probability for proton transfer through the formation of $-\text{SO}_3\text{H}_2^+$ is higher for structure c in Fig. 3. Starting from structure c, $-\text{SO}_3\text{H}_2^+$ was generated right at the beginning of BOMD simulations. Snapshots in Fig. 6d reveal that structure A acts as a precursor and the proton transfer could be mediated by $-\text{SO}_3\text{H}_2^+$ in both directions; from structures A to B to C, as well as from structures A to D to E. Since there is no water molecule to stabilize the product

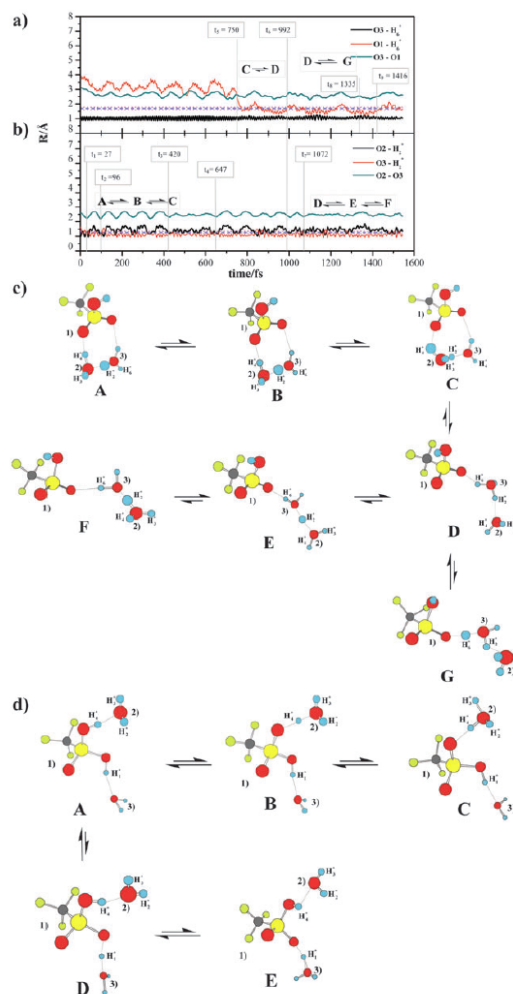


Fig. 6 Examples of proton transfer profiles for the $\text{CF}_3\text{SO}_3\text{H}-\text{H}_3\text{O}^+-\text{H}_2\text{O}$ 1 : 1 : 1 complexes, with snapshots of H-bond structures observed in the course of BOMD simulations. (a)–(b) BOMD simulations starting from structure A in Fig. 1. (c)–(d) Snapshots of H-bond structures.

(H_3O^+), both structures C and E return to structure A, as also recognized in the case of H_7O_3^+ .

The results in Fig. 7 show that, due to a limited number of water molecules, the products in elementary reactions I and II were observed in short times. $\langle\tau_{1:1:1}^{\text{I,C}}\rangle$ and $\langle\tau_{1:1:1}^{\text{II,C}}\rangle$ are 10.1 and 9.3 fs, respectively, compared to the lifetimes of the precursors, $\langle\tau_{1:1:1}^{\text{I,A}}\rangle$ and $\langle\tau_{1:1:1}^{\text{II,A}}\rangle$, of 51.0 and 54.6 fs, respectively. For elementary reaction I, the quasi-dynamic equilibrium between the precursor and the transition state ($\langle\tau_{1:1:1}^{\text{I,AB}}\rangle$) is 38.8 fs, with the average maximum proton transfer cycle time ($\langle\tau_{1:1:1}^{\text{I,PTmax}}\rangle$) of 79.9 fs; whereas those of elementary reaction II are 25.3 and 95.8 fs, respectively. The values of $g_{1:1:1}^{\text{I}}$ and $P_{1:1:1}^{\text{I,forw}}$, as well as $g_{1:1:1}^{\text{II}}$ and $P_{1:1:1}^{\text{II,forw}}$ in

Fig. 7, indicate that the degrees of coherence in elementary reactions I and II are comparable with H_3O_4^+ , with a lower probability for proton transfer in the forward direction; $P_{1:1:1}^{\text{I,forw}}$ and $P_{1:1:1}^{\text{II,forw}}$ are only 0.2. Elementary reaction III in Fig. 7 involves proton transfer through $-\text{SO}_3\text{H}_2^+$. Although elementary reaction III possesses the highest degree of coherence, $g_{1:1:1}^{\text{III}} = 0.8$, the probability for proton transfer from $-\text{SO}_3\text{H}_2^+$ and the lifetime of the product are the highest; $P_{1:1:1}^{\text{III,forw}} = 0.4$ and $\langle\tau_{1:1:1}^{\text{III,C}}\rangle = 23.9$ fs. These confirm the possibility that $-\text{SO}_3\text{H}_2^+$ could represent an effective transition state in proton transfer pathway at low hydration levels.²⁶

For the $\text{CF}_3\text{SO}_3\text{H}-\text{H}_3\text{O}^+-\text{H}_2\text{O}$ 1 : 1 : 2 complexes, five important proton transfer elementary reactions could be extracted from BOMD results. The extension of the H-bond network in the vicinity of $-\text{SO}_3\text{H}$ could bring about both stabilization and destabilization effects to H_3O^+ , depending upon the H-bond structures. Comparison of the results in Fig. 7 and 8 shows that, for elementary reaction I, the average lifetimes of the precursor ($\langle\tau_{1:1:2}^{\text{I,A}}\rangle$), as well as the quasi-dynamic equilibrium ($\langle\tau_{1:1:2}^{\text{I,ABC}}\rangle$), are increased when H_3O^+ is triply H-bonded; the former is 73.7 fs, and the latter is 29.0 fs. These are accompanied by an increase in the degree of coherence and a decrease in the average lifetime of the product, $g_{1:1:2}^{\text{I}} = 0.8$ and $\langle\tau_{1:1:2}^{\text{I,C}}\rangle = 7.8$ fs, as well as a decrease in the probability for proton transfer in the forward direction, $P_{1:1:2}^{\text{I,forw}} = 0.1$.

Elementary reactions II, III and IV in Fig. 8 represent three possibilities for proton transfers along the linear H-bonds at $-\text{SO}_3\text{H}$. For elementary reaction II, the extension of the H-bond network, through the formation of the $\text{O}-\text{H}\cdots\text{Ow}$ H-bond, brings about higher stability to H_3O^+ . This makes it difficult for H_3O^+ to transfer a proton to the adjacent water. Comparison of $P_{1:1:2}^{\text{II,forw}}$ and $P_{1:1:2}^{\text{III,forw}}$ in Fig. 7 and 8 shows that, due to an increase in the stability of H_3O^+ in elementary reaction II, the probability for proton transfer away from $-\text{SO}_3\text{H}$ is considerably decreased; structure C which is the product was rarely found in the course of BOMD simulations. Comparison of elementary reaction III in Fig. 7 and 8 reveals a similar trend, namely, the probability for H_3O^+ to protonate at $-\text{SO}_3\text{H}$ is reduced upon the $\text{Oh}-\text{Hh}\cdots\text{Ow}$ H-bond formation, with a shorter average lifetime of $-\text{SO}_3\text{H}_2^+$, $\langle\tau_{1:1:2}^{\text{III,C}}\rangle = 11.7$ fs, compared to $\langle\tau_{1:1:1}^{\text{III,A}}\rangle = 66.2$ fs. The elementary reaction IV shows a small probability to detect $-\text{SO}_3^-$ in the course of BOMD simulations, with $P_{1:1:2}^{\text{IV,forw}} = 0.03$. In this case, large-amplitude vibration with $g_{1:1:2}^{\text{IV}} \approx 1.0$, dominates and the charged product possesses very short average lifetime, $\langle\tau_{1:1:2}^{\text{IV,C}}\rangle = 4.7$ fs. The stability of H_3O^+ and the degree of coherence in the H-bond are substantially reduced upon larger cyclic H-bond network formation; $\langle\tau_{1:1:2}^{\text{V,A}}\rangle$ and $g_{1:1:2}^{\text{V}}$ for elementary reaction V are 10.2 fs and 0.14, respectively. The values are close to those in H_5O_2^+ . Since the average lifetimes of both precursor and product are small, the probability for proton transfer in the forward direction is the highest among the $\text{CF}_3\text{SO}_3\text{H}-\text{H}_3\text{O}^+-\text{H}_2\text{O}$ 1 : 1 : 2 complexes, with $P_{1:1:2}^{\text{V,forw}} = 0.6$.

Due to a high degree of freedom in the $\text{CF}_3\text{SO}_3\text{H}-\text{H}_3\text{O}^+-\text{H}_2\text{O}$ 1 : 1 : 3 complexes, only linear H-bonds were observed in the course of BOMD simulations. The elementary reactions I, II and III in Fig. 9 represent three possibilities for proton transfer along the H-bond network

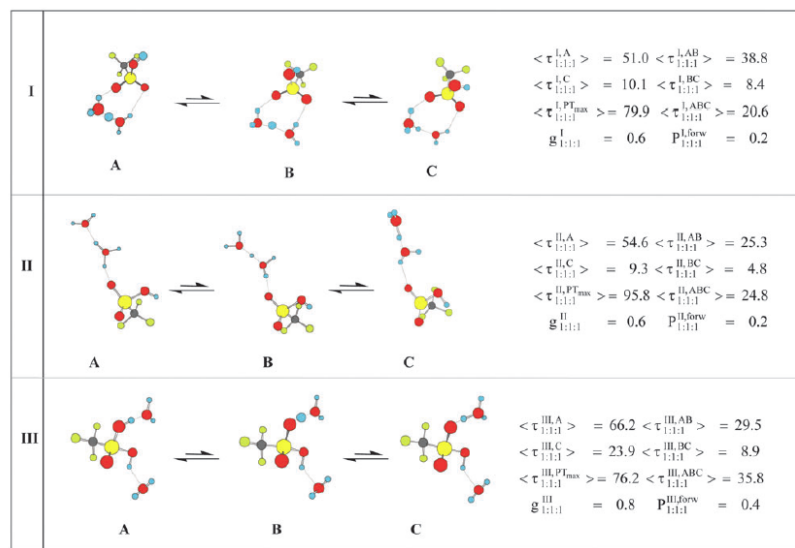


Fig. 7 Important elementary reactions in proton transfer in the $\text{CF}_3\text{SO}_3\text{H}-\text{H}_3\text{O}^+-\text{H}_2\text{O}$ 1 : 1 : 1 complexes, obtained from BOMD simulations. The symbols are explained in details in the text.

passing through $-\text{SO}_3\text{H}$. Large-amplitude vibrations seem to dominate in elementary reactions I and II, with $g_{1:1:3}^I$ and $g_{1:1:3}^{II}$ of 0.8. Elementary reactions I and II show that when the H-bond network is well connected on both sides of $-\text{SO}_3\text{H}$, the stability of H_3O^+ is increased. This tends to reduce the probability for the proton transfers from H_3O^+ to H_2O , as well as from H_3O^+ to $-\text{SO}_3\text{H}$; both $P_{1:1:3}^{I,forw}$ and $P_{1:1:3}^{II,forw}$ are only about 0.1. The former reflects the possibility for proton transfer away from $-\text{SO}_3\text{H}$, and the latter for the formation of $-\text{SO}_3\text{H}_2^+$. Elementary reaction III reveals a quite high possibility for proton transfer through the formation of $-\text{SO}_3^-$, through an ion-pair complex similar to structure e in Fig. 2. The results in Fig. 9 indicate further that, for elementary reaction III, large-amplitude vibration dominates, with $g_{1:1:3}^{III} = 0.9$, and the probability for proton transfer in the forward direction is the highest among the $\text{CF}_3\text{SO}_3\text{H}-\text{H}_3\text{O}^+-\text{H}_2\text{O}$ 1 : 1 : 3 complexes, with $P_{1:1:3}^{III,forw} = 0.7$. The latter is slightly higher than $P_{1:1:2}^{V,forw}$.

4. Conclusions

Attempt has been made in the present work to study proton transfer reactions at a hydrophilic functional group in model Nafion[®], using a theoretical method which takes into account the dynamics of formation and cleavage of covalent and H-bonds. Complexes formed from $\text{CF}_3\text{SO}_3\text{H}$, H_3O^+ and H_2O were employed as model systems, from which the dynamics of an excess proton and proton defects at and in the vicinity of $-\text{SO}_3\text{H}$ were systematically studied, with the emphasis on how $-\text{SO}_3\text{H}$ facilitates or mediates proton transfer reactions at low hydration levels.

It was found in general that all characteristic H-bond structures and trends of proton transfer in the $\text{H}_3\text{O}^+-\text{H}_2\text{O}$

1 : n and $\text{CF}_3\text{SO}_3\text{H}-\text{H}_3\text{O}^+-\text{H}_2\text{O}$ 1 : 1 : n complexes, $1 \leq n \leq 3$, could be predicted reasonably well by T-model, B3LYP/6-31G(d,p) and MP2/6-311++G(d,p) calculations. The theoretical results revealed possibilities for proton transfer along the H-bond network of water connecting the oxygen atoms of $-\text{SO}_3\text{H}$, as well as by relay-type mechanisms, in which proton hops across $-\text{SO}_3\text{H}$ through the formations of the $-\text{SO}_3\text{H}_2^+$ and $-\text{SO}_3^-$ transition states.

A series of BOMD simulations at 298 K was performed based on B3LYP/6-31G(d,p) calculations. Attention was focused on the precursors and transition states with H-bonds susceptible to proton transfers. Since the Zundel and Eigen complexes play the most important role in proton transfer reactions in aqueous solutions, their basic dynamic behavior was initially studied. It appeared that proton transfer in H_3O_2^+ depends strongly on the $\text{Oh}-\text{Hh} \cdots \text{Ow}$ H-bond separation, as well as its vibrational amplitude. Two extreme cases, namely, large- and small-amplitude vibrations, were analyzed and discussed in details based on proton transfer profiles. BOMD results showed that, due to the thermal energy fluctuation and coupled motions among H-bonds, a quasi-dynamic equilibrium between the Eigen and Zundel complexes could be established and considered to be one of the most important elementary reactions in the proton transfer process. Although our model systems lack of continuous H-bond network connecting the first and second hydration shells, the average lifetime of H_3O^+ in the Eigen complex is in reasonable agreement with the lowest limit estimated from low-frequency vibrational spectroscopy.

For the $\text{CF}_3\text{SO}_3\text{H}-\text{H}_3\text{O}^+-\text{H}_2\text{O}$ complexes, various temporary proton defects in H-bond structures were observed in the course of BOMD simulations. Due to the thermal energy fluctuation and dynamics at 298 K, proton transfer reactions at $-\text{SO}_3\text{H}$ seem to comprise various elementary reactions in

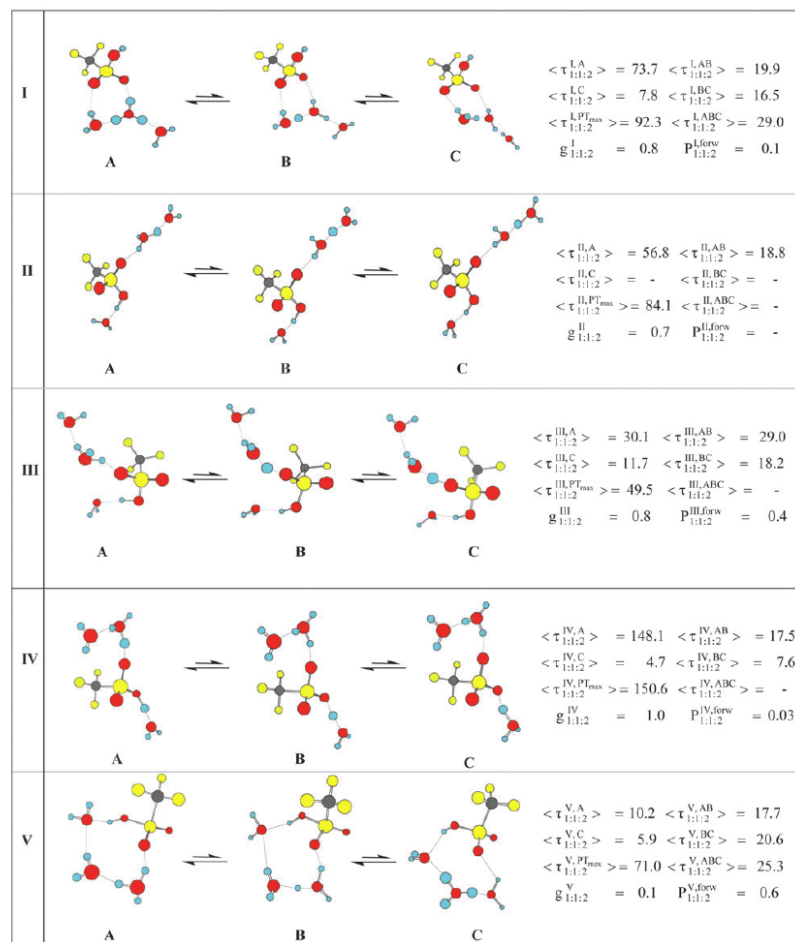


Fig. 8 Important elementary reactions in proton transfer in the $\text{CF}_3\text{SO}_3\text{H}-\text{H}_3\text{O}^+-\text{H}_2\text{O}$ 1 : 1 : 2 complexes, obtained from BOMD simulations. The symbols are explained in details in the text.

quasi-dynamic equilibria. These prohibit proton transfer reactions from being concerted, and confirm the observations that the proton motion is too fast to be a rate-determining step. Due to large- and small-amplitude vibrations in H-bond separations, the internal conversions between covalent and H-bonds, similar to the Grotthuss mechanism, were concluded to form the general basis for proton transfer processes at $-\text{SO}_3\text{H}$. Attempt was also made to describe these proton-relay type mechanisms in terms of coherence and incoherence effects. BOMD simulations showed that the proton-relay type mechanisms could take place among $-\text{SO}_3\text{H}$, H_3O^+ and H_2O , providing some effective proton transfer pathways, through the formations of the $-\text{SO}_3^-$, $-\text{SO}_3\text{H}_2^+$ and H_5O_2^+ transition states. The analyses of the average lifetimes of the precursors and elementary reactions suggested that when the H-bond structures are right, in order that $-\text{SO}_3\text{H}$ could effectively function as a mediator in proton transfer reactions, the probabilities for the elementary reactions to proceed in the

forward and reverse directions should be somewhat equivalent, otherwise the proton would be trapped at $-\text{SO}_3\text{H}$.

Finally, it should be emphasized that the present BOMD simulations focused on proton transfer processes at and in the proximity of a single $-\text{SO}_3\text{H}$ group, and within a narrow timescale. Therefore, H-bond structure reorganizations and molecular diffusions, which could contribute to proton conduction in different timescales, were not taken into account. It should be also added that the present theoretical investigations were performed at low hydration levels, in which the H-bond networks are not as extensive as in aqueous solutions, and strong interaction between proton and the polar environment could lead to a retardation of proton transfer. Therefore, direct comparisons between our model calculations and experiments seem not appropriate. However, some important insights, especially the interplays between local H-bond structures and dynamics, as well as the potential precursors and the proton transfer elementary reactions in an excess proton

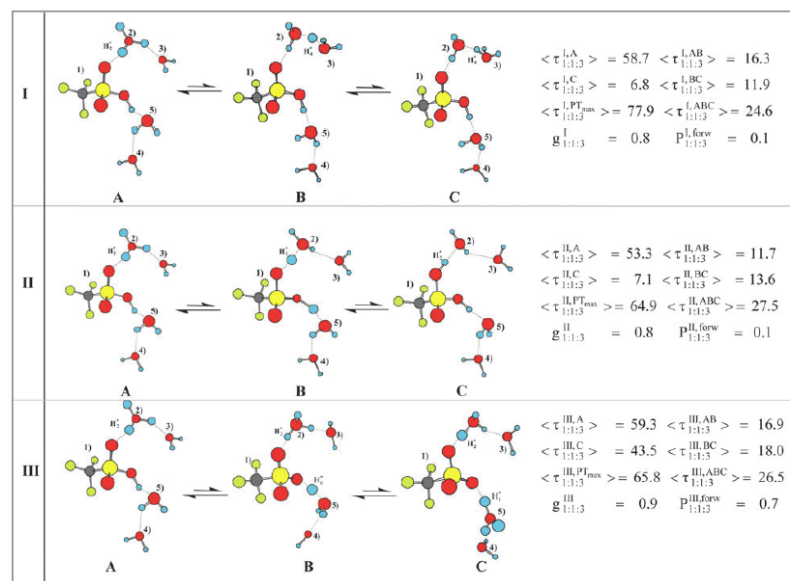


Fig. 9 Important elementary reactions in proton transfer in the $\text{CF}_3\text{SO}_3\text{H}-\text{H}_3\text{O}^+-\text{H}_2\text{O}$ 1 : 1 : 3 complexes, obtained from BOMD simulations. The symbols are explained in details in the text.

condition, could be obtained. The present BOMD results also iterated that the equilibrium structures and energetic obtained from MM or *ab initio* geometry optimizations could not provide complete information on chemical reactions, especially the reaction pathways. It appeared that the theoretical methods and the analyses adopted in the present work could provide the practical basis for study of proton transfer reactions in larger H-bond systems. Based on similar approaches, progress has been made in our laboratory to include more hydrophilic functional groups and appropriate solvent effects in model systems of Nafion[®].

Acknowledgements

The authors would like to acknowledge financial support from the Thailand Research Fund (TRF); the Advanced Research Scholarship (BRG-4880008) for Prof. Kritsana Sagarik; the Royal Golden Jubilee (RGJ) PhD Program, Grant No. PHD/0110/2548 for Mayuree Phonyiem; Grant No. PHD/0071/2547 for Sermsiri Chaiwongwattana; Grant No. PHD/0121/2549 for Charoensak Lao-ngam. Linux cluster facilities have been provided by School of Mathematics and School of Chemistry, SUT, as well as the Thai-Grid Project, National Electronics and Computer Technology Center (NECTEC) and National Nanotechnology Center (NANO-TEC), Thailand.

References

- 1 J. Larminie and A. Dicks, *Fuel Cell Syst.*, John Wiley & Sons Ltd, Chichester, 2001.
- 2 C. A. Vincent and B. Scrosati, *Modern Batteries: An introduction to electrochemical power sources*, John Wiley & Sons Ltd, New York, 1997.
- 3 T. Koppel, *Powering the Future: The Ballard fuel cell and the race to change the world*, John Wiley & Sons Ltd, New York, 1999.
- 4 J. T. Hinatsu, M. Mizuhata and H. Takenaka, *J. Electrochem. Soc.*, 1994, **141**, 1493.
- 5 K. A. Mauritz and R. B. Moore, *Chem. Rev.*, 2004, **104**, 4535.
- 6 T. D. Gierke, G. E. Munn and F. C. Wilson, *J. Polym. Sci. Polym. Phys.*, 1981, **19**, 1687.
- 7 S. J. Paddison, *Annu. Rev. Mater. Res.*, 2003, **33**, 289.
- 8 K. D. Kreuer, *Chem. Mater.*, 1996, **8**, 610.
- 9 K. D. Kreuer, S. J. Paddison, E. Spohr and M. Schuster, *Chem. Rev.*, 2004, **104**, 4637.
- 10 S. J. Paddison and T. Zawodzinski, Jr, *Solid State Ionics*, 1998, **115**, 333.
- 11 S. J. Paddison, L. R. Pratt and T. A. Zawodzinski, Jr, *J. New Mater. Electrochem. Syst.*, 1999, **2**, 183.
- 12 M. Laporta, M. Pegoraro and L. Zanderighi, *Phys. Chem. Chem. Phys.*, 1999, **1**, 4619.
- 13 A. Vishnyakov and A. V. Neimark, *J. Phys. Chem. B*, 2000, **104**, 4471.
- 14 R. Buzzoni, S. Bordiga, G. Ricchiardi, G. Spoto and A. Zecchina, *J. Phys. Chem.*, 1995, **99**, 11937.
- 15 A. Zecchina, F. Geobaldo, G. Spoto, S. Bordiga, G. Ricchiardi, R. Buzzoni and G. Petrini, *J. Phys. Chem.*, 1996, **100**, 16584.
- 16 S. J. Paddison, G. Bender, K. D. Kreuer, N. Nicoloso and T. A. Zawodzinski, Jr, *J. New Mater. Electrochem. Syst.*, 2000, **3**, 293.
- 17 N. G. Boyle, V. J. McBrierty and A. Eisenberg, *Macromolecules*, 1983, **16**, 80.
- 18 S. J. Paddison, L. R. Pratt, T. A. Zawodzinski, Jr and D. W. Reagor, *Fluid Phase Equilib.*, 1998, **150**, 235.
- 19 S. J. Paddison, L. R. Pratt and T. Zawodzinski, Jr, *J. Phys. Chem. A*, 2001, **105**, 6266.
- 20 S. J. Paddison, *J. New Mater. Electrochem. Syst.*, 2001, **4**, 197.
- 21 M. Eikerling, S. J. Paddison, L. R. Pratt and T. A. Zawodzinski, Jr, *Chem. Phys. Lett.*, 2003, **368**, 108.
- 22 M. Cappadonia, J. W. Erning, S. M. S. Niaki and U. Stimming, *Solid State Ionics*, 1995, **77**, 65.
- 23 S. J. Paddison and J. A. Elliott, *J. Phys. Chem. A*, 2005, **109**, 7583.

- 24 S. J. Paddison and J. A. Elliott, *Phys. Chem. Chem. Phys.*, 2006, **8**, 2193.
- 25 S. J. Paddison and J. A. Elliott, *Solid State Ionics*, 2006, **177**, 2385.
- 26 V. A. Glezakou, M. Dupuis and C. J. Mundy, *Phys. Chem. Chem. Phys.*, 2007, **9**, 5752.
- 27 J. M. Hermida-Ramon and G. Karlstroem, *J. Mol. Struct. (THEOCHEM)*, 2004, **712**, 167.
- 28 A. Botti, F. Bruni, S. Imberti, M. A. Ricci and A. K. Soper, *J. Mol. Liquid*, 2005, **117**, 77.
- 29 M. D. Newton, *J. Chem. Phys.*, 1978, **67**, 5535.
- 30 K. P. Sagarik and B. M. Rode, *Chem. Phys.*, 2000, **260**, 159.
- 31 K. P. Sagarik, S. Chaiwongwattana and P. Sisot, *Chem. Phys.*, 2004, **306**, 1.
- 32 K. P. Sagarik and S. Dokmaistrjan, *J. Mol. Struct. (THEOCHEM)*, 2005, **718**, 31.
- 33 K. Sagarik and S. Chaiyapongs, *Biophys. Chem.*, 2005, **117**, 18.
- 34 N. Deeying and K. Sagarik, *Biophys. Chem.*, 2007, **125**, 72.
- 35 K. D. Kreuer, *Solid State Ionics*, 2000, **136**, 149.
- 36 U. W. Schmitt and G. A. Voth, *J. Chem. Phys.*, 1999, **111**, 9361.
- 37 K. P. Sagarik and R. Ahlrichs, *J. Chem. Phys.*, 1987, **86**, 5117.
- 38 K. P. Sagarik, V. Pongpituk, S. Chiyapongs and P. Sisot, *Chem. Phys.*, 1991, **156**, 439.
- 39 K. P. Sagarik, *J. Mol. Struct. (THEOCHEM)*, 1999, **465**, 141.
- 40 K. P. Sagarik and E. Spohr, *Chem. Phys.*, 1995, **199**, 73.
- 41 K. P. Sagarik and P. Asawakun, *Chem. Phys.*, 1997, **219**, 173.
- 42 M. J. Frisch, G. W. Trucks, H. B. Schlegel, G. E. Scuseria, M. A. Robb, J. R. Cheeseman, V. G. Zakrzewski, J. A. Montgomery, Jr, R. E. Stratmann, J. C. Burant, S. Dapprich, J. M. Millam, A. D. Daniels, K. N. Kudin, M. C. Strain, O. Farkas, J. Tomasi, V. Barone, M. Cossi, R. Cammi, B. Mennucci, C. Pomelli, C. Adamo, S. Clifford, J. Ochterski, G. A. Petersson, P. Y. Ayala, Q. Cui, K. Morokuma, P. Salvador, J. J. Dannenberg, D. K. Malick, A. D. Rabuck, K. Raghavachari, J. B. Foresman, J. Cioslowski, J. V. Ortiz, A. G. Baboul, B. B. Stefanov, G. Liu, A. Liashenko, P. Piskorz, I. Komaromi, R. Gomperts, R. L. Martin, D. J. Fox, T. Keith, M. A. Al-Laham, C. Y. Peng, A. Nanayakkara, M. Challacombe, P. M. W. Gill, B. Johnson, W. Chen, M. W. Wong, C. Gonzalez and J. A. Pople, *GAUSSIAN 03 (Revision D.1)*, Gaussian, Inc., Wallingford, CT, 2005.
- 43 P. B. Balbuena and J. M. Seminario, *Theoretical and Computational Chemistry 7, Molecular dynamics; from classical to quantum methods*, Elsevier, Amsterdam, 1999.
- 44 C. J. Cramer, *Essentials of Computational Chemistry: Theory and models*, John Wiley & Sons, Ltd, 2002.
- 45 D. C. Young, *Computational Chemistry: A practical guide for applying techniques to real world problems*, Wiley Interscience, New York, 2001.
- 46 R. N. Barnett and U. Landman, *Phys. Rev.*, 1993, **B48**, 2081.
- 47 X. Jing, N. Troullier, D. Dean, N. Bingeli, J. R. Chelikowsky, K. Wu and Y. Saad, *Phys. Rev.*, 1994, **B50**, 122.
- 48 A. R. Leach, *Molecular Modelling: Principles and applications*, Longman, Edinburgh, 1996.
- 49 B. E. Conway, J. O. M. Bockris and H. Linton, *J. Chem. Phys.*, 1956, **24**, 834.
- 50 N. Agmon, *Chem. Phys. Lett.*, 1995, **244**, 456.
- 51 P. A. Giguere, *J. Chem. Educ.*, 1979, **56**, 571.
- 52 JMOL website <http://jmol.sourceforge.net/>.
- 53 X. Duan and St. Scheiner, *J. Mol. Struct.*, 1992, **270**, 173.
- 54 R. Janoscheck, *J. Mol. Struct.*, 1994, **231**, 45.
- 55 C. J. D. von Grotthuss, *Annu. Chim.*, 1806, **58**, 54.
- 56 K. D. Kreuer, *Solid State Ionics*, 1997, **94**, 55.
- 57 M. Eigen and L. De Maeyer, *Proc. R. Soc.*, 1958, **A247**, 505.
- 58 M. Eigen, *Angew. Chem.*, 1963, **75**, 489.
- 59 R. E. Glick and K. C. Tewari, *J. Chem. Phys.*, 1966, **44**, 546.
- 60 S. W. Rabideau and H. G. Hetch, *J. Chem. Phys.*, 1967, **47**, 544.

Proton transfer reactions and dynamics of sulfonic acid group in Nafion[®]†

Mayuree Phonyiem, Semsiri Chaiwongwattana, Charoensak Lao-ngam and Kritsana Sagarik*

Received 22nd February 2011, Accepted 1st April 2011

DOI: 10.1039/c1cp20469f

Proton transfer reactions and dynamics of the hydrophilic group ($-\text{SO}_3\text{H}$) in Nafion[®] were studied at low hydration levels using the complexes formed from $\text{CF}_3\text{SO}_3\text{H}$, H_3O^+ and $n\text{H}_2\text{O}$, $1 \leq n \leq 3$, as model systems. The equilibrium structures obtained from DFT calculations suggested at least two structural diffusion pathways at the $-\text{SO}_3\text{H}$ group namely, the “pass-through” and “pass-by” mechanisms. The former involves the protonation and deprotonation at the $-\text{SO}_3\text{H}$ group, whereas the latter the proton transfer in the adjacent Zundel complex. Analyses of the asymmetric O–H stretching frequencies (ν^{OH}) of the hydrogen bond (H-bond) protons showed the threshold frequencies (ν^{OH^*}) of proton transfer in the range of 1700 to 2200 cm^{-1} . Born–Oppenheimer Molecular Dynamics (BOMD) simulations at 350 K anticipated slightly lower threshold frequencies ($\nu_{\text{A}}^{\text{OH}^*,\text{MD}}$), with two characteristic asymmetric O–H stretching frequencies being the spectral signatures of proton transfer in the H-bond complexes. The lower frequency ($\nu_{\text{A}}^{\text{OH},\text{MD}}$) is associated with the oscillatory shuttling motion and the higher frequency ($\nu_{\text{B}}^{\text{OH},\text{MD}}$) the structural diffusion motion. Comparison of the present results with BOMD simulations on protonated water clusters indicated that the $-\text{SO}_3\text{H}$ group facilitates proton transfer by reducing the vibrational energy for the interconversion between the two dynamic states ($\Delta\nu_{\text{BA}}^{\text{OH},\text{MD}}$), resulting in a higher population of the H-bonds with the structural diffusion motion. One could therefore conclude that the $-\text{SO}_3\text{H}$ groups in Nafion[®] act as active binding sites which provide appropriate structural, energetic and dynamic conditions for effective structural diffusion processes in a proton exchange membrane fuel cell (PEMFC). The present results suggested for the first time a possibility to discuss the tendency of proton transfer in H-bond using $\Delta\nu_{\text{BA}}^{\text{OH},\text{MD}}$ and provided theoretical bases and guidelines for the investigations of proton transfer reactions in theory and experiment.

1. Introduction

Polymer electrolyte membrane widely used in proton exchange membrane fuel cells (PEMFC) is Nafion[®].^{1,2} Nafion[®] consists of Teflon[®] backbones and randomly attached hydrophilic side chains. The backbone and side chains of Nafion[®] are terminated by trifluoromethanesulfonic (triflic) acid groups. Experiments have shown that the triflic acid groups ($-\text{CF}_3\text{SO}_3\text{H}$) are preferentially hydrated, resulting in large interconnected hydrophilic domains which play important roles in proton transfer reactions.³ Although some basic information has been accumulated in the past decades, mechanisms of proton transfer reactions in Nafion[®], especially at the molecular level,

are not well understood.^{4–7} Some theoretical and experimental results pertinent to the present work will be summarized as follows.

Proton transfer reactions at the $-\text{SO}_3\text{H}$ group of Nafion[®] were investigated at low hydration levels, using the complexes formed from $\text{CF}_3\text{SO}_3\text{H}$, H_3O^+ and $n\text{H}_2\text{O}$, $1 \leq n \leq 3$, as model systems.⁸ With the emphasis on how $-\text{SO}_3\text{H}$ facilitates or mediates transportation of an excess proton, a series of BOMD simulations was conducted at 298 K, from which the intermediate states in the proton transfer pathways were identified, analyzed and categorized. It was observed that the proton transfer reactions at $-\text{SO}_3\text{H}$ are not concerted due to the thermal energy fluctuations and the quasi-dynamic equilibria among the Zundel complex, the Eigen complex and the $-\text{SO}_3\text{H}$ group could directly and indirectly mediate the proton transfer reactions through the formation of the proton defects, as well as the $-\text{SO}_3^-$ and $-\text{SO}_3\text{H}_2^+$ groups. It was concluded that static proton transfer potentials cannot provide complete description of the structural diffusion

School of Chemistry, Institute of Science, Suranaree University of Technology, Nakhon Ratchasima 30000, Thailand.
E-mail: kritsana@sut.ac.th; Fax: (6644) 224635; Tel: (6644) 224635
† Electronic supplementary information (ESI) available. See DOI: 10.1039/c1cp20469f

processes in H-bonds and it is necessary to incorporate thermal energy fluctuations and dynamics in the model calculations.^{8,9}

Since one of the most important evidence of the H-bond formation in aqueous solution is the red shift of the high-frequency hydroxyl (O–H) stretching mode, accompanied by its intensity increase and band broadening,^{10–12} attempt was made to correlate the O–H stretching frequency with the tendency of proton transfer in H-bonds;^{12–14} the broad and intense IR absorption bands ranging from 1000 to 3000 cm^{−1} were interpreted as spectral signatures of protonated water networks,¹⁴ whereas the tendency of proton transfer was measured from the strong red shift of the asymmetric O–H stretching frequency (ν^{OH}), compared with the corresponding “free” or “non-H-bonded” one.¹² The red shift cannot be determined easily in experiment due to the coupling and overlapping of various vibrational modes, as well as the detection limit of IR equipment;^{15,16} analyses of IR and Raman spectra of pure and concentrated solutions ($\text{H}_2\text{O}/\text{H}^+ = 3\text{--}4$) of H_2SO_4 , HCl and $\text{CF}_3\text{SO}_3\text{H}$,¹³ and FTIR study of water in cast Nafion[®] films¹⁷ revealed that the fingerprint of proton transfer from the undissociated $\text{CF}_3\text{SO}_3\text{H}$ to water at 1040 cm^{−1} could be masked by the strong C–F stretching bands at 1200–1300 cm^{−1}, as well as the stretching bands in the –SO₃H group at 910 and 1410 cm^{−1}. It was suggested that the classical interpretations of IR frequencies for concentrated acid solutions could be employed as criteria to roughly estimate the tendency of proton transfer;¹⁸ the stretching frequencies for the H-bond proton are divided into three groups, namely the internal (1300–2200 cm^{−1}), external (2500–3200 cm^{−1}), and outlayer groups (3300–3400 cm^{−1}). The H-bond proton in the internal group is considered to be susceptible to proton transfer.

In our previous study, characteristic IR frequencies of proton transfer in protonated water clusters were investigated using theoretical methods.¹⁹ DFT calculations revealed that the intermediate states in proton transfer pathways consist of the Zundel complex, with the threshold asymmetric O–H stretching frequencies (ν^{OH}) in the gas phase and aqueous solution at $\nu^{\text{OH}*} = 1984$ and 1881 cm^{−1}, respectively. Born–Oppenheimer MD (BOMD) simulations predicted slightly lower threshold frequencies, $\nu^{\text{OH},\text{MD}} = 1917$ and 1736 cm^{−1}, respectively, with two characteristic asymmetric O–H stretching frequencies ($\nu^{\text{OH},\text{MD}}$) being the IR spectral signatures of proton transfer. The lower-frequency band (at $\nu_{\text{A}}^{\text{OH},\text{MD}}$) could be associated with the “oscillatory shuttling motion”, whereas the higher-frequency band (at $\nu_{\text{B}}^{\text{OH},\text{MD}}$) with the “structural diffusion motion”.¹⁹

Although some important structural and dynamic results on the proton transfer reactions at the –SO₃H group of Nafion[®] have been reported in our previous work,⁸ several fundamental questions have to be answered, before the studies in condensed phases can proceed; as examples: (1) how to effectively monitor proton transfer reactions in condensed phases, both in theory and experiment; (2) according to our IR spectral analyses,^{9,19} what are the characteristic and threshold frequencies of proton transfers in Nafion[®]; (3) what are the basic intermediate states in the proton transfer pathways and how to estimate the activation energies of proton transfers at

and in the vicinities of the –SO₃H group; (4) how the proton transfer reactions can be facilitated or mediated by the –SO₃H group, *etc.* The answers to these questions are important since they could be used as guidelines for the studies in condensed phases and IR experiments.

In order to answer these questions, proton transfer reactions at the –SO₃H group of Nafion[®] were further investigated in the present study, using the complexes formed from $\text{CF}_3\text{SO}_3\text{H}$, H_3O^+ and $n\text{H}_2\text{O}$, $1 \leq n \leq 3$, as model systems.⁸ Since the dynamics of proton transfer can be characterized by vibrational behavior of the transferring proton, an attempt was made to correlate the tendency and population of proton transfer with the characteristic IR frequencies in H-bonds.^{9,20} Based on the theoretical results in the gas phase and continuum aqueous solution, the dynamics and mechanisms, as well as the IR spectral signatures, of proton transfer in the model systems were analyzed and discussed, in comparison with available theoretical and experimental data of the same and similar systems.

2. Computational methods

Since proton transfer reactions are complex, care must be exercised in selecting model systems and theoretical methods. Our previous experience showed that reactions and dynamics of proton transfer processes can be studied reasonably well using small model systems and the following three basic steps:⁸ (1) searching for all important equilibrium structures and intermediate states in the proton transfer pathways using the test-particle model (T-model) potentials;^{21–29} (2) refining of the computed structures using the DFT method; (3) BOMD simulations starting from the refined structures. These three basic steps were also adopted in the present investigations.

It should be noted that, although the DFT methods have been frequently chosen due to their ability to predict the effects of electron correlations with a reasonable degree of accuracy and computational effort, the performance of the DFT methods can be poor or fairly good, depending upon the chemical systems considered; the DFT methods tend to underestimate the interaction energies in van der Waals systems. Outstanding examples are the T-shaped and parallel-displaced (PD) structures of the phenol–benzene complex, from which the interplay between the electrostatic and dispersion interactions has been frequently studied;³⁰ the stability of the former is determined by the electrostatic interactions, whereas the latter by the dispersion interactions. B3LYP/6-311++G(d,p) calculations predicted that the PD structure is unstable, with a positive interaction energy (ΔE), whereas ΔE of the T-shaped structure (with the O–H $\cdots\pi$ H-bond) is -8.4 kJ mol^{−1}. This is considerably higher than the experimental value of -16.7 kJ mol^{−1} (ΔE of the cresol–benzene complex obtained from the picosecond photofragment spectroscopy).³¹ We are aware of this problem and therefore conducted a systematic comparison among B3LYP/6-31G(d,p), HF/6-311++G(d,p) and MP2/6-311++G(d,p) right at the beginning of this series of studies.⁸ It turned out that the size and shape of the potential energy surfaces for proton transfers in small protonated water clusters and the $\text{CF}_3\text{SO}_3\text{H}\text{--}\text{H}_3\text{O}^+\text{--}\text{H}_2\text{O}$ 1:1:1 complexes,

obtained from B3LYP/6-31G(d,p) and MP2/6-311++G(d,p) calculations, were quite similar, whereas HF/6-311++G(d,p) calculations yielded different results; minima were observed at shorter distances and a double-well potential appeared for the cyclic H-bonds in the protonated water cluster. Since forces in BOMD simulations are computed from energy gradients, which are determined by the structures of potential energy surfaces, we therefore adopted the DFT method with the B3LYP functional in all successive studies. The choice is justified by BOMD simulations on similar systems, in which spectroscopic and dynamic results are compared well with experiments.³²

As the electric field introduced by polar solvent can determine the potential energy surface, on which the transferring proton moves, a continuum model must be included in the model calculations. To account for the effects of the extended H-bond networks of water, a conductor-like screening model (COSMO), with the dielectric constant (ϵ) of 78, was employed in the present work. COSMO is a continuum solvent model,^{33,34} in which the solute molecule forms a cavity within a dielectric continuum solvent. The charge distribution of the solute molecule polarizes the dielectric solvent and the response of the solvent is described by the generation of screening charges on the cavity surface computed from atomic radii. Since the screening charges are updated in every cycle and the potential generated by these charges is included into the Hamiltonian, the variational principle is applied on both the molecular orbitals and screening charges, allowing the gradients to be computed in the presence of the continuum fields of solvent. The continuum fields are therefore varied in the course of BOMD simulations. As in the case of QM/MM methods, the solute within the cavity surface could be considered as the quantum mechanical (QM) system. Since the surrounding solvent medium does not have explicit solvent molecules, our BOMD simulations do not require periodic boundary conditions.

Static properties

Equilibrium structures and IR spectra. The equilibrium structures of the H-bond complexes formed from $\text{CF}_3\text{SO}_3\text{H}$, H_3O^+ and H_2O ,⁸ obtained from the T-model potentials, were reoptimized using the DFT method, both in the gas phase and continuum aqueous solution. In order to obtain reliable spectroscopic results, a tight SCF energy convergence criterion (less than 10^{-8} au), with the maximum norm of Cartesian gradients less than 10^{-4} au, was adopted in the DFT geometry optimizations. DFT calculations were performed using the B3LYP hybrid functional,^{35–36} with the triple-zeta valence basis sets augmented by polarization functions (TZVP).³⁷ The performance of B3LYP calculations and the TZVP basis sets on similar systems was discussed in detail.^{32,38} In the present work, B3LYP/TZVP calculations were performed using TURBOMOLE 6.0 software package.^{33,34}

The interaction energies (ΔE) of the H-bond complexes were computed from $\Delta E = E(\text{CF}_3\text{SO}_3\text{H}-\text{H}_3\text{O}^+-n\text{H}_2\text{O}) - [E(\text{CF}_3\text{SO}_3\text{H}) + E(\text{H}_3\text{O}^+) + nE(\text{H}_2\text{O})]$,¹⁹ where $E(\text{CF}_3\text{SO}_3\text{H}-\text{H}_3\text{O}^+-n\text{H}_2\text{O})$ are the total energies of the H-bond complexes; $E(\text{CF}_3\text{SO}_3\text{H})$, $E(\text{H}_3\text{O}^+)$ and $E(\text{H}_2\text{O})$ the

total energies of the isolated molecules at their optimized structures. The energetic effects of the continuum aqueous solvent (COSMO with $\epsilon = 78$) were estimated from the solvation energy (ΔE^{sol}); $\Delta E^{\text{sol}} = E(\text{CF}_3\text{SO}_3\text{H}-\text{H}_3\text{O}^+-n\text{H}_2\text{O})^{\text{COSMO}} - E(\text{CF}_3\text{SO}_3\text{H}-\text{H}_3\text{O}^+-n\text{H}_2\text{O})$; where $E(\text{CF}_3\text{SO}_3\text{H}-\text{H}_3\text{O}^+-n\text{H}_2\text{O})^{\text{COSMO}}$ and $E(\text{CF}_3\text{SO}_3\text{H}-\text{H}_3\text{O}^+-n\text{H}_2\text{O})$ are the total energies of the H-bond complexes, obtained from B3LYP/TZVP calculations with and without COSMO, respectively.

In order to discuss the tendency of proton transfer through the structural diffusion mechanism, the asymmetric stretching coordinate (Δd_{DA})^{9,20} and a concept of the “most active” H-bond were used.³⁹ The H-bond susceptible to proton transfer can be alternatively characterized by low to nonexistence energy barrier along the proton transfer coordinate. This is manifested by a broad IR band with the asymmetric O–H stretching frequency (ν^{OH}) lower than a threshold frequency ($\nu^{\text{OH}*}$).¹⁹ In the present work, based on the well-optimized H-bond structures, harmonic IR frequencies were derived from numerical second derivatives, from which analyses of normal modes in terms of internal coordinates were made. NUMFORCE and AOFORCE programs, included in TURBOMOLE 6.0 software package,^{33,34} were employed in the calculations of the second derivatives and the normal mode analyses, respectively. Since the vibrational frequencies obtained from quantum chemical calculations are generally overestimated compared to experiments, a scaling factor, which partially accounts for anharmonicities and systematic errors, had to be applied; the scaling factor of 0.9614⁴⁰ was shown to be appropriate for B3LYP/TZVP calculations.^{9,19} In order to quantitatively discuss the tendency of proton transfer in H-bond, ν^{OH} were plotted as a function of $R_{\text{O}-\text{O}}$ and $\nu^{\text{OH}*}$ were determined from the plot of ν^{OH} and Δd_{DA} .¹⁹

Dynamic properties

Quantum MD simulations. Elementary reactions and dynamics of rapid covalent bond formation and cleavage can be studied reasonably well using theoretical approaches that incorporate quantum chemical methods into MD simulations,⁴¹ among which BOMD simulations have been widely used.^{8,9,19,42,43} Within the framework of BOMD simulations, classical equations of motions of nuclei on the Born–Oppenheimer (BO) surfaces are integrated, whereas forces on nuclei are calculated in each MD step from quantum energy gradients, with the molecular orbitals (MO) updated by solving Schroedinger equations in the BO approximation; the nuclei thus undergo classical Newtonian dynamics on quantum potential hypersurface. BOMD simulations are therefore more accurate, as well as considerably CPU time consuming, compared to classical MD simulations, in which forces on nuclei are determined from predefined empirical or quantum pair potentials. Our experience showed that BOMD simulations with the DFT method represent an appropriate combination, due to the optimal accuracy *versus* CPU times.^{8,9,19} Therefore, BOMD simulations with the B3LYP/TZVP calculations were adopted in the present investigations.

Since proton transfer reactions especially in aqueous solution involve dynamic processes with different timescales,^{44–46} the

complexity of proton transfer processes could be reduced by selecting an appropriate timestep, from which the classical dynamic equations are solved. The observation that the actual proton transfer takes place in femtosecond (fs) timescale,⁴⁵ which is generally faster than solvent structure reorganization,⁴⁴ makes it reasonable to perform MD simulations by focusing only on short-lived phenomena. Our previous BOMD results showed that, for small H-bond clusters, only few structure reorganization took place within the simulation length of 1–2 ps.^{8,9}

All the equilibrium structures, including intermediate states, obtained from the B3LYP/TZVP geometry optimizations, were employed as starting configurations in BOMD simulations at 350 K, an operation temperature in PEMFC. Canonical ensemble (NVT) was employed in BOMD simulations, with a Nosé-Hoover chain thermostat applied to each degree of freedom in the model system. Since, in aqueous solution, rapid interconversion between the Zundel and Eigen complexes takes place within 100 fs,⁴⁶ the timestep used in solving dynamic equations was set to 1.0 fs. This choice is justified by the proton transfer profiles for the Zundel and the $\text{CF}_3\text{SO}_3\text{H-H}_3\text{O}^+-\text{H}_2\text{O}$ 1:1:1 complexes, in which the vibrations of normal O–H covalent bonds and those susceptible to proton transfers are clearly distinguished.⁸

In each BOMD simulation, 1000 fs were spent on equilibration, after which about 10 ps were devoted to property calculations. The choices are justified by BOMD simulations on H_5O_2^+ and H_7O_3^+ ,³² from which insights into fast dynamic processes in H-bonds (e.g. H-bond structures and IR spectra) could be obtained from relatively short BOMD trajectories (~ 2 ps). All BOMD simulations were performed using FROG program included in TURBOMOLE 6.0;^{33,34} FROG program employs the Leapfrog Verlet algorithm to turn the electronic potential energy gradients into new atomic positions and velocities.

The applicability and performance of NVE and NVT BOMD simulations in the studies of proton transfer reactions in small H-bond systems were investigated and discussed in details.⁴⁷ Since the energy released during the proton transfer process can be absorbed by the Nosé-Hoover thermostat bath, allowing the H-bond structure and the local temperature to maintain for a longer time (2–5 ps), NVT BOMD simulations were used in the present investigations. The Nosé-Hoover thermostats were applied every twenty BOMD steps; for the most active H-bond structure (structure A2C-[I] in Table 2), the average temperature was 349 K, with the standard deviation of 67 K, and the average total energy of -1191.7278058 au, with the standard deviation of 0.005439 au.

IR spectra and diffusion coefficients. Since proton transfers in H-bond are coupled with various degrees of freedom,^{4,9,48} attention was focused on the symmetric and asymmetric O–H stretching frequencies of the transferring protons, as well as the O–O vibrations. In the present study, IR spectra of the transferring protons were computed from BOMD simulations, by Fourier transformations of the velocity autocorrelation function (VACF).⁴⁹ This approach is appropriate as it allows the coupled vibrations to be distinguished, characterized and

analyzed separately. Fourier transformations of VACF were made within a short time limit of about 1000 fs. This is supported by the observation that the average lifetime of the most important intermediate state, the Zundel complex, is about 100 fs.⁴⁶

The diffusion coefficients (D) of the transferring protons were computed from BOMD simulations using the Einstein relation,^{50–51} for which D are determined from the slope of the mean-square displacements (MSD). Because the transferring proton is confined in a short H-bond distance, care must be exercised in selecting the time interval in which MSD are computed.⁵¹ Our experience showed that linear relationship between MSD and the simulation time could be obtained although the time intervals are not larger than 0.5 ps.^{9,19}

3. Results and discussion

In this section, all important results are discussed in comparison with available theoretical and experimental data. The static results obtained from B3LYP/TZVP calculations are analyzed and used as guidelines for the interpretations of the BOMD results. The emphases are on the effects of the $-\text{SO}_3\text{H}$ group on the H-bond structures, energetic and dynamics of proton transfer in the adjacent Zundel complex, as well as the tendency of protonation and deprotonation at the $-\text{SO}_3\text{H}$ group.

Static results

Equilibrium structures, energetic and IR spectra. The equilibrium structures, ΔE , ΔE^{sol} and $R_{\text{O} \cdots \text{O}}$ of the $\text{CF}_3\text{SO}_3\text{H-H}_3\text{O}^+-n\text{H}_2\text{O}$ complexes, $1 \leq n \leq 3$, in the gas phase and continuum aqueous solution are shown in Table 1, together with Δd_{DA} and ν^{OH} . The trends of ΔE and ΔE^{sol} with respect to the number of water molecules are presented in Fig. 1.

It appeared that the refined structures are the same as those obtained from B3LYP/6-31G(d,p) calculations.⁸ The trends of ΔE with respect to the number of water molecules in the gas phase and continuum aqueous solution are similar, with smaller variations in continuum aqueous solution. The destabilization effects caused by the continuum aqueous solvent are quite large, ranging from 120 kJ mol^{-1} in the $\text{CF}_3\text{SO}_3\text{H-H}_3\text{O}^+$ complex to 235 kJ mol^{-1} in the $\text{CF}_3\text{SO}_3\text{H-H}_3\text{O}^+-3\text{H}_2\text{O}$ complex; for the H-bond complexes with the same number of water molecules, the H-bonds inside the clusters experience comparable uniform electric field (COSMO). Fig. 1 also revealed that ΔE^{sol} are not substantially different. The environmental effects on the stabilities of charged H-bonds were investigated using *ab initio* SCRF (self-consistent reaction field) calculations at the Hartree-Fock level, from which the dependence of ΔE on a wide range of dielectric constant (ϵ) was established.⁵² It was demonstrated that small increases in ϵ from the gas-phase value ($\epsilon = 1$) rapidly reduce the stabilities of the charged H-bonds, which is in accordance with the present results.

The results in Table 1 anticipated three $\text{CF}_3\text{SO}_3\text{H-H}_3\text{O}^+-\text{H}_2\text{O}$ complexes as the most basic intermediate states in proton transfer pathways.

Table 1 Static results of the $\text{CF}_3\text{SO}_3\text{H}\cdot\text{H}_3\text{O}^+\cdot n\text{H}_2\text{O}$ complexes, $n = 1-3$, obtained from B3LYP/TZVP calculations. Energies, distances and IR frequencies are in kJ mol^{-1} , Å and cm^{-1} , respectively

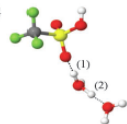
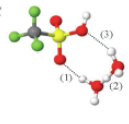
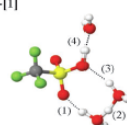
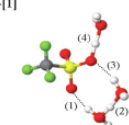
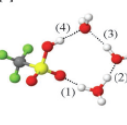
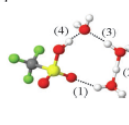
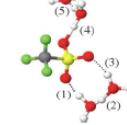
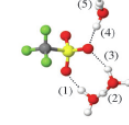
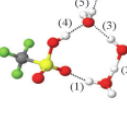
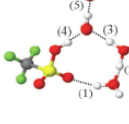
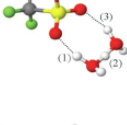
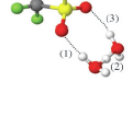
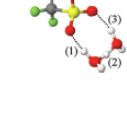
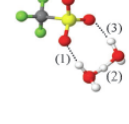
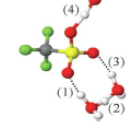
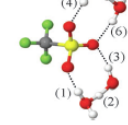
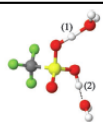
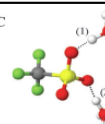
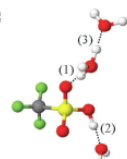
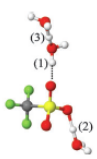
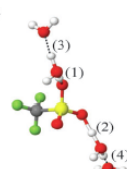
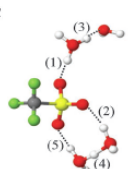
Gas	COSMO	ΔE	ΔE^{sol}	H-bond	$R_{\text{O}\cdots\text{O}}$	Δd_{DA}	ν^{OH}
A1G 	A1C 	−241.7 (−63.5)	−272.3	(1) (2) (3)	2.55 (2.75) 2.47 (2.43) — (3.05)	0.52 (0.83) 0.36 (0.20)* — (1.26)	2788 (3347) 2218(1223)* — (3577)
A2G-[1] 	A2C-[1] 	−316.9 (−109.0)	−276.3	(1) (2) (3) (4)	2.59 (2.72) 2.44 (2.43) 2.89 (2.96) 2.54 (2.41)	0.62 (0.79) 0.27* (0.21)* 1.01 (1.09) 0.47 (0.06)*	3029 (3320) 1893* (1230)* 3490 (3525) 2498 (905)*
A2G-[2] 	A2C-[2] 	−308.0 (−115.6)	−291.9	(1) (2) (3) (4)	2.54 (2.69) 2.45 (2.41) 2.85 (2.79) 2.79 (2.57)	0.56 (0.84) 0.30 (0.07)* 0.90 (0.84) 0.83 (0.51)	2873 (3422) 1985 (823)* 3396 (3292) 3233 (2509)
A3G-[1] 	A3C-[1] 	−398.3 (−155.6)	−275.3	(1) (2) (3) (4) (5)	2.54 (2.63) 2.44 (2.44) 2.74 (2.86) 2.43 (2.62) 2.54 (2.44)	0.50 (0.66) 0.27* (0.25)* 0.84 (0.96) 0.27* (0.61) 0.48 (0.26)*	2645(3071) 1848* (1345)* 3353 (3449) 1877* (2876) 2659 (1735)*
A3G-[2] 	A3C-[2] 	−380.3 (−146.1)	−283.8	(1) (2) (3) (4) (5)	2.56 (2.81) 2.43 (2.44) 2.73 (2.62) 2.70 (2.56) 2.65 (2.60)	0.58 (0.90) 0.21* (0.24)* 0.75 (0.61) 0.71 (0.48) 0.65 (0.58)	2940 (3460) 1335* (1374)* 3211 (2910) 2997 (2373) 3077 (2731)
B1G 	B1C 	−239.8 (−60.4)	−271.1	(1) (2) (3)	2.70 (2.81) 2.42 (2.43) 2.80 (3.01)	0.76 (0.93) 0.14* (0.18)* 0.96 (1.16)	3239 (3439) 1100* (1134)* 3454 (3537)
B2G 	B2C 	−327.6 (−117.0)	−273.6	(1) (2) (3) (4)	2.62 (2.69) 2.43 (2.43) 2.80 (2.81) 2.53 (2.45)	0.65 (0.73) 0.20* (0.17)* 0.91 (0.91) 0.45 (0.30)*	3026 (3163) 1333* (1068)* 3422 (3417) 2434 (1843)*
B3G 	B3C 	−398.7 (−162.9)	−282.2	(1) (2) (3) (4) (5) (6)	2.55 (2.65) 2.44 (2.43) 2.74 (2.81) 2.43 (2.66) 2.54 (2.43) — (2.81)	0.51 (0.68) 0.25* (0.22)* 0.83 (0.91) 0.26* (0.69) 0.50 (0.21)* — (0.90)	2691 (3085) 1407* (1276)* 3334 (3416) 1526* (3109) 2679 (1221)* — (3399)

Table 1 (continued)

Gas	COSMO	ΔE	ΔE^{sol}	H-bond	$R_{\text{O-O}}$	Δd_{DA}	ν^{OH}
C1G 	C1C 	-225.5 (-59.7)	-284.7	(1) (2)	2.44 (2.47) 2.49 (2.46)	0.23* (0.33) 0.37 (0.35)	1724* (1970) 2196 (2076)
C2G 	C2C 	-323.8 (-111.7)	-272.1	(1) (2) (3)	2.49 (2.61) 2.55 (2.43) 2.50 (2.45)	0.41 (0.61) 0.49 (0.21)* 0.42 (0.27)*	2324 (2967) 2599 (1413)* 2516 (1717)*
C3G 	C3C 	-387.1 (-159.7)	-290.6	(1) (2) (3) (4) (5)	2.44 (2.59) 2.43 (2.65) 2.55 (2.45) 2.55 (2.43) — (2.78)	0.24* (0.57) 0.22* (0.66) 0.51 (0.29)* 0.52 (0.20)* — (0.88)	1809* (2876) 1708* (3032) 2715 (1805)* 2760 (1201)* — (3390)

ΔE = interaction energy; ΔE^{sol} = solution energy; $R_{\text{O-O}}$ = H-bond distance; Δd_{DA} = asymmetric stretching coordinate; ν^{OH} = asymmetric frequency; (..) = continuum aqueous solution (COSMO); * = H-bond susceptible to proton transfer.

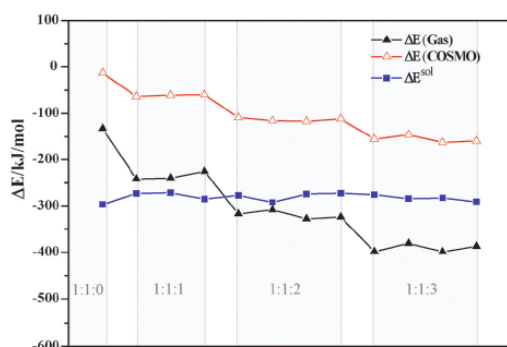
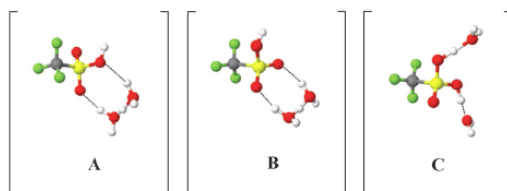


Fig. 1 The trends of the interaction (ΔE) and solvation energies (ΔE^{sol}) with respect to the number of water molecules, obtained from B3LYP/TZVP calculations: \blacktriangle = ΔE in the gas phase; \triangle = ΔE in continuum aqueous solution; \blacksquare = ΔE^{sol} .



Structures A and B are represented by the Zundel complex H-bonding at two oxygen atoms of the $-\text{SO}_3\text{H}$ group. In structure C, $-\text{SO}_3\text{H}$ separates H_3O^+ and H_2O . The H-bonding

features in structures A, B and C suggested two important structural diffusion mechanisms at the $-\text{SO}_3\text{H}$ group. Since the $-\text{SO}_3\text{H}$ group in structure C could be protonated or deprotonated and directly involved in proton transfer, one could regard the structural diffusion through structure C as the “pass-through” mechanism. Likewise, since the energetic and dynamics of the proton in the Zundel complex can be affected by the $-\text{SO}_3\text{H}$ group, one could consider the proton transfer through structures A and B as the “pass-by” mechanism.

In order to simplify the discussion, the H-bond structures in Table 1 are labeled with a three or four-character code; according to the basic intermediate states (A, B or C); the number of water molecules (n); in the gas phase (G) or continuum aqueous solution (C). Different H-bond structures with the same basic intermediate state and number of water molecule are distinguished by $[m]$. As examples, based on the four-character code, A2G-[1] and A2G-[2] represent different H-bond structures ([1] and [2]) with the same intermediate state and number of water molecules (A2) in the gas phase (G), whereas A2G-[1] and A2C-[1], the same H-bond structure with two water molecules (A2 and [1]) in the gas phase (G) and continuum aqueous solution (C), respectively.

Attempt was made to distinguish between normal and strong H-bonds in the protonated water clusters.¹⁹ B3LYP/TZVP calculations showed that the “critical distance” ($R_{\text{O-O}}^*$), the H-bond distance at which symmetric double-well potential with a barrier at the center is transformed into single-well potential without barrier, and the threshold asymmetric O-H stretching frequencies for proton transfers ($\nu^{\text{OH}*}$) could be

approximated from the plots of Δd_{DA} and $R_{\text{O-O}}$, ν^{OH} and $R_{\text{O-O}}$, and ν^{OH} and Δd_{DA} . The relationship between Δd_{DA} and $R_{\text{O-O}}$ could be represented by a linear function, ν^{OH} and $R_{\text{O-O}}$ by an exponential function similar to the integrated rate expression for the first order reaction, and ν^{OH} and Δd_{DA} by an exponential function resembling the normal distribution function. For the protonated water clusters,¹⁹ calculations of the second derivatives of the plots of ν^{OH} and Δd_{DA} gave two inflection points, in the gas phase at $\Delta d_{\text{DA}}^* = 0.33 \text{ \AA}$ and in continuum aqueous solution at $\Delta d_{\text{DA}}^* = 0.36 \text{ \AA}$. The values correspond to $\nu^{\text{OH}*} = 1984$ and 1881 cm^{-1} , respectively.

In the present study, to estimate $\nu^{\text{OH}*}$, Δd_{DA} and $R_{\text{O-O}}$, ν^{OH} and $R_{\text{O-O}}$ and ν^{OH} and Δd_{DA} for the pass-through mechanism were plotted and shown in Fig. 2a–c, respectively, whereas for the pass-by mechanism in Fig. 2d–f, respectively. The agreements between the fitted functions and the values obtained from B3LYP/TZVP calculations are shown in Fig. 2. For the pass-through mechanism in the gas phase, the inflection point is seen in Fig. 2c at $\nu^{\text{OH}*} = 2162 \text{ cm}^{-1}$ and $\Delta d_{\text{DA}}^* = 0.36 \text{ \AA}$, and in continuum aqueous solution at $\nu^{\text{OH}*} = 2001 \text{ cm}^{-1}$ and $\Delta d_{\text{DA}}^* = 0.36 \text{ \AA}$. For the pass-by mechanism, Fig. 2f shows the inflection points in the gas phase at $\nu^{\text{OH}*} = 1829 \text{ cm}^{-1}$ and $\Delta d_{\text{DA}}^* = 0.29 \text{ \AA}$, and in continuum aqueous solution at $\nu^{\text{OH}*} = 1714 \text{ cm}^{-1}$ and $\Delta d_{\text{DA}}^* = 0.30 \text{ \AA}$. Comparison of $\nu^{\text{OH}*}$ for the pass-by mechanism and those of the protonated water clusters¹⁹ suggested red-shifts of about 200 cm^{-1} due to the presence of the $-\text{SO}_3\text{H}$ group. It should be emphasized that the present work focused only on the asymmetric O–H stretching frequencies (ν^{OH}) which are directly related to the proton transfer processes. As ν^{OH} cannot be identified accurately in IR experiments, rigorous comparison cannot be made. One could however conclude that the asymmetric O–H stretching frequencies of the transferring protons in Table 1 are in good agreement with experiments.^{13,17}

Although the H-bond structures in the gas phase and continuum aqueous solution are approximately the same, the trends of proton transfers are quite different. Δd_{DA} and ν^{OH} in Table 1 revealed that the $-\text{SO}_3\text{H}$ group is not preferentially dissociated in the gas phase, whereas in continuum aqueous solution, $-\text{SO}_3\text{H}$ tends to deprotonate, resulting in $-\text{SO}_3^-$ in close contact with H_3O^+ , with the highest tendency of proton dissociation in structure A2C-[1] ($\Delta d_{\text{DA}} = 0.06 \text{ \AA}$ and $\nu^{\text{OH}} = 905 \text{ cm}^{-1}$). Δd_{DA} and ν^{OH} also indicated that, in continuum aqueous solution, structure A2C-[2] possesses the highest tendency of proton transfer through the pass-by mechanism ($\Delta d_{\text{DA}} = 0.07 \text{ \AA}$ and $\nu^{\text{OH}} = 823 \text{ cm}^{-1}$).

As in the case of IR experiments,^{10–12} Table 1 showed that ν^{OH} can vary in a quite wide range; in the gas phase from 1100 to 3500 cm^{-1} , in continuum aqueous solution from 820 to 3600 cm^{-1} . To resolve these broad IR bands, the H-bonds in Table 1 were divided into two groups; the H-bonds connecting directly to the $-\text{SO}_3\text{H}$ or $-\text{SO}_3^-$ group belong to **Group 1** (potentially involved in the protonation or deprotonation at the $-\text{SO}_3\text{H}$ group, as well as the pass-through mechanism) and the H-bonds in the adjacent $\text{H}_3\text{O}^+-\text{H}_2\text{O}$ or Zundel complex to **Group 2** (potentially involved in the pass-by mechanism). Investigation of the H-bond structures in Table 1 in details, allowed **Group 1** and **2** to be further

divided into four subgroups. The definitions of the groups and subgroups are summarized as follows:

Group 1: H-bonds connecting directly to the $-\text{SO}_3\text{H}$ or $-\text{SO}_3^-$ group.

Subgroup (I): Cyclic H-bonds between the Zundel complex or H_7O_3^+ and the two oxygen atoms of $-\text{SO}_3\text{H}$ or $-\text{SO}_3^-$, e.g. H-bonds (1) and (3) in structures A1C and B1C, and H-bonds (1) and (4) in structures A2G[2] and A2C[2].

Subgroup (II): Linear H-bond between an oxygen atom of the $-\text{SO}_3\text{H}$ or $-\text{SO}_3^-$ group and H_3O^+ , H_5O_2^+ or H_2O , e.g. H-bonds (1) and (2) in structures C1C and C2C, as well as H-bond (1) in structure C3C.

Group 2: H-bonds in the adjacent Zundel complex.

Subgroup (III): H-bond in the $\text{H}_3\text{O}^+-\text{H}_2\text{O}$ contact structure or the Zundel complex in the structure with Subgroup (II), e.g. H-bond (3) in structure C2G and C2C, respectively.

Subgroup (IV): H-bond of the Zundel complex in the structure with Subgroup (I), e.g. H-bond (2) in structures A1C and B1C.

The domains of ν^{OH} for the H-bond protons in **Group 1** (Subgroup (I) and (II)) and **Group 2** (Subgroup (III) to (IV)), in the gas phase and continuum aqueous solution, are shown in Fig. 3. Comparison of Fig. 3a and b revealed that the electric field introduced by the continuum aqueous solvent brings about significant shifts of ν^{OH} , especially for the pass-by mechanism, in which all the H-bonds in Subgroup (IV) are red shifted to ν^{OH} lower than $\nu^{\text{OH}*}$. For the pass-through mechanism, only some linear H-bonds in Subgroup (II) are red shifted to ν^{OH} lower than $\nu^{\text{OH}*}$. The cyclic H-bonds between the two oxygen atoms of $-\text{SO}_3\text{H}$ and the Zundel complex (Subgroup (I)) tend to be destabilized in continuum aqueous solution, leading to blue shifts of ν^{OH} above 3000 cm^{-1} . The red shifts reflect higher tendency for the deprotonation of the $-\text{SO}_3\text{H}$ group, as well as the pass-through mechanism, in continuum aqueous solution.

Dynamic results

In the present work, the neglect of extensive H-bond networks of water in the vicinities of the solute ($\text{CF}_3\text{SO}_3\text{H}$), as well as the thermal energy fluctuations in BOMD simulations, made it difficult to analyze the dynamics in the $\text{CF}_3\text{SO}_3\text{H}-\text{H}_3\text{O}^+-\text{H}_2\text{O}$ complexes. Therefore, attention was focused on the H-bond protons in the intermediate states.

Average H-bond structures and IR spectra. Before the dynamics in the $\text{CF}_3\text{SO}_3\text{H}-\text{H}_3\text{O}^+-\text{H}_2\text{O}$ complexes are discussed, the characteristic vibrations in the protonated water clusters will be analyzed.¹⁹ The IR spectra of the H-bond proton in the Zundel complex obtained from BOMD simulations at 350 K are given in Fig. 4a and b, in the gas phase and continuum aqueous solution, respectively. For the transferring proton ($\nu^{\text{OH}} < \nu^{\text{OH}*}$), the static proton transfer potential (B3LYP/TZVP calculations) predicted only one asymmetric O–H stretching band, whereas BOMD simulations showed in addition a higher frequency band. The two IR bands are labeled with A and B in Fig. 4a and b. Since the lower frequency band (at $\nu_{\text{A}}^{\text{OH,MD}}$) could be associated with the oscillatory shuttling motion and the higher frequency band

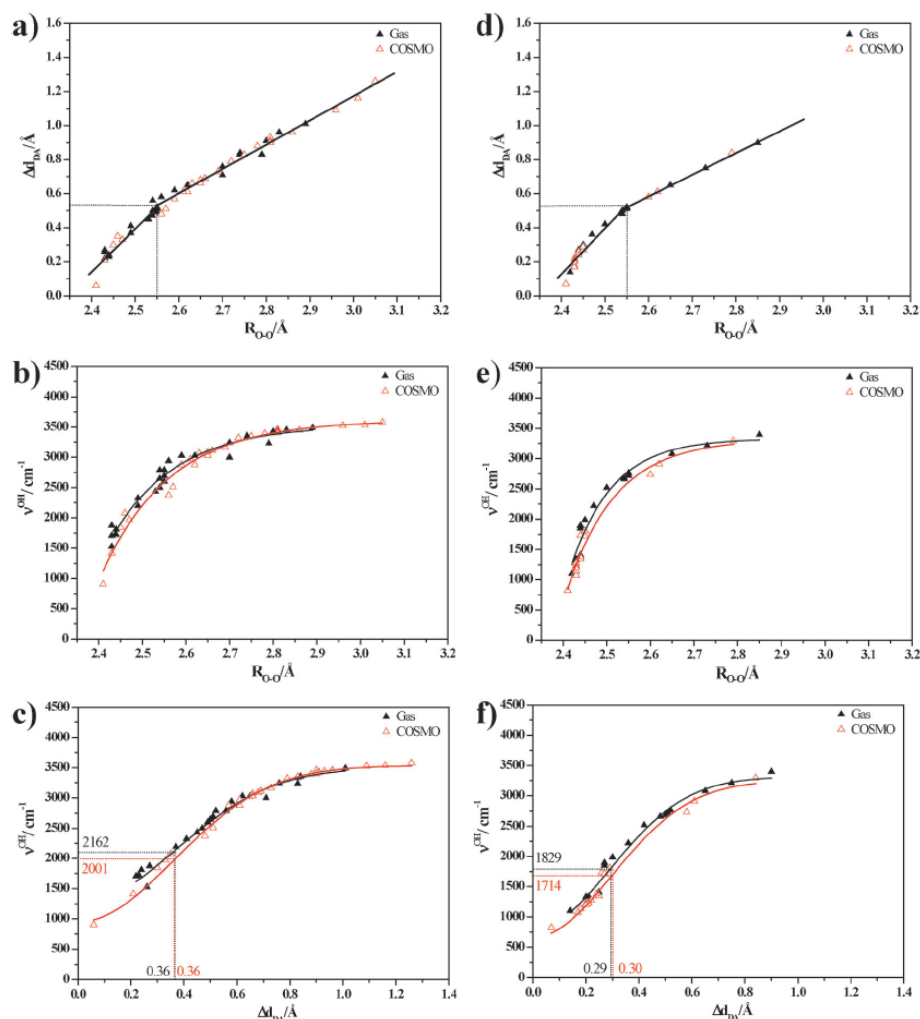


Fig. 2 Static results of the $\text{CF}_3\text{SO}_3\text{H}-\text{H}_3\text{O}^+-\text{H}_2\text{O}$ complexes obtained from B3LYP/TZVP calculations in the gas phase and continuum aqueous solution. (a) Plot of Δd_{DA} and $R_{\text{O-O}}$ for the pass-through mechanism. (b) Plot of ν^{OH} and $R_{\text{O-O}}$ for the pass-through mechanism. (c) Plot of ν^{OH} and Δd_{DA} for the pass-through mechanism. (d) Plot of Δd_{DA} and $R_{\text{O-O}}$ for the pass-by mechanism. (e) Plot of ν^{OH} and $R_{\text{O-O}}$ for the pass-by mechanism. (f) Plot of ν^{OH} and Δd_{DA} for the pass-by mechanism. (Δd_{DA} = asymmetric stretching coordinate; $R_{\text{O-O}}$ = O-H...O H-bond distance; ν^{OH} = asymmetric O-H stretching frequency).

(at $\nu_{\text{B}}^{\text{OH,MD}}$) with the structural diffusion motion,¹⁹ the vibrational energy for the interconversion between the two dynamic states ($\Delta\nu_{\text{BA}}^{\text{OH,MD}}$) can be approximated from the difference between $\nu_{\text{B}}^{\text{OH,MD}}$ and $\nu_{\text{A}}^{\text{OH,MD}}$, and the relative probability of finding these characteristic vibrations in the course of BOMD simulations could be estimated from the ratio of the IR intensities at B (I_{B}) and A (I_{A});¹⁹ the lower $I_{\text{B}}/I_{\text{A}}$ the higher the relative probability of finding the oscillatory shuttling motion. It should be noted that the discussion on $\Delta\nu_{\text{BA}}^{\text{OH,MD}}$ and $I_{\text{B}}/I_{\text{A}}$ is meaningful only when the H-bond considered is susceptible to proton transfer, $\nu_{\text{A}}^{\text{OH,MD}} < \nu_{\text{A}}^{\text{OH}^+, \text{MD}}$.

The intensities of the IR bands at A and B in Fig. 4a and b showed that the oscillatory shuttling motion dominates in the Zundel complex, especially in continuum aqueous solution; in the gas phase, $I_{\text{B}}/I_{\text{A}} = 0.5$, whereas in continuum aqueous solution, $I_{\text{B}}/I_{\text{A}} = 0.1$. The trend of $I_{\text{B}}/I_{\text{A}}$ in the gas phase and continuum aqueous solution can be explained using $\Delta\nu_{\text{BA}}^{\text{OH,MD}}$; in the gas phase, $\Delta\nu_{\text{BA}}^{\text{OH,MD}} = 724 \text{ cm}^{-1}$, and in continuum aqueous solution, $\Delta\nu_{\text{BA}}^{\text{OH,MD}} = 808 \text{ cm}^{-1}$. The latter reflects a higher vibrational energy for the interconversion between the oscillatory shuttling and structural diffusion motions, resulting in a higher population of the oscillatory shuttling motion for the Zundel complex in continuum aqueous solution. It should

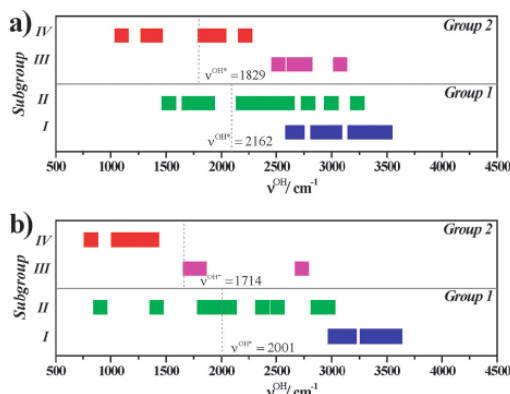


Fig. 3 The domains of ν^{OH} for the H-bond protons in Group 1 and 2, as well as Subgroup (I) to (IV). (a) gas phase. (b) continuum aqueous solution.

be noted that, due to a short BOMD simulation length, $I_{\text{B}}/I_{\text{A}}$ may not be determined precisely. Therefore, attempt was made to alternatively estimate the relative population of the oscillatory shuttling and structural diffusion motions from $\Delta\nu_{\text{BA}}^{\text{OH,MD}}$. For the protonated water clusters, an interesting relationship was observed when $\Delta\nu_{\text{BA}}^{\text{OH,MD}}$ and $\langle\Delta d_{\text{DA}}\rangle$ were plotted. Together with the plot of the standard deviations of the O–H distances ($\sigma_{\text{R}_{\text{O-H}}}$) and $\langle\Delta d_{\text{DA}}\rangle$, energetic aspects of the two characteristic vibrations in the protonated water cluster could be studied.

The plots of $\sigma_{\text{R}_{\text{O-H}}}$ and $\langle\Delta d_{\text{DA}}\rangle$ and $\Delta\nu_{\text{BA}}^{\text{OH,MD}}$ and $\langle\Delta d_{\text{DA}}\rangle$ are shown in Fig. 4c and d, respectively. The former could be represented by an exponential decay function, whereas the latter by a reflected normal distribution function. Due to the thermal energy fluctuations and dynamics, $\sigma_{\text{R}_{\text{O-H}}}$ as well as $\Delta\nu_{\text{BA}}^{\text{OH,MD}}$ in the gas phase and continuum aqueous solution are not well separated. Therefore, the discussion on the relative population of the oscillatory shuttling and structural diffusion motions will be made based on a combined data set. It appeared that, for the protonated water clusters, $\sigma_{\text{R}_{\text{O-H}}}$ decreases exponentially with $\langle\Delta d_{\text{DA}}\rangle$, reflecting characteristics of the oscillatory shuttling and structural diffusion motions; the oscillatory shuttling motion dominates in the H-bond with small $\langle\Delta d_{\text{DA}}\rangle$. $\Delta\nu_{\text{BA}}^{\text{OH,MD}}$ decreases exponentially with $\langle\Delta d_{\text{DA}}\rangle$ and reaches a minimum at $\langle\Delta d_{\text{DA}}\rangle = 0.28 \text{ \AA}$ ($\langle R_{\text{O-O}}\rangle = 2.46 \text{ \AA}$), corresponding to the lowest vibrational energy for the inter-conversion between the oscillatory shuttling and the structural diffusion motions, $\Delta\nu_{\text{BA}}^{\text{OH,MD}} = 473 \text{ cm}^{-1}$ or 5.7 kJ mol^{-1} . Since the probability of finding a physical system in a certain energy state is proportional to the Boltzmann factor, the probability of finding the structural diffusion motion relative to the oscillatory shuttling motion ($P_{\text{B}}/P_{\text{A}}$) is proportional to $e^{-\Delta\nu_{\text{BA}}^{\text{OH,MD}}/RT}$. For the protonated water clusters, $P_{\text{B}}/P_{\text{A}}$ and $\langle\Delta d_{\text{DA}}\rangle$ is plotted and shown in Fig. 4e. $P_{\text{B}}/P_{\text{A}}$ could be expressed in terms of $\langle\Delta d_{\text{DA}}\rangle$ using a normal distribution function. The agreement between the fitted function and the values obtained from BOMD simulations is included in Fig. 4e. The fitted function suggested the maximum probability of finding the structural diffusion motion relative to the

oscillatory shuttling motion, $P_{\text{B}}/P_{\text{A}} = 0.17$ at $\langle\Delta d_{\text{DA}}\rangle = 0.27 \text{ \AA}$. At larger $\langle\Delta d_{\text{DA}}\rangle$, the H-bond becomes weaker and $P_{\text{B}}/P_{\text{A}}$ decreases, especially when $\nu_{\text{A}}^{\text{OH,MD}} > \nu_{\text{A}}^{\text{OH},\text{MD}}$.

For the $\text{CF}_3\text{SO}_3\text{H-H}_3\text{O}^+-\text{H}_2\text{O}$ complexes, the average H-bond structures, $\langle R_{\text{O-O}}\rangle$ and $\langle\Delta d_{\text{DA}}\rangle$, obtained from BOMD simulations at 350 K, are summarized in Table 2, together with, $\nu_{\text{A}}^{\text{OH,MD}}$, $\nu_{\text{B}}^{\text{OH,MD}}$ and the proton diffusion coefficients (D). The H-bonds susceptible to proton transfers are designated by asterisks. The plots between $\langle\Delta d_{\text{DA}}\rangle$ and $\langle R_{\text{O-O}}\rangle$, $\nu_{\text{A}}^{\text{OH,MD}}$ and $\langle R_{\text{O-O}}\rangle$, and $\nu_{\text{A}}^{\text{OH,MD}}$ and $\langle\Delta d_{\text{DA}}\rangle$ for the pass-through mechanism are shown in Fig. 5a–c, respectively, and for the pass-by mechanism in Fig. 5d–f, respectively. The same types of functions, as in the case of the B3LYP/TZVP calculations in Fig. 2, were employed to represent the relationships in Fig. 5. The agreements between the fitted functions and the values obtained from BOMD simulations are illustrated in Fig. 5.

Since BOMD simulations were conducted in a short time, the average H-bond structures are not substantially different from the B3LYP/TZVP results. Comparison of $\nu_{\text{A}}^{\text{OH,MD}}$ in Table 2 with ν^{OH} in Table 1 showed a general trend. The inclusion of the thermal energy fluctuations and dynamics in the model calculations brought about red shifts of the oscillatory shuttling bands both in the gas phase and continuum aqueous solution, except for structures A2C-[1] and A2C-[2] in continuum aqueous solution; B3LYP/TZVP calculations predicted the H-bonds (4) and (2) in structures A2C-[1] and A2C-[2] to possess the highest tendencies of proton transfer through the pass-through and pass-by mechanisms, respectively, and coupling among various modes of vibrations in BOMD simulations led to blue shifts of about 43 and 52 cm^{-1} , respectively.

As in the case of protonated water clusters, according to the thermal energy fluctuations and dynamics, the results in the gas phase and continuum aqueous solution are not well separated. Fig. 5 showed the inflection points for the pass-through mechanism at $\nu_{\text{A}}^{\text{OH},\text{MD}} = 1656$ and 1684 cm^{-1} , respectively, and for the pass-by mechanism at $\nu_{\text{A}}^{\text{OH},\text{MD}} = 1733$ and 1741 cm^{-1} , respectively. The latter are 290 and 104 cm^{-1} lower than the corresponding values for the protonated water clusters.¹⁹ The red shifts represent energetic evidences for the promotion of proton transfer by the $-\text{SO}_3\text{H}$ group.

$\Delta\nu_{\text{BA}}^{\text{OH,MD}}$ and $P_{\text{B}}/P_{\text{A}}$ for the H-bond protons in the $\text{CF}_3\text{SO}_3\text{H-H}_3\text{O}^+-\text{H}_2\text{O}$ complexes are included in Table 2. Examples of the characteristic asymmetric O–H stretching bands for the pass-through and pass-by mechanisms, obtained from BOMD simulations at 350 K, are shown in Fig. 6a and e, respectively. For the pass-through mechanism, the plots of $\sigma_{\text{R}_{\text{O-H}}}$ and $\langle\Delta d_{\text{DA}}\rangle$, $\Delta\nu_{\text{BA}}^{\text{OH,MD}}$ and $\langle\Delta d_{\text{DA}}\rangle$, and $P_{\text{B}}/P_{\text{A}}$ and $\langle\Delta d_{\text{DA}}\rangle$ are illustrated in Fig. 6b to d, respectively, and for the pass-by mechanism in Fig. 6f to h, respectively.

All the outstanding features discussed in the protonated water clusters were observed in the $\text{CF}_3\text{SO}_3\text{H-H}_3\text{O}^+-\text{H}_2\text{O}$ complexes. The same types of functions, as in the case of the protonated water clusters in Fig. 4, represent the relationships in Fig. 6 quite well. For the pass-through mechanism, $\Delta\nu_{\text{BA}}^{\text{OH,MD}}$ in Fig. 6c decreases exponentially with $\langle\Delta d_{\text{DA}}\rangle$ and reaches a minimum at $\Delta\nu_{\text{BA}}^{\text{OH,MD}} = 469 \text{ cm}^{-1}$, corresponding to the

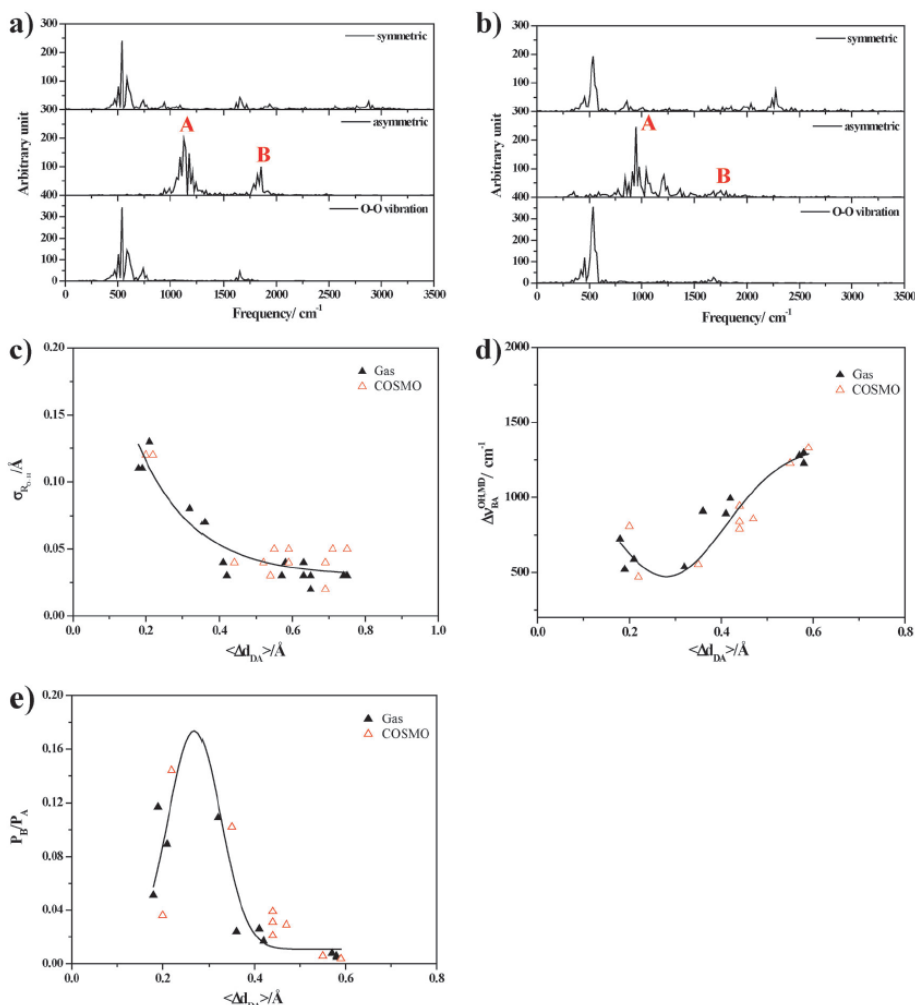


Fig. 4 BOMD results on the Zundel complex at 350 K. (a)–(b) IR spectra of the transferring proton in the gas phase and continuum aqueous solution, respectively.¹⁹ (c) Plot of $\sigma_{R_{O-H}}$ and $\langle\Delta d_{DA}\rangle$. (d) Plot of $\Delta\nu_{BA}^{OH,MD}$ and $\langle\Delta d_{DA}\rangle$. (e) Plot of P_B/P_A and $\langle\Delta d_{DA}\rangle$. $\sigma_{R_{O-H}}$ = standard deviations of the O–H distances; $\langle\Delta d_{DA}\rangle$ = average asymmetric stretching coordinate; P_B/P_A = probability of finding the structural diffusion motion relative to the oscillatory shuttling motion.

maximum probability of finding the structural diffusion motion (P_B/P_A) of 0.17; the H-bonds in the vicinities of the maximum are, for example, H-bond (1) in structures C1G and C1C, and H-bond (2) in structure C2G. For the pass-by mechanism, due to the presence of the $-\text{SO}_3\text{H}$ group, the vibrational energy for the interconversion between the oscillatory shuttling and the structural diffusion motions are decreased, from $\Delta\nu_{BA}^{OH,MD} = 473 \text{ cm}^{-1}$ in the protonated water clusters to $\Delta\nu_{BA}^{OH,MD} = 398 \text{ cm}^{-1}$ in the $\text{CF}_3\text{SO}_3\text{H}-\text{H}_3\text{O}^+-\text{H}_2\text{O}$ complexes. The values correspond to an increase in the relative probability of finding the structural diffusion motion, from $P_B/P_A = 0.17$ in the protonated water clusters to 0.21 in the $\text{CF}_3\text{SO}_3\text{H}-\text{H}_3\text{O}^+-\text{H}_2\text{O}$ complexes. The H-bonds in the vicinities of maximum P_B/P_A are, for examples, H-bond

(3) in structures C2C and C3C, and H-bond (5) in structure A3G-[1].

Dynamics of proton transfer and diffusion coefficients. To discuss the dynamics of proton transfer in the $\text{CF}_3\text{SO}_3\text{H}-\text{H}_3\text{O}^+-\text{H}_2\text{O}$ complexes, the distributions of the proton diffusion coefficients (D) for the H-bonds susceptible to proton transfer ($\nu_A^{OH,MD} < \nu_A^{OH^+,MD}$) were computed and shown in Fig. 7. It appeared that D can vary in a quite wide range, with maxima at 2.5×10^{-5} and $3.2 \times 10^{-5} \text{ cm}^2 \text{ s}^{-1}$, in the gas phase and continuum aqueous solution, respectively; the latter is represented by the H-bonds in **Group 2** (pass-by mechanism) and could be used in the discussion of the effects of the $-\text{SO}_3\text{H}$ group, by comparison with the results in the

Table 2. Dynamic results of the $\text{CF}_3\text{SO}_3\text{H}-\text{H}_3\text{O}^+-n\text{H}_2\text{O}$ complexes, $n = 1-3$, obtained from BOMD simulations at 350 K. Distances, IR frequencies and proton diffusion coefficients are in Å, cm^{-1} and $\text{cm}^2 \text{s}^{-1}$ respectively

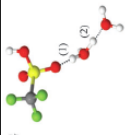
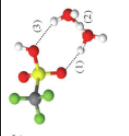
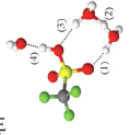
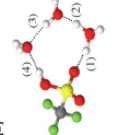
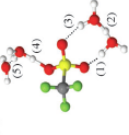
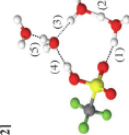
Gas	COSMO	H-bond	$\langle R_{\text{O-O}} \rangle$	$\sigma_{R_{\text{O-H}}}$	$\langle \Delta d_{\text{DA}} \rangle$	$\nu_{\text{A}}^{\text{OH,MD}}$	$\nu_{\text{B}}^{\text{OH,MD}}$	$\Delta \nu_{\text{BA}}^{\text{OH,MD}}$	$\mathbf{P}_{\text{B}}/\mathbf{P}_{\text{A}}$	D (10^{-5})
A1G			(1)	0.01 —	0.56 —	1750 —	2693 —	943 —	0.02 —	4.58 —
			(2)	0.03 (0.05)	0.36 (0.17)*	1515 (1043)*	2154 (1700)	673 (657)	0.06 (0.07)	2.48 (1.69)
			(3)	—	—	—	—	—	—	—
A2G-1[1]		(1)	2.6 (2.7)	0.02 (0.01)	0.65 (0.91)	1733 (1683)	2962 (3501)	1229 (1818)	0.01 (0.00)	5.06 (5.02)
		(2)	2.4 (2.4)	0.05 (0.08)	0.28* (0.21)*	1498* (959)*	2053 (1683)	555 (724)	0.10 (0.05)	2.45 (2.56)
		(3)	—	—	—	—	—	—	—	—
		(4)	2.5 (2.4)	0.02 (0.12)	0.55 (0.21)*	1818 (948)*	2693 (1717)	875 (769)	0.03 (0.04)	2.46 (2.67)
A2G-2[1]		(1)	2.5 —	0.02 —	0.58 —	1599 —	3046 —	1447 —	0.00 —	1.52 —
		(2)	2.5 (2.4)	0.08 (0.09)	0.26* (0.15)*	1531* (875)*	1969 (1834)	438 (959)	0.17 (0.02)	1.77 (2.91)
		(3)	— (2.8)	— (0.01)	— (0.94)	— (1666)	— (3366)	— (1700)	— (0.00)	— (7.42)
		(4)	— (2.6)	— (0.01)	— (0.54)	— (1296)	— (2592)	— (1296)	— (0.00)	— (2.91)
A3G-1[1]		(1)	2.5 (2.6)	0.02 (0.01)	0.53 (0.70)	1919 (1717)	2558 (3030)	639 (1313)	0.07 (0.00)	2.98 (3.01)
		(2)	2.4 (2.4)	0.06 (0.06)	0.27* (0.25)*	1363* (1313)*	1935 (1834)	572 (521)	0.10 (0.12)	1.65 (4.43)
		(3)	2.7 —	0.01 —	0.90 —	1548 —	3450 —	1902 —	0.00 —	2.51 —
		(4)	2.4 (2.6)	0.09 (0.01)	0.25* (0.66)	1010* (1515)	1750 (3080)	740 (1565)	0.05 (0.00)	4.38 (5.20)
		(5)	2.5 (2.4)	0.02 (0.07)	0.53 (0.26)*	1801 (1313)*	2727 (1733)	926 (420)	0.02 (0.18)	4.51 (3.29)
A3G-2[1]		(1)	2.6 —	0.02 —	0.64 —	1582 —	3013 —	1431 —	0.00 —	5.74 —
		(2)	2.4 (2.4)	0.08 (0.06)	0.20* (0.25)*	1094* (1397)*	1717 (1952)	623 (555)	0.08 (0.10)	2.00 (5.03)
		(3)	2.7 (2.6)	0.01 (0.01)	0.80 (0.66)	1801 (1599)	3349 (3063)	1548 (1464)	0.00 (0.00)	3.79 (6.17)
		(4)	2.7 (2.7)	0.01 (0.02)	0.75 (0.53)	1279 (1178)	3232 (2659)	1953 (1481)	0.00 (0.00)	3.59 (2.81)
		(5)	2.7 (2.6)	0.01 (0.01)	0.71 (0.64)	1885 (2323)	3299 (3046)	1414 (1060)	0.00 (0.01)	3.55 (4.10)

Table 2 (continued)

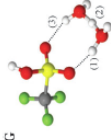
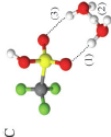
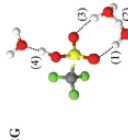
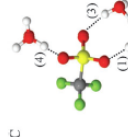
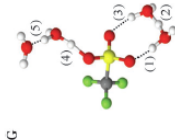
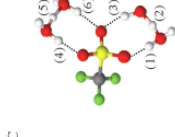
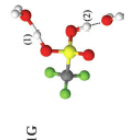
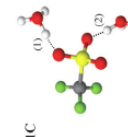
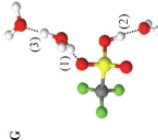
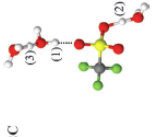
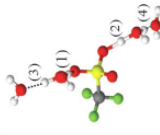
Gas	COSMO	H-bond	$\langle R_{O-O} \rangle$	$\sigma_{R_{O-H}}$	$\langle \Delta d_{DA} \rangle$	$\nu_A^{OH,MD}$	$\nu_B^{OH,MD}$	$\Delta\nu_{BA}^{OH,MD}$	P_B/P_A	D (10^{-5})
B1G			(1)	0.01	0.80	1599	3400	1801	0.00	3.48
			(2)	0.07 (0.07)	0.14* (0.16)*	1077* (993)*	1750 (1700)	673 (707)	0.06 (0.05)	2.18 (2.52)
			(3)	—	—	—	—	—	—	—
B2G			(1)	— (0.01)	— (0.79)	— (1666)	— (3400)	— (1734)	— (0.00)	— (3.32)
			(2)	0.08 (0.09)	0.20* (0.18)*	1066* (976)*	1868 (1700)	802 (724)	0.04 (0.03)	2.57 (2.12)
			(3)	—	—	—	—	—	—	—
			(4)	0.01 (0.12)	0.49 (0.28)*	1447 (1380)*	2609 (1902)	1162 (522)	0.01 (0.12)	1.17 (3.91)
B3G			(1)	0.02 (0.01)	0.54 (0.01)	1733 (1666)	2592 (3501)	859 (1835)	0.03 (0.00)	3.36 (4.32)
			(2)	0.07 (0.09)	0.26* (0.20)*	1313* (1077)*	1952 (1666)	639 (589)	0.07 (0.09)	3.27 (3.07)
			(3)	0.01 (0.01)	0.92 (1.00)	1565 (1548)	3484 (3535)	1919 (1987)	0.00 (0.00)	5.56 (2.64)
			(4)	0.09 (0.01)	0.22* (0.77)	976* (1599)	1751 (3282)	775 (1683)	0.04 (0.00)	2.20 (7.09)
			(5)	0.02 (0.08)	0.52 (0.20)*	1851 (1066)*	2760 (1717)	909 (651)	0.02 (0.07)	2.46 (4.58)
			(6)	—	—	—	—	—	—	—
C1G			(1)	0.06 (0.04)	0.26* (0.37)	1499* (1767)	2003 (2323)	504 (556)	0.13 (0.15)	1.33 (3.46)
			(2)	0.05 (0.08)	0.37 (0.33)	1902 (1851)	2306 (2356)	404 (505)	0.19 (0.13)	1.46 (3.15)
C2G			(1)	0.02	0.44	2272	2592	320	0.18	1.91
			(2)	0.02 (0.13)	0.52 (0.24)*	1582 (1161)*	2592 (2070)	1010 (909)	0.06 (0.02)	2.27 (3.15)
			(3)	0.04 (0.07)	0.43 (0.27)*	2171 (1414)*	2525 (1750)	556 (336)	0.10 (0.25)	3.65 (3.01)

Table 2 (continued)

Gas	COSMO	H-bond	$\langle R_{O-H} \rangle$	$\sigma_{R_{O-H}}$	$\langle \Delta \nu_{DA} \rangle$	$\nu_{A}^{OH,MD}$	$\nu_{B}^{OH,MD}$	$\Delta \nu_{BA}^{OH,MD}$	P_B/P_A	D (10^{-5})
C3G		(1)	2.4 (2.6)	0.11 (0.01)	0.26* (0.63)	1228* (1868)	1868 (3063)	640 (1195)	0.07 (0.01)	2.74 (4.39)
		(2)	2.4 (2.7)	0.11 (0.01)	0.22* (0.73)	1117* (1834)	2003 (3181)	886 (1347)	0.03 (0.00)	3.05 (6.82)
		(3)	— (2.5)	— (0.04)	— (0.30)*	— (1498)*	— (1868)	— (370)	— (0.22)	— (3.07)
		(4)	2.6 (2.4)	0.02 (0.08)	0.57 (0.19)*	1548 (1127)*	2895 (1700)	1347 (573)	0.00 (0.09)	4.25 (4.24)
		(5)	—	—	—	—	—	—	—	—

$\langle R_{O-H} \rangle$ = average H-bond distance; $\sigma_{R_{O-H}}$ = standard deviation of the O-H distance; $\langle \Delta \nu_{DA} \rangle$ = average asymmetric stretching coordinate; $\nu_A^{OH,MD}$ and $\nu_B^{OH,MD}$ = asymmetric O-H stretching frequencies; $\Delta \nu_{BA}^{OH,MD}$ = vibrational energy for the interconversion between the oscillatory shuttling and structural diffusion motions; P_B/P_A = relative probability of finding the oscillatory shuttling motion; D = proton diffusion coefficient; (.) = continuum aqueous solution (COSMO); * = H-bond susceptible to proton transfer.

protonated water clusters.¹⁹ It should be noted that the proton diffusion coefficients computed in the present work are comparable with the self-diffusion coefficient of liquid water ($2.3 \times 10^{-5} \text{ cm}^2 \text{ s}^{-1}$), but considerably lower than those in the protonated water clusters.^{19,53}

In order to obtain additional kinetics information from BOMD simulations, the lifetimes (τ) of the H-bonds with high relative probability of finding the structural diffusion motion (P_B/P_A) were computed from VACF of the O-O vibrations,⁴⁹ based on the observation that the relaxation behavior of the envelope of VACF can be approximated by an exponential function and the shared-proton structures possess shorter lifetimes than the contact structures ($\text{O-H}^+ \cdots \text{O}$).⁴⁶ The classical first-order rate constants (k) for the interconversion between these two limiting structures were approximated from the lifetimes. In the present study, the lifetimes of H-bond (1) in structure C1C and H-bond (3) in structure C2C are given as examples; $\tau = 90$ and 114 fs, respectively, and corresponding to $k = 15.4$ and 12.1 ps^{-1} , respectively. The lifetimes are shorter and the first-order rate constants are larger than those obtained for the protonated water cluster;¹⁹ in continuum aqueous solution, the shared-proton structure with the highest P_B/P_A possesses $\tau = 233$ fs and $k = 6.0 \text{ ps}^{-1}$. The values reflected a higher rate for the interconversion between the shared-proton and contact structures in the presence of the $-\text{SO}_3\text{H}$ group.

Remarks should be made on the dynamics and kinetics in the presence of the $-\text{SO}_3\text{H}$ group. Comparison of the most probable proton diffusion coefficient in the $\text{CF}_3\text{SO}_3\text{H-H}_3\text{O}^+-\text{H}_2\text{O}$ complexes ($D = 3.2 \times 10^{-5} \text{ cm}^2 \text{ s}^{-1}$, in continuum aqueous solution) and the corresponding value in the protonated water clusters¹⁹ leads to an important conclusion; the transferring proton in the protonated water cluster with an extended H-bond network possesses $D = 8.9 \times 10^{-5}$ and $8.2 \times 10^{-5} \text{ cm}^2 \text{ s}^{-1}$, in the gas phase and continuum aqueous solution, respectively. The values suggested that the $-\text{SO}_3\text{H}$ group suppresses the mobility of the transferring proton in the intermediate state, which could be explained by an increase of the electrostatic effect in the shared-proton structure. This results in lower proton diffusion coefficients in the $\text{CF}_3\text{SO}_3\text{H-H}_3\text{O}^+-\text{H}_2\text{O}$ complexes compared to the protonated water clusters. The increase of the electrostatic effect is accompanied by a decrease of $\Delta \nu_{BA}^{OH,MD}$ and an increase in the relative probability of finding the structural diffusion motion (P_B/P_A) in the shared-proton structure, leading eventually to higher first-order rate constants (k) in the $\text{CF}_3\text{SO}_3\text{H-H}_3\text{O}^+-\text{H}_2\text{O}$ complexes. One could therefore conclude that the $-\text{SO}_3\text{H}$ groups in Nafion[®] act as active binding sites which provide appropriate structural, energetic and dynamic conditions for effective structural diffusion processes in the intermediate states of proton transfer reactions.

4. Conclusion

Proton transfer reactions and dynamics at a hydrophilic group of Nafion[®] were investigated at low hydration levels using the complexes formed from $\text{CF}_3\text{SO}_3\text{H}$, H_3O^+ and $n\text{H}_2\text{O}$, $1 \leq n \leq 3$, as model systems. The theoretical investigations began with calculations of the equilibrium structures and interaction energies of the model systems in the gas phase and continuum

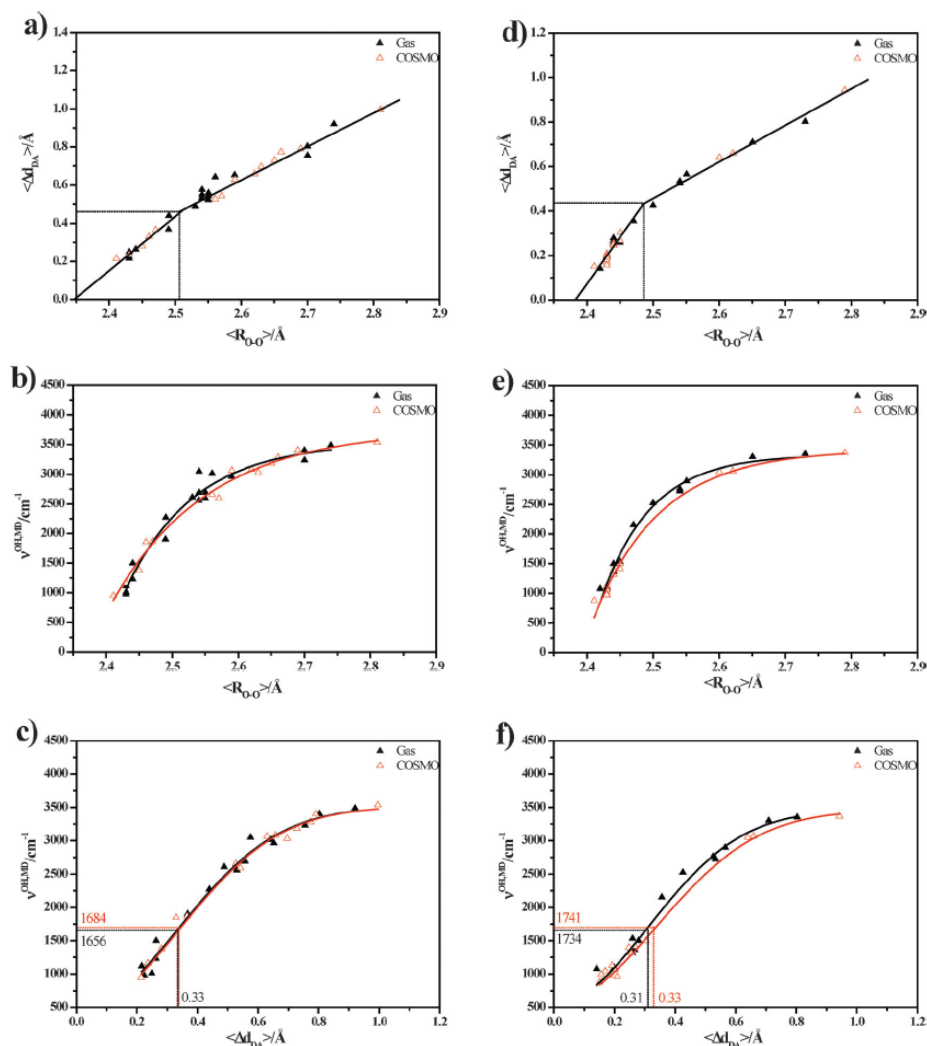


Fig. 5 The BOMD results on the $\text{CF}_3\text{SO}_3\text{H}-\text{H}_3\text{O}^+-\text{H}_2\text{O}$ complexes at 350 K. (a) Plot of $\langle \Delta d_{DA} \rangle$ and $\langle R_{O-O} \rangle$ for the pass-through mechanism. (b) Plot of ν^{OH} and $\langle R_{O-O} \rangle$ for the pass-through mechanism. (c) Plot of ν^{OH} and $\langle \Delta d_{DA} \rangle$ for the pass-through mechanism. (d) Plot of $\langle \Delta d_{DA} \rangle$ and $\langle R_{O-O} \rangle$ for the pass-by mechanism. (e) Plot of ν^{OH} and $\langle R_{O-O} \rangle$ for the pass-by mechanism. (f) Plot of ν^{OH} and $\langle \Delta d_{DA} \rangle$ for the pass-by mechanism. $\langle \Delta d_{DA} \rangle$ = average asymmetric stretching coordinate; $\langle R_{O-O} \rangle$ = average O-H...O H-bond distance; ν^{OH} = asymmetric O-H stretching frequency.

aqueous solution, using the DFT method at B3LYP/TZVP level of accuracy. The H-bond structures, asymmetric stretching coordinates (Δd_{DA}) and asymmetric O-H stretching frequencies (ν^{OH}) obtained from B3LYP/TZVP calculations were analyzed and categorized. The B3LYP/TZVP results suggested two types of structural diffusion mechanisms, namely the pass-through mechanism, involving the protonation and deprotonation at the $-\text{SO}_3\text{H}$ group, and the pass-by mechanism, the proton transfer in the adjacent Zundel complex. The plots of ν^{OH} and Δd_{DA} predicted the threshold frequencies (ν^{OH*}) for the proton transfer through the pass-through mechanism at 2162 and 2001 cm^{-1} , in the gas

phase and continuum aqueous solution, respectively, whereas for the pass-by mechanism at 1829 and 1714 cm^{-1} , respectively. The latter are about 200 cm^{-1} lower than those in the protonated water clusters and, therefore, represent a spectroscopic evidence for the promotion of proton transfer in the intermediate states (the shared-proton complexes) by the $-\text{SO}_3\text{H}$ group.

Inclusion of the thermal energy fluctuations and dynamics in the model calculations made it difficult to differentiate the results in the gas phase and continuum aqueous solution. For the pass-by mechanism, BOMD simulations at 350 K predicted similar characteristic asymmetric O-H stretching

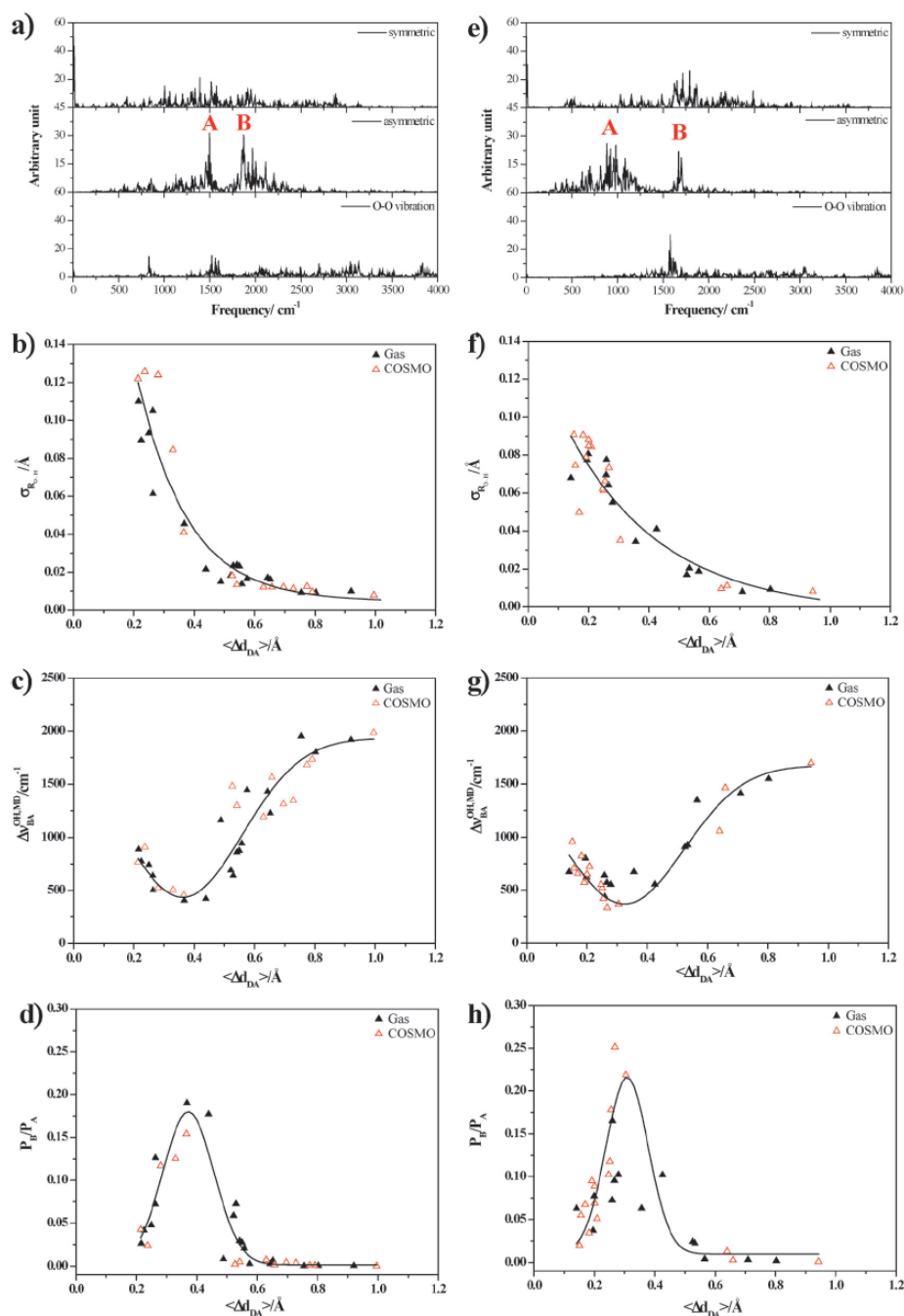


Fig. 6 BOMD results of the $\text{CF}_3\text{SO}_3\text{H}-\text{H}_3\text{O}^+-\text{H}_2\text{O}$ complexes at 350 K. (a) Example of the IR spectra of the transferring proton in the pass-through mechanism. (b) Plot of $\sigma_{R_{\text{O-H}}}$ and $\langle\Delta d_{\text{DA}}\rangle$ for the pass-through mechanism. (c) Plot of $\Delta\nu_{\text{O-H}}^{\text{OH,MD}}$ and $\langle\Delta d_{\text{DA}}\rangle$ for the pass-through mechanism. (d) Plot of $P_{\text{B}}/P_{\text{A}}$ and $\langle\Delta d_{\text{DA}}\rangle$ for the pass-through mechanism. (e) Example of the IR spectra of the transferring proton in the pass-by mechanism. (f) Plot of $\sigma_{R_{\text{O-H}}}$ and $\langle\Delta d_{\text{DA}}\rangle$ for the pass-by mechanism. (g) Plot of $\Delta\nu_{\text{O-H}}^{\text{OH,MD}}$ and $\langle\Delta d_{\text{DA}}\rangle$ for the pass-by mechanism. (h) Plot of $P_{\text{B}}/P_{\text{A}}$ and $\langle\Delta d_{\text{DA}}\rangle$ for the pass-by mechanism. $\sigma_{R_{\text{O-H}}}$ = standard deviations of the O-H distances; $\langle\Delta d_{\text{DA}}\rangle$ = average asymmetric stretching coordinate; $P_{\text{B}}/P_{\text{A}}$ = probability of finding the structural diffusion motion relative to the oscillatory shuttling motion.

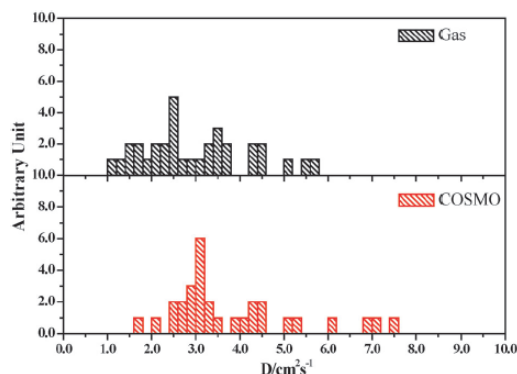


Fig. 7 Distributions of the diffusion coefficients (D) of the transferring proton in the $\text{CF}_3\text{SO}_3\text{H}-\text{H}_3\text{O}^+-\text{H}_2\text{O}$ complexes, obtained from BOMD simulations at 350 K. (a) gas phase. (b) continuum aqueous solution.

frequencies ($\nu_{\text{A}}^{\text{OH,MD}}$), with slightly lower threshold frequencies for proton transfer, $\nu_{\text{A}}^{\text{OH,MD}} = 1733$ and 1740 cm^{-1} , respectively. Additionally, BOMD simulations showed a second asymmetric O–H stretching band at a higher frequency ($\nu_{\text{B}}^{\text{OH,MD}}$). As in the case of protonated water clusters, $\nu_{\text{A}}^{\text{OH,MD}}$ and $\nu_{\text{B}}^{\text{OH,MD}}$ could be associated with the oscillatory shuttling and structural diffusion motions, respectively; the characteristic motions of the transferring proton in H-bond. The analyses of $\nu_{\text{A}}^{\text{OH,MD}}$ and $\nu_{\text{B}}^{\text{OH,MD}}$ suggested the lowest vibrational energies for the interconversion between the oscillatory shuttling and structural diffusion motions ($\Delta\nu_{\text{BA}}^{\text{OH,MD}}$), for the pass-through and pass-by mechanisms of 469 and 398 cm^{-1} , respectively. The latter is about 75 cm^{-1} lower than the protonated water clusters; an indication of a decrease of the vibrational energy for the interconversion between the oscillatory shuttling and structural diffusion motions in the presence of the $-\text{SO}_3\text{H}$ group.

Comparison of the proton diffusion coefficients obtained in the present work and those in the protonated water clusters indicated that the $-\text{SO}_3\text{H}$ group suppresses the mobility of the transferring proton in the intermediate states, by introducing strong electrostatic effect at the shared-proton structures. These are however accompanied by a decrease of the vibrational energy for the interconversion between the oscillatory shuttling and structural diffusion motions and a higher relative probability of finding the structural diffusion motion in the $\text{CF}_3\text{SO}_3\text{H}-\text{H}_3\text{O}^+-\text{H}_2\text{O}$ complexes, compared to those in the protonated water clusters. One could, therefore, conclude that the $-\text{SO}_3\text{H}$ groups in Nafion[®] act as active binding sites which provide appropriate structural, energetic and dynamic conditions for effective structural diffusion processes in the intermediate states of proton transfer reactions. The present results confirmed that, due to the coupling among various vibrational modes in H-bonds, the discussions on proton transfer reactions cannot be made based solely on static proton transfer potentials. Inclusion of thermal energy fluctuations and dynamics in the model calculations, as in the case of BOMD simulations, together with systematic IR spectral analyses, have been proved to be the most appropriate theoretical approaches.

Acknowledgements

The authors would like to acknowledge the financial supports from the Thailand Research Fund (TRF); the Advanced Research Scholarship (BRG-5180022) for Prof. Kritsana Sagarik; the Royal Golden Jubilee (RGJ) Ph.D. Program, Grant No. PHD/0110/2548 for Prof. Kritsana Sagarik and Mayuree Phonyiem; RGJ-PhD Program. Semsiri Chaiwongwattana was supported by SUT post-doctoral research fellowship. High-performance computer facilities provided by the following organizations are gratefully acknowledged: School of Mathematics and School of Chemistry, SUT; National Electronics and Computer Technology Center (NECTEC) and National Nanotechnology Center (NANOTEC), National Science and Technology Development Agency (NSTDA); the Thai National Grid Center (THAIGRID), Ministry of Information and Communication Technology (MICT).

References

- 1 J. Larminie and A. Dicks, *Fuel Cell Systems*, John Wiley & Sons Ltd, Chichester, 2001.
- 2 C. A. Vincent and B. Scrosati, *Modern Batteries: An introduction to electrochemical power sources*, John Wiley & Sons Ltd, New York, 1997.
- 3 J. T. Hinatsu, M. Mizuhata and H. Takenaka, *J. Electrochem. Soc.*, 1994, **141**, 1493.
- 4 K.-D. Kreuer, *Chem. Mater.*, 1996, **8**, 610.
- 5 K.-D. Kreuer, S. J. Paddison, E. Spohr and M. Schuster, *Chem. Rev.*, 2004, **104**, 4637.
- 6 S. J. Paddison, *Annu. Rev. Mater. Res.*, 2003, **33**, 289.
- 7 S. J. Paddison and T. A. Zawodzinski Jr, *Solid State Ionics*, 1998, **113–115**, 333.
- 8 K. Sagarik, M. Phonyiem, C. Lao-ngam and S. Chaiwongwattana, *Phys. Chem. Chem. Phys.*, 2008, **10**, 2098.
- 9 K. Sagarik, S. Chaiwongwattana, V. Vchirawongkwin and S. Prueksaaron, *Phys. Chem. Chem. Phys.*, 2010, **12**, 918.
- 10 J. B. Asbury, T. Steinel and M. D. Fayer, *J. Lumin.*, 2004, **107**, 271.
- 11 J. C. Jiang, C. Chaudhuri, Y. T. Lee and H. C. Chang, *J. Phys. Chem. A*, 2002, **106**, 10937.
- 12 C. C. Wu, C. Chaudhuri, J. C. Jiang, Y. T. Lee and H. C. Chang, *J. Phys. Chem. A*, 2004, **108**, 2859.
- 13 R. Buzzoni, S. Bordiga, G. Ricchiardi, G. Spoto and A. Zecchina, *J. Phys. Chem.*, 1995, **99**, 11937.
- 14 R. Ifimie, V. Thomas, S. Plessis, P. Marchand and P. Ayotte, *J. Am. Chem. Soc.*, 2008, **130**, 5901.
- 15 M. Okumura, L. I. Yeh, J. D. Myers and Y. T. Lee, *J. Phys. Chem.*, 1990, **94**, 3416.
- 16 C.-C. Wu, J. C. Jiang, D. W. Boo, S. H. Lin, Y. T. Lee and H.-C. Chang, *J. Chem. Phys.*, 2000, **112**, 176.
- 17 M. Ludvigsson, J. Lindgren and J. Tegenfeld, *Electrochim. Acta*, 2000, **45**, 2267.
- 18 G. C. Pimentel and A. L. McClellan, *The Hydrogen Bond*, W. H. Freeman, San Francisco, 1960.
- 19 C. Lao-ngam, P. Asawakun, S. Wannarat and K. Sagarik, *Phys. Chem. Chem. Phys.*, 2011, **13**, 4562.
- 20 M. Benoit and D. Marx, *ChemPhysChem*, 2005, **6**, 1738.
- 21 K. Sagarik, *J. Mol. Struct.: THEOCHEM*, 1999, **465**, 141.
- 22 K. Sagarik and P. Asawakun, *Chem. Phys.*, 1997, **219**, 173.
- 23 K. Sagarik, S. Chaiwongwattana and P. Siset, *Chem. Phys.*, 2004, **306**, 1.
- 24 K. Sagarik and S. Chaiyapongs, *Biophys. Chem.*, 2005, **117**, 119.
- 25 K. Sagarik and S. Dokmaisrijan, *J. Mol. Struct.: THEOCHEM*, 2005, **718**, 31.
- 26 K. Sagarik and B. M. Rode, *Chem. Phys.*, 2000, **260**, 159.
- 27 K. Sagarik and E. Spohr, *Chem. Phys.*, 1995, **199**, 73.
- 28 K. P. Sagarik and R. Ahlrichs, *J. Chem. Phys.*, 1987, **86**, 5117.
- 29 K. P. Sagarik, V. Pongpituk, S. Chaiyapongs and P. Siset, *Chem. Phys.*, 1991, **156**, 439.

-
- 30 K. Kwac, C. Lee, Y. Jung and J. Han, *J. Chem. Phys.*, 2006, **125**, 244508.
- 31 J. L. Knee, L. R. Knundkar and A. H. Zewail, *J. Chem. Phys.*, 1985, **82**, 4715.
- 32 V. Termath and J. Sauer, *Mol. Phys.*, 1997, **91**, 963.
- 33 R. Ahlrichs, M. Bär, M. Häser, H. Horn and C. Kölmel, *Chem. Phys. Lett.*, 1989, **162**, 165.
- 34 O. Treutler and R. Ahlrichs, *J. Chem. Phys.*, 1995, **102**, 346.
- 35 A. D. Becke, *J. Chem. Phys.*, 1993, **98**, 5648.
- 36 C. Lee, W. Yang and R. G. Parr, *Phys. Rev. B*, 1988, **37**, 785.
- 37 A. Schaefer, C. Huber and R. Ahlrichs, *J. Chem. Phys.*, 1994, **100**, 5829.
- 38 G. Santambrogio, M. Bruemmer, L. Woeste, J. Doeblér, M. Sierka, J. Sauer, G. Meijer and K. R. Asmis, *Phys. Chem. Chem. Phys.*, 2008, **10**, 3992.
- 39 D. Marx, M. E. Tuckerman, J. Hutter and M. Parrinello, *Nature*, 1999, **367**, 101.
- 40 A. P. Scott and L. Radom, *J. Phys. Chem.*, 1996, **100**, 16502.
- 41 P. B. Balbuena and J. M. Seminario, *Theoretical and Computational Chemistry 7*, Elsevier, Amsterdam, 1999.
- 42 R. N. Barnett and U. Landman, *Phys. Rev. B: Condens. Matter*, 1993, **48**, 2081.
- 43 X. Jing, N. Troullier, D. Dean, J. R. N. Binnigeli, Chelikowsky, K. Wu and Y. Saad, *Phys. Rev.*, 1994, **B50**, 122.
- 44 N. Agmon, *Chem. Phys. Lett.*, 1995, **244**, 456.
- 45 P. A. Giguere, *J. Chem. Educ.*, 1979, **56**, 571.
- 46 K. D. Kreuer, *Solid State Ionics*, 2000, **136–137**, 149.
- 47 R. R. Sadeghi and H. Cheng, *J. Chem. Phys.*, 1999, **111**, 2086.
- 48 H.-P. Cheng and J. L. Krause, *J. Chem. Phys.*, 1997, **107**, 8461.
- 49 P. Bopp, *Chem. Phys.*, 1986, **106**, 205.
- 50 J. M. Haile, *Molecular Dynamics Simulations*, John Wiley & Sons Ltd, New York, 1997.
- 51 D. C. Rapaport, *The Art of Molecular Dynamics Simulation*, Cambridge University Press, London, 1995.
- 52 J. Chen, M. A. McAllister, J. K. Lee and K. N. Houk, *J. Org. Chem.*, 1998, **63**, 4611.
- 53 Y. Wu, H. Chen, F. Wang, F. Paesani and G. A. Voth, *J. Phys. Chem. B*, 2008, **112**, 467.

CURRICULUM VITAE

Ms. MAYUREE PHONYIEM

Educations:

- 2006 - 2011 Ph.D. Candidate (Chemistry), Suranaree University of Technology,
Thailand
- 1999 – 2003 B.Sc. (Chemistry), Ramkhamhaeng University, Thailand

Work Experiences:

- 2003 – 2003 Chemist, Global Chemical Co., Ltd. Samut Prakan, Thailand.
- 2003 – 2005 Analyst, I.Q.A. Norwest Labs Co., Ltd., Bangkok, Thailand.

Research Experience:

- 08/2011-11/2011 Visiting scholar, Hirata group at University of Illinois at Urbana-
Champaign, U.S.

Grant and Fellowship:

- 2006 - 2011 Royal Golden Jubilee (RGJ) Ph. D. research scholarship from
Thailand Research Fund (TRF)
- 2009-2011 SUT Teaching Assistantship